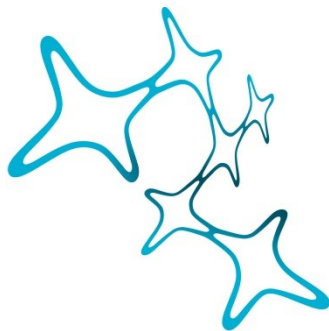

EXPLORING MOLECULAR MECHANISMS DICTATING ASTROCYTE IDENTITY AND IMPLICATIONS FOR NEURONAL REPROGRAMMING

Poornemaa Natarajan



Graduate School of
Systemic Neurosciences

LMU Munich



Dissertation at the
Graduate School of Systemic Neurosciences
Ludwig-Maximilians-Universität München

21.08.2023

Supervisor

Prof. Dr. Magdalena Götz

Head of LMU Department of Physiological Genomics

BioMedical Center – BMC

Ludwig-Maximilians-Universität München

Institute Stem Cell Research, Helmholtz Center Munich

First Reviewer: Prof. Dr. Magdalena Götz

Second Reviewer: Dr. Francois Guillemot

External Reviewer: Prof. Dr. Elly Hol

Date of Submission: 21.08.2023

Date of Defense : 12.03.2024

TABLE OF CONTENTS

SUMMARY	4
1. INTRODUCTION	5
1.1 Manipulation of cell fate	6
1.2 Direct neuronal reprogramming of astrocytes	7
1.3 Challenges faced during direct neuronal reprogramming	9
1.3.1 Reprogramming TF and DNA accessibility.....	9
1.3.2 Erasure of starter cell identity	11
1.3.3 Cell proliferation.....	12
1.3.4 Cell death	13
1.3.5 Metabolic and mitochondrial changes	13
1.4 Astrocytes.....	14
1.4.1 Astrocytogenesis.....	15
1.4.2 Astrocyte heterogeneity	16
1.4.3 Astrocytes in the context of injury and disease.....	17
1.4.4 Transcription factors influencing astrocyte functions.....	18
1.5 Aims of the study.....	21
2. RESULTS	22
2.1 Project 1.....	22
2.2 Project 2.....	52
3. DISCUSSION	105
3.1 Metabolic and mitochondrial remodeling are crucial to the success of astrocyte to neuron fate conversion	105
3.1.1 Astrocytes and neurons have a distinct mitochondrial proteome.....	105
3.1.2 Mitochondria undergoes dynamic remodeling during direct neuronal reprogramming of astrocytes	106
3.1.3 Early induction of neuron-enriched mitoproteins aids direct neuronal reprogramming	107
3.1.4 Inhibiting astrocyte specific metabolic pathways improves direct neuronal reprogramming.....	110
3.2 Astrocyte specific Sox9, Trps1 deletion affects glial crosstalk and injury response	112
3.2.1 Intra-regional heterogeneity in the expression of individual TFs at protein and RNA levels.....	112
3.2.2 Sox9 and Trps1 deletion reveals crucial roles in adult cortical astrocytes.....	114
3.2.3 Astrocyte specific Sox9 and Trps1 loss affects injury response of several cells in the tissue microenvironment	117
3.3 Concluding remarks	121
4. References	123
Declaration of Author contributions	139
Curriculum vitae	141
List of Publications	143
Affidavit	144
Acknowledgements	145

SUMMARY

A major breakthrough in the field of regenerative medicine is the possibility of cellular reprogramming and extensive research in the recent years has brought to light the immense potential this holds for replacement of damaged neurons in injury or disease conditions. Even though considerable success has been achieved in converting several cell types to neurons *in vivo*, much remains to be understood about the mechanisms underlying this process. Among the different cell sources in the brain for direct neuronal reprogramming, astrocytes are the most favored as they display a dormant neurogenic capacity. In addition, astrocytes are also integral to a multitude of homeostatic functions across the central nervous system. However, we are yet to understand the diverse nature of astrocyte identity and functions, how this is altered in the pathological context of disease or inflammation. Bridging the gaps in our understanding of astrocyte identity and functions (in homeostatic and disease conditions) and their impact in the outcome of reprogramming would be crucial to moving this field forward.

In pursuit of this, my first PhD project focused on understanding the metabolic and mitochondrial differences between astrocytes and neurons, how this information can be exploited to improve reprogramming. A pivotal feature of astrocyte identity is their preference for glycolysis and fatty acid β -oxidation while neurons are restricted to oxidative phosphorylation for metabolism. Thus, we compared the mitochondrial proteome of astrocytes and neurons. Expectedly, the proteomes differed significantly (Russo et al., 2021). We made use of this data to understand if precocious expression of neuron-enriched mitochondrial proteins aids the process of direct neuronal reprogramming. Interestingly, this improved the efficiency by accelerating the speed of reprogramming, survival of the reprogrammed neurons and even resulted in cells with more mature morphology. Incidentally, disrupting an astrocyte specific metabolic pathway, fatty acid β -oxidation, also improved the efficiency of neuronal reprogramming, highlighting that metabolic and mitochondrial remodeling is a crucial step while converting astrocytes to neurons (Russo et al., 2021).

In the second project, we delved deeper into the molecular mechanisms dictating astrocyte identity and functions by focusing on the roles of two key astrocyte transcription factors (TFs), Sox9 and Trps1. After characterizing their expression pattern in the cortical gray matter (GM) at single cell protein and RNA level, we set out to identify how the astrocyte functions are altered upon deletion of Sox9 and Trps1. Our study revealed novel and hitherto unknown

functions of these two factors in cortical GM astrocytes, loss of these TFs affected vital astrocyte functions like immune response, glial crosstalk and synapse maintenance.

In summary, we observed that astrocytes have specialized mitochondria with a distinct mitochondrial proteome to meet their unique metabolic requirements, which would be hallmark feature of astrocyte identity. In addition to establishing neuron specific programs, these astrocyte specific features would have to be downregulated for efficient conversion of cell fate from astrocyte to neuron. Further, we show that important astrocyte TFs may display intra-regional variations in their expression levels at RNA and protein level. We were able to identify how these TFs may be involved in dictating several vital astrocyte functions, as loss of these TFs may have widespread effects, even on the surrounding cells in the tissue microenvironment.

1. INTRODUCTION

The functional impairment in Central Nervous System (CNS) is the main result of irreversible loss of neurons, both in degenerative diseases or traumatic brain injury (TBI). Though the mammalian brain exhibits high levels of plasticity at the level of synapses and circuits, its potential for regeneration in case of TBI/ disease is limited and this further decreases with age. Regenerative therapies thus aim to replace the damaged neurons and restore the original circuitry for functional rescue and such strategies can also be potentially used to rectify malformed circuits in case of developmental disorders. Several methods have been tried so far for this purpose, like transplantation of embryonic cells/ induced pluripotent stem cells (iPSCs), recruitment of endogenous cells either locally or from neurogenic niches and direct neuronal reprogramming of the cells in the local environment. Considerable success has been achieved by transplantation of cells, even resulting in integration of the transplanted cells into pre-existing circuitry and functional rescue (Falkner, Grade et al., 2016), also in a primate model of Parkinson's (Kikuchi et al., 2017). One major risk of cell transplantations is graft rejection when the cells are derived from exogenous origin. Although this can be overcome by using patient-derived autologous cells for transplantation (Schweitzer et al., 2020), it can be expensive and time-consuming to generate personalized iPSCs of consistent quality for transplantation. On the other hand, direct reprogramming of endogenous cells from the local environment overcomes this disadvantage, making it an attractive therapeutic strategy. Direct reprogramming refers to the conversion of a terminally differentiated cell of one type (like

astrocyte, oligodendrocyte or microglia) into another functionally distinct cell type (like neurons of a desired subtype), often by forced expression of transcription factors (TFs) without having to undergo an intermediate multipotent cell stage. This is an exciting strategy because in case of brain injury and inflammation, it can simultaneously reduce the formation of non-functional glial scar by converting the reactive glial cells itself into neurons. So far, direct neuronal reprogramming of non-neuronal cells such as astrocytes (Chen et al., 2020; Gascón, Murenu et al., 2016; Guo et al., 2014; Mattugini, Bocchi et al., 2019), oligodendrocytes (Heinrich et al., 2014; Pereira et al., 2017; Torper et al., 2015), microglia (Matsuda et al., 2019) and pericytes (Karow, Camp et al., 2018) into functional neurons has been demonstrated successfully *in vitro* and *in vivo* (for an extensive list, see reviews Bocchi et al., 2022; Gascón et al., 2017). In general, successful reprogramming involves establishment of the desired end cell type, and the simultaneous erasure of the starter cell identity. I will first introduce some of the existing approaches in the field of direct neuronal reprogramming and the general hurdles faced in this process.

Even if we can convert one cell type to another with relative ease, the identity of a cell is maintained stably and such conversions do not happen naturally. It is imperative to understand the mechanisms that maintain the functions and identity of the starter cell type. This will help us overcome the road blocks faced in the process of neuronal reprogramming and improve the outcome. In addition, several studies implicate astrocytes in disease etiology (Bustos and Sattler, 2023; Caldwell et al., 2022; Franklin et al., 2021; Monterey et al., 2021) and the therapeutic options are not only from a neuronal perspective anymore. Accordingly, it has become even more important to understand the biology of these cells in greater detail and I will introduce about astrocytes, our starter cells of interest.

1.1 Manipulation of cell fate

All the cells in an organism arise from a single cell, which over the course of development divides and gives rise to many diverse cell types with unique functions. Such fate specification requires precise and concerted spatiotemporal changes in transcriptional and epigenetic programs. For a long time, it was believed that once specified during development, the fate of a cell is irreversible. Seminal studies in the 1950s changed this idea; in amphibians, the transfer of nuclei from various stages of development into an unfertilized egg could give rise to new organisms that underwent normal development (Briggs and King, 1952; Gurdon, 1962; Gurdon

et al., 1958). Further developments in the field established the possibility of converting a terminally differentiated cell of one type into another functionally distinct cell type even without having to undergo an intermediate multipotent cell stage, a process referred to as “direct reprogramming”. Initially it was explored to convert cells that were developmentally closer, and by using TFs that were known to be essential for the developmental cell fate specification of the desired end cell type. For example, fibroblasts were converted to muscle cells, both of which are of mesodermal origin; by forced expression of MyoD which is essential for myogenesis during development (Davis et al., 1987). Similarly, non-neuronal cells of the brain could be converted into neurons by forced expression of TFs such as Pax6, Ascl1, Dlx2 or Neurogenin2 (Ngn2) successfully, generating even the subtypes of neurons that these factors would instruct during development (Heinrich et al., 2010; Heins, Malatesta et al., 2002). Such conversion was shown to be possible even *in vivo*, reactive glial cells from the region of brain injury could be converted into immature neurons (Buffo et al., 2005; Heinrich et al., 2014). Yet another breakthrough in this field was when it was shown that cells could even be converted across germ layers. For example, fibroblasts that are of mesodermal origin could be converted into neurons that developmentally arise from the ectoderm (Vierbuchen et al., 2010). Together, these studies shed light on the immense translational potential direct reprogramming has, either to target local non-neuronal cells for direct neuronal reprogramming or to potentially use patient derived fibroblasts that can be used for cell transplantation based regenerative therapies. Indeed, direct reprogramming of fibroblasts into several other cell types has also been accomplished with a cocktail of TFs (see reviews Carter et al., 2020; Morris, 2016).

1.2 Direct neuronal reprogramming of astrocytes

While the direct reprogramming with patient derived fibroblasts is an exciting strategy for disease modelling and potential cell transplantation based regenerative approaches, the use of endogenous non-neuronal cells in the environment is even more alluring.

Among all the cell sources, astrocytes are highly attractive as they are known to have a latent neurogenic potential (summarized in *Figure 1*). Upon injury, some cortical reactive astrocytes can proliferate and give rise to multipotent neurospheres when cultured *in vitro* (Buffo et al., 2008; Sirko, Behrendt et al., 2013). Interestingly, these cells also share similarities with neural stem cells (NSCs) in gene expression (Götz et al., 2015). Similar to cortical astrocytes, even striatal astrocytes have a latent neurogenic potential, which is regulated by Notch signaling (Magnusson et al., 2014). In general, striatal astrocytes could give rise to Dcx⁺ neuroblasts after

stroke; downregulation of *Rbpj-k* to interfere with the Notch signaling activated the latent neurogenic potential of striatal astrocytes giving rise to neuroblasts even in the absence of stroke (Magnusson et al., 2014). Manipulation of the same pathway in cortical astrocytes did not automatically have the same effect (Magnusson et al., 2020), but the plasticity of these cells could be elicited when ablation of Notch signaling was combined with a stab wound injury (SWI) (Zamboni et al., 2020). These data highlight the unique nature of astrocytes that makes them an attractive cell source for further manipulation. Furthermore, this also highlights the diversity and versatility of these cells between different brain regions, the understanding of which would be essential to exploit them for regenerative purposes.

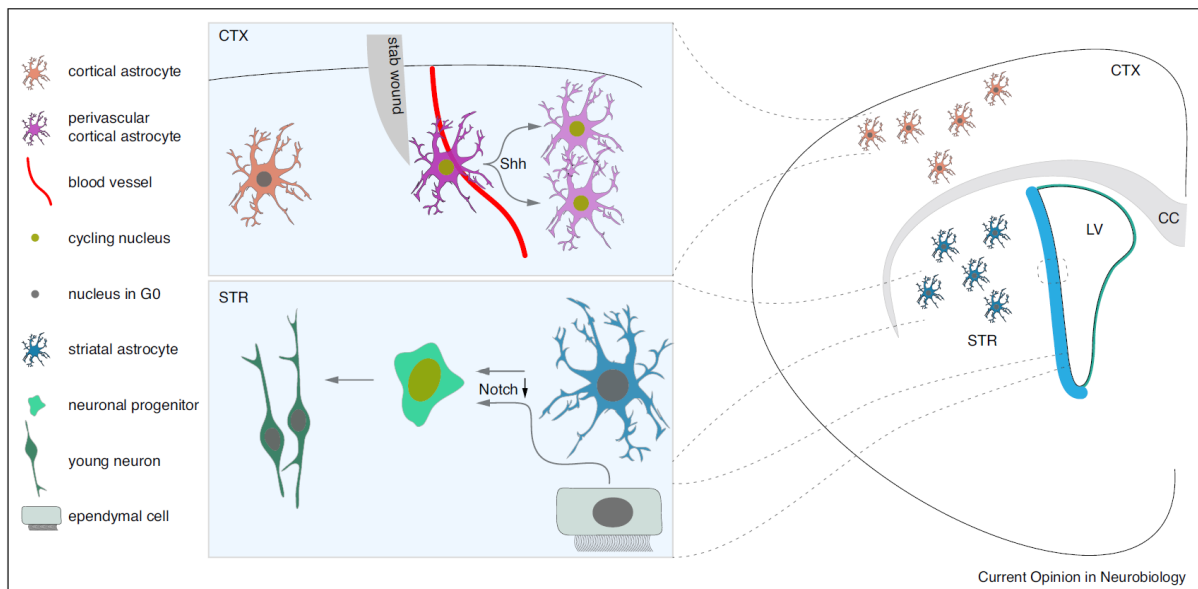


Figure 1. This image is from Falk and Götz, 2017, an open-access article distributed under the terms of the Creative Commons Attribution License (CC BY-NC-ND 4.0). This illustrates the differences in the neurogenic potential of astrocytes between brain regions. Some cortical astrocytes proliferate after injury in response to Sonic hedgehog signaling, their neurogenic potential is activated when cultured *in vitro*, giving rise to multipotent neurospheres (Sirko, Behrendt et al., 2013). In contrast, striatal astrocytes can give rise to neuroblasts *in vivo* and this is regulated by Notch signaling (Magnusson et al., 2014), similar to the ependymal cells (Carlén et al., 2009).

As mentioned earlier, several studies have demonstrated successful *in vivo* direct neuronal reprogramming of astrocytes (Chen et al., 2020; Gascón, Murenu et al., 2016; Guo et al., 2014; Mattugini, Bocchi et al., 2019; Niu et al., 2015), achieving even generation of layer and subtype

specific neurons (Mattugini, Bocchi et al., 2019). However, much of the understanding of direct neuronal reprogramming comes from *in vitro* studies that shed light on several fundamental concepts underlying this process. For example, direct neuronal reprogramming of cortical astrocytes with *Dlx2* or *Ngn2* gives rise to GABAergic and glutamatergic induced neurons (iNs) respectively (Heinrich et al., 2010). Similarly, *Ascl1* and *Ngn2* instruct distinct neurogenic cascades in murine astrocytes, which also vary depending on the region of origin within the CNS, i.e., cortical or spinal cord astrocytes (Kempf, Knelles, Hersbach et al., 2021; Masserdotti et al., 2015).

Even when using the same reprogramming TF, the source of starter cell plays an important role in the efficiency of reprogramming and influences the subtype of iNs that can be obtained. For example, while reprogramming of striatal astrocytes with *Ascl1* gives rise to iNs that are glutamatergic and GABAergic (Liu, Miao et al., 2015), *Ascl1* gives rise to predominantly glutamatergic iNs when fibroblasts are the starter cells (Chanda et al., 2014). Even if *Ascl1* can reprogram fibroblasts alone, the efficiency of conversion is much higher when a cocktail of TFs (*Ascl1*, *Brn2* and *Myt1l*) are used (Vierbuchen et al., 2010; Wapinski, Vierbuchen et al., 2013). This could stem from the fact that fibroblasts are more developmentally distant from neurons, thus requiring more factors. Overall, the efficiency and outcome of reprogramming varies depending on the starter cells and the TFs used for reprogramming, hinting at cell type specific hurdles that are faced during this process.

1.3 Challenges faced during direct neuronal reprogramming

Although considerable success has been achieved in the field of neuronal reprogramming, the reprogramming efficiency can be improved further by understanding the mechanisms underlying the process of cell fate conversion. Furthermore, we are yet to understand in detail how specific neuronal subtypes that successfully integrate into the host circuitry can be obtained and the impact astrocyte heterogeneity may have in this process. So far, several hurdles that can be detrimental to the process of direct neuronal reprogramming have been identified (summarized in *Figure 2*) and I will elaborate on some of them below.

1.3.1 Reprogramming TF and DNA accessibility

The first challenge during this process is the genomic accessibility to the reprogramming TF, which dictates successful instruction of the neuronal fate and this is highly dependent on the chromatin landscape in the starter cell type. As shown in *Figure 3a*, most of the common

neuronal reprogramming TFs such as *Ascl1*, *Ngn2* and *NeuroD1* are thought to be pioneer factors, that can bind to closed chromatin and induce downstream target gene expression during reprogramming (Matsuda et al., 2019; Wapinski, Vierbuchen et al., 2013; Wapinski, Lee et al., 2017) or during differentiation (Aydin et al., 2019; Pataskar et al., 2016). Even so, the epigenetic environment in different starter cell types heavily influences the binding of these TFs. For example, *Ngn2* that reprograms astrocytes very efficiently (Berninger et al., 2007; Heinrich et al., 2010; Masserdotti et al., 2015), can do so in fibroblasts only in the presence of small molecules such as forskolin (activator of adenylate cyclase) and dorsomorphin (inhibitor of BMP signaling) that increase *Ngn2* binding to chromatin (Smith et al., 2016). Even with astrocytes as starter cells, the efficiency of reprogramming is drastically reduced when the *Ngn2* target sites are gradually blocked by REST, which accumulates as astrocyte grow more mature and older (Masserdotti et al., 2015). Thus, epigenetic barriers are among the foremost of hurdles encountered during reprogramming.

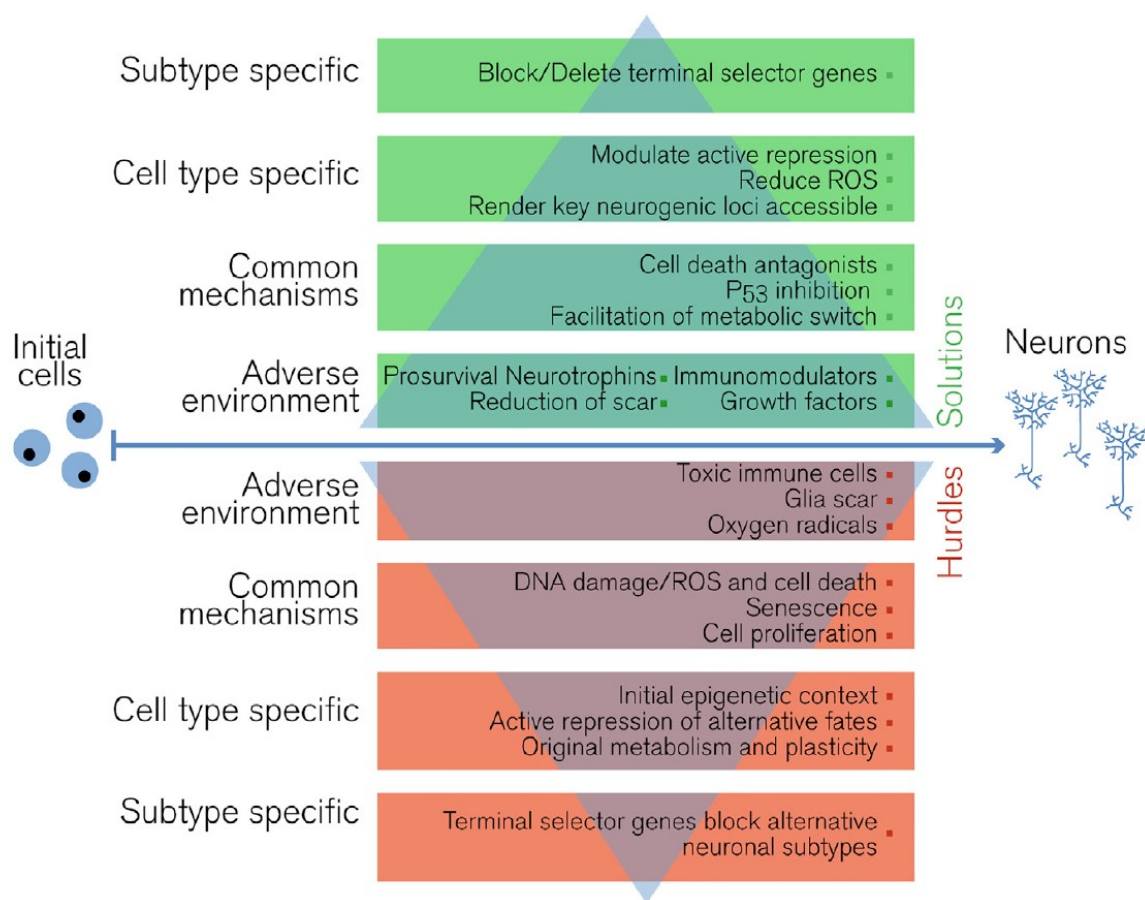


Figure 2. Summary of the hurdles faced during direct neuronal reprogramming (Gascón et al., 2017, permission to use the figure for the non-commercial purpose granted by Elsevier)

In some cases, due to similar binding motifs or chromatin accessibility, certain reprogramming TFs may bind to promiscuous sites and induce expression of genes not related to the intended cell type (as depicted in *Figure 3c*). For example in fibroblasts, ideally Myod1 would induce the expression of myogenic transcriptional program while Ascl1 would induce a neurogenic program. However, it has been shown that Ascl1 can induce expression of myogenic genes like *Myo18b*, *Tnnc2* during direct neuronal reprogramming of fibroblasts (Treutlein et al., 2016; Wapinski et al., 2017). Similarly, Myod1 can induce expression of neurogenic genes in fibroblasts and in the presence of Myt11, the neurogenic potential is further increased (Lee et al., 2020). Thus, the choice of reprogramming TF and the chromatin landscape of the starter cell type can pose several challenges. Using additional reprogramming factors like Brn2 or Myt11 has been shown to overcome these (Lee et al., 2020; Treutlein et al., 2016; Wapinski et al., 2013). Alternatively, a cocktail of small molecules can be used to promote chromatin accessibility (Smith et al., 2016; Wang et al., 2022). In fact, many studies have even demonstrated direct reprogramming by use of a combination of small molecules alone, without even the need for exogenous expression of a bonafide neurogenic TF (Yin, Zhang et al., 2019; Zhang et al., 2015).

1.3.2 Erasure of starter cell identity

As mentioned earlier, successful conversion requires establishment of new cell fate accompanied by erasure of the starter cell identity. While most focus has been on understanding establishment of neuronal fate, the dynamics of starter cell identity erasure is yet to be unraveled. The TFs used for direct reprogramming (may) have different propensities to erase the starter cell identity, similar to the differences in (but independent of) their ability to induce successful reprogramming in fibroblasts (Hersbach et al., 2022). Neuronal reprogramming of human adult fibroblasts with miRNAs show erasure of fibroblast identity followed by consequent establishment of neuronal fate (Cates et al., 2021). Such a systematic mechanistic breakdown of fate erasure has not yet been carried out in the context of astrocyte to neuron reprogramming. However, it has been noticed that several genes related to astrocytes (*Id3*, *Slc1a3*, *Trps1*, *Aqp4*, *Gjal1*, *Bhlhe40*, *Fgfr3*, *Klf15*, *Aldoc*, *Ank2*) are downregulated in Ascl1 or Ngn2 mediated astrocyte to neuron reprogramming (Kempf, Knelles, Hersbach et al., 2021), highlighting the potential of the pioneer reprogramming TFs to suppress various aspects of the starter cell identity (as depicted in *Figure 3b*). Understanding the dynamics of astrocyte identity erasure could help in faster and more efficient reprogramming *in vivo*, which may be key to functional restoration of damaged neuronal circuits.

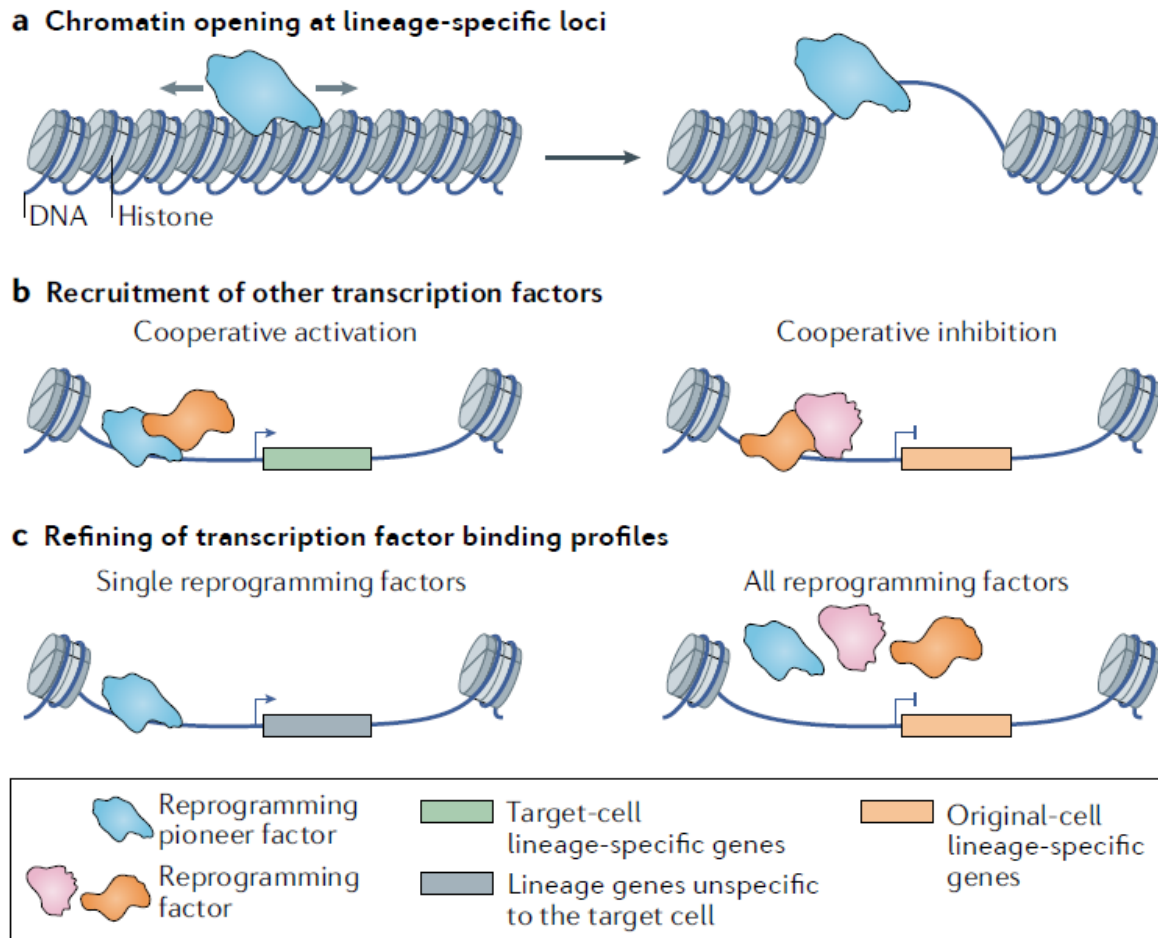


Figure 3. Overview of how reprogramming factors such as *Ascl1*, *Ng2* bind to closed chromatin and induce expression of neuronal genes; how multiple reprogramming factors (or reprogramming factors along with some co-factors) may act in tandem to either activate the desired cell type specific genes or inhibit genes related to starter cell identity; In some cases, reprogramming TFs may induce expression of genes unrelated to the starter cell and desired cell type. This image is from Wang et al., 2021, License number 5603650390639.

1.3.3 Cell proliferation

Another challenge during reprogramming could be proliferation. While proliferation can be beneficial for reprogramming into proliferative fates like iPSCs (Ruiz et al., 2011; Velychko et al., 2019), live imaging during direct neuronal reprogramming of astrocytes showed proliferation is not necessary (Gascón, Murenu et al., 2016; Heinrich et al., 2010). As neurons are non-proliferating post-mitotic cells, absence of proliferation may in fact be beneficial to reprogramming. In line with this, *Ascl1* mediated reprogramming elicits the expression of anti-proliferative genes such as *Cdkn1c* in astrocytes (Kempf, Knelles, Hersbach et al., 2021;

Masserdotti et al., 2015). Similarly, neuronal reprogramming of fibroblasts with microRNAs miR-9/9* and miR-124 elicits cell cycle exit prior to establishment of neuronal identity (Cates, McCoy, Kwon, Liu et al., 2021). While proliferation may not be necessary for successful neuronal reprogramming, it may be beneficial under certain contexts; a subset of fibroblasts that have high levels of proliferation in addition to high levels of transcription reprogrammed more effectively than fibroblast populations that had only high levels of either proliferation or transcription (Babos et al., 2019). Active transcription is essential for establishment of the neuronal identity, and proliferation (at least in the earlier stages of reprogramming) maybe beneficial as activation of topoisomerases could alleviate the genomic DNA stress induced by overexpression of reprogramming TF. Thus, cell proliferation may play context dependent roles, acting either as a barrier or as a promoter of reprogramming.

1.3.4 Cell death

The live-imaging experiments by Gascón , Murenu et al., 2016 identified yet another major hurdle during astrocyte reprogramming: cell death. The process of cell fate conversion results in an increase in the production of reactive oxygen species (ROS) and peroxidised lipids. Such increase in ROS has also been observed during stem cell differentiation (Khacho et al., 2016), which is also accompanied by mitochondrial remodeling.

This bottleneck could be overcome by expression of anti-apoptotic genes like Bcl2 or by treatment with anti-oxidants such as vitamin E (α -Tocotrienol) during the process of reprogramming (Gascón, Murenu et al., 2016). Interestingly, among the cell death pathways, it was found that ferroptosis posed the largest hurdle, as both cell survival and reprogramming efficiency were maximally improved only when an inhibitor of this pathway (liproxstatin-1) was applied. Inhibition of apoptosis in general with a pan-caspase/apoptosis inhibitor (ZVAD), or inhibition of necroptosis (Necrostatin-1) only improved cell survival, but no improvement in the reprogramming efficiency was observed (Gascón, Murenu et al., 2016).

1.3.5 Metabolic and mitochondrial changes

Astrocytes though capable of oxidative phosphorylation, predominantly use fatty acid β -oxidation (FAO) and glycolysis (Rose et al., 2020). FAO is a hallmark of astrocytes (Eraso-Pichot et al., 2018) and it is one of the ways in which astrocytes contribute to neuronal health and brain homeostasis (Ioannou et al., 2019), but this is absent in neurons. On the other hand, neurons predominantly use oxidative phosphorylation. Similar to astrocytes, NSCs have higher levels of glycolysis and FAO. Activation of adult NSCs and subsequent neuronal differentiation

is accompanied by a shift from glycolysis to oxidative phosphorylation (Llorens-Bobadilla et al., 2015; Zheng et al., 2016). Direct differentiation of human embryonic stem cells into iNs using Ngn2 also shows dynamic remodeling of mitochondria over the time course of differentiation (Ordureau et al., 2021). Thus, conversion of cell fate from astrocyte to neuron would also involve a metabolic shift from glycolysis and FAO to oxidative phosphorylation. This would require dynamic mitochondrial changes, which in addition to the metabolic burden of increased ROS could be a major hurdle. In fact, reprogramming astrocytes in media containing Oligomycin A, an inhibitor of oxidative phosphorylation (thereby forcing glycolysis) drastically reduces the neuronal reprogramming efficiency (Gascón, Murenu et al., 2016).

Expectedly, the different cell types in the brain have a distinct mitochondrial proteome to suit their unique metabolic requirements (Fecher et al., 2019). Similarly, we found that the mitochondrial proteome of cortical astrocytes and neurons are distinct (Russo et al., 2021). Indeed, successful metabolic and mitochondrial remodeling are critical to efficient neuronal reprogramming (Russo et al., 2021), I will be elaborate on this in detail in later sections as one of the key findings of the work done during my PhD. Likewise, other organelles may also have to undergo extensive remodeling during the course of reprogramming to suit the needs of the end cell type.

While most of the above-mentioned aspects describe the hurdles faced during the process of neuronal reprogramming, one primary challenge is also to understand the nature of astrocytes, the mechanisms that maintain the functions and identity of the starter cell type.

In the following section, I will discuss about the role of astrocytes in health and disease or injury, astrocytogenesis and the importance of astrocyte heterogeneity and how TFs may be important in mediating key astrocyte functions and maintaining cell identity.

1.4 Astrocytes

Astrocytes play key roles in brain functions as summarized in *Figure 4A-C* (image from Linnerbauer and Rothhammer, 2020). They are integral to ion homeostasis (Chever et al., 2010; Djukic et al., 2007; Kelley et al., 2018) and play key roles in synapse formation and maintenance (Blanco-Suarez et al., 2018; Caldwell et al., 2022; Lee et al., 2021), see review Allen and Eroglu, 2017. Astrocytes are also involved in cross-talk with other glial and immune cells (see review Han et al., 2021), required for maintenance of blood brain barrier (BBB)

(Heithoff et al., 2021; Hösli et al., 2022) and aid in metabolism via fatty acid oxidation (Ioannou et al., 2019; Rose et al., 2020) and by shuttling lactate to neurons (Magistretti and Allaman, 2018). Indeed, several of these homeostatic functions may be affected in the context of disease (as depicted in and *Figure 4D-F*).

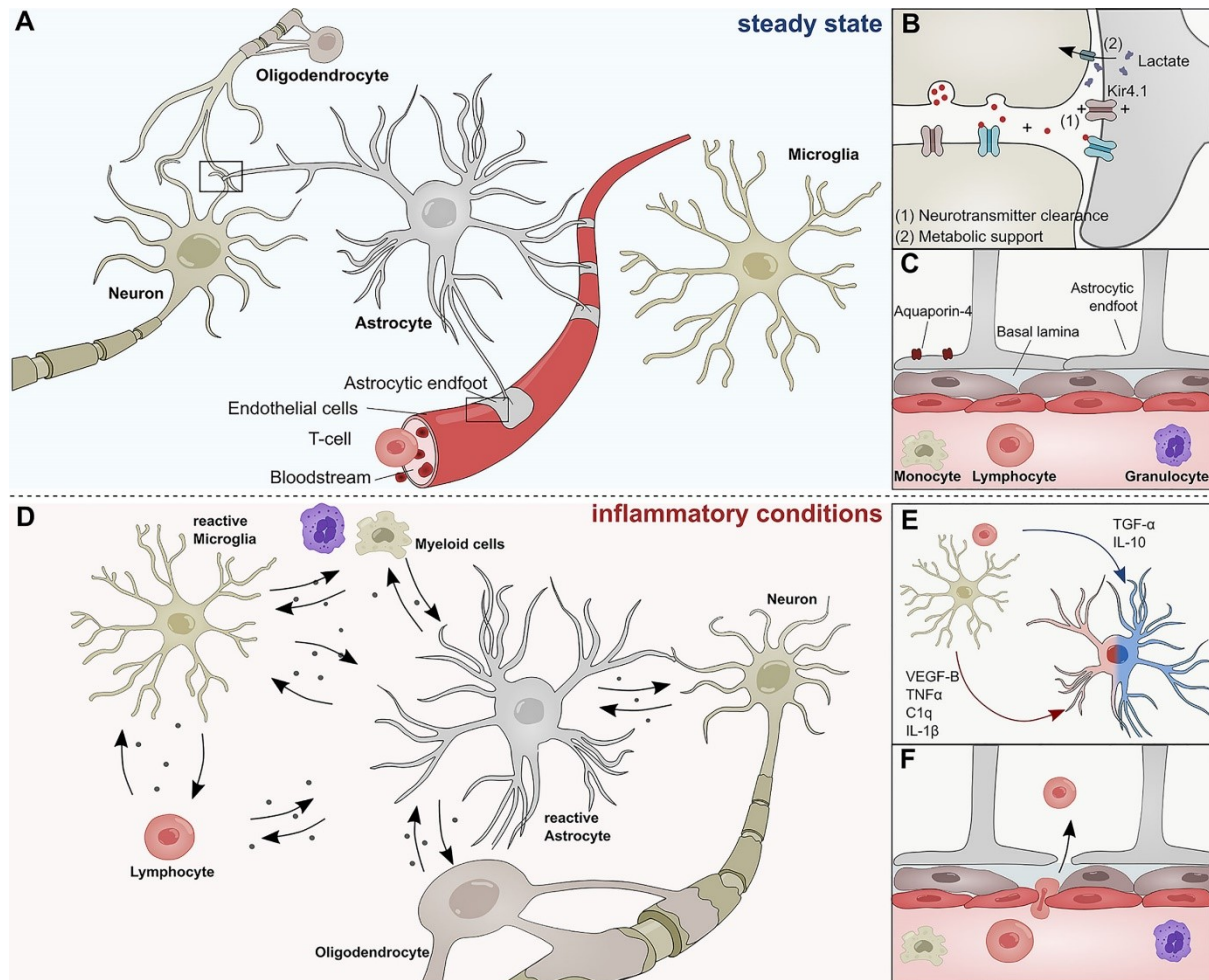


Figure 4. Overview of astrocyte functions in health and disease. This image is from Linnerbauer and Rothhammer, 2020, an open-access article distributed under the terms of the Creative Commons Attribution License (CC BY-NC-ND 4.0). Abbreviations: C1q, Complement component 1q; IL-1 β , Interleukin-1 β ; IL-10, Interleukin 10; TNF- α , Tumor necrosis factor α ; TGF- α , Transforming growth factor α ; VEGF-B, Vascular endothelial growth factor B)

1.4.1 Astrocytogenesis

Like all events in development, astrocytogenesis requires precise expression of several transcriptional cascades (Tiwari, Pataskar et al., 2018). During development, the end of neurogenesis is accompanied by a gradual switch to gliogenesis, and many cortical astrocytes arise from radial glial cells, a large fraction of which expand by local proliferation during early

postnatal days (Clavreul et al., 2019; Ge et al., 2012; Ge and Jia, 2016). A fraction of the cortical astrocytes also arises from oligodendrocyte lineage cells (Olig2 or NG2 expressing cells) and progenitors from the ventral forebrain (Clavreul et al., 2019; Sánchez-González et al., 2020; Zhu et al., 2008), but the exact contribution is yet to be deciphered. In fact, a small proportion of Olig2+ cells (around 5-8%) gives rise to astrocytes even in the adult cortical grey matter (GM) (Dimou et al., 2008).

At the molecular level, astrocyte fate specification requires timely expression of Sox9 and subsequent induction of Nfia, which then together instructs expression of several genes like *Apcdd1*, *Mmd2*, *Zcchc24* that are required for migration and metabolism of astrocyte precursors (Kang, Lee et al., 2012). Sox9 is not just essential for astrocyte fate specification, but may also be essential to prevent precocious astrocyte and oligodendrocyte gene expression (Klum, Zaouter et al., 2018), to suppress neurogenesis and facilitate the gliogenic switch (Vong et al., 2015). Over the years, more TFs like Zbtb20 (Nagao et al., 2016), Atf3, Runx2 (Tiwari, Pataskar et al., 2018) that are essential for various stages of astrocytogenesis have been identified. Overexpression of these factors by in-utero electroporation (IUE) at embryonic day (E) 15.5 resulted in an increase in the number of Sox9 expressing astrocytes by postnatal day (P) 5 or 7, at the expense of Satb2 or Cux1 expressing neurons (Nagao et al., 2016; Tiwari, Pataskar et al., 2018).

1.4.2 Astrocyte heterogeneity

Astrocytes display significant heterogeneity between (Boisvert et al., 2018; Endo et al., 2022) and even within (Batiuk et al., 2020; Bayraktar et al., 2020; Ohlig, Clavreul et al., 2021) various brain regions, perhaps to meet the local metabolic and functional demands of each region. This heterogeneity, at least partly, endows astrocytes also with special region-specific functions, like prolonged astrogenesis in the diencephalon (Ohlig, Clavreul et al., 2021), increased cholesterol biosynthesis in cortical astrocytes in contrast to higher lipid metabolism in hypothalamic astrocytes (Boisvert et al., 2018) etc.

Such heterogeneity could arise partly from differences in developmental origin. For example, the expression of Pax6 or Nkx6.1 determines the positional heterogeneity of the astrocytes in ventral spinal cord, giving rise to only Reelin+ or Reelin+Slit1+ or only Slit1+ astrocytes (Hochstim et al., 2008). Such heterogeneity due to developmental position can have a functional relevance, the ventral spinal cord astrocytes express higher levels of *Sema3a* than the dorsal counterparts and this influences motor neuron survival, synaptogenesis and axon guidance for the sensory neurons (Molofsky et al., 2014). The heterogeneity may also be

influenced local environmental cues. For example in the cortical GM, it was shown that neuronal layer specific expression of *Satb2* is important for the astrocyte identity specific to superficial layers and in Reelin deficient mice, both neuronal and astrocyte layer specificity is inverted (Bayraktar et al., 2020; Lanjakornsiripan, Pior, Kawaguchi et al., 2018).

Recent studies have highlighted that there may be (at least) two distinct astrocyte precursor cell types characterized by the expression of *Sparc* or *Sparc11*, which appear at distinct developmental time points (Liu, Wu et al., 2022). *Sparc*⁺ cells emerge in both the ganglionic eminence and the dorsal forebrain during embryonic development, *Sparc11*⁺ cells emerge in restricted regions of the ventral brain and the pallium-subpallium boundary during embryonic development, and later appear in the dorsal brain postnatally. Even so, both the astrocyte precursor populations are present in the dorsal and ventral forebrain, showing that the astrocyte heterogeneity may not be solely dependent on the region of origin, but heterogeneity may already be present prior to gliogenesis (Liu, Wu et al., 2022). Such a convergence between dorsal and ventral astrocyte precursors has also been observed at the single cell transcriptome level, an extensive single cell sequencing with lineage tracing technique has also pointed that the astrocytes from the dorsal and ventral forebrain converge transcriptomically (Bandler, Vitali et al., 2022).

Similar to astrocyte heterogeneity between different brain regions, neurons have a region specific transcriptional signature, some of which are regionally shared between astrocytes and this has an impact on the outcome of direct neuronal reprogramming as well (Herrero-Navarro et al., 2021; Hu et al., 2019; Kempf, Knelles, Hersbach et al., 2021). Thus, understanding the relevance and importance of astrocyte heterogeneity would be essential to deciphering its impact in direct neuronal reprogramming. Furthermore, astrocyte heterogeneity is also present in their response to injury (Koupourtidou, Schwarz et al., 2023), inflammation (Hasel et al., 2021), disease (Sadick, O'Dea et al., 2022) and in ageing and it may have both neuroprotective and neurotoxic effects. As mentioned earlier, astrocytes from different brain regions may have different neurogenic potential regulated by different signaling pathways (Magnusson et al., 2020, 2014; Sirko, Behrendt et al., 2013; Zamboni et al., 2020). Thus, understanding astrocyte heterogeneity in response to injury and disease in detail would give us significant insights into developing successful regenerative therapy strategies.

1.4.3 Astrocytes in the context of injury and disease

In addition to their diverse roles in healthy CNS, astrocytes also respond to injury and disease (similar to the depiction in Figure 3D-F). Upon injury or in disease, astrocytes become

“reactive”, a process characterized by gene expression and functional changes. Such reactive astrocytes also have unique functions, they become hypertrophic and some astrocytes located at juxtavascular sites even proliferate (Bardehle et al., 2013; Buffo et al., 2008). The extent of proliferation and the *in vitro* potential of these astrocytes to form multipotent neurospheres is dependent on the type of injury, with fewer proliferating astrocytes and a lower neurosphere forming capacity in an Alzheimer’s mouse model (APPPS1) than in a SWI paradigm (Sirko, Behrendt et al., 2013).

Astrocyte response to injury or disease is controlled in a temporal manner. In case of SWI, astrocyte reactivity peaks at 5 days post SWI (dpSWI) while microglia reactivity, immune cell infiltration and oligodendrocyte proliferations are higher earlier, at 3dpSWI (Frik et al., 2018; Koupourtidou, Schwarz et al., 2023). In addition, astrocytes interact with the invading immune cells and coordinate with other glial cells to respond to the injury (Frik et al., 2018; Koupourtidou, Schwarz et al., 2023) and contribute to scar-forming tissue (Anderson et al., 2016, see reviews Sofroniew, 2020; Yang et al., 2020). In case of spinal cord injury, monocyte invasion seems to be more beneficial for promoting functional recovery (Wattananit et al., 2016) but in case of SWI injury in the cortical GM, blocking monocyte invasion promoted astrocyte proliferation and reduced scar formation (Frik et al., 2018). This highlights region and injury specific differences in astrocyte response and how glial crosstalk influences different outcomes.

In general, neurotoxic astrocytes are thought to be induced by activated microglia (Liddelow et al., 2017) and such neurotoxic astrocytes induce oligodendrocyte and neuronal cell death by producing long-chain saturated free fatty acids (Guttenplan et al., 2021). Even though the astrocyte response to injury and inflammation is diverse, the exact sub-states that are specifically neurotoxic or neuroprotective are yet to be distinguished in finer detail.

Targeting the more detrimental sub-states of astrocytes for neuronal reprogramming or for other astrocyte based therapies may help in a more favorable prognosis of the disease. It is thus essential to understand the basis and effects of astrocyte heterogeneity and their response in disease or injury to unravel their implications in regenerative therapies.

1.4.4 TFs influencing astrocyte functions

Long after astrocytogenesis, mature astrocytes continue to express some TFs like Sox9, Nfia that are required for astrocyte fate specification in addition to expressing genes and TFs unique to the identity and functions of adult astrocytes. These TFs would dictate specific downstream transcriptional cascades that maintain astrocyte identity. Understanding the roles of these TFs

in astrocyte functions and identity would be an important step in furthering our understanding of astrocytes in health and disease. This will help us decipher how the starter cell identity can be erased to improve neuronal reprogramming.

Interestingly, even pan-astrocyte TFs may have unique and region-specific functions during astrocyte maturation (Cheng et al., 2023), in adult astrocytes (Huang, Woo et al., 2020; Ung, Huang et al., 2021), astrocyte response to injury and disease (Glasgow et al., 2017; Laug, Huang et al., 2019; Sardar, Chen et al., 2022). This could be partly due to region specific expression of other key TFs that may act as co-factors or chromatin remodelers, which will heavily influence the region-specific functions of pan-astrocyte TFs.

Though Sox9 and Nfia are required for astrocyte fate specification during development, they have region specific roles during postnatal astrocyte maturation. Sox9 or Nfia deletion during postnatal development impairs astrocyte response to inhibitory neurons by influencing the levels of *Gabbr1* in olfactory bulb and cortical astrocytes respectively and this reduces the morphological complexity of astrocytes in the respective regions (Cheng et al., 2023). Surprisingly, Sox9 or Nfia rescue by overexpression restored Nfia dependent *Gabbr1* expression in the cortex, but Sox9 overexpression alone failed to restore *Gabbr1* expression in the olfactory bulb highlighting the complexity of transcriptional cascades controlling astrocytic functions in different brain regions.

In adult astrocytes, loss of Nfia has a prominent effect only in the astrocytes of the hippocampus, the astrocytes become less complex morphologically and results in an impaired neuron-astrocyte cross talk in the region (Huang, Woo et al., 2020). Even though Nfia is expressed in other brain regions such as the olfactory bulb, its deletion does not have an observable effect here, as the transcriptional cascades are less dependent on Nfia which preferentially binds Nfib instead of DNA (Huang, Woo et al., 2020). Similarly, loss of Sox9 in adult astrocytes has a prominent effect only in the astrocytes of the olfactory bulb and not elsewhere (Ung, Huang et al., 2021). Sox9 deletion reduces the morphological complexity of olfactory bulb astrocytes, reduces calcium signaling and neuronal activity, influencing sensory processing circuits in the olfactory bulb (Ung, Huang et al., 2021).

Apart from the unique roles Nfia has during astrocyte development and in adult astrocytes, Nfia also dictates unique astrocyte functions in response to injury. Nfia deletion affects the BBB and reduces oligodendrocyte differentiation, remyelination in the context of lysolecithin induced spinal cord injury, but a similar effect is not observed in the corpus callosum (Laug, Huang et al., 2019). On the other hand, in a photothrombotic model of cortical ischemic stroke, Nfia deletion resulted in reduced reactive astrogliosis (measured based on GFAP expression on

astrocytes at the site of injury). This highlights that these TFs have region specific and even injury specific roles in astrocytes. In conclusion, it would be vital to understand how TFs influence astrocyte functions in the different brain regions and in various injury or disease conditions to devise better treatment strategies.

Along this line, we were mainly interested in two TFs, Sox9 (SRY-Box Transcription Factor 9) and Trps1 (Transcriptional Repressor GATA Binding 1 or Tricho-Rhino-Phalangeal Syndrome Type I Protein). The role of Sox9 in astrocytes has been relatively well established. As outlined in the above sections, Sox9 is required for astrocyte fate specification during development (Kang, Lee et al., 2012; Klum, Zaouter et al., 2018; Stolt et al., 2003) and has prominent roles in the astrocytes of adult olfactory bulb (Ung, Huang et al., 2021). In contrast, the role of Trps1 in astrocytes is unknown. Although initially identified as a transcriptional repressor (Elster, Tollot et al., 2018; Fantauzzo et al., 2012; Malik, 2001), Trps1 may act as a transcriptional activator as well (Fantauzzo and Christiano, 2012; Witwicki, Ekram et al., 2018; Wuelling et al., 2020). The function of this TF has been studied in the context of breast cancer survival (Cornelissen et al., 2020; Elster et al., 2018; Witwicki et al., 2018; Yang et al., 2021) and chondrogenesis (Tan, Niu et al., 2018; Wuelling et al., 2020, 2009) and hair epithelium (Fantauzzo et al., 2012; Fantauzzo and Christiano, 2012). Interestingly, Sox9 and Trps1 may be involved in similar transcriptional cascades; Trps1 is predicted to be upstream of Sox9 in the context of hair follicle development (Fantauzzo et al., 2012) or vice-versa in the context of chondrocyte differentiation (Tan, Niu et al., 2018). Thus, it was of interest to understand the roles of these two TFs in astrocytes simultaneously. I will be elaborate on this in detail in later sections, as the second key finding of the work done during my PhD.

1.5 Aims of the study

The first aim of my PhD was to understand the impact of mitochondrial remodeling and metabolic shift during direct neuronal reprogramming of astrocytes. First, the mitochondrial proteome of astrocytes and neurons was characterized. Interestingly, the expression of these proteins changed during the course direct neuronal reprogramming. Using this information, I was able to demonstrate that astrocyte to neuron conversion can indeed be improved by CRISPRa (Clustered Regularly Interspaced Short Palindromic Repeats activation)/ dCas9 mediated precocious expression of neuron enriched mitochondrial proteins.

In addition, I interfered with the starter cell specific metabolic pathway, i.e., impaired fatty acid oxidation in astrocytes during reprogramming and observed that this too helped in the process of reprogramming.

As a second aim, I wanted to explore the concept of manipulating the starter cell identity further. The effects of deleting key TFs that are essential in maintaining cell identity may have a higher impact in reprogramming, instead of just interfering with the astrocyte metabolism. However, even before understanding the impact of astrocyte fate manipulation in reprogramming, I first wanted to explore how deletion of key TFs affects astrocyte identity and functions in cortical astrocytes *in vivo*. I decided to focus on Sox9, a well-known astrocyte TF and Trps1, a novel TF and understand how they influence astrocyte functions. The roles of Sox9 in astrocyte development and some of its functions in the adult astrocytes have been studied (and outlined in previous sections), but its functions in adult cortical astrocytes is not known. Similarly, the role of Trps1 in astrocytes is unknown even though it has been identified in several astrocyte transcriptomic studies before (Endo et al., 2022; Ohlig, Clavreul et al., 2021; Sirko et al., 2015). In other lineages, Sox9 and Trps1 participate in related transcriptional cascades, frequently engaging other elements associated with Hedgehog signaling pathway (Fantauzzo et al., 2012; Tan, Niu et al., 2018). Thus, it was of interest to understand the roles of these two TFs in astrocytes simultaneously.

For this, I deleted these TFs in the adult somatosensory cortex either one at a time, or both simultaneously using a CRISPR/ Cas9 based approach. This has led to the discovery of how these TFs may be essential for key astrocyte functions, glial crosstalk which is a very important feature of astrocytes in both healthy brain homeostasis and in mediating response to injury.

2. RESULTS

2.1 Project 1

The aim of the first project was to understand the metabolic and mitochondrial changes during direct neuronal reprogramming of astrocytes and how manipulation of the same can influence this process.

CRISPR-Mediated Induction of Neuron-Enriched Mitochondrial Proteins Boosts Direct Glia-to-Neuron Conversion

<https://doi.org/10.1016/j.stem.2020.10.015>

Russo, G. L., Sonsalla, G.#, **Natarajan, P.#**, Breunig, C. T., Bulli, G., Merl-Pham, J., Schmitt, S., Giehl-Schwab, J., Giesert, F., Jastroch, M., Zischka, H., Wurst, W., Stricker, S. H., Hauck, S. M., Masserdotti, G.*, & Götz, M.* (2021) “CRISPR-Mediated Induction of Neuron-Enriched Mitochondrial Proteins Boosts Direct Glia-to- Neuron Conversion” *Cell Stem Cell*, 28(3): 524–534.e7.

These authors contributed equally

*Co-last author

For this paper, I performed and analyzed the data of the following experiments; Giacomo Masserdotti contributed to statistical analysis and data visualization of the same.

- I performed neuronal reprogramming experiments of astrocytes *in vitro*, demonstrating that early expression of neuron enriched mitochondrial proteins by a CRISPRa strategy increases the efficiency of reprogramming and gives rise to neurons that are more morphologically mature (Figure 3).
- By live imaging experiments, I was also able to demonstrate that early induction of these mitochondrial proteins accelerated the speed of reprogramming and the survival of the induced neurons (Figure 4).
- Furthermore, I validated the specificity of all the gRNAs used for activation of the selected candidate mitochondrial proteins (Figure S4).

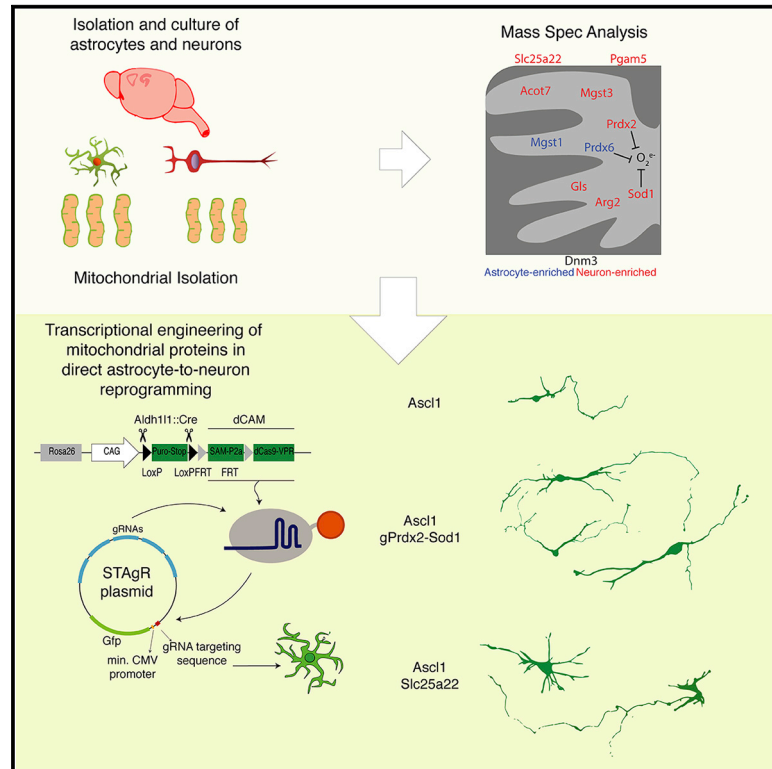
- In addition, I was also able to show that interfering with astrocyte metabolism by using a chemical inhibitor of Cpt1a (etomoxir) which is essential for FAO in astrocytes, enhances both Ascl1 and Ngn2 mediated reprogramming of astrocytes (Figure S2).

The results of this project have been published as Russo et al., 2021 in the journal *Cell Stem cell*. This is an open access article, and is available under the terms of the Creative Commons Attribution License (CC BY-NC-ND 4.0). As a co-author, I have the right to include it in my dissertation, provided it is not commercially published.

Due to elevated number of pages, Supplementary Table 1 (List of differentially enriched mitochondrial proteins), Supplementary Table 2 (GO, GSEA analysis of differentially enriched proteins) and the live imaging videos demonstrating CRISPRa-Mediated Direct Neuronal Reprogramming are not included in the PDF version of this thesis, but they are provided separately.

CRISPR-Mediated Induction of Neuron-Enriched Mitochondrial Proteins Boosts Direct Glia-to-Neuron Conversion

Graphical Abstract



Authors

Gianluca L. Russo, Giovanna Sonsalla, Poornema Natarajan, ..., Stefanie M. Hauck, Giacomo Masserdotti, Magdalena Götz

Correspondence

magdalena.goetz@helmholtz-muenchen.de

In Brief

Russo et al. identify mitochondrial proteins enriched in neurons or astrocytes. Astrocyte-enriched mitochondrial proteins are often only partially downregulated during astrocyte-to-neuron direct reprogramming. Neuron-enriched ones are upregulated late and mainly in reprogrammed neurons. CRISPRa-mediated early induction of neuron-enriched mitochondrial proteins boosts direct neuronal reprogramming speed and efficiency.

Highlights

- Mitochondrial proteomes of cortical astrocytes and neurons are distinct
- Astrocyte-enriched mitochondrial proteins are downregulated late in neuronal conversion
- Neuron-enriched mitochondrial proteins are upregulated late in neuronal conversion
- Early induction of neuronal mitochondrial proteins improves neuronal reprogramming



Short Article

CRISPR-Mediated Induction of Neuron-Enriched Mitochondrial Proteins Boosts Direct Glia-to-Neuron Conversion

Gianluca L. Russo,^{1,2,3} Giovanna Sonsalla,^{1,2,3,15} Poornema Natarajan,^{1,2,3,15} Christopher T. Breunig,^{4,5} Giorgia Bulli,^{1,2} Juliane Merl-Pham,⁶ Sabine Schmitt,⁷ Jessica Giehl-Schwab,⁸ Florian Giesert,^{8,9} Martin Jastroch,¹⁰ Hans Zischka,^{7,11} Wolfgang Wurst,^{8,9,12} Stefan H. Stricker,^{4,5} Stefanie M. Hauck,^{6,16} Giacomo Masserdotti,^{1,2,16} and Magdalena Götz^{1,2,13,14,16,*}

¹Physiological Genomics, Biomedical Center (BMC), Ludwig-Maximilians-Universität (LMU), Planegg-Martinsried, Germany

²Institute for Stem Cell Research, Helmholtz Center Munich, BMC LMU, Planegg-Martinsried, Germany

³Graduate School of Systemic Neurosciences, BMC, LMU, Planegg-Martinsried, Germany

⁴MCN Junior Research Group, Munich Center for Neurosciences, BMC, LMU, Planegg-Martinsried, Germany

⁵Epigenetic Engineering, Institute of Stem Cell Research, Helmholtz Zentrum, Planegg-Martinsried, Germany

⁶Research Unit Protein Science, Helmholtz Center Munich, Neuherberg, Germany

⁷Institute of Toxicology and Environmental Hygiene, School of Medicine, Technical University Munich (TUM), Munich, Germany

⁸Institute of Developmental Genetics, Helmholtz Center Munich, Neuherberg, Germany

⁹Developmental Genetics, TUM, Munich-Weihenstephan, Germany

¹⁰Department of Molecular Biosciences, The Wenner-Gren Institute, The Arrhenius Laboratories F3, Stockholm University, Stockholm, Sweden

¹¹Institute of Molecular Toxicology and Pharmacology, Helmholtz Center Munich, Neuherberg, Germany

¹²German Center for Neurodegenerative Diseases (DZNE) Site Munich, Munich, Germany

¹³Excellence Cluster of Systems Neurology (SYNERGY), Munich, Germany

¹⁴Lead Contact

¹⁵These authors contributed equally

¹⁶These authors contributed equally

*Correspondence: magdalena.goetz@helmholtz-muenchen.de

<https://doi.org/10.1016/j.stem.2020.10.015>

SUMMARY

Astrocyte-to-neuron conversion is a promising avenue for neuronal replacement therapy. Neurons are particularly dependent on mitochondrial function, but how well mitochondria adapt to the new fate is unknown. Here, we determined the comprehensive mitochondrial proteome of cortical astrocytes and neurons, identifying about 150 significantly enriched mitochondrial proteins for each cell type, including transporters, metabolic enzymes, and cell-type-specific antioxidants. Monitoring their transition during reprogramming revealed late and only partial adaptation to the neuronal identity. Early dCas9-mediated activation of genes encoding mitochondrial proteins significantly improved conversion efficiency, particularly for neuron-enriched but not astrocyte-enriched antioxidant proteins. For example, Sod1 not only improves the survival of the converted neurons but also elicits a faster conversion pace, indicating that mitochondrial proteins act as enablers and drivers in this process. Transcriptional engineering of mitochondrial proteins with other functions improved reprogramming as well, demonstrating a broader role of mitochondrial proteins during fate conversion.

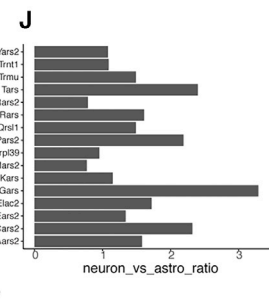
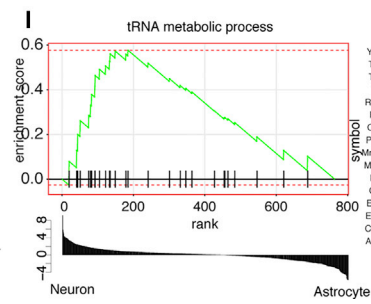
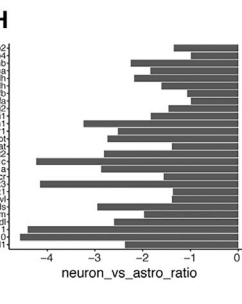
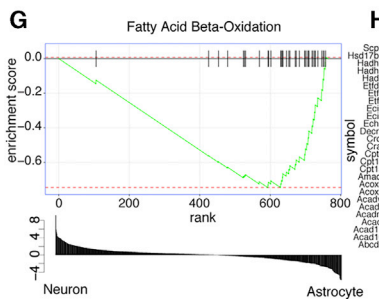
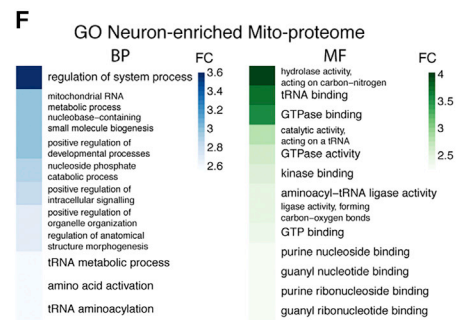
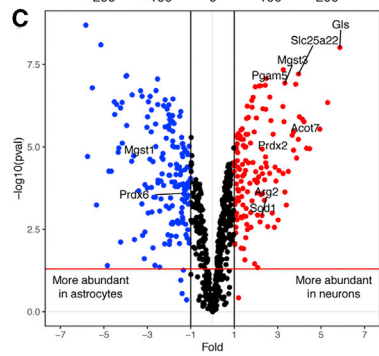
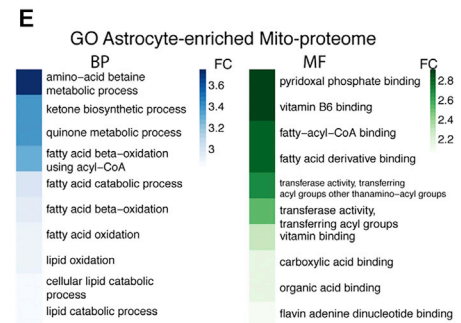
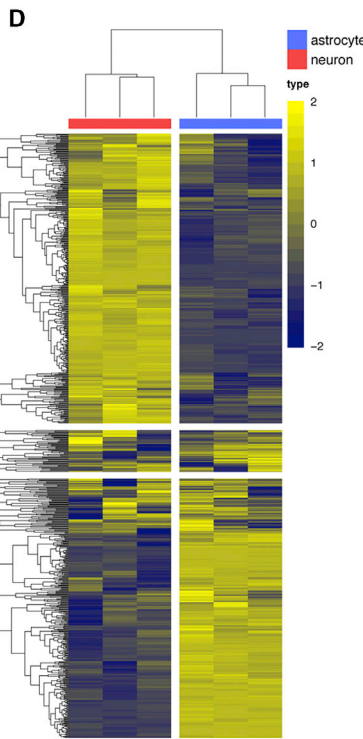
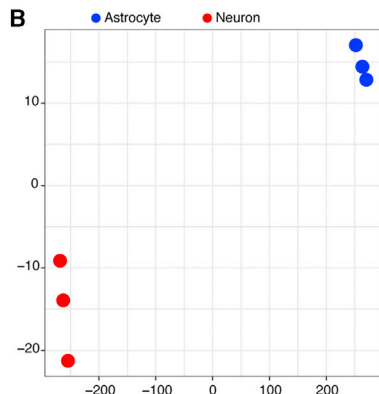
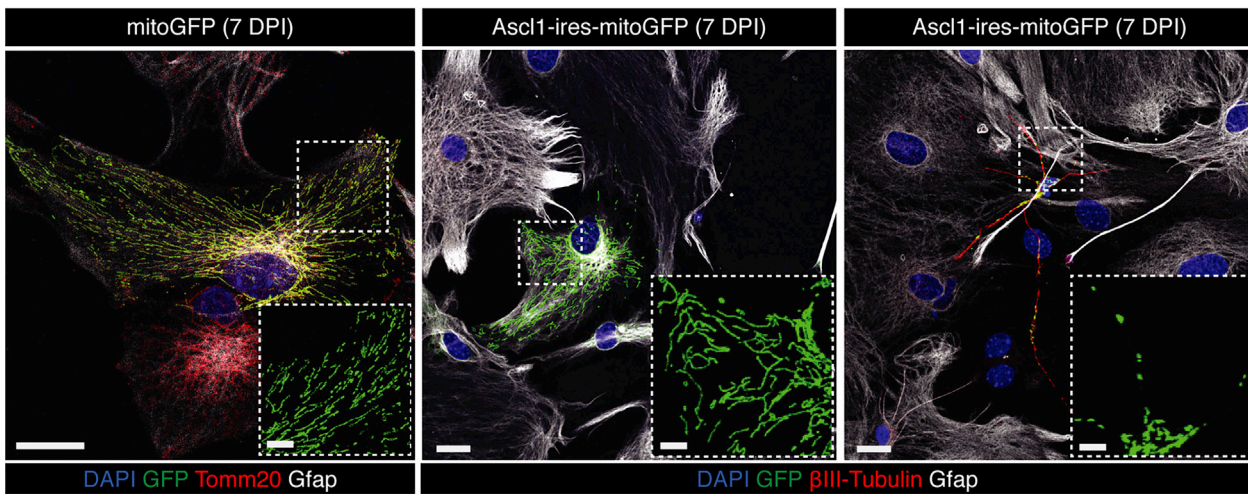
INTRODUCTION

The ability to regenerate lost neurons after an injury or in neurodegenerative disease is still a key challenge in the field of regenerative medicine. Among different therapeutic approaches (Barker et al., 2018; Grade and Götz, 2017), direct conversion of local glia into neurons has become a viable option to replace functional neurons (Vignoles et al., 2019). Because direct neuronal conversion is dramatically hindered by increased generation of reactive oxygen species (ROS) during the process,

Bcl2 or pharmacological application of antioxidants could drastically improve neuronal generation *in vitro* and *in vivo* (Gascón et al., 2016). At the same time, neurons rely on oxidative phosphorylation (OxPhos) (Harris et al., 2012; Herrero-Mendez et al., 2009), so an increase in mitochondrial activity is required during neuronal conversion. Mitochondria perform a plethora of additional functions (Spinelli and Haigis, 2018), and specific mitochondrial proteins may be required to implement the cell-type-specific metabolic needs (Calvo and Mootha, 2010; Folmes et al., 2012; Pagliarini et al., 2008). Because changes in



A



(legend on next page)

mitochondrial proteins have not yet been investigated in neuronal reprogramming, we assessed the similarities and differences in mitochondrial composition for cultured neurons and astrocytes and aimed to improve mismatching during reprogramming by regulating the respective genes by CRISPRa (clustered regularly interspaced short palindromic repeat activation)-mediated transcriptional engineering.

RESULTS

Mitochondrial Morphology Changes during Cortical Astrocyte-to-Neuron Reprogramming *In Vitro*

We first monitored morphological changes of mitochondria during reprogramming. Astrocytes isolated from postnatal day 5 (P5) murine cerebral cortex (Heinrich et al., 2011) were transduced with a retrovirus encoding mitochondrion-targeted green fluorescent protein (*mitoGFP*) with or without the reprogramming proneural factor Achaete-scute homolog 1 (*Ascl1-ires-mitoGFP*, *ires* [intra ribosome entry site]), shown previously to reprogram astrocytes into GABAergic neurons (Heinrich et al., 2010; Masserdotti et al., 2015). *MitoGFP* co-localized with Tomm20, a pan-mitochondrial marker protein, revealing an elongated and ramified mitochondrial network in astrocytes (Figure 1A, left panel). This was maintained in *Ascl1*-transduced astrocytes failing to reprogram (positive for the astroglial protein glia fibrillary acidic protein [Gfap], negative for neuron-specific β III-tubulin; Figure 1A, center panel), whereas successfully converted neuronal cells (β III-tubulin+, Gfap-) had smaller mitochondria with shorter and rounder morphology (Figure 1A, right panel). These data are in line with neurons *in vivo* possessing smaller mitochondria and higher fission properties (Misgeld and Schwarz, 2017), whereas astrocytes have more elongated mitochondria and fusion events (Motori et al., 2013). To gain a better understanding of mitochondrial restructuring during the reprogramming process, we investigated the proteins that mediate morphological and functional changes in mitochondria.

Astrocytes and Neurons Differ in Mitochondrial Structure and Function *In Vitro*

To determine the comprehensive mitochondrial proteome of neurons and astrocytes, we chose highly pure neuronal cultures derived from embryonic day 14 (E14) cerebral cortex, cultured for 7 days (Walcher et al., 2013); i.e., young neurons comparable with reprogrammed neurons at 7 days post-transduction (DPT) in reprogramming) and primary cultures of astrocytes as used

in direct neuronal reprogramming. Functional bio-energetic differences of neurons and astrocytes from these cultures were confirmed by Seahorse analysis (Figures S1A–S1C). A cell fractionation-based method (Schmitt et al., 2013) enriched mitochondria, as assessed by western blot (Figure S1D) and electron microscopy (EM) (Figure S1E), and functional assays confirmed the isolation of intact mitochondria from both cell types (Figures S1F and S1G). EM confirmed the cell-type-specific differences in mitochondrial morphology (Figures 1A and 1E) and also revealed some other organelles in the neuronal samples, probably because small mitochondria are tightly linked to the cytoskeleton in the thin neuronal processes and the endoplasmic reticulum (ER) (Fecher et al., 2019).

Astrocytes and Neurons Exhibit Profound Differences in Their Mitochondrial Proteome

We then used liquid chromatography-tandem mass spectrometry (LC-MS/MS) to identify proteins in neuronal and astrocytic mitochondria. A *t*-distributed stochastic neighbor embedding (*t*-SNE) plot for all identified proteins normalized for abundance (Figures S1J; normalization in Figure S1H) or mitochondrion-specific proteins (Figure 1B; normalization in Figure S1K), as classified by MitoCarta 2.0 (Table S1; Calvo et al., 2016), revealed clear separation of neurons and astrocytes. Unsupervised cluster analysis confirmed the cell type dependent similarity, considering whole proteins (Figure S1I) or only mitochondrial proteins (Figure S1L). Overall, we detected 757 (± 1) mitochondrial proteins in astrocytes and 738 (± 1) in neurons (Figures S1M and S1N) of which 164 (22%) were more abundant in astrocytes and 141 (19%) more abundant in neurons ($p < 0.05$ and 2-fold enrichment; Figure 1C; Table S1), with high reproducibility across samples (Figure 1D). Thus, about a fifth of the mitochondrial proteome differs significantly between these cell types. Western blotting of whole-cell lysates from independent cultures confirmed enrichment of *Sfxn5* and *Cpox* in astrocytes (Figure S1O, left and center panel) and glutaminase (Gls) in neurons (Figure S1O, right panel).

Gene Ontology (GO) term analysis of mitochondrial proteins significantly enriched in astrocytes (Figure 1E, left panel; top 10 enriched biological processes [BPs]; Fisher's exact test < 0.01 ; see Table S2A for a complete list) revealed terms such as fatty acid catabolic process, fatty acid β -oxidation, and lipid catabolic process, also relevant pathways for astrocytes *in vivo* (van Deijk et al., 2017). This was supported by the analysis of molecular function (MF) GO terms (Figure 1E, right panel; Table

Figure 1. Astrocytes and Neurons Differ in Mitochondrial Structure and Proteome

(A) Micrograph of mitochondrial morphology in control (*mitoGFP*) astrocytes (left panel), *Ascl1*-non-reprogrammed astrocytes (center panel), and *Ascl1*-induced neurons (right panel, *Ascl1-mitoGFP*), 7 DPI. Scale bars, 20 μ m and 6 μ m (insets).

(B) *t*-SNE plot of samples considering only mitochondrial proteins.

(C) Volcano plot of mitochondrial proteins with \log_2 ratio of abundance of neurons/astrocytes (*x* axis) and the $-\log_{10}$ of the corresponding significance value (*p* value, *y* axis); 2-fold changes (vertical lines), significance cutoff $p = 0.05$ (horizontal line). Proteins significantly more abundant in astrocytes are shown in blue and more abundant in neurons in red. Names highlight proteins covered in this study.

(D) Unsupervised heatmap cluster analysis of all detected mitochondrial proteins. Astrocytes, blue; neurons, red. $n = 3$ for each group. The color scale indicates Z score.

(E and F) GO terms of the top 10 biological processes (BPs; blue, left panels) and molecular functions (MFs; green, right panels) for astrocyte-enriched (E) and neuron-enriched (F) mitochondrial proteins. The color bar represents the fold change compared with the expected number of genes for each term. Terms were considered if exact Fisher test < 0.01 .

(G–J) Examples of 2 terms identified by gene set enrichment analysis (GSEA) (G and I) and barplots (H and J) of the main genes associated with the respective terms (in G or I).

S2A), including terms such as fatty-acyl-coenzyme A (CoA) binding, in line with a recent study of mitochondria of Bergmann glia from adult mice (Fecher et al., 2019). Likewise, gene set enrichment analysis (GSEA) identified fatty acid β -oxidation-related proteins in astrocytes (Figure 1G; Table S2E), comprising key regulators such as Acads, Cpt1a, and Cpt2 (Figure 1H; Tables S1 and S2E).

To explore the functional relevance of the fatty acid β -oxidation pathway in direct reprogramming, we blocked this pathway using etomoxir, an inhibitor of Cpt1a (Jernberg et al., 2017), early during the conversion process (Figure S2A). Medium to high doses of etomoxir (25 μ M and 100 μ M, respectively) improved reprogramming compared to the control (no etomoxir) upon Ascl1 (Figures S2B and S2C) or Neurogenin2 (Neurog2) expression (Figures S2D and S2E). Interestingly, co-treatment with α -tocotrienol, an analog of the ROS scavenger vitamin E, reduced Ascl1-mediated reprogramming efficiency, suggesting that the positive effect of etomoxir might be partly due to an increase in ROS, as shown previously (O'Connor et al., 2018). Thus, β -oxidation is a general hurdle in glia-to-neuron reprogramming.

GO terms significant for neuron-enriched mitochondrial proteins were associated with RNA metabolism and function (BP in Figure 1F, left panel, and Table S2C; MF in Figure 1F, right panel, and Table S2D) and further supported by GSEA (Figures 1I and 1J, tRNA metabolic process; full list in Table S2E). This highlights the notion that tRNA biogenesis is an important activity in neuronal mitochondria and its dysfunction is associated with neurodevelopmental disease (Schaffer et al., 2019). Among neuron-enriched mitochondrial proteins, we also detected Glis, the enzyme regulating glutamine metabolism and glutamate neurotransmitter levels (Márquez et al., 2009), and ATP citrate lyase (Acl), involved in production of cytosolic acetyl-CoA (Lin et al., 2013; Table S1).

Enrichment of the mitochondrial fusion protein Mitofusin 1 (Mfn1) in astrocytes is in line with the presence of more elongated mitochondria in such cells (Figure 1A), whereas the fission master regulator Dynamin-related protein (Dnm1, also known as Drp1) is more prevalent in the neuronal mitochondrial proteome (Table S1). Interestingly, the antioxidant proteins Gpx1, Gpx4, Prdx6, and Mgst1 were more enriched in astrocytes (Table S1), whereas Mgst3, Prdx2, and Sod1 were more abundant in neurons (Table S1), suggesting that different members of antioxidant protein families (e.g., peroxiredoxins and microsomal glutathione S-transferases) are enriched in specific cell types. This raised the intriguing question of whether these proteins (Prdx2 and Prdx6 or Mgst1 and Mgst3) are functionally similar and only expressed in a cell-type-specific manner or whether the neuron-enriched antioxidant proteins may be specifically required in neurons and, hence, during the direct conversion process.

We also compared our data with mitochondrial proteins isolated from adult murine cerebellum (Purkinje cells, granule cells, and astrocytes; Fecher et al., 2019). Despite the very different experimental conditions (*in vivo* versus *in vitro*, adult versus postnatal, cerebellum versus cortex, immunoprecipitation [IP]-based versus fractionation-based-method), we found 117 proteins enriched in both astrocyte-derived samples; i.e., 60% of all mitochondrial proteins identified by Fecher et al. (2019) were also

present in our astrocyte-enriched mitochondrial proteome (Figure S1P). Likewise, 46% of neuron-enriched mitochondria identified by Fecher et al. (2019) were common to our neuronal dataset (Figure S1Q).

Thus, the mitochondrial proteome already differs profoundly in astrocytes and neurons *in vivo* and *in vitro*, comprising broad categories of protein functions from metabolism to tRNA synthesis and mitochondrial translation.

Mitochondrial Protein Changes during Astrocyte-to-Neuron Reprogramming

To determine whether and when astrocytes downregulate their characteristic mitochondrial proteins and express neuron-enriched ones during reprogramming, we chose differentially enriched functionally relevant candidates detectable by immunostaining (Table S1). The immunofluorescence intensity of the candidates was quantified and normalized to the signal intensity of the pan-mitochondrial protein Tomm20, preventing any bias of the total mitochondrial mass on quantification.

Sfxn5, a mitochondrial transporter of citrate (Miyake et al., 2002), an essential intermediate of the tricarboxylic acid cycle (TCA), was enriched in astrocyte-derived mitochondria (Table S1). Accordingly, its level was much higher in astrocytes or DsRed-transduced controls than in reprogrammed neurons (Figures 2A, 2B, and 2D). During Ascl1-mediated reprogramming, Sfxn5 was similar to control astrocytes at early stages (Figures 2A and 2D), whereas β III-tubulin+ reprogrammed neurons had significantly lower levels (Figures 2B and 2D). Notably, Sfxn5 and Tomm20 showed a greater colocalization in Ascl1-transduced cells at 1 than 7 DPT (Figure 2C), supporting the notion that Sfxn5 is mitochondrially localized in astrocytes and disappears in induced neurons (iNeurons). Likewise, the astrocyte-enriched mitochondrial protein Cpx (Mori et al., 2013), highly expressed in astrocytes (Figures S3A, S3B, and S3D) was downregulated significantly in Ascl1-transduced cells (Figures S3B and S3D, center panel), but to a lower degree in Ascl1-transduced astrocytes than in Ascl1-iNeurons (Figures S3C and S3D). These data show a relatively late (5–7 DPT) regulation of Sfxn5 and Cpx. The lack of downregulation in reprogramming-resistant astrocytes prompts the suggestion that this may contribute to failure of reprogramming.

Among neuron-enriched mitochondrial proteins, we examined Prdx2, which catalyzes the reduction of peroxides and, hence, protects against oxidative stress (Boulos et al., 2007). Prdx2 was not detected in astrocytes (Figures 2E, 2F, and 2H), while Ascl1-transduced cells had some Prdx2 signal at 3 DPT, with the strongest increase at 5–7 DPT in Ascl1-iNeurons (Figures 2F and 2H). At 7 DPT, Prdx2 reached a level similar to that observed in primary neurons (Figure 2H) and co-localized with Tomm20 (Figure 2G). Similarly, Glis, fundamental for glutamate production and glutamate and GABA transmitter levels as well as neuronal differentiation (Velletri et al., 2013), showed the strongest expression in iNeurons (5–7 DPT; Figures S3F and S3H), where it colocalized with Tomm20 (Figure S3G). Notably, its upregulation started earlier, at 1 DPT (Figure S3H), but did not reach the levels of primary cortical neurons (Figure S3H, right panel).

Mitochondrial proteins enriched in astrocytes (Sfxn5 and Cpx) or neurons (Prdx2 and Glis) change relatively late during

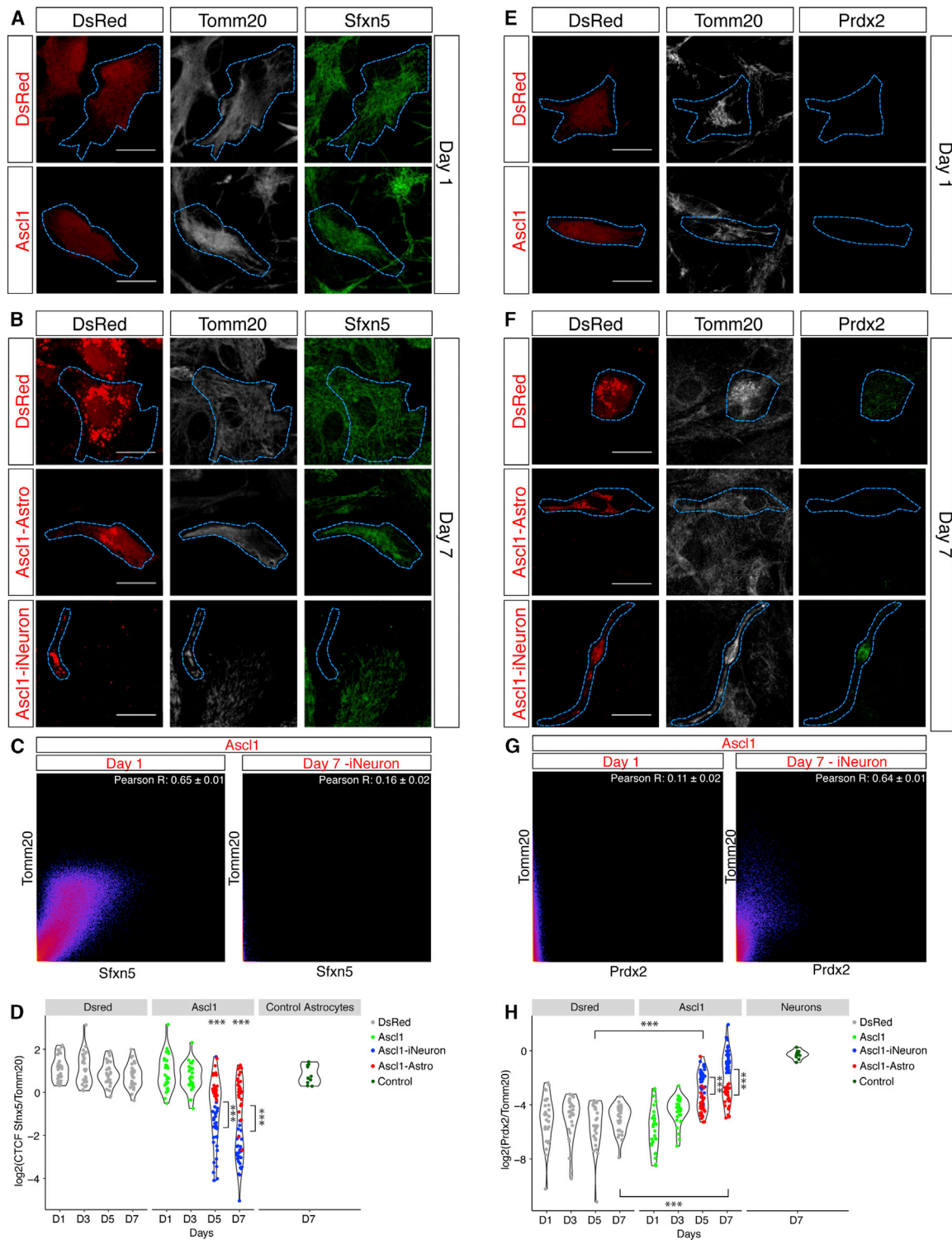
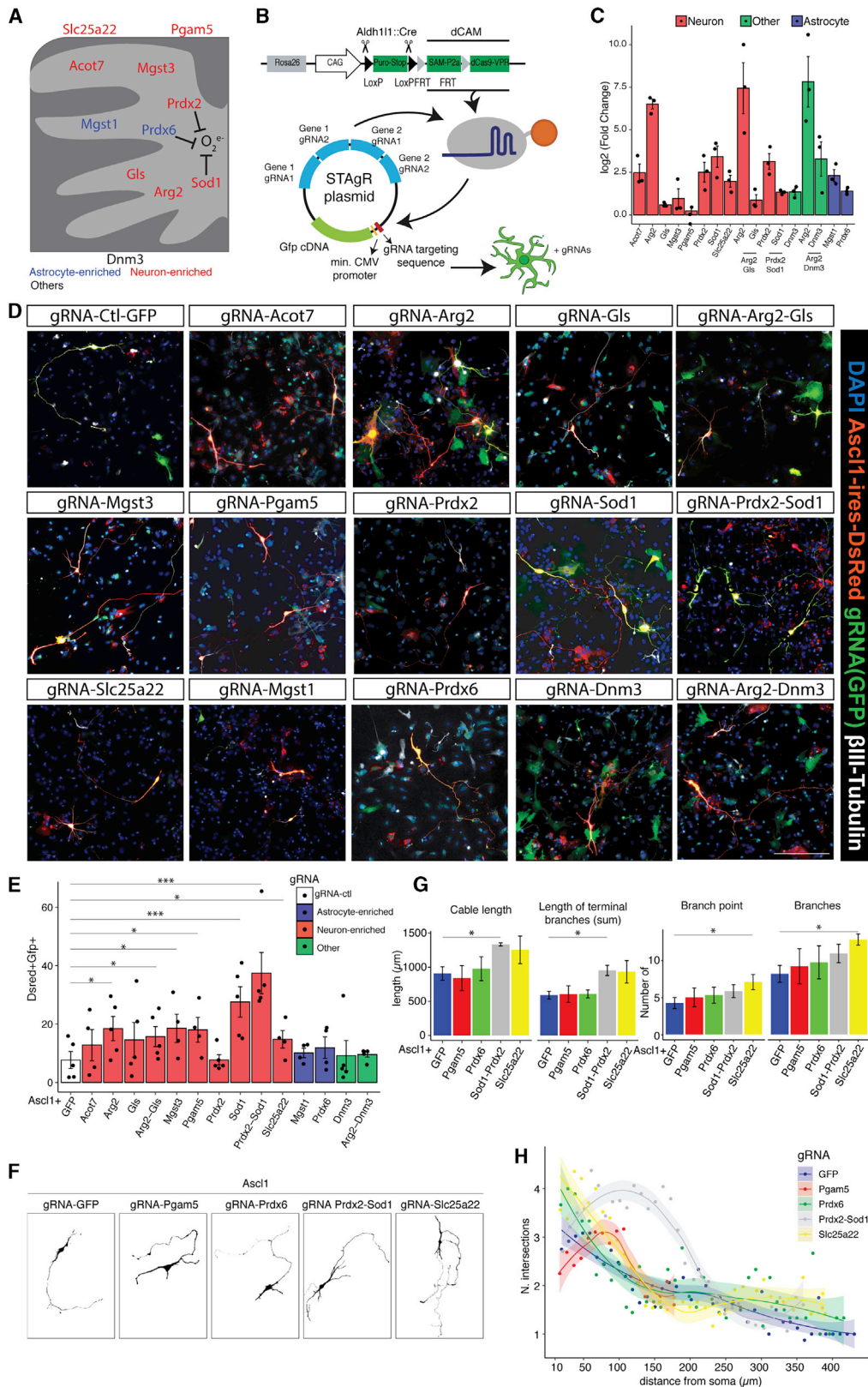


Figure 2. Mitochondrial Protein Changes during Astrocyte-to-Neuron Reprogramming

(A, B, E, and F) Micrographs showing immunostaining in astrocytes transduced with DsRed or Ascl1-ires-DsRed as indicated. Scale bars, 20 μ m.

(C and G) Examples of scatterplots of the pixel intensity correlation between Tomm20 and Sfxn5 (C) or Prdx2 (G) in Ascl1-transduced cells on day 1 (left panel) and in reprogrammed cells on day 7 (right panel). Pearson's coefficient as average of 3 cells/biological replicate; n = 3 biological replicates.

(D and H) Violin plots of the log₂ ratio of the intensity of the expression of Sfxn5 (D) or Prdx2 (H) normalized to Tomm20 intensity over time. Each dot represents 1 cell. 10 cells analyzed/biological replicate/condition/day. n = 3 biological replicates; ***p \leq 0.001.



(legend on next page)

neuronal reprogramming. Remarkably, the changes correlated with the degree of conversion, prompting the hypothesis that they may be functionally relevant.

CRISPRa-Mediated Induction of Neuron-Enriched Mitochondrial Proteins Improves the Efficiency of Direct Neuronal Reprogramming

To test the above prediction, we chose 8 candidates enriched in neuronal mitochondria (Figures S4A and S4B; Table S1; Fecher et al., 2019): *Sod1* and *Prdx2* for their antioxidant activity in neurons (Liu et al., 2020; Rosen, 1993), acyl-CoA thioesterase 7 (*Acot7*), arginase 2 (*Arg2*), Gls, microsomal Gst3 (*Mgst3*), mitochondrial serine/threonine protein phosphatase (*Pgam5*), and solute carrier 25 member 22 (*Slc25a22*) (Figure 3A). Among astrocyte-enriched antioxidant mitochondrial proteins, we selected *Prdx6* (Fisher, 2011) and the microsomal glutathione S-transferase *Mgst1*, a member of the membrane-associated proteins in eicosanoid and glutathione metabolism (MAPEG) family, as *Mgst3* (Bresell et al., 2005). Dynamin 3 (*Dnm3*) was included as a protein with mitochondrion-unrelated functions (Gu et al., 2010; Figure 3A).

Quantitative RT-PCR from cells isolated by fluorescence-activated cell sorting (FACS) 48 h after transfection of the dCas9-VPR coding plasmid (Breunig et al., 2018b) and non-targeting control gRNAs or gRNAs designed to target the promoter region of the above candidates showed different levels of induction (Figure 3C; *Arg2*, ~94-fold; *Acot7*, *Prdx2*, *Sod1*, *Slc25a22*, *Dnm3*, *Mgst1*, and *Prdx6*, ~ 5-fold; *Gls*, *Mgst3*, and *Pgam5*, ~2-fold). Multiple gRNAs targeting different genes (e.g., *Arg2*+*Gls*) did not alter the induction levels of their specific targets, and no significant induction was detectable for six putative off targets of each gRNA (Figure S4C).

gRNAs for the selected candidates were cloned in a plasmid with a GFP reporter module whose activation depends on the presence of the self-transcribed gRNAs (e.g., for *Sod1*) and dCas9-CAM (Figure 3B). Then, primary cultures of astrocytes, obtained by crossing a transgenic mouse line in which the dCas9 gene is fused to three transactivating domains (VP64, p65, and RTA[R transactivator]) and SAM (synergistic activator Mediator) components (dCAM) (Chavez et al., 2015; Konermann et al., 2015; STAR Methods) with the astrocyte-specific *Aldh1l1*:*Cre* mouse line (Tien et al., 2012; Figure 3B), were co-transfected with the constructs for *Ascl1-ires-DsRed* and the control STAgR-GFP (*gRNA-GFP*) or gene-specific gRNA, and neuronal conversion was examined 8 DPT. Strikingly, the induction of many, but not all, genes coding for neuron-enriched mitochondrial proteins

improved the reprogramming efficiency (Figures 3D and 3E). Induction of *Sod1* resulted in the highest reprogramming efficiency alone or in combination with *Prdx2* (Figure 3D and 3E; Figure S4D). In addition, induction of *Arg2* and *Mgst3* as well as *Pgam5* and *Slc25a22*, which do not have any reported antioxidant activity, significantly improved the conversion efficiency (Figures 3D and 3E). Remarkably, the induction of genes coding for astrocyte-enriched mitochondrial proteins, even with antioxidant function (*Mgst1* and *Prdx6*), was not beneficial for reprogramming, like *Dnm3* (Figures 3D and 3E). This highlights the need for neuron-enriched antioxidants (e.g., *Sod1* and *Mgst3*) and shows that members of the same family (e.g., *Mgst1* and *Mgst3*) are clearly not functionally redundant. The expression of neuron-enriched candidates also resulted in a more complex morphology of iNeurons, with more neurite outgrowth in *Ascl1-Sod1+Prdx2*-co-expressing neurons and more branches in *Ascl1-Slc25a22*-co-expressing neurons (Figures 3F and 3G).

These data suggest that neuron-specific mitochondrial proteins are particularly important during the conversion process and that their earlier and/or higher expression improves reprogramming.

CRISPRa-Mediated Induction of *Prdx2* and *Sod1* Improves Neuronal Reprogramming by Faster Conversion into Neurons with a Longer Lifespan

To investigate the effect of the early activation of mitochondrial proteins on neuronal conversion, we followed single cells by live imaging as described before (Costa et al., 2011), from 28 h after the transfection for 6 days with GFP/DsRed pictures taken every 4 h (Figure 4A; Figure S2F; Video S1). *Ascl1-Prdx2-Sod1*-co-transfected cells with neuron-like morphology (smaller cell soma and processes longer than 3× the soma length; Gascón et al., 2016) were already increased significantly at 75 h compared with *Ascl1*-only cells (Figure 4B). *Prdx2* and *Sod1* co-activation significantly increased the lifespan of all tracked cells (Figure 4C), mainly because of an increased lifespan of the converted neurons (Figures 4E and 4F), but not of non-reprogrammed astrocytes (Figure 4D), consistent with the cell-type-specific role of antioxidants. Measuring the conversion speed (when cells first acquire a neuron-like morphology) showed a bi-phasic distribution in *Ascl1*-transfected cells (Figure 4G). Cells turning into neurons fast (red dots) typically died before the end of the experiment, whereas those that reprogrammed at a slower pace (blue dots) survived until the end of the video session at 6 DPT (Figure 4G). This was remarkably different in *Ascl1-Prdx2-Sod1*-expressing cells: many cells

Figure 3. CRISPRa-Mediated Activation of Neuron-Enriched Mitochondrial Proteins Improves Neuronal Reprogramming

- (A and B) Schemes of the selected candidates in mitochondria and the dCas9-CAM-STAgR (string assembly gRNA) system employed here.
- (C) Real-time quantitative PCR (qPCR) of the candidates in dCas9-CAM gene-specific gRNA-expressing cells. Data are shown as log₂ fold change over the gRNA scramble control (mean ± SEM). n = 3 for each group.
- (D) Micrographs showing reprogrammed cells (βIII-tubulin⁺-DsRed⁺-GFP⁺) upon co-transfection of *Ascl1-ires-DsRed* (red) and different STAgR constructs (green). Scale bar, 100 μm.
- (E) Reprogramming efficiency as the percentage of βIII-tubulin⁺/DsRed⁺/GFP⁺ at 7 DPT. Data are shown as mean ± SEM. *p < 0.05, ***p < 0.001. n = 5 per experimental condition.
- (F) Examples of the morphology of reprogrammed neurons co-expressing *Ascl1* and the indicated gRNAs.
- (G) Morphological analysis of reprogrammed neurons upon induction of selected candidates (x axis). Data are shown as mean ± SEM. Paired t test, *p ≤ 0.05; n = 4 biological replicates.
- (H) Sholl analysis of reprogrammed neurons co-expressing *Ascl1* and the indicated candidates. Data are shown as mean ± SEM. Paired t test, *p ≤ 0.05; n = 4 biological replicates.

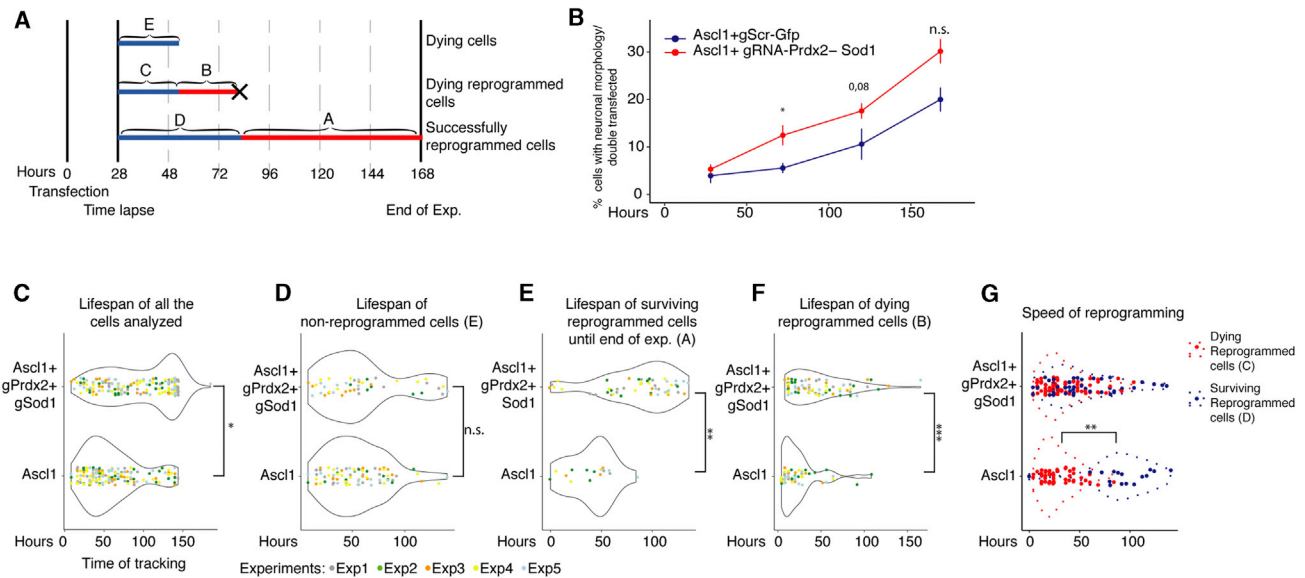


Figure 4. Continuous Single-Cell Live Imaging Reveals Several Roles of Prdx2-Sod1 Activation in Neuronal Reprogramming

(A) Scheme of continuous live imaging and the analysis performed.

(B) Time course analysis of the percentage of cells acquiring neuronal morphology over double-transfected cells at the indicated time points. Data are shown as mean \pm SEM. * $p \leq 0.05$. $n = 3$ biological replicates for each group.

(C and D) Violin plot showing the lifespan of all cells analyzed irrespective of their final identity (C) and cells that died without converting (D), following expression of *Ascl1-gRNA-GFP* or *Ascl1-gRNA-Prdx2-Sod1*. $n = 5$ biological replicates for each group. * $p \leq 0.05$

(E–G) Violin plots showing the lifespan (E and F) and speed of reprogramming (G) upon expression of *Ascl1-gRNA-GFP* or *Ascl1-gRNA-Prdx2-Sod1*. $n = 5$ biological replicates (color-coded) for each group. * $p \leq 0.05$, ** $p \leq 0.01$, *** $p \leq 0.001$.

reprogrammed fast and survived until the end of the experiment (Figure 4G). Importantly, this is not due to improved survival of the fast-converting cells that would die under the *Ascl1*-only condition because a similar number of cells converting fast and dying (blue dots and curve in Figure 4G) was observed among *Ascl1-Prdx2-Sod1* cells. Rather, many more cells were recruited for reprogramming under the *Ascl1-Prdx2-Sod1* condition and in a fast manner (Figure 4G). We therefore conclude that activation of these neuron-enriched mitochondrial proteins speeds up the conversion process in addition to its role in protecting neurons from cell death.

DISCUSSION

Here we describe the comprehensive mitochondrial proteomes of cortical astrocytes and neurons that show quantitative differences in a fifth of the identified proteins. The functional relevance of these differences is shown by the fact that cells failing to up-regulate neuron-enriched mitochondrial proteins often do not reprogram; activating their expression improved the reprogramming efficiency, and astrocyte-enriched mitochondrial proteins, even with known antioxidant function, have no such effects.

Astrocyte Metabolism and Its Influence on Neuronal Reprogramming

Astrocytes share similarities with neural stem cells (NSCs) (Götz et al., 2015). For example, we and others (Fecher et al., 2019) found the mitochondrial proteome of astrocytes to be enriched for the GO terms lipid metabolism and fatty acid β -oxidation, also highly represented in neural stem cells (NSCs) and downre-

gulated during adult neurogenesis (Knobloch et al., 2017; Llorens-Bobadilla et al., 2015). Despite the fast transcriptional changes at early stages of reprogramming (Gascón et al., 2016; Masserdotti et al., 2015), genes associated with lipid metabolism (e.g., *Cpt1a*) are not yet downregulated after 48 h (Gascón et al., 2016; Masserdotti et al., 2015), suggesting slow metabolic conversion, a limiting factor in induced pluripotent stem cell (iPSC) reprogramming (Wu et al., 2016). Accordingly, etomoxir-mediated reduction of fatty acid β -oxidation improved neuronal reprogramming (Figure S3), indicating that the manipulation of specific metabolic pathways might substantially contribute to remove hurdles during the conversion. The addition of ROS scavenger reduced the reprogramming efficiency combined with etomoxir, suggesting potential beneficial effects of ROS under this condition. It will be interesting to determine the level of ROS above which it shows deleterious effects.

Early Activation of Neuron-Enriched Mitochondrial Proteins with a Wide Functional Spectrum Improves Astrocyte-to-Neuron Conversion

The comprehensive mitochondrial proteome revealed cell-type-specific enrichment of antioxidant proteins; e.g., *Mgst1* and *Mgst3* were enriched in the mitochondrial proteome of astrocytes and neurons, respectively. Remarkably, early CRISPR-mediated induction of the latter, but not the former, improved direct neuronal conversion, demonstrating the key functional role of cell-type-specific but similar antioxidant proteins. *Sod1* activation had the most potent effect, in line with its functional relevance in neurodegeneration (Kaur et al., 2016). However, other mitochondrial proteins with antioxidant functions, such

as Prdx6 and Prdx2 (enriched in astrocytes and neurons, respectively) did not improve reprogramming, showing that only some antioxidants perform highly cell-type-specific functions relevant in direct neuronal reprogramming.

The early activation of neuron-enriched mitochondrial proteins without any reported antioxidant activity also significantly increased direct reprogramming efficiency. Pgam5, a mitochondrial phosphatase that associates with the RIP1/RIP3/MLKL (Mixed lineage kinase domain-like pseudokinase) complex, doubled *Ascl1*-induced reprogramming efficiency, possibly by inhibiting necroptosis (Gascón et al., 2016; Lu et al., 2016). In addition, Pgam5 regulates mitochondrial homeostasis and dynamics by dephosphorylating Drp1, BCL-xL (B-cell lymphoma extra large), and FUNDC1 (Ma et al., 2020), a key process for neuronal function and survival (Lu et al., 2014). Likewise, the mitochondrial glutamate transporter Slc25a22, which also improved reprogramming by 2-fold, is important for brain function (Cohen et al., 2014; Molinari et al., 2005, 2009; Poduri et al., 2013) by regulating glutamate levels (Goubert et al., 2017).

Conversely, the activation of Glis did not significantly improve reprogramming, suggesting that glutamate biogenesis does not have a major role in this process. Likewise, the activation of a non-mitochondrial protein, Dnm3, expressed at similar levels in astrocytes and neurons, had no effect. These results confirm our cutoff criteria and highlight a potent role of only some neuron-enriched mitochondrial proteins in direct conversion by influencing several functional pathways.

Notably, astrocyte-enriched mitochondrial proteins, like Sfnx5 and CpoX, were only partially downregulated in reprogramming and maintained a higher expression in cells that failed to convert. This indicates that these cells face a “confused” metabolic state that may hinder reprogramming and highlights the importance to further ease the metabolic transition for proper conversion. Indeed, “on-memory” genes not shut off during reprogramming from the original starter cell limit the conversion process (Hormanseder et al., 2017).

Neuron-Enriched Mitochondrial Protein Activation as an Enabler and Driver in Reprogramming

Most improvement in reprogramming efficiency was achieved by early expression of the neuron-enriched mitochondrial proteins Sod1 and Prdx2: they increased recruitment of more cells into the conversion process and improved survival only of reprogrammed neurons and their differentiation. Thus, early activation of these neuron-enriched mitochondrial antioxidants protects neurons, but not astrocytes, against aberrant ROS levels (Gascón et al., 2016).

Remarkably, *Ascl1*-expressing cells showed a significant difference in conversion speed between neurons that survive and those that do not survive for 6 days, with the former converting much slower. This is reminiscent of natural neurogenesis, where the transition from progenitors to neurons often occurs more gradually via intermediate progenitors (Khacho et al., 2016; Llorens-Bobadilla et al., 2015), suggesting the need for a period of adaptation to support the new identity. Surprisingly, the expression of *Prdx2* and *Sod1* speeds up the conversion process in cells surviving until the end of the time lapse, similarly to co-expression of *Bcl2* (Gascón et al., 2016). Thus, different mitochondrion-dependent pathways may speed up the conversion

rate by improving cell survival and/or protecting against ROS damage. We therefore propose that failure or late activation of neuron-enriched mitochondrial proteins may impair the conversion process at several levels, ultimately causing cells to die. Importantly, this occurs despite the expression of a multitude of antioxidant and metabolic proteins present in astrocytes. Thus, direct neuronal reprogramming sheds new light on the function of cell-type-enriched mitochondrial proteins.

Limitations of Study

Clearly, it would be desirable to follow the mitochondrial proteome in a comprehensive manner during the reprogramming process, which will be made easier by newly developed mouse lines with tagged mitochondrial proteins (Fecher et al., 2019), also in the murine brain *in vivo* or human cells *in vitro*. Ideally, these could be compared with fully differentiated neurons; here we choose culture conditions and time points to match the reprogramming protocol.

STAR★METHODS

Detailed methods are provided in the online version of this paper and include the following:

- KEY RESOURCES TABLE
- RESOURCE AVAILABILITY
 - Lead Contact
 - Materials Availability
 - Data and Code Availability
- EXPERIMENTAL MODEL AND SUBJECT DETAILS
 - Wild-type mice (Primary Cell culture, Proteomics, IHC)
 - Aldh1-Cre and Cre-inducible dCas9-VPR mice
 - Primary cultures of cortical astrocytes
 - Cells undergoing direct neuronal conversion
 - Primary cultures of cortical neurons
- METHOD DETAILS
 - Transfection and Transduction
 - Fluorescence-activated Cell Sorting
 - Mitochondria isolation
 - Characterization of isolated mitochondria
 - Seahorse experiments
 - Proteome analysis
 - Western Blot Analysis
 - Immunocytochemistry
 - RNA extraction, retro-transcription and Real Time Quantitative PCR (qRT-PCR)
 - STAgR cloning
 - Live-Imaging Microscopy
- QUANTIFICATION AND STATISTICAL ANALYSIS

SUPPLEMENTAL INFORMATION

Supplemental Information can be found online at <https://doi.org/10.1016/j.stem.2020.10.015>.

ACKNOWLEDGMENTS

Particular thanks go to Caroline Fecher and Thomas Misgeld (Technical University of Munich) for providing the antibodies against Sfnx5 and Glis and sharing their proteome data and expertise about mitochondria. We are very

grateful to Tatiana Simon (BMC, Munich) and Andrea Steiner-Mezzadri (Helmholtz Center Munich) for technical assistance, Daniel Brandt for technical support with the Seahorse analyzer, Uli Ohmayer for initial proteomic analysis, Andreas Beyerlein and Hannah Busen from Core Facility Statistical Consulting (all from Helmholtz Center Munich), Tobias Straub (Bioinformatic Core Facility of the BMC, LMU, Munich) and Pawel Smialowski (Helmholtz Zentrum, Munich) for help with R coding, Tamas Schauer for advice regarding DHARMA, and Nicola Mattugini for comments on the manuscript. This work was funded by the Fondation Rodger de Spoelberch, the German Research Foundation (SFB870 and SPP1757), the advanced ERC ChroNeuroRepair and ERANet (to M.G.), SPP2127 (to S.M.H.), and ExNet-0041-Phase2-3 (SyNergy-HMGU) and AMPPro Project (Aging and Metabolic Programming) network funds of the Helmholtz Association (to W.W.).

AUTHOR CONTRIBUTIONS

M.G. conceived and designed the project. G.L.R. and G.M. shaped the project, and G.L.R. performed experiments and analysis. G.S. contributed to the time course analysis. P.N. performed and analyzed the experiment with etomoxir, gRNA, and continuous live imaging. C.T.B. and S.H.S. provided CRISPR-Cas expertise and developed and designed the STAgR approach, and C.T.B. helped with cloning of the constructs. G.B. performed western blots. J.M.-P. and S.M.H. provided proteomics expertise and performed experiments and analysis. S.S. and H.Z. performed mitochondrial isolation and electron microscopy. J.G.-S., F.G., and W.W. generated and provided dCAM transgenic mice. M.J. provided expertise regarding metabolism and Seahorse analysis. G.M. analyzed the data; provided expertise and training of G.L.R., G.S., P.N., and G.B. regarding reprogramming; and co-directed the project together with M.G. G.L.R., G.M., and M.G. wrote the manuscript, and all authors contributed corrections and comments.

DECLARATION OF INTERESTS

The authors declare no competing interests.

Received: August 5, 2019

Revised: August 11, 2020

Accepted: August 20, 2020

Published: November 16, 2020; corrected online: December 2, 2020

REFERENCES

Barker, R.A., Götz, M., and Parmar, M. (2018). New approaches for brain repair—from rescue to reprogramming. *Nature* 557, 329–334.

Boulos, S., Meloni, B.P., Arthur, P.G., Bojarski, C., and Knuckey, N.W. (2007). Peroxiredoxin 2 overexpression protects cortical neuronal cultures from ischemic and oxidative injury but not glutamate excitotoxicity, whereas Cu/Zn superoxide dismutase 1 overexpression protects only against oxidative injury. *J. Neurosci. Res.* 85, 3089–3097.

Bresell, A., Weinander, R., Lundqvist, G., Raza, H., Shimoji, M., Sun, T.H., Balk, L., Wiklund, R., Eriksson, J., Jansson, C., et al. (2005). Bioinformatic and enzymatic characterization of the MAPEG superfamily. *FEBS J.* 272, 1688–1703.

Breunig, C.T., Durovic, T., Neuner, A.M., Baumann, V., Wiesbeck, M.F., Köferle, A., Götz, M., Ninkovic, J., and Stricker, S.H. (2018a). One step generation of customizable gRNA vectors for multiplex CRISPR approaches through string assembly gRNA cloning (STAgR). *PLoS ONE* 13, e0196015.

Breunig, C.T., Neuner, A.M., Giehl-Schwab, J., Wurst, W., Götz, M., and Stricker, S.H. (2018b). A Customizable Protocol for String Assembly gRNA Cloning (STAgR). *J. Vis. Exp.* (142), e58556.

Calvo, S.E., and Mootha, V.K. (2010). The mitochondrial proteome and human disease. *Annu. Rev. Genomics Hum. Genet.* 11, 25–44.

Calvo, S.E., Clauser, K.R., and Mootha, V.K. (2016). MitoCarta2.0: an updated inventory of mammalian mitochondrial proteins. *Nucleic Acids Res.* 44 (D1), D1251–D1257.

Chavez, A., Scheiman, J., Vora, S., Pruitt, B.W., Tuttle, M., P R Iyer, E., Lin, S., Kiani, S., Guzman, C.D., Wiegand, D.J., et al. (2015). Highly efficient Cas9-mediated transcriptional programming. *Nat. Methods* 12, 326–328.

Cohen, R., Basel-Vanagaite, L., Goldberg-Stern, H., Halevy, A., Shuper, A., Feingold-Zadok, M., Behar, D.M., and Straussberg, R. (2014). Two siblings with early infantile myoclonic encephalopathy due to mutation in the gene encoding mitochondrial glutamate/H⁺ symporter SLC25A22. *Eur. J. Paediatr. Neurol.* 18, 801–805.

Costa, M.R., Ortega, F., Brill, M.S., Beckervordersandforth, R., Petrone, C., Schroeder, T., Götz, M., and Berninger, B. (2011). Continuous live imaging of adult neural stem cell division and lineage progression in vitro. *Development* 138, 1057–1068.

Fecher, C., Trovò, L., Müller, S.A., Snaidero, N., Wettmarshausen, J., Heink, S., Ortiz, O., Wagner, I., Kühn, R., Hartmann, J., et al. (2019). Cell-type-specific profiling of brain mitochondria reveals functional and molecular diversity. *Nat. Neurosci.* 22, 1731–1742.

Ferreira, T.A., Blackman, A.V., Oyrer, J., Jayabal, S., Chung, A.J., Watt, A.J., Sjöström, P.J., and van Meyel, D.J. (2014). Neuronal morphometry directly from bitmap images. *Nat. Methods* 11, 982–984.

Fisher, A.B. (2011). Peroxiredoxin 6: a bifunctional enzyme with glutathione peroxidase and phospholipase A₂ activities. *Antioxid. Redox Signal.* 15, 831–844.

Folmes, C.D., Dzeja, P.P., Nelson, T.J., and Terzic, A. (2012). Metabolic plasticity in stem cell homeostasis and differentiation. *Cell Stem Cell* 11, 596–606.

Gascón, S., Murenu, E., Masserdotti, G., Ortega, F., Russo, G.L., Petrik, D., Deshpande, A., Heinrich, C., Karow, M., Robertson, S.P., et al. (2016). Identification and Successful Negotiation of a Metabolic Checkpoint in Direct Neuronal Reprogramming. *Cell Stem Cell* 18, 396–409.

Gibson, D.G. (2011). Enzymatic assembly of overlapping DNA fragments. *Methods Enzymol.* 498, 349–361.

Götz, M., Sirko, S., Beckers, J., and Irmeler, M. (2015). Reactive astrocytes as neural stem or progenitor cells: In vivo lineage, in vitro potential, and Genome-wide expression analysis. *Glia* 63, 1452–1468.

Goubert, E., Mircheva, Y., Lasorsa, F.M., Melon, C., Profilo, E., Sutura, J., Becq, H., Palmieri, F., Palmieri, L., Aniksztejn, L., and Molinari, F. (2017). Inhibition of the Mitochondrial Glutamate Carrier SLC25A22 in Astrocytes Leads to Intracellular Glutamate Accumulation. *Front. Cell. Neurosci.* 11, 149.

Grade, S., and Götz, M. (2017). Neuronal replacement therapy: previous achievements and challenges ahead. *NPJ Regen. Med.* 2, 29.

Gu, C., Yaddanapudi, S., Weins, A., Osborn, T., Reiser, J., Pollak, M., Hartwig, J., and Sever, S. (2010). Direct dynamin-actin interactions regulate the actin cytoskeleton. *EMBO J.* 29, 3593–3606.

Harris, J.J., Jolivet, R., and Attwell, D. (2012). Synaptic energy use and supply. *Neuron* 75, 762–777.

Hartfuss, E., Galli, R., Heins, N., and Götz, M. (2001). Characterization of CNS precursor subtypes and radial glia. *Dev. Biol.* 229, 15–30.

Hartig, F., and Lohse, L. (2020). DHARMA: Residual Diagnostics for Hierarchical (Multi-Level/Mixed) Regression Models. R package version 0.3.2.0. <https://cran.r-project.org/web/packages/DHARMA/index.html>.

Heinrich, C., Blum, R., Gascón, S., Masserdotti, G., Tripathi, P., Sánchez, R., Tiedt, S., Schroeder, T., Götz, M., and Berninger, B. (2010). Directing astroglia from the cerebral cortex into subtype specific functional neurons. *PLoS Biol.* 8, e1000373.

Heinrich, C., Gascón, S., Masserdotti, G., Lepier, A., Sanchez, R., Simon-Ebert, T., Schroeder, T., Götz, M., and Berninger, B. (2011). Generation of subtype-specific neurons from postnatal astroglia of the mouse cerebral cortex. *Nat. Protoc.* 6, 214–228.

Heins, N., Malatesta, P., Cecconi, F., Nakafuku, M., Tucker, K.L., Hack, M.A., Chapouton, P., Barde, Y.A., and Götz, M. (2002). Glial cells generate neurons: the role of the transcription factor Pax6. *Nat. Neurosci.* 5, 308–315.

Herrero-Mendez, A., Almeida, A., Fernández, E., Maestre, C., Moncada, S., and Bolaños, J.P. (2009). The bioenergetic and antioxidant status of neurons is controlled by continuous degradation of a key glycolytic enzyme by APC/C-Cdh1. *Nat. Cell Biol.* 11, 747–752.

Hormanseder, E., Simeone, A., Allen, G.E., Bradshaw, C.R., Figlmüller, M., Gurdon, J., and Jullien, J. (2017). H3K4 Methylation-Dependent Memory of

- Somatic Cell Identity Inhibits Reprogramming and Development of Nuclear Transfer Embryos. *Cell Stem Cell* 21, 135–143.e6.
- Jernberg, J.N., Bowman, C.E., Wolfgang, M.J., and Scafidi, S. (2017). Developmental regulation and localization of carnitine palmitoyltransferases (CPTs) in rat brain. *J. Neurochem.* 142, 407–419.
- Kaur, S.J., McKeown, S.R., and Rashid, S. (2016). Mutant SOD1 mediated pathogenesis of Amyotrophic Lateral Sclerosis. *Gene* 577, 109–118.
- Khacho, M., Clark, A., Svoboda, D.S., Azzi, J., MacLaurin, J.G., Meghaizel, C., Sesaki, H., Lagace, D.C., Germain, M., Harper, M.E., et al. (2016). Mitochondrial Dynamics Impacts Stem Cell Identity and Fate Decisions by Regulating a Nuclear Transcriptional Program. *Cell Stem Cell* 19, 232–247.
- Knobloch, M., Pilz, G.A., Ghesquière, B., Kovacs, W.J., Wegleiter, T., Moore, D.L., Hruzova, M., Zamboni, N., Carmeliet, P., and Jessberger, S. (2017). A Fatty Acid Oxidation-Dependent Metabolic Shift Regulates Adult Neural Stem Cell Activity. *Cell Rep.* 20, 2144–2155.
- Konermann, S., Brigham, M.D., Trevino, A.E., Joung, J., Abudayyeh, O.O., Barcena, C., Hsu, P.D., Habib, N., Gootenberg, J.S., Nishimasu, H., et al. (2015). Genome-scale transcriptional activation by an engineered CRISPR-Cas9 complex. *Nature* 517, 583–588.
- Korotkevich, G., Sukhov, V., and Sergushichev, A. (2019). Fast gene set enrichment analysis. *bioRxiv*. <https://doi.org/10.1101/060012>.
- Lin, R., Tao, R., Gao, X., Li, T., Zhou, X., Guan, K.L., Xiong, Y., and Lei, Q.Y. (2013). Acetylation stabilizes ATP-citrate lyase to promote lipid biosynthesis and tumor growth. *Mol. Cell* 51, 506–518.
- Liu, J., Su, G., Gao, J., Tian, Y., Liu, X., and Zhang, Z. (2020). Effects of Peroxiredoxin 2 in Neurological Disorders: A Review of its Molecular Mechanisms. *Neurochem. Res.* 45, 720–730.
- Llorens-Bobadilla, E., Zhao, S., Baser, A., Saiz-Castro, G., Zwadlo, K., and Martin-Villalba, A. (2015). Single-Cell Transcriptomics Reveals a Population of Dormant Neural Stem Cells that Become Activated upon Brain Injury. *Cell Stem Cell* 17, 329–340.
- Lu, W., Karuppagounder, S.S., Springer, D.A., Allen, M.D., Zheng, L., Chao, B., Zhang, Y., Dawson, V.L., Dawson, T.M., and Lenardo, M. (2014). Genetic deficiency of the mitochondrial protein PGAM5 causes a Parkinson's-like movement disorder. *Nat. Commun.* 5, 4930.
- Lu, W., Sun, J., Yoon, J.S., Zhang, Y., Zheng, L., Murphy, E., Mattson, M.P., and Lenardo, M.J. (2016). Mitochondrial Protein PGAM5 Regulates Mitophagic Protection against Cell Necroptosis. *PLoS ONE* 11, e0147792.
- Ma, K., Zhang, Z., Chang, R., Cheng, H., Mu, C., Zhao, T., Chen, L., Zhang, C., Luo, Q., Lin, J., et al. (2020). Dynamic PGAM5 multimers dephosphorylate BCL-xL or FUNDC1 to regulate mitochondrial and cellular fate. *Cell Death Differ.* 27, 1036–1051.
- Márquez, J., Tosina, M., de la Rosa, V., Segura, J.A., Alonso, F.J., Matés, J.M., and Campos-Sandoval, J.A. (2009). New insights into brain glutaminases: beyond their role on glutamatergic transmission. *Neurochem. Int.* 55, 64–70.
- Masserdotti, G., Gillotin, S., Sutor, B., Drechsel, D., Irmeler, M., Jørgensen, H.F., Sass, S., Theis, F.J., Beckers, J., Berninger, B., et al. (2015). Transcriptional Mechanisms of Proneural Factors and REST in Regulating Neuronal Reprogramming of Astrocytes. *Cell Stem Cell* 17, 74–88.
- Misgeld, T., and Schwarz, T.L. (2017). Mitostasis in Neurons: Maintaining Mitochondria in an Extended Cellular Architecture. *Neuron* 96, 651–666.
- Miyake, S., Yamashita, T., Taniguchi, M., Tamatani, M., Sato, K., and Tohyama, M. (2002). Identification and characterization of a novel mitochondrial tricarboxylate carrier. *Biochem. Biophys. Res. Commun.* 295, 463–468.
- Molinari, F., Raas-Rothschild, A., Rio, M., Fiermonte, G., Encha-Razavi, F., Palmieri, L., Palmieri, F., Ben-Neriah, Z., Kadhon, N., Vekemans, M., et al. (2005). Impaired mitochondrial glutamate transport in autosomal recessive neonatal myoclonic epilepsy. *Am. J. Hum. Genet.* 76, 334–339.
- Molinari, F., Kaminska, A., Fiermonte, G., Boddaert, N., Raas-Rothschild, A., Plouin, P., Palmieri, L., Brunelle, F., Palmieri, F., Dulac, O., et al. (2009). Mutations in the mitochondrial glutamate carrier SLC25A22 in neonatal epileptic encephalopathy with suppression bursts. *Clin. Genet.* 76, 188–194.
- Mori, M., Gotoh, S., Taketani, S., Hiai, H., and Higuchi, K. (2013). Hereditary cataract of the Nakano mouse: Involvement of a hypomorphic mutation in the coproporphyrinogen oxidase gene. *Exp. Eye Res.* 112, 45–50.
- Motori, E., Puyal, J., Toni, N., Ghanem, A., Angeloni, C., Malaguti, M., Cantelli-Forti, G., Berninger, B., Conzelmann, K.K., Götz, M., et al. (2013). Inflammation-induced alteration of astrocyte mitochondrial dynamics requires autophagy for mitochondrial network maintenance. *Cell Metab.* 18, 844–859.
- O'Connor, R.S., Guo, L., Ghassemi, S., Snyder, N.W., Worth, A.J., Weng, L., Kam, Y., Philipson, B., Trefely, S., Nunez-Cruz, S., et al. (2018). The CPT1a inhibitor, etomoxir induces severe oxidative stress at commonly used concentrations. *Sci. Rep.* 8, 6289.
- Pagliarini, D.J., Calvo, S.E., Chang, B., Sheth, S.A., Vafai, S.B., Ong, S.E., Walford, G.A., Sugiana, C., Boneh, A., Chen, W.K., et al. (2008). A mitochondrial protein compendium elucidates complex I disease biology. *Cell* 134, 112–123.
- Poduri, A., Heinzen, E.L., Chitsazzadeh, V., Lasorsa, F.M., Elhosary, P.C., LaCourse, C.M., Martin, E., Yuskaitis, C.J., Hill, R.S., Atabay, K.D., et al. (2013). SLC25A22 is a novel gene for migrating partial seizures in infancy. *Ann. Neurol.* 74, 873–882.
- Rosen, D.R. (1993). Mutations in Cu/Zn superoxide dismutase gene are associated with familial amyotrophic lateral sclerosis. *Nature* 364, 362.
- Schaffer, A.E., Pinkard, O., and Collier, J.M. (2019). tRNA Metabolism and Neurodevelopmental Disorders. *Annu. Rev. Genomics Hum. Genet.* 20, 359–387.
- Schmitt, S., Saathoff, F., Meissner, L., Schropp, E.M., Lichtmanegger, J., Schulz, S., Eberhagen, C., Borchard, S., Aichler, M., Adamski, J., et al. (2013). A semi-automated method for isolating functionally intact mitochondria from cultured cells and tissue biopsies. *Anal. Biochem.* 443, 66–74.
- Spinelli, J.B., and Haigis, M.C. (2018). The multifaceted contributions of mitochondria to cellular metabolism. *Nat. Cell Biol.* 20, 745–754.
- Tien, A.C., Tsai, H.H., Molofsky, A.V., McMahon, M., Foo, L.C., Kaul, A., Dougherty, J.D., Heintz, N., Gutmann, D.H., Barres, B.A., and Rowitch, D.H. (2012). Regulated temporal-spatial astrocyte precursor cell proliferation involves BRAF signalling in mammalian spinal cord. *Development* 139, 2477–2487.
- van Deijk, A.F., Camargo, N., Timmerman, J., Heistek, T., Brouwers, J.F., Mogavero, F., Mansvelde, H.D., Smit, A.B., and Verheijen, M.H. (2017). Astrocyte lipid metabolism is critical for synapse development and function in vivo. *Glia* 65, 670–682.
- Velletri, T., Romeo, F., Tucci, P., Peschiaroli, A., Annicchiarico-Petruzzelli, M., Niklison-Chirou, M.V., Amelio, I., Knight, R.A., Mak, T.W., Melino, G., and Agostini, M. (2013). GLS2 is transcriptionally regulated by p73 and contributes to neuronal differentiation. *Cell Cycle* 12, 3564–3573.
- Vignoles, R., Lentini, C., d'Orange, M., and Heinrich, C. (2019). Direct Lineage Reprogramming for Brain Repair: Breakthroughs and Challenges. *Trends Mol. Med.* 25, 897–914.
- Walcher, T., Xie, Q., Sun, J., Irmeler, M., Beckers, J., Öztürk, T., Niessing, D., Stoykova, A., Cvekl, A., Ninkovic, J., and Götz, M. (2013). Functional dissection of the paired domain of Pax6 reveals molecular mechanisms of coordinating neurogenesis and proliferation. *Development* 140, 1123–1136.
- Wiśniewski, J.R., Zougman, A., Nagaraj, N., and Mann, M. (2009). Universal sample preparation method for proteome analysis. *Nat. Methods* 6, 359–362.
- Wu, J., Ocampo, A., and Belmonte, J.C.I. (2016). Cellular Metabolism and Induced Pluripotency. *Cell* 166, 1371–1385.
- Zhang, X., Smits, A.H., van Tilburg, G.B., Ovaa, H., Huber, W., and Vermeulen, M. (2018). Proteome-wide identification of ubiquitin interactions using UblA-MS. *Nat. Protoc.* 13, 530–550.
- Zischka, H., Larochette, N., Hoffmann, F., Hamöller, D., Jägemann, N., Lichtmanegger, J., Jennen, L., Müller-Höcker, J., Roggel, F., Göttlicher, M., et al. (2008). Electrophoretic analysis of the mitochondrial outer membrane rupture induced by permeability transition. *Anal. Chem.* 80, 5051–5058.

STAR★METHODS

KEY RESOURCES TABLE

REAGENT or RESOURCE	SOURCE	IDENTIFIER
Antibodies		
Rabbit anti-CS	Novus Biologicals	NBP2-13878
Rabbit anti-VDAC	Cell Signaling	Cat# 4866; RRID: AB_2272627
Goat anti-ANT	Santa Cruz	Cat# sc.9299; RRID: AB_671086
Total Oxphos Rodent Ab cocktail	Abcam	Cat# ab110413; RRID: AB_2629281
Mouse anti- β -III-Tubulin	Sigma-Aldrich	Cat# T8660; RRID: AB_477590
Mouse anti-GFAP	Dako	Cat# Z0334; RRID: AB_100013482
Rabbit anti-GFAP	Sigma-Aldrich	Cat# G3893; RRID: AB_477010
Rat anti-RFP	Chromotek	Cat# 5F8; RRID: AB_2336064
Rabbit anti-RFP	Rockland	Cat# 600-401-379; RRID: AB_2209751
Chicken anti-GFP	Aves Labs	Cat# GFP-1020; RRID: AB_10000240
Rabbit anti-CPOX	Abcam	Cat# Ab169766
Rabbit anti-Prdx2	Abcam	Cat# Ab109367; RRID: AB_10862524
Rabbit anti-Gls	Proteintech	Cat# 20170-1-AP; RRID: AB_10665373
Rabbit anti-Sfxn5	Abcam	Cat# Ab172971
Anti-Aldh111	Merck Millipore	Cat# MABN495; RRID: AB_2687399
Anti-Tomm20	Abnova	Cat# H00009804-M01; RRID: AB_1507602
Anti-Mouse-HRP linked	Invitrogen	Cat#626520; RRID: AB_2533947
Anti-Mouse, HRP linked	Cell Signaling	Cat# 7076; RRID: AB_330924
Anti-Rabbit, HRP linked	Cell Signaling	Cat# 7074; RRID: AB_2099233
Anti-Rabbit, HRP, linked	GE Healthcare	Cat#NA934; RRID: AB_2722659
Anti-Goat, HRP linked	Santa Cruz	Cat# sc-2020; RRID: AB_631728
Anti-Mouse Alexa Fluor 488	Molecular Probes	Cat# A-21202; RRID: AB_141607
Anti-Chicken Alexa Fluor 488	Thermo Fisher	Cat# A-11039; RRID: AB_2534096
Anti-Rat Cy3	Dianova	Cat# 112-165-167; RRID: AB_2338251
Anti-Mouse IgG2b 633	Innovative Research	Cat# A21146; RRID: AB_1500899
Anti-Mouse IgG1 647	Molecular Probes	Cat# A21240; RRID: AB_141658
Anti-Rabbit Alexa Fluor 488	Molecular Probes	Cat# A21206; RRID: AB_141708
Anti-Mouse IgG1 Biotin	Southernbiotech	Cat# 1070-08; RRID: AB_2794413
Streptavidin Alex Fluor 405	Thermo Fisher	Cat# S32351
Bacterial and Virus Strains		
RV CAG-Neurog2-ires-DsRedExpress2	Gascón et al., 2016	N/A
RV CAG-Ascl1-ires-DsRed	Gascón et al., 2016	N/A
RV CAG-DsRedExpress2	Gascón et al., 2016	N/A
RV CAG-mitoGFP	This study	N/A
RV CAG-Ascl1-ires-mitoGFP	This study	N/A
RV CAG-Ascl1-ires-mitoRFP	This study	N/A
Chemicals, Peptides, and Recombinant Proteins		
EGF	GIBCO	Cat# PHG0311
bFGF	GIBCO	Cat# 13256029
Poly-D-Lysine	Sigma-Aldrich	Cat# P0899
B27	GIBCO	Cat# 17504044
HBSS medium	Thermo Fisher	Cat# 24020117
HEPES	Thermo Fisher	Cat# 15630080
DMEM/F12	Thermo Fisher	Cat# 10565018

(Continued on next page)

Continued

REAGENT or RESOURCE	SOURCE	IDENTIFIER
trypsin/EDTA 0,25%	Thermo Fisher	Cat# 25200056
Neurobasal Medium	GIBCO	Cat# 21103149
Glucose	GIBCO	Cat# A2494001
GlutaMAX	GIBCO	Cat# 35050061
OptiMEM – GlutaMAX	Thermo Fisher	Cat# 51985-026
EGTA	Sigma-Aldrich	Cat# E3889
Lipofectamine 2000	Thermo Fisher	Cat# 11668019
Rhodamine 123	Thermo Fisher	Cat# R302
Oligomycin A	Sigma-Aldrich	Cat# 73351
FCCP	Sigma-Aldrich	Cat# C2920
Rotenone	Sigma-Aldrich	Cat# R8875
Antimycin A	Sigma-Aldrich	Cat# A8674
2-Deoxy-D-glucose	Sigma-Aldrich	Cat# D8375
Triton X-100	Sigma-Aldrich	Cat# T9284
Etomoxir	Sigma-Aldrich	Cat# E1905
Bovine Serum Albumine (BSA)	Sigma-Aldrich	Cat# A9418
Critical Commercial Assays		
Arcturus PicoPure RNA Isolation Kit	Thermo Fisher	Cat# 12204-01
Bradford Protein Assay Kit	BioRad	Cat# 5000201
First Strand cDNA Synthesis Kit	Thermo Fisher	Cat# K1621
PowerUp SYBR Green Master Mix	Thermo Fisher	Cat# A25742
Agencourt AMPure XP	Beckman Coulter	Cat# 10136224
RC DC Protein assay	BioRad	N/A
Deposited Data		
mitoProteomic data, identifier: PXD014886	This study	https://www.ebi.ac.uk/pride
Experimental Models: Organisms/Strains		
C57BL/6	LMU animal Facility	N/A
Aldh111-Cre	LMU animal Facility	N/A
Rosa26-LoxP-Stop-LoxP-dCAM	HMGU	N/A
Oligonucleotides		
See Methods S1	This study	N/A
Recombinant DNA		
STAgR_Neo	Addgene	RRID:Addgene_102992
STAGR_gRNAScaffold_hU6	Addgene	RRID:Addgene_102843
STAGR_gRNAScaffold_hH1	Addgene	RRID:Addgene_102841
STAGR_gRNAScaffold_h7SK	Addgene	Addgene_102841
STAGR_gRNAScaffold_mU6	Addgene	RRID:Addgene_102844
pCDNA-miniCMV-GFP	This study	N/A
STAgR_cntrl	This study	N/A
STAgR_Acot7	This study	N/A
STAgR_Arg2	This study	N/A
STAgR_Gls	This study	N/A
STAgR_Mgst3	This study	N/A
STAgR_Pgam5	This study	N/A
STAgR_Sod1	This study	N/A
STAgR_Slc25a22	This study	N/A
STAgR_Dnm3	This study	N/A
STAgR_Mgst1	This study	N/A
STAgR_Prxd6	This study	N/A

(Continued on next page)

Continued		
REAGENT or RESOURCE	SOURCE	IDENTIFIER
STAgR_Arg2-Gls (A-G)	This study	N/A
STAgR_Prxd2-Sod1 (P-S)	This study	N/A
STAgR_Arg2-Dnm3 (A-D)	This study	N/A
Software and Algorithms		
ZEN software	Zeiss	https://www.zeiss.com/microscopy/en_us/products/microscope-software/zen.html RRID:SCR_013672
ImageJ	ImageJ	https://imagej.net/Downloads RRID: SCR_003070
Morphometric analysis	SNT	Ferreira et al., 2014
Sholl Analysis	ImageJ	N/A
Co-localization	Coloc2	https://imagej.net/Coloc_2
Proteome discoverer 2.2 software	Thermo Fisher	https://www.thermofisher.com/order/catalog/product/IQLAEGABSFJMAUH RRID:SCR_014477
SwissProt Database Mouse	NCBI Protein	https://www.ncbi.nlm.nih.gov/protein RRID:SCR_003257
mitoCARTA 2.0 database	Calvo et al., 2016	N/A
Perseus Software	Perseus	http://maxquant.net/perseus/ RRID:SCR_015753
GraphPad Prism 7.0	GraphPad Software	https://www.graphpad.com:443/ RRID:SCR_002798
Adobe Illustrator	Adobe Illustrator	https://www.adobe.com/de/products/catalog.html RRID:SCR_010279
Zeiss AxioVision 4.7 software	Zeiss	http://www.zeiss.com/microscopy/us/products/microscope-software/zen-core.html?vaURL=www.zeiss.com/microscopy/us/products/microscope-software/axiovision.html
Microsoft Excel	Microsoft Excel	https://www.microsoft.com/en-gb/ RRID:SCR_016137
Seahorse Wave	Agilent Technologies	https://www.agilent.com/en-us/products/cell-analysis-(seahorse)/software-download-for-wave-desktop RRID:SCR_014526
RStudio		https://rstudio.com
	DHARMA	https://cran.r-project.org/web/packages/DHARMA/vignettes/DHARMA.html
	DEP	https://www.bioconductor.org/packages/release/bioc/html/DEP.html
	ggplot2	https://ggplot2.tidyverse.org
	Pheatmap	https://www.bioconductor.org/packages/release/bioc/html/heatmaps.html
	fgsea	https://bioconductor.org/packages/release/bioc/html/fgsea.html
	TopGo	https://bioconductor.org/packages/release/bioc/html/topGO.html
Other		
Aqua Poly/Mount	Polysciences	Cat# 18606-20

RESOURCE AVAILABILITY

Lead Contact

Further information and requests for resources and reagents should be directed to and will be fulfilled by the Lead Contact, Prof. Magdalena Götz (magdalena.goetz@helmholtz-muenchen.de).

Materials Availability

- Plasmids generated in this study are available upon request.
- gRNA sequences used to activate gene-specific loci are listed in [Methods S1](#).
- Aldh1-Cre transgenic mice are available at Jackson Lab (stock n.023748).
- There are restrictions to the availability of dCAM mice due to MTA request.

Data and Code Availability

- Mass spectrometry proteomics data have been deposited to the ProteomeXchange Consortium via the PRIDE, partner repository, with dataset identifier PXD014886.

EXPERIMENTAL MODEL AND SUBJECT DETAILS

Wild-type mice (Primary Cell culture, Proteomics, IHC)

All experimental procedures in this study, done at the LMU München, were performed in accordance with German and European Union guidelines and were approved by the government of Upper Bavaria. For most of the experiments, primary cultures of astrocytes were obtained from brains of C57BL/6J mice of 5-7 days of age; no specific gender was considered. Primary cultures of cortical neurons were obtained from brains of C57BL/6J embryos at 14.5 days post conception (14.5 dpc or E14.5). Mice were fed *ad libitum* and housed with 12/12 h light and dark cycle and kept under specific-pathogen-free (SPF) conditions.

Aldh1-Cre and Cre-inducible dCas9-VPR mice

The activation of specific mitochondria-coding genes was performed in primary cultures of astrocytes obtained from Aldh111-Cre (Tien et al., 2012) crossed with dCAM mice (Rosa26-loxP-Stop-LoxP-dCas9VPR-SAM mice (J.G.-S., unpublished data). Both strains were used as heterozygotes. The background strain of the mice was C57BL/6.

Primary cultures of cortical astrocytes

Astrocytes were isolated and cultured as previously described, with small changes (Heins et al., 2002). After removal of the meninges, gray matter tissue from cerebral cortex of C57BL/6J mice at postnatal day 5-7 (P5-P7) was dissected and dissociated mechanically. Subsequently, cells were centrifuged for 5 min at 1,300 rpm, re-suspended, and plated in a T25 flask in medium consisting of DMEM/F12 (1:1), 10% fetal bovine serum (FBS), penicillin/streptomycin, and 1x B27 serum-free-supplement, 10 ng/ml epidermal growth factor (EGF), and 10 ng/ml basic fibroblast growth factor (bFGF) (astro-medium). Cells were passaged at 80%-90% confluency after 7-10 days using trypsin/EDTA and plated on poly-D-lysine coated glass coverslips at a density of 50,000-60,000 cells per coverslip (in 24-well plates) in fresh astro-medium. The vast majority of the cells (> 90%) in these cultures were positive for glial fibrillary acidic protein (Gfap) as previously described. Primary cultures of astrocytes were maintained in an incubator for 6-8 days at 37°C and 5% CO₂.

Cells undergoing direct neuronal conversion

One day after transduction or transfection, astro-medium was replaced with fresh medium consisting of DMEM/F12 (1:1), penicillin/streptomycin, supplemented with 1x B27 and Glutamax, but not FBS, EGF and FGF (differentiation medium). Small molecules were added once, at the time of medium replacement (24h after transduction or transfection). Cultures were maintained in an incubator for 6-8 days at 37°C and 9% CO₂.

Primary cultures of cortical neurons

Cerebral cortices were dissected from embryonic day (E) 14 mice as described before (Hartfuss et al., 2001; Walcher et al., 2013). Cortices were isolated, meninges removed and samples mechanically dissociated in 1x HBSS medium containing 10mM HEPES, on ice. Subsequently, cells were digested for 15 min in trypsin-EDTA (0.05%) and centrifuged for 5 min at 1,000 rpm. The pellet was resuspended in medium containing 10% FBS to stop trypsin, then centrifuged again and resuspended in 1x Neurobasal Medium, supplemented with 1x Glutamax, penicillin/streptomycin, and 1x B27. Cells were counted and plated at a density of 600,000 cells per well in 6-well plates, pre-coated with poly-D-lysine. After one week in culture the cells had mostly differentiated into neurons, with a high purity and little contamination by other cell types.

METHOD DETAILS

Transfection and Transduction

For transfection, DNA-liposome complexes were prepared in OptiMem medium using the retroviral plasmids described below and Lipofectamine 2000. Astrocytic cultures, plated the day before in 24-well plates at a density of 60,000-80,000 cells per well, were transfected with DNA-liposome complexes composed of 0.6 µg total DNA, mixed with 0,75µl of Lipofectamine2000 per well, in 400µl of OptiMem medium for 4 hours. Then, transfection medium was replaced by a solution composed to 1:1 ratio of fresh astro-medium and astro-medium collected from the same cells before the transfection (and filtered). One day later, the medium was replaced with differentiation medium and cells maintained in culture until 6-7 days post-transfection in 9% CO₂ incubator. For FACS sorting, RNA extraction and RT-PCR, astrocytes were plated in 6-well plates pre-coated with PDL at a concentration of 350,000 cells per well. The following day, cells were transfected with DNA-liposome complexes containing 1µg total DNA and 1,25µl Lipofectamine 2000 per 1ml of OptiMem medium for 4 hours and cultured in astro-medium for 48hours before sorting. For STAgR experiments, primary cultures of astrocytes, obtained from double positive Aldh111-Cre dCAM mice (Rosa26-loxP-Stop-LoxP-dCas9VPR-SAM mice (Giehl-Schwab J. et al., in revision), were transfected with plasmids encoding the indicated STAgR and *Ascl1* with a molar ratio 1:1. For transduction, astrocytes were infected with 1µl of virus per well one day after plating. The viruses used are listed in the key resource table and were produced as previously described (Gascón et al., 2016).

Fluorescence-activated Cell Sorting

WT astrocytes were transfected with gRNAs-GFP and dCas9-VPR-DsRed plasmids. Cells were collected 48 hours after transfection and sorted for RFP⁺/GFP⁺, using the FACSria III (BD Bioscience) system at high purity mode and a flow rate lower than 600 cells per second. Alternatively, astrocytes obtained from Aldh111-Cre x dCAM transgenic mice were transfected only with gRNA-expressing plasmids and subjected to FACS analysis at 48 hours, collecting GFP⁺ cells. Cells were washed twice with 1x PBS, treated with trypsin (0,05% in EDTA) for 5%, then astro-medium was added. Cells were harvested by centrifugation (1,000 rpm, 5min, 4°C), washed twice with 1x PBS and, then, resuspended in 400µl of DMEM/F12 (1:1), phenol-red-free. Single cell suspension was filtrated using a 70-µm cell strainer. Cells were sorted using the FACS Aria III (BD). Gates were set by using un-transfected cells, as well cells expressing GFP or DsRed as positive control. 15,000 cells were sorted directly in extraction buffer (Picopure RNA isolation kit) to enhance RNA quality and efficiency, for subsequent extraction and qRT-PCR.

Mitochondria isolation

Mitochondria isolation from cultured astrocytes and neurons was performed as previously described (Schmitt et al., 2013) using the pump-controlled cell (PCC) rupture method; a cell homogenizer (Isobiotec, Germany) combined with 1 mL Luer Lock Gas-Tight Syringes (4.608 mm i.d., SGE Supelco, USA) and a high-precision pump (Pump 11, Harvard Apparatus, USA). The homogenizer was pre-cooled on ice to ensure cooling of the samples during the isolation, the tungsten carbide ball (6µm diameter) was inserted and the homogenizer was equilibrated with isolation buffer (300 mM sucrose, 5 mM TES, and 200 µM ethyleneglycoltetraacetic acid [EGTA], pH 7.2). The sample of dissociated astrocytes or neurons was added to 1 mL of isolation buffer and passed three (neurons) to six (astrocytes) times through the system at a constant rate (700 µl/min). To recover the homogenate, the system was rinsed once with 1 mL of isolation buffer. The sample preparation and the tunable parameters of the PCC, such as the clearance and the number of strokes, were optimized for each sample. Yield and functionality (mitochondrial transmembrane potential, $\Delta\psi_m$) of the isolated mitochondria were used to assess the optimal parameters. Around 1 million astrocytes and neurons respectively were used to obtain a sufficient amount of mitochondria for further processing. The pooled homogenate was cleared from cell debris and nuclei by centrifugation (800 × g, 5 min at 4°C), and mitochondria were pelleted at 9000 × g (10 min at 4°C). After the isolation, syringes were rinsed 3-4 times with double distilled water (ddH₂O). The tungsten carbide ball and the cell homogenizer were cleaned with isopropanol followed by ddH₂O to allow processing of the next sample without contamination.

Characterization of isolated mitochondria

The functional analysis of isolated mitochondria was performed by measuring Rhodamine 123 (Rh123) fluorescence quenching in order to determine $\Delta\psi_m$, as well as measuring the absorbance change at 540nm (Synergy 2, BioTek, USA) to determine mitochondrial swelling, as described previously (Schmitt et al., 2013). Protein concentrations were determined by the Bradford assay. For immunoblotting analysis, 10 µg of protein was subjected to sodium dodecyl sulfate-polyacrylamide gel electrophoresis (SDS-PAGE), and separated proteins were transferred onto PVDF membrane. Equal protein loading and proper transfer were controlled by Ponceau red staining. The primary and secondary antibodies used for Western Blot analysis are listed in the Key Resource table.

Electron microscopy analysis of the isolated mitochondria was done as described previously (Zischka et al., 2008). ZE-FFE-separated mitochondrial fractions were immediately pelleted, fixed in 2.5% glutaraldehyde, post-fixed with 1% osmium tetroxide, dehydrated with ethanol and embedded in Epon. Ultrathin sections were negatively stained with uranyl acetate and lead citrate and then analyzed on a Zeiss EM 10 CR electron microscope.

Seahorse experiments

Primary cortical astrocytes or neurons were plated onto XF24 V3 PET cell culture microplates from Seahorse biosciences, pre-coated with PDL, and analyzed the day after plating. Cells were seeded at 20,000, 30,000, 50,000 for neurons; and 15,000, 25,000 or 40,000 for astrocytes. The final cell number was assessed by counting DAPI⁺ nuclei and measuring DNA content to normalize the data to µg DNA or 1000 cells. Before measuring cellular respiration, cells were washed twice with assay medium (XF DMEM + 25 mM glucose) and then incubated in 750 µL of assay medium for 10 min in an air incubator without CO₂ at 37°C. The XF24 plate was then transferred to the XF24 Extracellular Flux analyzer (Seahorse Bioscience). Basal respiration was determined with 4-5 assay cycles (2 min. mix, 2 min. measuring), and all parameters were obtained after the respective drug application. Basal OCR and PPR were measured prior to oligomycin treatment. For the measurement of different mitochondrial respiration states, oligomycin A (Oligo, 5 µg/ml) was used to inhibit the ATP synthase, followed by Carbonyl cyanide-4-(trifluoromethoxy)phenylhydrazone (FCCP, 1 µM) to induce maximal substrate oxidation capacity, and a cocktail containing rotenone (Rot, 5 µM) and antimycin A (Ant, 2 µM) to inhibit ETC activity and determine non-mitochondrial oxygen uptake. Finally, 2-deoxyglucose (2-DG, 100mM) was added to block glycolysis. Extracellular acidification rate (ECAR) was converted to proton production rate (PPR) based on machine algorithms and the buffer capacity of the medium. The OCR/PPR ratio was calculated over the averaged basal values. Each value is calculated averaging 3-5 time points from 3 technical replicates.

Proteome analysis

Isolated mitochondria (10 µg) were used per biological replicate. SDS was added to a final concentration of 2% for efficient solubilization, prior to tryptic protein digest using a modified FASP protocol (Wiśniewski et al., 2009). Proteomic measurements were performed on a Q-Exactive HF mass spectrometer (Thermo Scientific) online coupled to an Ultimate 3000 nano-RSLC (Dionex). Peptides

were separated on a C18 nanoEase MZ HSS T3 column (100Å, 1.8 μm, 75 μm x 250 mm; Waters) in a 95 min non-linear acetonitrile gradient. Precursor (scan range 300 – 1500 m/z) and TOP10 fragment spectra of charges 2-7 were acquired in the orbitrap mass detector of the mass spectrometer, at resolutions of 60,000 and 15,000 respectively with a maximum injection time of 50 ms and a dynamic exclusion of 30 s for each one. The individual raw-files were loaded to the Proteome discoverer 2.2 software (Thermo scientific) allowing for peptide identification and label-free quantification using the Minora node. Searches were performed using Sequest HT as a search engine in the Swissprot mouse database with the following search settings: 10 ppm precursor tolerance, 0.02 Da fragment tolerance, two missed cleavages allowed, carbamidomethyl on cysteine as fixed modification, deamidation of glutamine and asparagine allowed as variable modification, as well as oxidation of methionine and Met-loss combined with acetylation at the N terminus of the protein. Proteins were quantified by summing up the abundances of allocated unique and razor peptides; resulting protein abundances are given in Table S1. Mitochondrial proteins were classified using the mitoCARTA 2.0 database (Calvo et al., 2016). Data were analyzed in RStudio (version 3.5.3), using the package DEP (Zhang et al., 2018). First, we filtered for proteins identified in all replicates of at least one condition; then, data were normalized using variance stabilizing transformation (vsn). Differential enrichment analysis was performed based on linear model. Identified proteins were considered as enriched in neurons if the log₂(fold-change value) was > 1 and enriched in astrocytes if the log₂(fold-change value) was < -1 and pvalue < 0.05 (according to DEP output). Differentially enriched proteins (DEP) data are provided in Table S1. T-Distributed Stochastic Neighbor Embedding (t-SNE) was computed from data normalized in DEP package in RStudio, as well as the heatmap of all considered proteins and the distance matrix including hierarchical clustering. Gene Ontology analysis was performed in RStudio using the package “TopGO,” using exact Fisher test. Proteins were considered differentially enriched if log₂(fold-change) > |1| and pval < 0.05. Complete list of GO term is provided in Table S2. For Gene Set Enrichment Analysis (GSEA) the package “fgsea” in Rstudio was employed (Korotkevich et al., 2019). Complete list of GSEA term is provided in Table S2E.

Western Blot Analysis

Primary cultures of astrocytes or neurons were collected and lysed in RIPA buffer. Protein concentration was evaluated with RC DC Protein assay (Bio-Rad Laboratories); 60 μg of lysate was loaded in sodium dodecyl sulfate-polyacrylamide gel electrophoresis (SDS-PAGE) and transferred onto a polyvinylidene fluoride (PVDF) membrane. Depending on the size of the protein analyzed, different gel concentration was used. The primary and secondary antibodies used for Western Blot analysis are listed in Key Resources Table.

Immunocytochemistry

Cells were fixed in 4% paraformaldehyde (PFA) in PBS1X for 10 min. at room temperature, washed in PBS1X twice for 5 minutes, and stored up to a month at 4°C before staining. For Prdx2 staining, cells were fixed in ice-cold Methanol 20% for 10 minutes, washed twice in PBS1X for 10 minutes, and subsequently stored and treated as other samples. Specimen were incubated in primary antibodies (for concentration see Key Resources Table) in PBS1X containing 3% Bovine Serum Albumin (BSA) and 0.5% Triton X-100 for 2 hours at room temperature or overnight at 4°C. After washing twice for 5 minutes with PBS, cells were incubated with the appropriate species- or subclass-specific secondary antibodies, with or without DAPI to label nuclei (blue), diluted 1:10000, for 1 hour in the dark at room temperature. Optionally, after incubating with primary antibodies and washing with PBS, biotin-labeled secondary antibodies were used at a dilution of 1:200 for 1 hour, followed by streptavidin-coupled fluorophores (1:500) for another hour. Coverslips were then mounted with Aqua Poly/Mount (Polysciences, Warrington, PA). Samples were imaged at the LSM710 laser-scanning confocal or Axio Observer Z1 epifluorescence microscope (Carl Zeiss). Digital images were acquired using the ZEN software (Carl Zeiss) at 80X, 40X or 25x.

RNA extraction, retro-transcription and Real Time Quantitative PCR (qRT-PCR)

RNA was extracted using Arcturus PicoPure RNA Isolation Kit (Thermo Fisher Scientific) according to the manufacturer’s instructions, including removal of genomic DNA. 100ng RNA was reverse transcribed using the ThermoFisher cDNA first strand kit. Each cDNA sample was diluted 1:5. qPCR reactions were performed on an Applied Biosystems QuantStudio 6 Flex Real-Time PCR System, or Roche LightCycler 480. Each 10 μL reaction consisted of 5 μL of PowerUp SYBR Green Master Mix (Thermo Fisher), 0.05 μL of forward and reverse primer (100 μM) and 5 μL of DNA appropriately diluted. qRT-PCR primers can be found in Key Resource table. The expression of each gene was analyzed in triplicate. Data were subjected to normalization by using *Gapdh* as housekeeping genes and expressed as mRNA fold change compared to control. Quantification was performed on 3 independent biological samples, each time as technical triplicate. Off targets were selected from the UCSC genome browser, potentially targeting intergenic as well as exon regions. Primers are listed in Methods S1.

STAgR cloning

For generation of STAgR cloning fragments, we followed previously published protocols (Breunig et al., 2018a, 2018b; Gibson, 2011). In particular, we generated individual cloning fragments for Gibson assembly by PCRs on 10 ng of vector templates (STAgR_Neo, STAgR_gRNAScaffold_hU6, STAgR_gRNAScaffold_hH1, STAgR_gRNAScaffold_h7SK and/or STAgR_gRNAScaffold_mU6). The mix contained 10 μl of high fidelity (HF) buffer, 1 μl of 10 mM dNTPs, 0.25 μl of overhang-primers (see key resources), 0.5 μl of HF polymerase, 1.5 μl of dimethyl sulfoxide (DMSO) and enough H₂O to reach a final volume of 50 μl. Reactions were incubated on a thermocycler as follows: 1 cycle of 98°C for 1 min 30 s; 38 cycles of 98°C for 10 s, 59°C (for gRNA scaffold)/ 68°C (for SAM loop) for 10 s, 72°C for 30 s (for inserts) / 1 min 30 s (for vectors); 1 cycle of 72°C for 10 min. 44.5 μl of the PCR reaction were mixed

with 0.5 μl of DpnI enzyme (10 units) and 5 μl of buffer, then incubated for 1 h at 37°C. DNA purification was achieved through incubation with 90 μl of magnetic beads for 2 min at room temperature (RT). Beads were pelleted through a magnet and washed twice with 70% ethanol without complete resuspension. The pellet was then dissolved in 20 μl H₂O and separated from the beads. DNA concentration was measured using a spectrophotometer. Gibson Assembly has been performed following a homemade Gibson assembly mix. The 5x isothermal reaction buffer is composed as follows: 1 M Tris (Tris(hydroxymethyl)aminomethane)-HCl (pH 7.5), 300 μl of 1 M MgCl₂, 60 μl of 100 mM dGTP (deoxyguanosine triphosphate), 60 μl of 100 mM dATP (deoxyadenosine triphosphate), 60 μl of 100 mM dTTP (deoxythymidine triphosphate), 60 μl of 100 mM dCTP (deoxycytidine triphosphate), 300 μl of 1 M DTT (dithiothreitol), 1.5 g of PEG-8000 (polyethylene glycol), 300 μl of 100 mM NAD (nicotinamide adenine dinucleotide) and enough H₂O to obtain 6 ml. For the assembly master mix, 320 μl of 5x isothermal reaction buffer was combined with 697 μl of H₂O, 3 μl of 10 U/ μl T5 exonuclease, 20 μl of 2 U/ μl DNA polymerase and 160 μl of 40 U/ μl Taq DNA ligase. 7.5 μl of assembly master mix have been mixed with 2.5 μl of insert and vector. A vector to insert ratio of 1:3 was used. Samples were incubated at 50°C for 60 min and subsequently transformed into *E. Coli*. Resulting plasmids have been sequenced by the Sanger sequencing method with the following primers: StAgR_seq_fwd1 (GAGTTAGGGGCGGGACTATG), StAgR_seq_fwd2 (ACTGGATCCGGTACCAAGG) and StAgR_seq_rev (TTACGGTTCCTGGCCTTTTG). Verified inserts have been cut with KpnI and subcloned into pCDNA-miniCMV-GFP. Primers for gRNA are listed in [Methods S1](#) table.

Live-Imaging Microscopy

Continuous live imaging was performed with a Cell Observer (Zeiss) at a constant temperature of 37°C and at 5% CO₂. Phase-contrast images were acquired every 10 min and fluorescence pictures every 4 hours for 6 days using a 10x phase contrast objective (Zeiss) and an AxioCam HRm camera with a self-written VBA module remote controlling Zeiss AxioVision 4.7 software (TAT, Prof. Dr. Timm Schroeder). Movies were assembled and analyzed using ImageJ (NIH) software, as also described in [Gascón et al. \(2016\)](#). In [Figure 4B](#) data are shown as pool of five independent biological replicates; in [Figures 4C–4G](#) all cells considered from all biological replicates are shown, indicated by different colors; statistics was performed on the 5 biological replicates using linear regression in Rstudio (see below).

QUANTIFICATION AND STATISTICAL ANALYSIS

When virus was used to induce neuronal conversion ([Figure 1](#); [Figure S2](#); [Figure 3](#); [Figure S3](#); [Figure 4](#)), astrocytes were fixed at the days after transduction, as indicated in the figures. Quantification for neuronal cells was based on β -III-tubulin immunoreactivity and morphological parameters, e.g., appearance of processes longer than 3x the cell soma as in [Gascón et al. \(2016\)](#). Astrocytes were quantified based on morphological features and Gfap expression, though Gfap is downregulated following direct conversion. For quantification in [Figure 2](#) and [Figure S2](#), we selected 10 transduced cells per each condition (DsRed, Ascl1-ires-DsRed at day 1 and day 3, and DsRed, Ascl1-ires-DsRed with neuronal morphology or astrocytic morphology at day 5 and 7). ImageJ (v1.52p) was used to define a region of interest (ROI) outlining a selected cell in order to measure the signal intensity for a given protein. To prevent a possible bias due to the different mitochondrial content in astrocytes and neurons, we also evaluated the intensity of Tomm20, a pan-mitochondrial protein. For each ROI, after subtracting the background value, we divided the intensity of the protein of interest by the corresponding Tomm20 expression, and log transformed the value. The colocalization analysis was conducted using the Coloc2 plugin for ImageJ.

For time-lapse experiment quantifications ([Figure 4](#) and [Figure S4](#)), cells were tracked in every frame of the movie. GFP⁺/DsRed⁺ cells acquiring neuronal morphology, with processes longer than 3x the cell soma, were quantified among the total GFP⁺/DsRed⁺ cells, as previously published ([Gascón et al., 2016](#)). In total, 158 cells were tracked in controls and 177 in Ascl1+Prdx2-Sod1 over n = 5 biological replicates.

Morphological analysis of reprogrammed neuronal cells ([Figures 3F–3H](#)) was performed with the ImageJ plugin SNT (simple Neurite tracer) ([Ferreira et al., 2014](#)) and different parameters were measured. Sholl analysis, also in ImageJ, was performed on each of the traced neurons: a step size of 10 μm was maintained constant, with the first radius defined according to the soma of each cell. We evaluated 3–4 neurons per condition, in 4 biological replicates. Data were analyzed with Microsoft Excel, GraphPad Prism 7.0 software and linear regression using “lm” function (R Stats package) in RStudio. Evaluation of the residuals for fitted linear models was performed with the package “DHARMA” ([Hartig and Lohse, 2020](#)) in RStudio.

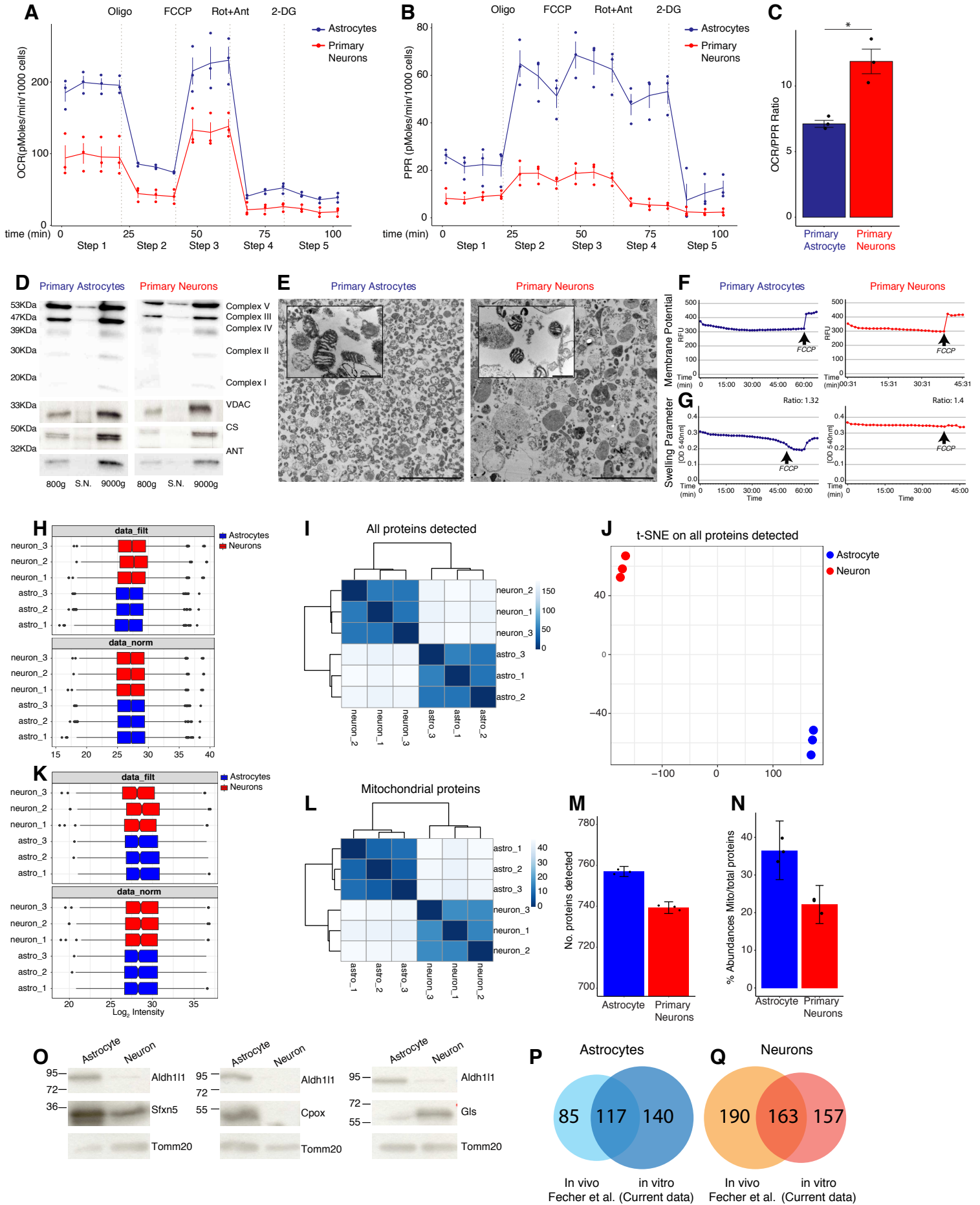
Statistics on the reprogramming efficiency in [Figure S2](#) and [Figure 4](#) was performed as follows: reprogramming efficiency was log₂ transformed, in order to reduce differences in variance across experiments and to fit the data to a normal distribution. Then, linear regression model was used, together with “DHARMA” package to evaluate the residuals. Statistics on [Figure 2](#) and [Figure S3](#) was performed log₂-transformed ratio. Statistics on [Figure 4](#) was evaluated using paired t test. The number of biological replicates is indicated in the corresponding Figure legends. Data are plotted as mean \pm standard error of the mean (SEM). Significance is based on the p value indicated on the graphs as * p \leq 0.05, ** p \leq 0.01, ***p \leq 0.001.

Supplemental Information

**CRISPR-Mediated Induction
of Neuron-Enriched Mitochondrial Proteins
Boosts Direct Glia-to-Neuron Conversion**

Gianluca L. Russo, Giovanna Sonsalla, Poornema Natarajan, Christopher T. Breunig, Giorgia Bulli, Juliane Merl-Pham, Sabine Schmitt, Jessica Giehl-Schwab, Florian Giesert, Martin Jastroch, Hans Zischka, Wolfgang Wurst, Stefan H. Stricker, Stefanie M. Hauck, Giacomo Masserdotti, and Magdalena Götz

Figure S1



SUPPLEMENTAL MATERIAL

Figure S1, related to Figure 1. Astrocytes and neurons from cerebral cortex differ in mitochondrial function

- (A-B) Longitudinal traces of extracellular flux analysis measured by Seahorse XF analyzer, comparing the Oxygen Consumption Rate (A) and the Proton Production Rate (B) of astrocytes (blue) versus neurons (red) over time, after challenging the cells with different ETC inhibitors. Values are normalized per 1000 cells. Each time point is shown as mean \pm SD. n=3 experimental batches for each group.
- (C) Barplot showing OCR/PPR ratio in cultures of primary astrocytes versus neurons, as measured by Seahorse XF analyzer. * $p \leq 0.05$. n=3 for each group.
- (D) Immunoblot detection of mitochondrial proteins in different fractions (800g, nuclear; S.N., cytosolic; 9000g, mitochondria and other organelles) isolated from astrocytes or neurons.
- (E) Electron Microscopy images of mitochondria isolated from astrocyte and neuron cultures. Scale bar: 5 μ m. Magnifications scale bar: 500nm.
- (F) Graphs showing the membrane potential of mitochondria isolated from astrocytes (*upper panel*) and neurons (*lower panel*) measured by Rhodamine 123 assay, indicating their healthy functional state.
- (G) Graphs showing the swelling parameter of mitochondria isolated from astrocytes (*upper panel*) and neurons (*lower panel*) by absorbance at 540nm indicating their healthy functional state.
- (H) Boxplot depicting abundances of all proteins before (*upper panel*) and after (*lower panel*) normalization.
- (I) Unsupervised cluster analysis of the samples considering all quantified proteins.
- (J) *t*-SNE of the samples, based on all proteins after normalization.
- (K) Boxplot depicting abundances of mitochondrial proteins selected according to mitoCarta before (*upper panel*) and after (*lower panel*) normalization.
- (L) Unsupervised cluster analysis of the samples considering only mitochondrial proteins.
- (M) Barplot showing the number of mitochondrial proteins identified by mass spec in astrocytes (blue) and neurons (red). Each dot represents a biological replicate.
- (N) Barplot depicting the percentage of mitochondrial protein abundance over total protein abundance in astrocytes (blue) and neurons (red). Each dot represents a biological replicate.
- (O) Western blots of total lysates from cultured astrocytes or neurons confirming the selective cell enrichment by high amounts of Adlh111 in astrocyte lysates, equal mitochondrial protein loading by Tomm20 and the higher amount of Sfxn5 and CpoX in astrocytes and Glis in neurons.
- (P,Q) Venn Diagrams of all astrocyte-enriched (I) and neuron-enriched (J) mitochondrial proteins detected by Fecher et al. and our analysis showing a high degree of overlap given that mitochondrial proteins were isolated at different stages (adult versus postnatal), from different regions (cerebellum versus cortex) and in different conditions (*in vivo* versus *in vitro*).

Figure S2

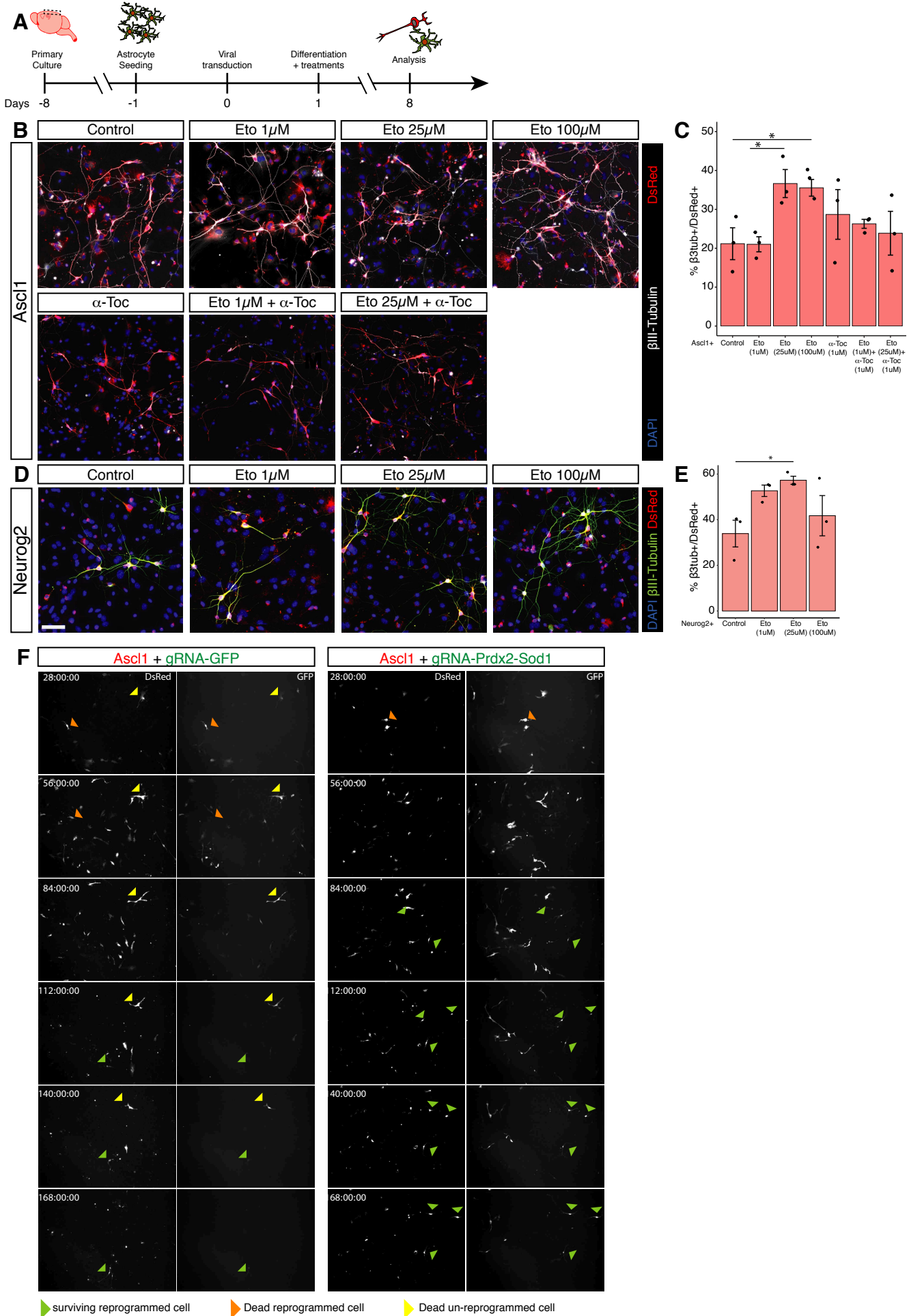


Figure S2, related to Figure 1 and 4. Etomoxir treatment improves direct neuronal reprogramming.

(A) Schematic drawing of the experimental setup.

(B) Micrographs showing the Ascl1-transduced cells (DsRed⁺) that are β III-tubulin⁺ neurons (in white), nuclei labeled in DAPI (Blue), in the treatment conditions indicated. Scale bar: 50 μ m.

(C) Histogram depicting the percent of β III-tubulin⁺ cells amongst Ascl1-transduced DsRed⁺ cells at 8 DPI. Data are shown as mean \pm SEM. Each dot represents a biological replicate (n=3 for experimental condition). *p \leq 0.05

(D) Micrographs showing the efficiency of neuronal conversion in upon Neurog2 expression together with treatment of different concentration of Etomoxir. Reprogrammed neurons (DsRed⁺) are β III-tubulin⁺ (in white). Nuclei labeled in DAPI (Blue). Scale bar: 50 μ m.

(E) Histogram depicting the percentage of β III-tubulin⁺ cells amongst Neurog2-transduced DsRed⁺ cells at 8 DPI. Data are shown mean \pm SEM. Each dot represents a biological replicate (n=3 for experimental condition). *p \leq 0.05

(F) Example of fluorescent pictures acquired during the imaging and used for analysis (related to **Figure 4**).

Figure S3

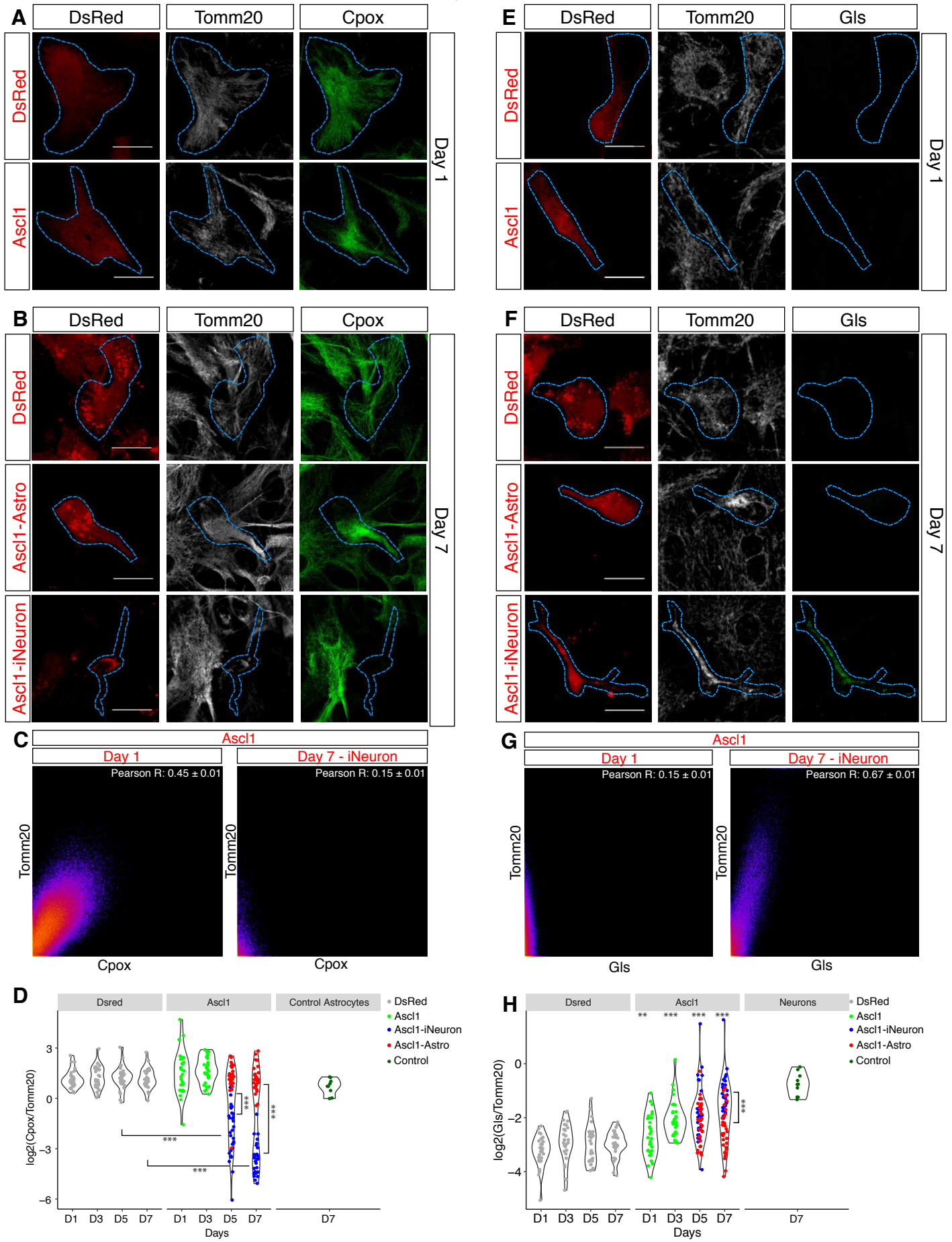


Figure S3, related to Figure 2. Mitochondrial protein changes during astrocyte-to-neuron reprogramming

(A, B) Micrographs showing immunostainings of the astrocyte-enriched mitochondrial protein Cpx in astrocytes transduced with DsRed (control) or Ascl1-ires-DsRed at 1 (A) or 7 (B) DPI as indicated. Mitochondria are identified by the expression of Tomm20. Scale bar: 20 μ m.

(C) Example of scatter plot of the pixel intensity correlation between Tomm20 and Cpx in Ascl1-transduced cells at 1 (*left panel*) and 7 (*right panel*) DPI. Pearson's coefficient as average of 3 cells/biological replicate; n=3 biological replicates.

(D) Violin plot depicting the log₂-ratio of the intensity of the expression of Cpx versus Tomm20 over time (D1, D3, D5, D7) and in cortical astrocyte cultures at day 7. Each dot represents 1 analyzed cell. 10 cells analyzed per biological replicate, each condition. n=3 biological replicates; ***p \leq 0.001.

(E, F) Micrographs showing the expression of the neuron-specific mitochondrial protein Prdx2 in astrocytes transduced with DsRed (control) or Ascl1-ires-DsRed at 1 (E) and 7 (F) DPI. Mitochondria are identified by the expression of Tomm20. Scale bar: 20 μ m.

(G) Example of scatter plot of the pixel intensity correlation between Tomm20 and Gls in Ascl1-transduced cells at 1 (*left panel*) and 7 (*right panel*) DPI. Pearson's coefficient as average of 3 cells/biological replicate; n=3 biological replicates.

(H) Violin plot depicting the log₂-ratio of the intensity of the expression of Gls versus Tomm20 over time (D1, D3, D5, D7) and in E14 cortex-derived cultures at 7 days in vitro. Each dot represents 1 analyzed cell. 10 cells analyzed per biological replicate, each condition. n=3 biological replicates; ***p \leq 0.001.

Figure S4

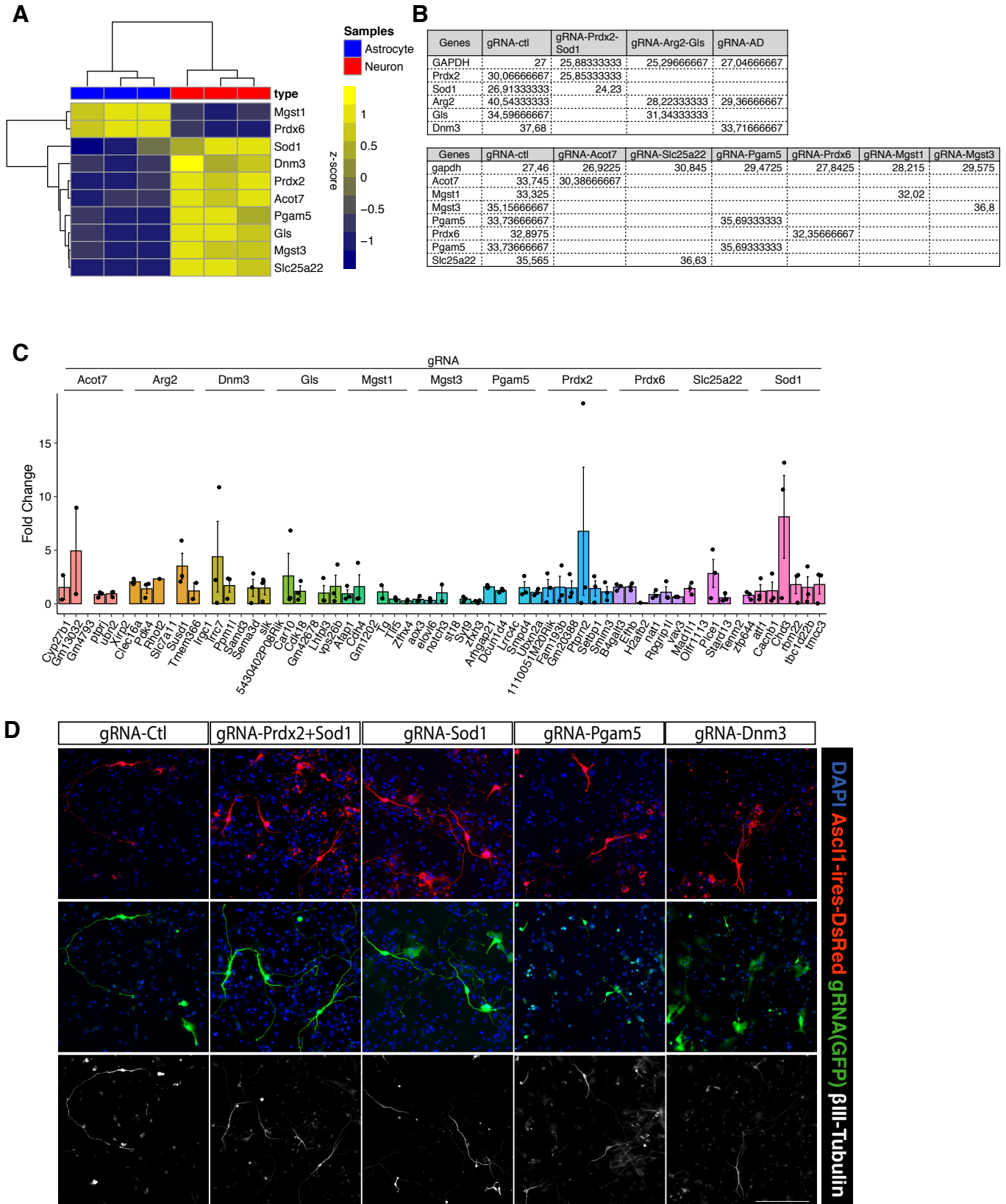


Figure S4, related to Figure 3. Characterization of selected candidates

(A) Unsupervised heatmap depicting the relative expression of the selected candidates.

(B) Graphs depicting the log₂-normalized abundance of the astrocyte-enriched (blue dots) and neuron-enriched (red dots) candidates, as analyzed in Figure 2. Each dot represents a biological replicate.

(C) Real Time quantitative PCR (RT-qPCR) showing the fold change of putative off-targets following the transfection of gene-specific gRNA. Data are shown as fold change over the gRNA-scramble control (mean ± SEM). None of this is significant over Paired t-test used. control. n=3 biological replicates for each group.

(D) Single channel immunofluorescence images showing reprogrammed neurons (β III-tubulin⁺-DsRed⁺-GFP⁺) transfected by Ascl1-ires-DsRed (red) and different STAgR constructs (green). Scale bar: 100 μ m.

2.2 Project 2

The aim of the second project was to understand the molecular mechanisms governing astrocyte identity and functions better. In this regard, we studied how the diverse functions of astrocytes in cortical GM is mediated by key TFs such as Sox9 and Trps1.

Single cell deletion and analysis of the transcription factors Sox9 and Trps1 reveals novel functions in astrocyte

Poornemaa Natarajan^{1,2,3,4}, Christina Koupourtidou^{2,3,5}, Thibault de Resseguier¹, Riccardo Bocchi^{1,2,6}, Judith Fischer-Sternjak^{1,2}, Sarah Gleiss¹, Diana Rodrigues¹, Mike Myoga¹, Jovica Ninkovic^{5,7}, Giacomo Masserdotti^{1,2*}, Magdalena Götz^{1,2,7*#}

Manuscript ready for submission

Author contributions:

M.G. and G.M. conceived and designed the project. **P.N. contributed to shaping the project, performed all experiments and data analysis.** C.K. helped performing stRNA-seq experiment, C.K. and J.N. provided the 5dpSWI scRNA-seq dataset for comparison with stRNA-seq data. T.D.R. characterized Trps1 expression in Olig2+ cells and contributed to the GFAP intensity analysis. R.B. helped with animal experiments, R.B. and J.F-S. provided the intact adult cortical GM scRNA-seq dataset. S.G., D.F. and M.M. performed the collection of cells for Patch-seq based scRNA-seq experiment. **P.N., G.M. and M.G. wrote the manuscript.** M.G. provided all the funding.

Due to elevated number of pages, Data tables S1-S6 are not included in the PDF version of this thesis, but they are provided separately.

Single cell deletion and analysis of the transcription factors Sox9 and Trps1 reveals novel functions in astrocyte

Poornemaa Natarajan^{1,2,3,4}, Christina Koupourtidou^{2,3,5}, Thibault de Resseguier¹, Riccardo Bocchi^{1,2,6}, Judith Fischer-Sternjak^{1,2}, Sarah Gleiss¹, Diana Rodrigues¹, Mike Myoga¹, Jovica Ninkovic^{5,7}, Giacomo Masserdotti^{1,2*}, Magdalena Götz^{1,2,7*#}

¹Physiological Genomics, Biomedical Center (BMC), Ludwig-Maximilians-Universität (LMU), Planegg-Martinsried, Germany

²Institute for Stem Cell Research, Helmholtz Center Munich, German Research Center for Environmental Health (GmbH), Neuherberg, Germany

³Graduate School of Systemic Neurosciences, Biocenter, LMU, Munich, Germany

⁴Max-Planck-Institute for Biochemistry, International Max Planck Research School for Life Sciences, Munich, Germany

⁵Department of Cell Biology and Anatomy, BMC, LMU, Planegg-Martinsried, Germany

⁶Current address: Department of Basic Neuroscience, University of Geneva

⁷Excellence Cluster of Systems Neurology (SYNERGY), Munich, Germany

* These authors contributed equally

Correspondence to: magdalena.goetz@helmholtz-munich.de

Abstract

Astrocytes play many roles in brain function, yet it is still poorly understood how these are orchestrated by pan-astrocyte transcription factors (TFs). Here we examined the function of a well-known pan-astrocyte TF Sox9 and the novel astrocyte TF Trps1 (Transcriptional Repressor GATA Binding 1) by Cas9-mediated deletion in vivo using Mokola-pseudotyped lentiviral delivery into the adult cerebral cortex. The consequences of deletion of either Sox9, Trps1 alone or simultaneously were explored at single cell level (by patch-seq based single cell transcriptomics) and tissue level (by spatial transcriptomics). This revealed TF-specific astrocyte functions like synapse maintenance and immune response and generally reduced effects when both TFs were deleted, implicating them in common regulatory networks. Most importantly, we noticed unexpected changes in oligodendrocytes and other immune cells upon astrocyte specific TF deletion. Our study reveals hitherto unknown functions of Sox9 and Trps1 in astrocytes and their communication with neurons, other glial and immune cells.

Introduction

Astrocytes are integral to numerous homeostatic functions throughout the central nervous system. While the importance of transcription factors (TF) is well documented in astrocyte fate specification (Kang et al., 2012; Tiwari et al., 2018), their roles in mature astrocytes and their involvement in astrocyte heterogeneity is largely elusive. For example, the TFs Sox9 and Nfia, Nfib have been implicated in astrocyte specification (Deneen et al., 2006; Kang, Lee et al., 2012; Klum, Zaouter et al., 2018) and are still rather ubiquitously expressed in adult astrocytes (Sun et al., 2017). Such pan-astrocyte TFs may play unique and region specific roles in astrocytes during postnatal development (Cheng et al., 2023), in the intact adult brain (Huang, Woo et al., 2020; Ung, Huang et al., 2021), in astrocyte response to injury (Laug, Huang et al., 2019) or disease (Glasgow et al., 2017; Sardar, Chen et al., 2022). Interestingly, Sox9 was shown to have a role only in specific brain regions, and no role for Sox9 has been discovered yet in the cerebral cortex (Cheng et al., 2023; Ung, Huang et al., 2021).

We therefore set out to explore the function of Sox9 at the single cell level in the cortical grey matter (GM) astrocytes, thereby taking into account possible cellular heterogeneity. We further examined the expression and function of a novel TF Trps1 (Transcriptional Repressor GATA Binding 1 or Tricho-Rhino-Phalangeal Syndrome Type I), that has been found in many gene expression studies in astrocytes (Endo et al., 2022; Ohlig, Clavreul et al., 2021; Sirko et al., 2015). Notably, in other cell types such as chondrocytes or hair follicle epithelium, Trps1 and Sox9 are involved in similar transcriptional cascades (Fantauzzo et al., 2012; Tan, Niu et al., 2018) and this prompted us to explore the roles of Sox9 and Trps1 in the adult cortical GM astrocytes. Furthermore, Trps1 was also predicted to be a TF driving both astrocyte and oligodendrocyte fate during development (Weng, Wang et al., 2019), but its precise expression, especially at the protein levels, and function in adult astrocytes is entirely unknown.

In pronounced difference to previous analysis of adult astrocyte TF functions, we scrutinized the expression and performed functional analysis at the single cell level to unravel possible subtype-specific functions. To explore the possible intra-regional heterogeneity, we characterized the Sox9 and Trps1 expression in the adult cortex GM and noticed a remarkable degree of heterogeneity at protein level. This highlights the need to explore their function at the single cell level. To do so, we deleted Sox9 and Trps1 either alone or simultaneously using Cas9-mediated strategy, targeted to astrocytes by use of pseudotyped lentiviruses and analyzed the effects at the single cell level using Patch-seq based single cell RNA-sequencing (scRNA-

seq). This analysis revealed TF-dependent alterations in gene expression related to unique astrocyte functions, involved in synaptic regulation and the immune reaction elicited by the viral vector injection. As these pointed to non-cell autonomous functions, we performed spatial transcriptomics (10x Visium, stRNA-seq) which revealed unexpected effects of astrocyte specific TF deletion in their surrounding onto oligodendrocytes as well as several cell types from the immune system. Most strikingly, we found that Sox9 and Trps1 function is often antagonistic with the double deletion abolishing effects of the single deletions. Their most prominent roles affect synaptic maintenance, oligodendrocyte differentiation and immune cell reaction to injury. Thus, Sox9 and Trps1 are involved in governing several functions of mature cortical astrocytes with widespread effects upon their loss, placing them at the nexus of brain homeostasis.

Results

Cortical astrocytes show heterogeneity in Sox9 and Trps1 levels

As Trps1 has been detected in several RNA-seq studies of astrocytes, but never explored at the protein level in the brain, we examined its expression along with Sox9 and S100 β (as a general marker for astrocytes) by immunohistochemistry in the cerebral cortex of young adult mice (2-3 months old) (Figure 1A and B). First, we monitored the distribution of immunopositive cells across a cortical column divided into five equal bins and quantified the percentage Sox9+S100 β + or Trps1+S100 β + astrocytes per bin (Figure 1D and E). Most S100 β astrocytes were also positive for Sox9 (Figure 1H) and this did not vary much across the bins (Figure 1D). Conversely, only 40% of the S100 β + astrocytes were immunopositive of Trps1, most of which were also Sox9+ (Figure 1H). We also observed a non-significant trend of S100 β + astrocytes positive for Trps1 higher in the upper than lower bins (Figure 1E). Among all the Sox9+ cells in the cortical GM, most were immunopositive for S100 β or Trps1 (ED Figure 1A), but only 35.5% of the Trps1+ cells were immunopositive for S100 β or Sox9 (ED Figure 1B). To verify if other glial cells express Trps1, we performed immunostainings for Trps1, Olig2 and S100 β in the adult cortex. To our surprise, about 50% of the Olig2 positive oligodendroglial lineage cells were also positive of Trps1 (ED Figure 1C) suggesting that like in the developing brain, Trps1 is expressed in both astrocyte and oligodendrocyte lineage also in the adult brain. To evaluate whether Sox9 and Trps1 show heterogeneity at the protein level we measured their fluorescence intensity within each bin of the cortical column. The normalized corrected total cell fluorescence (CTCF) for Sox9 and Trps1 showed remarkable heterogeneity (as observed

in the color-coded dot plot; Figure 1C). While the fluorescence intensity of Sox9 did not show considerable variation across the bins (Figure 1F), Trps1 expression was more layer dependent (Figure 1G). More cells with lower levels of Trps1 were present in the upper layers (UL, bins 1-2), while Trps1-high cells were present in the deeper layers (DL, bin 4 & 5, with significantly more Trps1-high cells in bin 5 than bin 1, $p < 0.05$). This suggests that more S100 β ⁺ astrocytes expressing Trps1 but at lower level are present in the UL, while Trps1-high cells located in cortical DL are likely not astrocytes but rather oligodendrocyte lineage cells.

As intra-regional heterogeneity in astrocytes at the level of transcriptome has been observed before (Bayraktar et al., 2020; Lanjakornsiripan, Pior, Kawaguchi et al., 2018; Ohlig, Clavreul et al., 2021), we wanted to explore if Sox9 and Trps1 RNA are also expressed heterogeneously within cortical GM astrocytes. For this, we made use of scRNA-seq data (10x) from Bocchi et al., (*submitted*) where cells from cortical GM, white matter (WM) and sub-ependymal zone (SEZ) were taken by means of a biopsy punch without any specific selection for astrocytes. We subsetted this dataset for cells from the cortical GM that were annotated as astrocytes and re-clustered this data. This resulted in 3150 cells which separated into 6 clusters (ED Figure 1D) showing a clear astrocyte signature (“Astrocyte score”, genes shown in Data Table S6). Interestingly Sox9 and Trps1 show a huge variation; cells in cluster C expressed lowest levels of both *Sox9* and *Trps1*, while clusters A and E expressed high levels of both (ED Figure 1E). These express almost no, or very low levels of other glial lineage specific genes such as *Olig2* or *Sox10* for the oligodendrocyte lineage and *Tmem119* or *Aif1* (*Ibal*) for microglia (ED Figure 1F). Remarkably, each cluster had unique gene expression profile (ED Figure 1G; Data Table S1), Gene Ontology (GO) for genes enriched in each cluster revealed specialized functions (ED Figure 1H). For example, cluster C astrocytes (with low levels of *Sox9* & *Trps1*) expressed genes involved in pathways like “mitochondrial respirasome” and “myelin sheath formation”, while cluster E (with high levels of both *Sox9* & *Trps1*) expressed genes involved in “gliogenesis”, “fatty acid metabolic process”.

CRISPR mediated deletion of Sox9 and Trps1 in astrocytes

Given the interesting heterogeneity observed above, we aimed to explore the effects of Sox9 and Trps1 deletion in cortical GM astrocytes at the single cell level. To do so we used a CRISPR (Clustered Regularly Interspaced Short Palindromic Repeats)/ Cas9 mediated strategy, delivering the respective gRNAs to astrocytes by Mokola- pseudotyped lentivirus (Mok-LV) (Watson et al., 2002) in a transgenic mice expressing Cas9-GFP ubiquitously (Platt et al., 2014). Two gRNAs per gene, targeting different exons for efficient knockdown were used and

multiplexed (Breunig et al., 2018) targeting either only Sox9, only Trps1 or Sox9 and Trps1 simultaneously, in a vector also expressing a fluorescent reporter in the transduced cells under a CMV promoter (Figure 2A). First, we confirmed the specificity of Mok-LV to target astrocytes injecting with the control gRNA (g-Control) Mok-LV at a titer of $1-5 \times 10^8$ titer units per milliliter (TU/ml) into the somatosensory cortex. This resulted in a substantial number of infected cells in the injected region both at 7 or 21 days post injection (dpi, Figure 2B); more than 80% of the transduced cells were immunopositive for astrocyte markers such as S100 β or GFAP (Figure 2C) at both time points. Thus as previously shown, the Mokola pseudotype targets astrocytes with high specificity and efficiency.

We next injected Mok-LV expressing gRNAs against Sox9 (g-Sox9) or Trps1 (g-Trps1) or both (g-Sox9+Trps1) and examined the protein levels of these TFs in the targeted astrocytes. Animals injected with g-Sox9 or g-Sox9+Trps1 showed a significant reduction in the number of Sox9+ cells at 7 (Figure 2D and D') and 21dpi (ED Figure 2C and E); likewise, almost no Trps1+ astrocytes were found in animals injected with g-Trps1 (Figure 2E and E'; ED Figure 2D and F). Conversely, Trps1 levels were more variable in the g-Sox9+Trps1 injections (Figure 2E').

Next, we examined if astrocytes retain their main hallmarks, such as their morphology and pan-astrocyte marker expression. Indeed, most astrocytes had their normal bushy morphology (Figures 2D, E). Likewise, most infected cells retained S100 β and GFAP protein at 7dpi (Figure 2F & G, ED Figure 2A) and 21dpi (ED Figure 2B).

Patch-seq based scRNA-seq reveals changes in a multitude of astrocyte functions after deletion of Sox9, Trps1

To examine the consequences of Sox9 and Trps1 deletion in astrocytes at the single cell level, we performed Smart-seq2 based Patch-seq of astrocytes (Cadwell, Palasantza et al, 2015; Cadwell et al, 2017). For this, individual astrocytes were patched establishing a gigaOhm seal in acute cortical slices of animals injected with g-Control, g-Sox9, g-Trps1 and g-Sox9+Trps1 to collect their cytoplasm and nucleus (Figure 3A). Overall, we collected 40 g-Control, 57 g-Sox9, 45 g-Trps1 and 39 g-Sox9+Trps1 cells across the two time points (7 and 21dpi). For a systematic and comprehensive analysis, we also collected 56 astrocytes from the intact cortex of Aldh1l1-eGFP animals, and several "slice-controls", in which the patch-clamp pipette was briefly in touch with the brain slices, but no gigaOhm seal was established and no cells were intentionally collected. Among the collected slice-controls, less than half (12 samples out of 30) had sufficient RNA and passed the quality control steps (ED Figure 3A). The cells could

broadly be divided into four clusters (PS0, PS1, PS2, PS3; Figure 3B). Surprisingly, though we collected cells over multiple batches, there was no apparent batch effects (ED Figure 3B) and the slice-control samples were distributed mostly in clusters PS1, PS2, and PS3. Further grouping based on the individual TF deleted (Figure 3B) or the time point (ED Figure 3B) could not be clearly inferred.

The intact astrocytes were distributed mostly in cluster PS0 and PS2, which show some level of astrocyte heterogeneity even within such few cells. Cluster PS1 appeared only in the condition of gRNA injection (irrespective of whether the cells were from control or deletion conditions), which pointed to the possibility that this signature may partly arise as a response to the mild injury of the Mok-LV injection. Expectedly, GO analysis for the differentially expressed genes (DEG) between g-Control cells and intact astrocytes show upregulation of terms like “positive regulation of response to external stimulus”, “response to interferon-gamma”, “antigen processing and presentation” in the g-Control cells (Figure 3D). This indicates an injury response signature that arises because of our mild injury during Mok-LV gRNA injection, also reflecting the reaction to injection of viral vectors (see also Mattugini, Bocchi et al., 2019 for reaction to different viral vectors).

To get a general overview of the effect of Sox9/ Trps1 deletion, we performed pairwise comparison of the deletion conditions with the g-Control cells to understand the gene expression changes irrespective of the time point. Indeed, the deletion of each TF elicited profound changes in gene expression changes unique to each condition (Figure 3C). Upon Sox9 deletion, 646 significant DEGs were detected (457 upregulated, 189 downregulated). Remarkably, most g-Sox9 downregulated genes were also downregulated after Trps1 or Sox9+Trps1 deletion (ED Figure 3E), suggesting a common signature following deletion of either of these TFs. Conversely, most of the up-regulated genes were exclusive to the Sox9 deletion condition (Figure 3D, ED Figure 3D). Trps1 deletion resulted in 767 significant DEGs (414 up-, 353 down regulated), many of which were significant only in the g-Trps1 condition. Following g-Sox9+Trps1 deletion, fewer significant DEGs were detected, most of which were downregulated (70%, 266 genes) only in this condition (Figure 3D, ED Figure 3D and E). These data suggest that Sox9 may be involved in upregulation of the DEGs after Trps1 deletion. Vice versa, Trps1 seems to help upregulating, directly or indirectly, the DEGs upregulated upon Sox9 deletion, as these upregulated DEGs virtually vanished in the double-deletion (Figure 3C).

Although Sox9 is traditionally known as an activator of transcription, it may be involved in indirectly repressing genes by competing for co-factors (Yang, Gomez et al., 2023). Similarly, Trps1 although initially identified as a transcriptional repressor (Fantauzzo et al., 2012; Malik,

2001), it has also been found to act as a transcriptional activator (Fantauzzo and Christiano, 2012; Witwicki, Ekram et al., 2018; Wuelling et al., 2020). Thus, both Sox9 and Trps1 may function as either an activator or a repressor depending on the context.

To get a better idea about possible direct targets of Sox9 and Trps1, we overlapped the significant DEGs with the known targets of Sox9 and Trps1 based on ChIP data for Sox9 in chondrocytes (Ohba, He et al., 2015) and Trps1 in breast cancer cells (Witwicki, Ekram et al., 2018). Notably, a number of genes were commonly predicted as Sox9 and Trps1 targets (3293 genes, i.e., 53% of Trps1 targets were shared with 33.3% of Sox9 targets) (ED Figure 3F). More than 50% of the up or downregulated genes were predicted to be either an exclusive Sox9 target or a common predicted target of Sox9 and Trps1 in all conditions (ED Figure 3G). Very few of the DEGs were predicted to be an exclusive target of Trps1 (10% or lesser), suggesting that more genes may be regulated by Sox9 or co-regulated by Sox9 and Trps1 in astrocytes.

To gain more function-oriented insights into the consequences of deleting these TFs, we performed GO analysis for the significant DEGs in each condition. Interestingly, in all the three deletion conditions (g-Sox9, g-Trps1 and g-Sox9+Trps1), pathways related to immune response such as “response to interferon-gamma” and “response to interferon-beta” were downregulated (i.e., *Igtp*, *Gbp3*; Figure 3F-H), as well as “antigen presentation” when deleting Trps1 (Figure 3G) or “regeneration” was downregulated when deleting Trps1 and Sox9 (Figure 3H). This may imply an attenuated injury response upon deletion of these TFs.

Common pathways related to the astrocytic function of synapse maintenance (like “synapse organization”, “neurotransmitter transport” or “secretion”) were upregulated in the g-Sox9 and g-Trps1 conditions, albeit with different genes enriched in both the cases (Figure 3E, F, Data Table S2). Interestingly, pathways related to gliogenesis (with genes such as *Fgfr3*, *Hes5*, *Nfix*, *Zfp365* in case of g-Sox9, Figure 3E) or glial cell differentiation (with genes such as *Zfp365*, *Hes1* in case of g-Trps1, see Data Table S2) were also upregulated. The deletion of both, Sox9 and Trps1, showed upregulation of genes related to GTPase activity and morphogenesis (Figure 3H). Thus, both of these TFs regulate synaptic functions, signaling and gliogenesis. Specifically for the Sox9 deletion, however, mostly terms related to metabolic functions were upregulated (Figure 3F). This is of interest as the cluster C of cortical GM astrocytes with endogenously low levels of Sox9 and Trps1 had mostly metabolic functions.

To understand the dynamics of gene regulation better, we distinguished the early and late time points (7 and 21dpi). The comparison of the TF deletions at 7 and 21dpi with the g-Control cells of the corresponding time points showed dynamic change in the direction of up- and down

DEGs. While most of the DEGs were exclusively upregulated in the g-Sox9 condition at 7dpi, very few genes were upregulated by 21dpi, suggesting that repressive functions, possibly indirect, dominate the earlier time point, while gene activation dominates the later time point of Sox9 deletion (ED Figure 4A and B). Notably at 21dpi, more than half of the DEGs upregulated in the g-Sox9 condition were also upregulated in the g-Trps1 condition. Notably, the Trps1 deletion profile was opposite of Sox9 with most downregulated DEGs in the g-Trps1 condition at 7dpi, while a large fraction of the DEGs were upregulated by 21dpi. At both the time points, fewer genes were among significant DEGs in the g-Sox9+Trps1 condition, suggesting that Sox9 and Trps1 mediate some of the DEGs in the single deletion conditions, respectively. GO analysis of the DEGs specific to each condition and time point showed consistent downregulation of immune response related pathways such as “response to interferon-gamma”, “response to interferon-beta”, “antigen processing and presentation” in all the conditions, at both 7 & 21dpi (ED Figure 4C-E). On the other hand, many pathways related to translation and signal transduction by p53 class mediator were only transiently regulated in both g-Sox9 and g-Trps1 conditions (see Data Table S3).

Loss of Sox9 and Trps1 triggers alteration in the surrounding synapses

As GO terms related to pathways involved in synapse organization were regulated after Trps1 (Figure 3F) and Sox9 (Data Table S2) deletion, we explored if the number of synapses may be affected in any of the conditions. Towards this aim, we immunostained for the pre-synaptic protein synaptophysin, and excitatory post-synaptic protein Homer1 in sections from animals injected with the gRNAs. Confocal images were taken at a magnification of 40X (with a 2.5x zoom) and each image contained 1-3 infected astrocytes. The images were deconvolved and the astrocyte surface was reconstructed on Imaris. Following this, we calculated the number of pre- and post-synaptic puncta in the regions surrounding the astrocyte (within a distance of 0-1.5 μ m from the astrocyte surface). All post-synaptic puncta closest to a pre-synaptic puncta (within a distance of 0.2 μ m) was considered as a “synapse”. While we did not see any change in the number of pre-synaptic puncta and post-synaptic puncta individually (data not shown), we see a trend towards decrease in the number of synaptic puncta where both synaptic markers coincide within 1.5 μ m distance around astrocytes after Trps1 deletion (Figure 3H).

Non-cell autonomous effects of Sox9 and Trps1 deletion in cortical astrocytes revealed by spatial transcriptomics

Astrocytes are essential for brain homeostasis and we noticed changes in the synapse numbers at the tissue level upon *Trps1* loss in astrocytes. To gain unbiased insights into how alterations of astrocytes lacking *Sox9* and/or *Trps1* may affect the surrounding cells and tissue microenvironment, we performed spatial transcriptomics (10x Visium, stRNA-seq) of the adult mouse cortex after injection of g-Control, g-*Sox9*, g-*Trps1* or g-*Sox9+Trps1* Mok-LVs. We chose the 7dpi time point to also gain insights into the astrocyte response to the injury and reaction to the Mok-LV injection.

Brains of the animals injected with the Mok-LVs were dissected at 7dpi, and 10 μ m thick sections were made at the cryostat. The sections were briefly checked for the presence of infected cells (Tdtomato⁺ cells) in the expected injection region (somatosensory cortex). Once in the region of injection, two consecutive sections containing infected cells were placed in one capture area each. The region of injection for each condition was defined based on the fluorescence images taken before tissue processing (Figure 4B). These are referred to as g-Control, g-*Sox9*, g-*Trps1* or g-*Sox9+Trps1* injection and the remaining regions are defined as the background tissue for the respective tissues henceforth. After quality control steps to remove spots with low gene numbers, counts or high mitochondrial or hemoglobin reads (ED Figure 5A and B), we performed clustering of the data. The initial clustering highlighted differences in the sub-cortical tissue regions (data not shown), and this can indeed be seen also in the anatomical position, the tissue was more rostral in one of the conditions (g-*Sox9*). As the injection of the Mok-LV was limited to the cortical GM, in line with our interest to understand the role of *Sox9/Trps1* in this region, we subsetted for spots located in the cortex GM in all four tissues and performed further downstream analysis. Clustering of these spots gave rise to 11 clusters, which were present in distinct anatomical regions, such as the different cortex layers (Figure 4C). These spatial clusters were rather unique, and had their own gene expression signature (Figure 4D). Of particular interest were clusters 0 and 4, which dominated the Mok-LV injection region, but the representation of these clusters was dependent on the condition in consideration (ED Figure 5C). The spots from the g-Control and g-*Sox9* injection were represented in clusters 0 and 4 at comparable levels. On the other hand, cluster 4 dominated the region of g-*Sox9+Trps1* injection with very few spots of cluster 0 in this condition. In the g-*Trps1* injection, cluster 4 was completely absent, and most spots were represented by cluster 0. Thus, deleting *Sox9* or *Trps1* in astrocytes resulted in gene expression differences at tissue level. Apart from cluster 0 and 4, cluster 8 also seemed to be a possible “injury” or *Sox9/Trps1* deletion specific feature. Unlike cluster 0 and 4, which were concentrated at the injection site, cluster 8 seemed to be more sparsely located. Overall, there were very few genes specific to

cluster 8 and only a small fraction of the genes unique to the injury specific clusters showed overlap (ED Figure 5D).

GO analysis showed that terms such as “antigen processing and presentation of peptide antigen” were upregulated in all three injury specific clusters, while terms such as “synapse organization”, “ion transport” and “microglial cell activation” were upregulated only in clusters 0 and 4, i.e. the clusters mostly found after Trps1 or Trps1 and Sox9 deletion. The GO term “response to interferon-gamma” was upregulated in clusters 4 and 8. These data thus demonstrate that Sox9 and/or Trps1 deletion in astrocytes affects the entire reaction of the cortical tissue to injury. Interestingly, only in the cluster 0 dominant after Trps1 deletion genes involved in metabolism such as “cellular respiration”, “mitochondrial metabolism” were upregulated (ED Figure 5E and Data table S4). This is particularly intriguing as such GO terms were also observed in the cortical GM astrocyte cluster C with endogenously low level of Sox9 or Trps1 (ED Figure 1).

Interestingly, the canonical cortical layering was largely maintained in the background tissue across all the four conditions. While clusters 7, 5, 9 and 1 represented the DL, clusters 2 and 3 represented the UL (Figure 4C). The expression pattern of known or predicted UL and DL neuronal and astrocyte markers (ED Figure 5F) in these clusters pointed to the same. A prominent exception to this was in the tissue of g-Sox9+Trps1, where the cluster 10 replaced the UL cluster 2. Even though located in the same anatomical position as cluster 2, cluster 10 showed a unique gene expression signature with only 8% of the genes being common with cluster 2 (ED Figure 5G). GO analysis of genes unique to this cluster showed enrichment of pathways like “cytoplasmic translation”, “antigen processing and presentation”, “exocytosis”, etc. (ED Figure 5H and Data table S4), pointing to possible widespread tissue level effects unique to the simultaneous deletion of Sox9 and Trps1 in astrocytes.

To get a general overview of the differences in the Mok-LV injection regions after deletion of Sox9 or Trps1, we performed pairwise-comparisons of g-Sox9, g-Trps1 and g-Sox9+Trps1 injection regions with the g-Control injection region. Fewer genes were significantly upregulated in all three conditions with more than 50% of the upregulated DEGs significant only in one of the conditions (Figure 4E). The condition of g-Trps1 and g-Sox9+Trps1 elicited downregulation of more genes, most of which were significant only in the respective conditions (Figure 4G). On the other hand, the g-Sox9 injection area showed downregulation of fewer genes, most of which were also downregulated in the g-Trps1 or g-Sox9+Trps1 injection region (Figure 4G). We performed GO analysis for the significant DEGs and this revealed some intriguing changes, some of which were in line with the observations from the Patch-seq data

(Figure 4F & H). We first focused on the comparison to the Patch-seq data (i.e. largely occurring in astrocytes), to separate changes in the targeted astrocytes from non-cell-autonomous changes and gain insights into the tissue wide non-cell-autonomous changes. Patch-seq had shown downregulation of immune response in all three conditions, but the stRNA-seq data indicated downregulation of immune response related pathways only in the g-Sox9 and g-Trps1 injection regions (Figure 4H), and the same was upregulated in the g-Sox9+Trps1 condition (Figure 4F). Similarly, the astrocytes analyzed by Patch-seq showed an upregulation of synapse related pathways, but terms such as “synapse organization”, “learning and memory” were actually downregulated in the g-Sox9 and g-Sox9+Trps1 injection region (Figure 4H). This is particularly intriguing given the tendency to a reduced synapse number observed by immunostainings.

Most interestingly, the stRNA-seq also revealed new GO terms like “oligodendrocyte differentiation” (with genes such as *Olig1*, *Enpp2*, *Tspan2*, etc.) upregulated in the g-Sox9 and g-Sox9+Trps1 injection (Figure 4F). This suggests that astrocyte specific deletion of Sox9/Trps1 affects oligodendrocyte differentiation in a crosstalk between glial cells governed by these TFs in astrocytes.

Crosstalk of astrocytes after Sox9 and Trps1 deletion with other cell types after injury

To exploit the stRNA-seq further towards a better understanding how astrocyte-specific manipulations affect other cell types, we used gene module scores as previously done in other studies (Hasel et al., 2021; Sadick, O'Dea et al., 2022). Indeed, the spots in the UL and DL showed a higher score for the corresponding modules of UL and DL neuronal markers (ED Figure 6A).

We then computed the module score for genes known to be specifically upregulated in reactive astrocytes (Figure 5A) and as expected, this was significantly upregulated in all the injection regions in comparison to their corresponding background tissue (Figure 5B, see Table 2 for summary of injection specific changes). Among the injection regions, only the g-Sox9 scored significantly less in this module than the g-Control injection (see Table 1 for summary of changes unique to Sox9/Trps1 deletion in comparison to control). However, the g-Trps1 background tissue scored significantly less in this module when compared to the g-Control background tissue, suggesting some more wide-spread effects in the sections. On the other hand, the g-Sox9+Trps1 background tissue scored significantly higher. This conveyed a

possible broader tissue level inflammatory effect, more idiosyncratic to the simultaneous deletion of Sox9 and Trps1.

GFAP in astrocytes is a good measure of general tissue pathology (Escartin et al., 2021; Hol and Pekny, 2015). We therefore examined the level of GFAP by fluorescence intensity measurement after immunostainings. While there were no differences in the GFAP intensity between cells from the g-Sox9 and g-Sox9+Trps1 condition, cells from the g-Trps1 condition showed significantly higher levels of GFAP at 7dpi (ED Figure 6B). Given that the dynamics of gene regulation could differ at the RNA and protein level, we performed the same analysis at the later time point of 21dpi. At 21dpi, cells from the g-Sox9 and g-Trps1, but not g-Sox9+Trps1 showed significantly lower levels of GFAP (ED Figure 6C). Overall, these data demonstrated reduced astrocyte reactivity upon Sox9 and/or Trps1 deletion and changes in the immune response in the region after Sox9 and Trps1 deletion.

These changes are likely due to a crosstalk with other cell types. A multitude of invading immune cells enter the brain as a result of compromised blood brain barrier (BBB), and contribute to the immune response in injury and disease (Mira et al., 2021; Puntambekar et al., 2018). The responses from the various cell types are orchestrated in a temporal manner and would involve significant crosstalk between the cells in the environment (Frik et al., 2018), all of which would be essential for eventual recovery and circuit restoration after injury. The impaired immune response in case of g-Sox9 and g-Trps1 injection regions and the exacerbated nature of the same in g-Sox9+Trps1 injection region could thus arise from altered crosstalk between Sox9, Trps1 deleted astrocytes and other cells contributing to immune response after injury. To check this, we made use of the scRNA-seq dataset generated by Koupourtidou, Schwarz et al., 2023. While they characterized responses to stab wound injury (SWI) in the cortical GM at 3- and 5-days post SWI (dpSWI), we made use of the 5dpSWI data as it is closer to our time point of 7dpi. In addition to several clusters of neurons, astrocytes, microglia and oligodendrocytes, several cell types like B cells, NKT (natural killer T cells)/ T cells, border-associated macrophages (BAM), dendritic cells (DC), vascular endothelial cells (venous) (VECV), vascular smooth muscle cells (VSMCs), etc. were present in this dataset. Apart from the scRNA-seq data, this study also identified the presence of an injury specific spatial cluster in their stRNA-seq. We first computed module score for the top 50 genes of their injury specific cluster to verify that their experimental paradigm was comparable to ours. Indeed, we noticed that the expression of these injury specific genes were significantly higher in all the regions that we defined as injection regions in comparison to the corresponding background regions (ED Figure 6D and E).

To understand if the representation of the different cell types from 5dpSWI scRNA-seq data were altered in the tissue regions after Sox9, Trps1 deletion, we computed module scores based on the top DEGs for each of these annotated cell type clusters. While the module score for genes known to be upregulated in reactive astrocytes was significantly higher in all the injection regions (Figure 5A and B), the module scores for the various astrocyte clusters were largely unaltered (ED Figure 6F-I). Only the g-Sox9 injection region showed a significant downregulation in two of the astrocyte clusters (4_Astrocytes and 10_Astrocytes), while the g-Trps1 injection region scored slightly higher in one of the astrocyte clusters (8_Astrocytes). Module score for the various oligodendrocyte lineage clusters reiterated the effects observed earlier in the GO term analysis, of increased oligodendrocyte differentiation (Figure 4F). Only the g-Trps1 injection region showed a slightly elevated score for the OPCs module (oligodendrocyte precursor cells, Figure 5D). Interestingly, both g-Sox9 and g-Sox9+Trps1 scored significantly higher in the modules for committed oligodendrocyte progenitors (COPs, Figure 5E), and mature oligodendrocytes (MOL, Figure 5F).

To understand the effects on microglia and other immune cell types, we computed module scores for these as well. Similar to the reactive astrocyte module, all the injection regions showed a significantly elevated microglia module score (for all three microglia substates) in comparison to the corresponding background tissue region, indicating injury specific microglial activation (Figure 5G-I, Table 2). Among the injection regions, g-Sox9 injection scored significantly lesser than the g-Control injection in all the microglia cluster modules (Table 1), while the g-Trps1 background tissue scored less than the g-Control background tissue in all. Thus, we observed a generally reduced microglia reaction upon deletion of Sox9 or Trps1 in astrocytes, which was not apparent in the double deletion condition. Notably, the reduced immune response in astrocytes upon Sox9 or Trps1 deletion may thus also be due to reduced microglial activation.

Similar to the reactive astrocyte module, the immune cell types such as B cells (Figure 5J), monocytes and macrophages (Figure 5K, L), T cells (ED Figure 6J), BAM (ED Figure 6K), and DC (ED Figure 6L) showed significant elevation in all the injection regions in comparison to the corresponding background tissue, indicating this is an injury specific response (Table 2). Interestingly, the g-Sox9+Trps1 injection and background region scored higher than the g-Control injection and background tissue respectively in the B cells module, indicating broad tissue level increase in B cell representation (Figure 5J, Table 1). While neither of the monocytes (13_Macrophages/Monocytes and 29_Monocytes) modules were altered significantly in the g-Sox9+Trps1 injection in comparison to the g-Control injection region, the

g-Sox9+Trps1 background tissue scored significantly higher in both these modules in comparison to the g-Control background tissue (Figure 5K, L). The background tissue is especially relevant here, as the immune cells are migratory and may well spread beyond the lesion area (see Data Table S6 for summary of changes in background tissue). In contrast, the g-Trps1 injection and background tissue scored less than the g-Control tissue in all these modules (Figure 5J-L). The module scores of NKT/ T cells (ED Figure 6J) was not significantly altered between the injection regions, but the g-Trps1 background region scored significantly less than the g-Control background region. Both the BAM and DC modules were significantly reduced in the g-Sox9 injection region in comparison to the g-Control injection region (ED Figure 6K, L), while only the DC module was reduced in the g-Trps1 injection region. Thus, Sox9 and Trps1 mediate communication with immune cells after the injury caused by viral vector injection which is mostly reduced upon deleting these TFs.

Taken together (see Table 1 & 2 or Data table S6 for summary), Trps1 deletion in astrocytes resulted in a generally reduced immune cell activation or invasion (microglia, B cells, macrophages, monocytes), while the background tissue showed a general increase in the immune cell scores in the double deletion of Sox9 and Trps1 in astrocytes, lending further support to a partially antagonistic function of Sox9 and Trps1 in astrocytes and the ensuing signaling to immune cells. All of these data demonstrate clear tissue level changes in immune cell responses, depending on the TF being manipulated. This reveals that manipulation of astrocytes by deleting key TFs elicits a multitude of non-cell autonomous effects, affecting the injury response by attenuating astrocyte, microglia and immune cell reactions in various combinations, but promoting oligodendrocyte differentiation and thus most likely repair.

Table 1. Comparison of cell type specific module scores between gRNA injection regions

Module scores	g-Sox9 injection vs g-Control injection	g-Trps1 injection vs g-Control injection	g-Sox9+Trps1 injection vs g-Control injection
Reactive astrocyte module (Figure 5A, B)	----	NS	NS
Injury specific gene expression module (ED Figure 6D, E)	--	NS	NS
0_Astrocytes (ED Figure 6F)	NS	NS	NS
4_Astrocytes (ED Figure 6G)	--	NS	NS

8_Astrocytes (ED Figure 6H)	NS	+	NS
10_Astrocytes (ED Figure 6I)	----	NS	NS
14_OPCs (Figure 5D)	NS	+	NS
18_COPs (Figure 5E)	+	NS	++++
7_MOL (Figure 5F)	+++	NS	++++
1_Microglia (Figure 5G)	-	NS	NS
5_Microglia (Figure 5H)	--	NS	NS
11_Microglia (Figure 5I)	-	NS	NS
26_B cells (Figure 5J)	NS	NS	++++
13_Macrophages/ Monocytes (Figure 5K)	NS	--	NS
29_Monocytes (Figure 5L)	NS	----	NS
16_NKT/ T cells (ED Figure 6J)	NS	NS	NS
19_BAM (ED Figure 6K)	----	NS	NS
27_DC (ED Figure 6L)	---	----	NS

Table 2 Comparison of cell type specific module scores between gRNA injection region and corresponding background tissue (indicative of the presence of injury response)

Module scores	g-Control injection vs background	g-Sox9 injection vs background	g-Trps1 injection vs background	g-Sox9+Trps1 injection vs background
Reactive astrocyte module (Figure 5A, B)	++++	++++	++++	++++
Injury specific gene expression module (ED Figure 6D, E)	++++	++++	++++	++++
0_Astrocytes (ED Figure 6F)	---	NS	NS	NS
4_Astrocytes (ED Figure 6G)	NS	NS	NS	NS
8_Astrocytes (ED Figure 6H)	NS	NS	NS	NS
10_Astrocytes (ED Figure 6I)	NS	NS	++++	NS
14_OPCs (Figure 5D)	NS	NS	++++	NS
18_COPs (Figure 5E)	-	NS	NS	NS
7_MOL (Figure 5F)	---	NS	-	NS
1_Microglia (Figure 5G)	++++	++++	++++	++++
5_Microglia (Figure 5H)	++++	++++	++++	++++

11_Microglia (Figure 5I)	++++	++++	++++	++++
26_B cells (Figure 5J)	++++	++++	++++	++++
13_Macrophages/ Monocytes (Figure 5K)	++++	++++	++++	++++
29_Monocytes (Figure 5L)	++++	++++	++++	++++
16_NKT/ T cells (ED Figure 6J)	++++	++++	++++	++++
19_BAM (ED Figure 6K)	++++	++++	++++	++++
27_DC (ED Figure 6L)	++++	++++	NS	++++

(“+” and “-” indicates higher or lower module score; Values of statistical significance are denoted as: +p ≤ 0.05, ++p ≤ 0.005, +++p ≤ 0.0005, ++++ p ≤ 0.0001; -p ≤ 0.05, - -p ≤ 0.005, - - - p ≤ 0.0005, - - - -p ≤ 0.0001)

Discussion

Here we unraveled novel functions of the TFs Sox9 and Trps1 in astrocytes of the cerebral cortex GM by astrocyte-specific deletion followed by single cell and tissue-wide transcriptome analysis. This reveals a common role in regulating synapse function with only Trps1 loss reducing synapse numbers and pathways involved in oligodendrocyte differentiation. Notably, both factors regulate immune cell reaction and invasion after a mild injury. Interestingly, we find fewer genes regulated when both factors are deleted highlighting their function within the same molecular pathway.

Sox9 and Trps1 are expressed heterogeneously in cortical GM astrocytes

Given that Trps1 was never characterized in astrocytes at the protein level, despite its expression in several astrocyte datasets (Endo et al., 2022; Sirko et al., 2015; Weng et al., 2019; Zhang et al., 2014), we first showed that about 40% of the S100β+ astrocytes are Trps1-immunopositive and always also Sox9+ (Figure 1H). Thus, Trps1 levels sufficiently high to be detected by immunostaining are in a subset of astrocytes, and we observed highest Trps1 levels in the DL of the cortex (Figure 1C and G). Astrocyte diversity at the level of cortical layers has already been characterized (Bayraktar et al., 2020; Lanjakornsiripan, Pior, Kawaguchi et al., 2018) and is influenced by neurons when establishing the layers. While the cause and effect of the layer specific expression of Trps1 is not known yet, it is intriguing to note that it is highest in the layers with highest myelination in the cortex (refs). This is of interest, as Trps1 has been reported as a possible transcriptional regulator of both astrocyte and oligodendrocyte fate in development (Weng et al., 2019). In line with this, we observed that around 50% of the Olig2+

oligodendrocyte lineage cells were also immunopositive for Trps1. In addition, we noted Trps1⁺ cells that are neither positive for S100 β nor Olig2. While formally these could be astrocytes that express neither S100 β nor Sox9 or oligodendrocytes that do not express Olig2, it is also possible they are a non-glial cell type as Trps1 has been observed, at least at the level of RNA in some neuronal cell types (Bakken et al., 2021) or they may be non-neural cells.

In contrast to Trps1 protein, Sox9 immunostaining was widespread, in all astrocytes and throughout the cortex, even though with varying levels throughout the cortical column (Figure 1C). Interestingly, the heterogeneity at the protein level may relate to heterogeneity at the mRNA level (Bocchi et al., *submitted*) where we identified a cluster of cortex GM astrocytes with low Sox9 and Trps1 expression (ED Figure 1D, E). It is interesting to note that GO term analysis highlighted metabolic functions to be specific in these astrocytes, and we also detected such a function after deleting Trps1 (see below).

Several studies in the recent past have highlighted the substantial heterogeneity of astrocytes in their morphology and gene expression patterns between brain regions (Boisvert et al., 2018; Endo et al., 2022) and even within the same brain region (Bayraktar et al., 2020; Lanjakornsiripan, Pior, Kawaguchi et al., 2018; Ohlig, Clavreul et al., 2021). In addition to this diversity in the intact brain, astrocyte response to injury (Koupourtidou, Schwarz et al., 2023), inflammation (Hasel et al., 2021) or disease (Sadick, O'Dea et al., 2022) is also quite diverse. In general, TFs unique to the variety of astrocyte subsets may play a key role in conferring heterogeneity by dictating specific downstream cascades. Alternatively, the heterogeneity itself may bestow pan-astrocyte TFs with region or subset specific functions due to differences in availability of co-factors, chromatin remodelers, etc., which might further reinforce the existence of distinct astrocyte subsets. Thus, it is exciting that variations in the expression levels of key TFs like Sox9 and Trps1 can be seen at single cell protein and RNA levels. The levels of TFs may regulate the extent of downstream cascade expression, this may be important in fine-tuning astrocyte functions or even identity, as has been observed in other cell types previously (Pali et al., 2019).

Sox9, Trps1 deletion sheds light on their functions in cortical GM astrocytes

We were able to demonstrate that Mokola pseudotyping is an efficient way to achieve astrocyte specific targeting, as most infected cells are immunopositive for S100 β , GFAP and even Sox9 (in case of g-Control injection) at 7 and 21dpi (Figure 2B and D, ED Figure 2E). CRISPR/ Cas9

mediated deletion of these TFs was efficient and rather quick, we could see a considerable reduction in the number of cells expressing Sox9 or Trps1 already at 7dpi (Figure 2D and E).

Patch-seq based scRNA-seq revealed more genes to be upregulated after Sox9 deletion while Trps1 deletion resulted in a comparable number of up and downregulated genes, which fits with the versatile role of Trps1 as a transcriptional repressor (Fantauzzo et al., 2012; Malik, 2001) and activator (Fantauzzo and Christiano, 2012; Witwicki, Ekram et al., 2018; Wuelling et al., 2020). Interestingly, simultaneous deletion of Sox9 and Trps1 resulted in fewer DEGs, with the least number of upregulated genes, hinting at a possible requirement of Sox9 to activate the targets de-repressed by Trps1. In the hair follicle epithelium, Trps1 has been shown to negatively regulate Sox9 expression (Fantauzzo et al., 2012) while in chondrocytes, Sox9 has been shown to induce Trps1 expression (Tan, Niu et al., 2018), highlighting that these TFs may be involved in related transcriptional cascades in several lineages. Indeed, here we show that deletion of Sox9 and Trps1 show interacting effects and partial overlapping functions with the GO terms detected in Sox9 and Trps1 low astrocytes. GO analysis of Sox9/ Trps1 deleted astrocytes show that both Sox9 and Trps1 deletion seems to affect several astrocyte functions like synapse organization and immune response. Both Sox9 and Trps1 loss triggered upregulation of genes related to gliogenesis (like *Fgfr3*, *Hes5*, *Zfp365* or *Hes1*, *Zfp365*), which possibly indicate that the glial identity is reinforced by upregulation of alternate glial specific genes, thus maintaining astrocyte identity even in the absence of Sox9 or Trps1.

Astrocyte specific Sox9, Trps1 loss triggers non-astrocyte specific tissue level changes

While the Patch-seq based scRNA-seq revealed upregulation of synapse related pathways both in the g-Sox9 (Data Table S2) and g-Trps1 (Figure 3F) condition, the number of synaptic puncta in close proximity to Trps1 deleted astrocytes condition was significantly reduced (Figure 3H). It could be hypothesized that Trps1 deleted astrocytes upregulate synapse related pathways to compensate for the fewer synapses in the surroundings. This implicates the role of pan-astrocyte TFs in intrinsic astrocyte functions such as synapse maintenance and highlights broad tissue level changes upon astrocyte manipulation. While synaptophysin is a generic pre-synaptic marker, Homer1 specifically labels excitatory post-synapses. It is possible that Sox9, Trps1 loss has a specific or more pronounced effect on inhibitory post-synapses. Sox9 (in the olfactory bulb) and Nfia (in the cortex) have been shown to regulate astrocyte response to inhibitory neurons during development (Cheng et al., 2023). Thus, it would be interesting to see if Sox9 loss in the adult cortical astrocytes has a selective effect on inhibitory synapses and characterize

the effect of Sox9 and Trps1 in synapse maintenance by electrophysiological characterization of the surrounding neurons.

Sox9, Trps1 loss in astrocytes creates an imbalance in glial and immune cell response

Our stRNA-seq after Sox9, Trps1 deletion revealed novel and widespread tissue level changes upon astrocyte manipulation. Among the injury responsive spatial clusters, cluster 0 was characterized by expression of known reactive glial genes like *Gfap*, *Serpina3n*, *Vim*; while cluster 4 was characterized by expression of genes like *Igtp*, *Cxcl10* involved in interferon response (Figure 4D). Similar to the prediction of patch-seq based scRNA-seq, stRNA-seq indicated dampened immune responses in the tissue where Sox9 or Trps1 was deleted. In contrast, simultaneous deletion of Sox9 and Trps1 showed an exacerbated immune activation at the level of whole tissue. It is possible that in the case of g-Sox9+Trps1, the inability of astrocytes to coordinate the immune response either results in, or is compensated by activation of other cells like microglia, invading monocytes which results in a broader tissue level exacerbated immune response in that region.

Indeed this was the case, comparison of our stRNA-seq data after astrocyte specific Sox9, Trps1 deletion with the scRNA-seq data of cells from cortical GM after a SWI (Koupourtidou, Schwarz et al., 2023) revealed an increase in the representation of B cells, monocytes and DC in the tissue after simultaneous Sox9, Trps1 deletion. On the other hand, the tissue with only Sox9 or Trps1 deletion (i.e., in g-Sox9 or g-Trps1 condition) had significantly lesser representation of microglia or monocytes or T cells or DC (see Table 1.1 and 1.2 for summary).

Most intriguingly, astrocyte specific Sox9 or Sox9+Trps1 deletion elicited a prominent increase in representation of oligodendrocytes (18_COPs and 7_MOL), upregulation of GO terms “oligodendrocyte differentiation”. In the zebrafish brain, increased OPC proliferation and accumulation at the site of injury was shown to be influenced by immune response (Tlr2, Cxcr3) pathways (Sanchez-Gonzalez et al., 2022). Reactive astrocytes may also influence the rate of oligodendrocyte differentiation via endothelin-1/ Ednrb signaling (Hammond, McEllin et al., 2015). While we observe an increase in the representation of oligodendrocytes, we do not know whether this is mediated directly by astrocytes lacking Sox9 or if it is a protracted side effect of the alterations in the immune response in the region. Future experiments with BrdU/ EdU based lineage tracing to see if there is an increase in OPC proliferation following Sox9 or

Sox9+Trps1 deletion would give us more definitive answers about the changes in glial cell dynamics when astrocyte specific TFs are deleted.

In conclusion, we observe remarkable heterogeneity in the expression levels of pan-astrocyte TF Sox9 and pan-glial TF Trps1 at both single cell protein and RNA level within the cortical GM. The role of Sox9 by deletion has already been explored in the adult brain (Ung, Huang et al., 2021) and postnatal development (Cheng et al., 2023), however these studies noticed no prominent effects in cortical astrocytes, but rather had a significant impact in the astrocytes of the olfactory bulb. Nonetheless, these previous studies did not carry out a systematic analysis of the transcriptomic changes after Sox9 deletion. Conversely, we studied the transcriptomic changes resulting from Sox9, Trps1 loss at both the single cell and tissue level, which helped us unravel the previously unidentified roles of these TFs in the cortical GM astrocytes. It is to be noted that our experimental paradigm for Sox9 (and Trps1) deletion is significantly different from the Cre mediated deletion performed by Ung, Huang et al., 2021. Our experiment involves injection of Mok-LV encoding gRNAs against the TF of interest for eventual deletion by CRISPR strategy. This may be disadvantageous on certain accounts: only a limited number of cells are targeted and there may be a relative unpredictability in the nature of indels in each targeted cell. However, in our case, the TF deletion is accompanied by a “mild injury” like condition. It is possible that this challenges the astrocytes and the effect of TF loss is more prominent and sheds light on astrocytic functions that are compromised in the absence of key TFs like Sox9 and Trps1. Even previously, *Rbpj-k* knockdown in cortical astrocytes had an observable effect only when combined with a SWI (Zamboni et al., 2020), and cortical astrocytes may in general be more resistant to gene perturbations (at least in the context of genes like *Rbpj-k*, Sox9 and *Nfia* that have been studied so far).

Thus, our study provides an overview of the roles of Sox9 and Trps1 in the cortical GM astrocytes, the deletion of which affects several astrocyte functions like synapse maintenance and response to injury, with a pronounced effect on oligodendrocyte differentiation and other immune cells in the tissue microenvironment.

Acknowledgements

We would like to thank Tatiana Simon-Ebert (BMC, Munich) for help with the stRNA-seq library preparation, Tobias Straub (Bioinformatic Core Facility of the BMC, LMU, Munich)

for the alignment of Patch-seq based scRNA-seq data, Ines Muehlhahn for help with cloning (BMC, Munich), Paulina Chlebik (BMC, Munich) for help with lentiviral production and titration. We acknowledge the support of the Bioimaging Core Facility and Bioinformatic Core Facility at BMC, LMU Munich and the Laboratory for Functional Genome Analysis (LAFUGA). We are particularly grateful to all the members of the Götz lab for their valuable inputs throughout the course of this project.

This study was supported by the German Research Foundation TRR274 (Nr. 408885537), FOR2879/2 (Nr. 405358801), the SPP 2306 Ferroptosis (Project Nr 461629173) and SyNergy (EXC2145/Project-ID 390857198) as well as by the EU in the consortium NSC Reconstruct (H2020, Nr. 874758) and the advanced ERC grant (Nr. 885382) to M.G.

Author contributions

M.G. and G.M. conceived and designed the project. P.N. contributed to shaping the project, performed all experiments and data analysis. C.K. helped performing stRNA-seq experiment, C.K. and J.N. provided the 5dpSWI scRNA-seq dataset for comparison with stRNA-seq data. T.D.R. characterized Trps1 expression in Olig2+ cells and contributed to the GFAP intensity analysis. R.B. helped with animal experiments, R.B. and J.F-S. provided the intact adult cortical GM scRNA-seq dataset. S.G., D.F. and M.M. performed the collection of cells for Patch-seq based scRNA-seq experiment. P.N., G.M. and M.G. wrote the manuscript. M.G. provided all the funding.

Figure Legends

Figure 1. Characterization of Sox9 and Trps1 expression in the cortical GM

- A. Overview of Sox9, Trps1 and S100 β expression in the cortex shown by immunostaining (scale 50 μ m).
- B. Zoomed image of area highlighted in yellow box of the overview image, yellow arrowheads point to cells positive for Sox9, Trps1 and S100 β while the white arrowheads point to cells positive for Trps1 alone.
- C. The cortical column is divided into 5 bins, the variation in Sox9 and Trps1 expression (measured by fluorescence intensity) along the bins is shown in a color-coded dotplot.
- D-G. Boxplots showing bin-wise percentage of S100b+ astrocytes expressing (F) Sox9 and (G) Trps1 (n = 4). Quantification for the normalized (H) Sox9 and (I) Trps1 intensity across bins (n = 4).
- H. Percentage of Sox9, Trps1 or S100 β positive cells normalized to the total number of S100 β + cells in the cortical GM (n= 4, data labels indicate %Mean \pm SEM cells throughout the length of the cortical GM, irrespective of bins or layers

Data in D-G shown as box plots, showing median, minimum and maximum values. Statistics for comparison of normalized Trps1 intensity across the bins was done with Friedman test and Dunn's multiple comparison test, * $p \leq 0.05$. Bar plots depict Mean \pm SEM, n = 4 for g-Control, g-Sox9 and g-Sox9+Trps1, n = 3 for g-Trps1; statistics for comparison was performed with One-way Anova and Dunnett's multiple comparison test: * $p \leq 0.05$, ** $p \leq 0.01$, *** $p \leq 0.001$.

Figure 2. CRISPR mediated deletion of Sox9 and Trps1 in adult cortical astrocytes

- A. Scheme for mokola pseudotyped lentivirus (Mok-LV) constructs expressing control gRNA (g-Control) or gRNAs against Sox9 and Trps1 which are injected into the adult cortex, analysis is performed at 7 or 21dpi.
- B. Overview images of g-Control injection in the cortex and expression of astrocyte specific markers S100 β , GFAP at 7 and 21dpi shown by immunostaining (scale = 50 μ m).
- C. Barplots showing the quantification for the percentage of g-Control infected cells expressing S100 β , GFAP at 7 and 21dpi.
- D-E. Images showing gRNA infected cells expressing (D) Sox9 or (E) Trps1 at 7dpi (yellow arrowheads point to gRNA infected cells positive for Sox9/ Trps1, while the white arrowheads

point to cells negative for Sox9/ Trps1, scale = 20 μ m). Barplots showing quantification for the percentage of gRNA infected cells expressing (D') Sox9 and (E') Trps1 at 7dpi respectively. **F-G.** Barplots showing the quantification for the percentage of gRNA infected cells expressing (F) S100 β and (G) GFAP at 7dpi in all conditions.

Figure 3. Patch-seq based single-cell sequencing of Sox9 and Trps1 deleted astrocytes

- A.** Scheme for patch-seq of gRNA infected astrocytes from adult cortex.
- B.** UMAP plots depicting clusters and distribution of experimental conditions across the various clusters.
- C.** Stacked barplots showing number of significantly up and downregulated genes (p val < 0.05) in g-Sox9, g-Trps1, and g-Sox9+Trps1 condition in comparison to g-Control.
- D-G.** Barplots depicting top 5 up- and down-regulated pathways enriched in (D) g-Control astrocytes compared to intact astrocytes collected and processed by the same method; in astrocytes after (E) Sox9 deletion, (F) Trps1 deletion, (G) Sox9+Trps1 deletion in comparison to g-Control (the number of genes enriched in each pathway is shown as 'Count', enrichGO was performed on genes enriched in each condition with p val < 0.05, and further simplified with Rrvgo package. See Data table S2 for more details)
- H.** Representative images showing synaptic puncta (in green, post-synaptic puncta co-localizing with pre-synaptic puncta) in close proximity to gRNA (red) infected astrocytes, across all conditions and quantification of the same shown in violin plots for several ROIs (each containing 1-3 infected astrocytes) and in barplots for the average of all cells from each biological replicate. Statistics for comparison performed with Kruskal-wallis test with Dunn's test for multiple comparison, p -values mentioned above lines denoting groups in comparison.

Figure 4. Tissue level effects of Sox9 and Trps1 loss in cortical astrocytes explored by Spatial transcriptomics

- A.** Scheme for Spatial transcriptomics (10x Visium, stRNA-seq) in the cortex of adult animals injected with Mok-LV expressing gRNA (Brains from animals injected with either g-Control, g-Sox9, g-Trps1 or g-Sox9+Trps1 were manually resected and two consecutive sections with infected cells were placed in one capture area each of a 10x Visium slide).

- B.** Spatial location of the gRNA injection region (defined based on the fluorescence signal in the images taken before tissue processing steps) is highlighted for each condition, and the remaining tissue is considered as background tissue for each condition.
 - C.** Spatial distribution of clusters for spots specific to cortical GM across all conditions.
 - D.** Dotplot showing expression of top 5 genes for each of the spatial clusters.
 - E-H.** Pie charts depicting overlap of (E) up- and (G) down-regulated genes in the injection regions after Sox9/ Trps1 deletion in comparison to Control injection.
- Barplots depicting top 5 (F) upregulated and (H) downregulated pathways enriched in the injection regions after Sox9/ Trps1 deletion in comparison to Control injection (the number of genes enriched in each pathway is shown as 'Count', enrichGO was performed on genes enriched in each condition with $pval < 0.05$ and further simplified with Rrvgo package, see Data table S5 for more details).

Figure 5. Altered immune response after Sox9, Trps1 deletion

- A-B.** The extent of 'Reactive astrocyte module' gene expression in different conditions shown in (A) SpatialFeatureplots and (B) Violin plots (stratified based on region of gRNA injection and corresponding background tissue) respectively.
- C.** Umap plot depicting distribution of cells collected 5days post stab wound injury (dpSWI) in the cortex GM, clusters are color coded according to the cell type annotation (Koupourtidou, Schwarz, et. al. 2023)
- D-L.** Violin plots (stratified based on region of gRNA injection and corresponding background tissue) depicting module scores for various cell types like (D) 14_OPCs, (E) 18_COPs, (F) 7_MOLs, (G) 1_Microglia, (H) 5_Microglia, (I) 11_Microglia, (J) 26_B cells, (K) 13_Macrophages/ Monocytes, (L) 29_Monocytes contributing to injury response. Module scores computed based on the top 25 DEG for each of the annotated cell type clusters present in the 5dpSWI scRNA-seq of Koupourtidou, Schwarz, et. al.

Statistics for comparing module scores **B, D-L** done using Kruskal-wallis test and Dunn's multiple comparison. Significance for comparisons of the injection regions with the corresponding background tissue depicted with lines and * above; significance for comparisons of experimental injection regions with the control-injection or experimental background tissue with Control-background tissue depicted with * above the respective violins; * $p \leq 0.05$, ** $p \leq 0.005$, *** $p \leq 0.0005$, **** $p \leq 0.0001$.

Refer to Data table S6 for the list of genes used for module score calculation and a summary of the changes in different conditions; Abbreviations: dpSWI = days post stab wound injury, OPCs = oligodendrocyte progenitor cells, COPs = committed oligodendrocyte progenitors, MOL = mature oligodendrocytes

Extended data figures

Extended data Figure 1 (for Figure 1).

A-B. Percentage of Sox9, Trps1 or S100 β positive cells normalized to the total number of (A) Sox9⁺ cells, or (B) Trps1⁺ cells in the cortical GM (n= 4, data labels indicate %Mean \pm SEM cells throughout the length of the cortical GM, irrespective of bins or layers).

C. Barplot indicating the percentage of Olig2⁺ cells expressing S100 β or Trps1 in the cortex GM (n=3, as Mean \pm SEM)

D. UMAP plots depicting sub-clusters of cortical GM astrocytes, astrocyte score.

E. UMAP plots depicting heterogeneity in expression of *Sox9* and *Trps1* RNA across the clusters.

F. UMAP plots depicting expression of markers for other cell types such as *Olig2*, Sox10 (oligodendroglial lineage) and *Tmem119*, *Aif1* (microglia) in the cortical GM astrocytes.

G. Dotplot depicting expression of known astrocyte genes and top ten genes specific to each of the cortical GM astrocyte subclusters.

H. Barplots depicting top 5 pathways enriched in the different clusters of cortical GM astrocytes (the number of genes enriched in each pathway is shown as 'Count', enrichGO was performed on genes enriched in each cluster with padj < 0.05, see Data table S1).

Extended data Figure 2 (for Figure 2).

A. Overview images of g-Sox9, g-Trps1 and g-Sox9+Trps1 injection in the cortex and expression of astrocyte specific markers S100 β , GFAP at 7dpi shown by immunostaining (scale = 50 μ m).

B. Overview images of g-Sox9, g-Trps1 and g-Sox9+Trps1 injection in the cortex and expression of astrocyte specific markers S100 β , GFAP at 21dpi shown by immunostaining (scale = 50 μ m), and the corresponding quantifications as barplots

C-F. Images showing gRNA infected cells expressing (C) Sox9 or (D) Trps1 at 21dpi (yellow arrowheads point to gRNA infected cells positive for Sox9/ Trps1, while the white arrowheads point to cells negative for Sox9/ Trps1, scale = 20 μ m). Barplots showing quantification for the percentage of gRNA infected cells expressing (E) Sox9 and (F) Trps1 at 7dpi respectively.

Extended data Figure 3 (for Figure 3).

A. Violin plot showing number of counts and genes detected per cell.

B. UMAP plots showing distribution of cells by experimental batch and time point of analysis.

C. Dotplot showing expression of top five genes specific to each condition.

D-F. Venn diagram showing overlap of (D) up- and (E) down-regulated genes after Sox9, Trps1, or Sox9+Trps1 deletion, (F) overlap in the genes predicted to be targets of Sox9 and Trps1, based on ChIP data for Sox9 from Ohba, He et al., 2015, for Trps1 from Witwicki, Ekram et al., 2018.

G. Stacked barplots showing number of genes that are predicted Sox9, Trps1 or common targets among the significantly up and downregulated genes (p val < 0.05) in g-Sox9, g-Trps1, and g-Sox9+Trps1 condition in comparison to g-Control.

Extended data Figure 4 (for Figure 3)

A-B. Venn diagrams showing overlap in the significantly (p val < 0.05) up and downregulated genes at (A) 7 and (B) 21dpi after Sox9, Trps1 or Sox9+Trps1 deletion.

C-E. Barplots depicting top 5 up- and down-regulated pathways enriched at 7 and 21dpi after (C) Sox9 or (D) Trps1 or (E) Sox9+Trps1 deletion (the number of genes enriched in each pathway is shown as 'Count', enrichGO was performed on genes enriched in each condition with p val < 0.05, and further simplified with Rrvgo package, see Data table S3 for more details).

Extended data Figure 5 (for Figure 4)

- A. Violin plots showing the number of genes, number of counts, percentage mitochondrial and hemoglobin reads for all the spots in the stRNA-seq, across the four conditions.
- B. SpatialFeaturePlot showing the number of genes detected in individual spots, across the four conditions.
- C. Distribution of tissue regions specific to gRNA injection and the corresponding background tissue from each condition, across the spatial clusters (for spots specific to cortical GM).
- D. Venndiagram showing overlap in genes enriched in injury specific spatial clusters.
- E. Barplots depicting top upregulated pathways enriched in spatial clusters specific to injection region or Sox9/ Trps1 deletion.
- F. Dotplot showing expression of known/ predicted UL, DL neuronal and astrocyte markers across the spatial clusters (clusters ordered based on their anatomical location as follows: injury specific (4, 0, 8), medial (6), upper layer (2/ 10, 3), lower layers (1, 5, 9, 7).
- G. Venndiagram showing overlap of DEG specific to spatial cluster 2 and 10 (in comparison to clusters 0, 1, 3-9).
- H. Barplot depicting top upregulated pathways enriched in spatial cluster 10 (which is unique to the background tissue of Sox9+Trps1 condition and anatomically similar to spatial cluster 2).

E & H: the number of genes enriched in each pathway is shown as 'Count', enrichGO was performed on genes enriched in each spatial cluster with $pval < 0.01$ and simplified further with Rrvgo package, see Data table S4 for more details.

Extended data Figure 6 for Figure 5

- A. SpatialFeature plots showing the expression pattern of UL and DL Neuron module, for validation of the use of 'Module score'.
- B-C. GFAP expression by fluorescence intensity measurement in control or Sox9/ Trps1 deleted sections immunostained for Gfap and Tdtomato (gRNA), shown in a violin plot for individual cells or in a bar plot for showing the average intensity of all cells per mice at (B) 7dpi and (C) 21dpi. Intensity values are normalized to the area of the individual cells and expressed as a fold-change in comparison to the control condition. Statistics for comparison at the individual cell level is done with Kruskal-wallis test with Dunn's test for multiple comparison, for averaged data at the level of mice is not significant; * $p \leq 0.05$, ** $p \leq 0.01$, *** $p \leq 0.001$.

D-E. SpatialFeatureplot (D) and the corresponding violin plot (E) showing the expression of genes expressed in the injury specific spatial cluster (based on Koupourtidou, Schwarz et al., 2023)

F-L. Violin plots (stratified based on region of gRNA injection and corresponding background tissue) depicting module scores for various cell types like (F) 0_Astrocytes, (G) 4_Astrocytes, (H) 8_Astrocytes, (I) 10_Astrocytes, (J) 16_NKT/ Tcells, (K) 19_BAM, (L) 27_DC that contribute to injury response.

Module scores computed based on the top 25 DEG for each of the annotated cell type clusters present in the 5dpSWI scRNA-seq of Koupourtidou, Schwarz, et. al. See Data table S6 for the list of genes and summary.

E-L: Statistics for module scores comparison done using Kruskal-wallis test and Dunn's multiple comparison. Significance for comparisons of the injection regions with the corresponding background tissue depicted with lines and * above; significance for comparisons of experimental injection regions with the control-injection or experimental background tissue with Control-background tissue depicted with * above the respective violins; * $p \leq 0.05$, ** $p \leq 0.005$, *** $p \leq 0.0005$, **** $p \leq 0.0001$.

(Abbreviations: dpSWI = days post stab wound injury, NKT = natural killer T cells, BAM = border-associated macrophages, DC = dendritic cells).

Materials and Methods

Animals

For immunostainings to characterize the expression of Sox9 and Trps1 in the adult cortical GM, 2-5 month old C57BL/6J mice (Charles River Laboratories; Sulzfeld, Germany) were used. R26-Cas9-Fezh mice (Platt et al., 2014, Jackson Laboratories; Gt(ROSA)26Sortm1.1(CAG-cas9*,-EGFP)Fezh/J, JAX stock #024858) expressing Cas9-GFP in all cells constitutively were used for Sox9, Trps1 deletion experiments. Animals were bred as homozygotes and housed under specified pathogen-free conditions and a 12:12h light/dark cycle, with 2–3 adult animals per filter top cages. All experimental procedures were performed in accordance with animal welfare policies and approved by the Government of Upper Bavaria (Germany).

gRNA cloning and viral vector preparation

For cloning multiple gRNAs targeting the TFs, we used the STAgR approach (Breunig et al., 2018). In brief, the gRNA-insert and gRNA-vector fragments were generated by PCR with gRNA-scaffold-Fwd and gRNA(rev)-hU6-Rev primers (see Resources Table) as described in (Breunig et al., 2018). The PCR amplified gRNA-insert and gRNA-vector fragments were purified using AMPure XP Beads and assembled into a 2X-STAgR or 4X-STAgR construct by use of Gibson assembly (Gibson, 2011). The assembled fragments were transformed into chemically competent TOP10 *E. coli* bacteria and gRNA positive clones were selected by colony PCR and the isolated plasmids were further verified by Sanger sequencing using StAgR_seq_fwd2 and StAgR_seq_rev primers. The gRNA sequences were further sub-cloned into a lentiviral construct as following: gRNA containing sequences were cut out from the STAgR plasmids by KpnI or AfeI+BsrBI digestion and ligated into a similarly generated lentiviral sticky or blunt end fragment (LTR-CMV-TdTomato-WPRE-LTR) using T4 DNA ligase (incubated at 16°C overnight) and transformed into chemically competent TOP10 *E. coli* bacteria. gRNA positive clones were selected by colony PCR and further verified by Sanger sequencing using either of the following primers: lentiSeq_fwd, StAgR_seq_fwd2, seqWPRE_Fwd, STAGRseq_pLKOI_rev. The final assembled lentiviral constructs are as depicted in Figure 2A.

The lentiviral production was carried out as described in Heinrich et al., 2014, with few improvements. The gRNA lentiviral plasmids were transfected into HEK293T cells along with the pMokola-G plasmid (for pseudotyping) and pCMVdr8.91 packaging plasmid. The viral

particles were harvested from the medium 4 days after. The media was collected in 50ml tubes, spun down at 3500rpm for 5min, and filtered with a 0.45 μ m filter into a conical-bottom ultracentrifuge tube containing Optiprep. After ultracentrifugation at 24000rpm for 2 h, most of the supernatant was removed without disturbing the Optiprep interface and re-suspended thoroughly in cold TBS-5 buffer (ensuring complete mixing with OptiPrep now) and subject to a second round of ultracentrifugation at 24000 rpm for 2 h. After discarding the supernatant, the viral pellet was re-suspended in an appropriate volume of TBS-5 buffer and stored at -80°C until further use. The titer of the Mok-LVs was determined by infecting primary astrocyte cultures with serial dilutions of the concentrated viral stock, the titer was calculated based on the number of cells expressing TdTomato 3d after transduction, expressed as titer units per milliliter (TU/ml).

The gRNA sequences and primer sequences are:

gRNA sequences	
g-Control (non-targeting sequence)	GCTGCATGGGGCGCGAATCA
g-Sox9_exon1	GTACCCGCATCTGCACAACG
g-Sox9_exon2	GCTGGTACTTGTAATCGGGG
g-Trps1_exon1	TAGGACTGCATAATCGCACC
g-Trps1_exon3	AGAGGGGCAGACATCCTACG

Primers for gRNA cloning	
g-Sox9_exon1_Scaffold-fwd	GTACCCGCATCTGCACAACGGTTTTAGAGCTAGAAA TAGCAAGTT
g-Sox9_exon1_hU6_Rev	CGTTGTGCAGATGCGGGTACCGGTGTTTCGTCCTTT
g-Sox9_exon2_Scaffold-fwd	GCTGGTACTTGTAATCGGGGGTTTTAGAGCTAGAAA TAGCAAGTT
g-Sox9_exon2_hU6_Rev	CCCCGATTACAAGTACCAGCCGGTGTTCGTCCTTT
g-Trps1_exon1_Scaffold_fw d	TAGGACTGCATAATCGCACCGTTTTAGAGCTAGAAA TAGCAAGTT
g-Trps1_exon1_hU6_Rev	GGTGCGATTATGCAGTCCTACGGTGTTCGTCCTTT

g-Trps1_exon3_Scaffold_fwd	AGAGGGGCAGACATCCTACGGTTTTAGAGCTAGAA ATAGCAAGTT
g-Trps1_exon3_hU6_Rev	CGTAGGATGTCTGCCCCTCTCGGTGTTTCGTCCTTT
g-Control_Scaffold-fwd	GCTGCATGGGGCGCGAATCAGTTTTAGAGCTAGAAA TAGCAAGTT
g-Control_hU6_Rev	TGATTCGCGCCCCATGCAGCCGGTGTTCGTCCTTT

Primers for Sanger sequencing	
StAgR_seq_fwd2	ACTGGATCCGGTACCAAGG
StAgR_seq_rev	TTACGGTTCCTGGCCTTTTG
STAGRseq_pLKOI_rev	ACCAATGACTTACAAGGCAGC
seqWPRE_Fwd	TCCTTCTGCTACGTCCCTTC
lentiSeq_fwd	ATCGTTTCAGACCCACCTCC

Viral injection in R26-Cas9-Fezh mice

Adult (2- 4months old) animals homozygous for Cas9 were used for lentiviral injection to achieve CRISPR mediated deletion of astrocyte TFs. Briefly, animals were anesthetized and injected with the Mok-LV virus at a titer of $1-5 \times 10^8$ TU/ml in one hemisphere, Bregma: RC: -0.4 to -1.4 mm; ML: -1.0 mm; DV: -0.65mm. The animals were killed 7 or 21 days after the Mok-LV injection by transcardial perfusion with phosphate-buffered saline (PBS), followed by 4% paraformaldehyde (PFA) in PBS. The brains from these animals were removed and post-fixed for 24 h in 4% PFA, following which the 40 μ m thick sections were cut at the vibratome and the brain slices were stored in PBS with azide at 4°C until further analysis by immunostainings. The animals used for Sox9, Trps1 characterization by immunostainings were perfused and processed in a similar manner, but without any viral injections.

Immunohistochemistry

For immunohistology, sections stored in PBS with azide were washed with PBS three times, for 10 minutes each and pre-incubated for 90 minutes in blocking solution (3% bovine serum albumin, 0.5% Triton X-100 in PBS). The primary antibodies were diluted in the blocking solution (as mentioned in the Resources Table); the and the sections were incubated with the

appropriate combination for 48 hours at 4°C. Then, the slices with PBS three times, 10 minutes. Following this, the slices were incubated for 2 hours with the appropriate species- or subclass-specific secondary antibodies and 4', 6-diamidino-2-phenylindole (DAPI, to label the nuclei) diluted in the blocking solution (as mentioned in the Resources Table). After washing the slices in PBS again, they were mounted with Aqua Poly/Mount (Polysciences, Warrington, PA). For Trps1, synaptophysin and Homer1 immunostainings, antigen retrieval steps with 0.01 M Sodium citrate (pH 6) at 90°C for 20 min was performed before incubation with the corresponding primary antibodies. The following primary and secondary antibodies were used at the mentioned dilutions:

Primary antibody	Dilution	Company/ Catalogue number
Rabbit anti-Sox9	1: 1500	Merck/ Millipore (AB5535)
Rabbit anti-Trps1	1: 300	Abcam (ab209664)
Mouse IgG1 anti-S100β	1: 300	Sigma (S2532)
Goat anti-Sox9	1:500	AF3075-SP
Mouse IgG1 anti-Gfap	1:300	Sigma (G3893)
Mouse IgG1 anti-Synaptophysin	1: 500	Synaptic Systems (SYSY101011)
Rabbit anti-Homer1	1: 500	Synaptic systems (SYSY 160 003)
Goat anti-mcherry	1: 1000	Acris/ Origene (AB0081-200)
Rabbit anti-RFP	1: 1000	Rockland (600-401-379)
Mouse IgG2a anti-Olig2	1: 250	Merck/ Millipore (MABN50)
Secondary antibody	Dilution	Company/ Catalogue number
Donkey anti mouse IgG A488	1: 250	Life Technologies (A21202)
Donkey anti-goat A594	1:1000	Life Technologies (A-11058)
Donkey anti-rabbit Cy3	1: 1000	Dianova, 711-165-152
Donkey anti-Rabbit IgG Alexa Fluor 647	1: 1000	Jackson (Biozol) JIM-711-165-152
Goat Anti-Mouse IgG1 Alexa Fluor 488	1: 1000	Life Technologies (A21121)
Goat anti-Mouse IgG2a Antibody, Alexa Fluor 647	1: 1000	Invitrogen A21241
DAPI (nuclear staining)	1: 1000 (0.1 µg/ml)	Sigma, D9564

Quantification and statistical analysis for Immunohistochemistry

Images were obtained using Confocal laser scanning (Zeiss LSM710) microscope and analyzed using ImageJ or Imaris (for synapse analysis).

Images for Sox9 and Trps1 characterization in adult cortex were taken as a tiled image at a magnification of 25X to cover the entire cortical column in the somatosensory cortex area, with 12-20 μm thick z stacks. The proportion of Sox9 or Trps1 positive (or double positive cells) was obtained by counting all the S100 β ⁺ astrocytes or Olig2⁺ oligodendroglial lineage cells. To understand the layer wise distribution, the cortical GM was divided into five equal bins, with bins 1, 2 corresponding to the upper cortical layers and bin 3 in the middle and bins 4 and 5 corresponding to the deeper cortical layers. The intensity of Sox9 and Trps1 was calculated for all the cells in the cortical column, based on ROIs drawn for DAPI signal. A cell was considered positive for Sox9 or Trps1 if the normalized corrected total cell fluorescence was more than 0.3 or 0.15 respectively.

Images for validation of Sox9, Trps1 deletion after Mok-LV injection were taken as tiled images at a magnification of 25X to cover the entire region of injection along the cortical column, with 12-20 μm thick z stacks. The proportion of infected cells (TdTomato⁺) cells expressing Sox9, Trps1, S100 β or Gfap was expressed as a percentage of gRNA-TdTomato⁺ cells.

Images for synapse analysis were taken at a magnification of 40X (+2.5x zoom) with 4.5-7 μm thick z stacks. Each image contained on to three infected astrocytes, and at least five ROIs were imaged for each animal. The images were deconvolved and the astrocyte surface was reconstructed on Imaris. Following this, the number of pre- and post-synaptic puncta in the regions surrounding the astrocyte (within a distance of 0-0.5 μm , 0.5-1.5 μm from the astrocyte surface) were calculated with the “Spots” option on Imaris. All post-synaptic puncta closest to a pre-synaptic puncta (within a distance of 0.2 μm) were considered as a “synapse”.

All statistical tests were performed with GraphPad Prism 9.5. Parametric One-way Anova with Tukey’s test for comparison was performed if all the conditions in a comparison passed Shapiro-Wilk test for normality. Otherwise Kruskal-wallis test with Dunn’s test for multiple comparison was performed. The exact test used for each graph is also mentioned in the corresponding figure legends, all barplots are represented as Mean \pm SEM.

Patch-seq based scRNA-seq

Smart-seq2 based Patch-seq of astrocytes was performed using a protocol similar to the one established for neurons (Cadwell et al., 2017, 2016). Animals injected with g-Control, g-Sox9, g-Trps1 or g-Sox9+Trps1 Mok-LVs were killed at 7 or 21dpi and acute cortical slices of 300 μ m thickness were cut on a Vibratome. The brain slices were incubated in oxygenated ACSF for 30min at 37 \pm 0.5 $^{\circ}$ C and subsequently, infected astrocytes (identified based on signal for TdTomato in the Mok-LV construct) were collected using a patch-clamp pipette, in individual tubes containing the lysis buffer (Cadwell et al., 2017). Subsequent reverse-transcription and cDNA amplification steps were carried out using Superscript II Reverse Transcriptase (SSIIRT; Thermo Fisher Scientific, cat. no. 18064014) and KAPA Biosystems HiFi HotStart Ready Mix (Thermo Fisher Scientific, cat. no. NC0295239) respectively. The generated cDNA was purified with Axygen AxyPrep mag PCR clean-up kit (Thermo Fisher Scientific, cat. no. 14223151) using a ratio of 0.6:1 (vol beads: vol PCR reaction) and the purified cDNA was checked by running 1 μ l of the sample on an Agilent Bioanalyzer or Qubit, as per manufacturer's instructions. Samples with good quality cDNA were sent to Laboratory for Functional Genome Analysis (LAFUGA), Gene center Munich, where further downstream steps such as Tagmentation reaction and sequencing were carried out as mentioned in the protocol by (Cadwell et al., 2017). After sequencing, raw reads were de-multiplexed on in-house high-performance-cluster (HPC) using Je (version 2.0.2). The raw sequencing reads were aligned to Ensembl GRCm38 mouse reference genome using STAR aligner (version 2.7.1) with the GeneCounts parameter on. See "Data analysis for scRNA-seq of cortical GM astrocytes, Patch-seq based scRNA-seq and stRNA-seq" for details about data analysis.

Spatial transcriptomics (stRNA-seq) analysis

Animals injected with Mok-LV gRNAs were killed at 7dpi and the extracted brains were embedded and snap frozen in an isopentane and liquid nitrogen bath as recommended by 10x Genomics (Protocol: CG000240). The brains were resected to generate smaller samples (as shown in Figure 4B) at the cryostat (in Thermo Scientific CryoStar NX50) and 10 μ m thick coronal sections of the dorsal brain were cut. The sections were checked for the presence of infected cells (Tdtomato+ cells) briefly. After confirming that we were at the region of injection, two consecutive 10 μ m thick sections containing infected cells were placed in one capture area each. The tissue was stained using H&E staining and imaged with the Carl Zeiss Axio Imager.M2m Microscope using 10x objective (Protocol: CG0001600). The libraries were prepared with Visium Spatial Gene Expression Reagent Kits (CG000239) with 18min

permeabilization time and sequenced on an Illumina HiSeq1500 instrument and a paired-end flowcell (High output) according to manufacturer protocol. Sequencing was performed in the Laboratory for Functional Genome Analysis (LAFUGA). Data was mapped against the mouse reference genome mm10 (GENCODE vM23/Ensembl 98; builds versions 1.2.0 and 2020A from 10xGenomics) with Space Ranger 1.2.2. Further downstream analysis of this data was performed in Rstudio using Seurat and Bioconductor packages. For quality control, spots with less than 30% mitochondrial reads, less than 20% hemoglobin reads and at least 250 detectable genes were selected for further analysis. The four samples were merged on Seurat and spots specific to the cortical GM were selected based on the anatomical position. Data was analyzed as explained below.

Data analysis for scRNA-seq of cortical GM astrocytes, Patch-seq based scRNA-seq and stRNA-seq

All the scRNA-seq and stRNA-seq data were analyzed on Rstudio, using packages from Bioconductor and Seurat and the GO analysis was performed with the enrichGO function and simplified with the Rrvgo package to avoid redundant GO terms. scRNA-seq for cortical GM astrocytes (10x) was kindly provided by Bocchi et al., (*submitted*). Cells annotated as astrocytes in this dataset was subsetted to select astrocytes from the cortical GM, which resulted in 3150 cells. The FindClusters function was used at a resolution of 0.5 and this gave rise to 6 clusters with distinct gene expression patterns. For the Patch-seq based scRNA-seq data and the stRNA-seq data, the cells were clustered similarly with a resolution of 0.8. For comparison of our stRNA-seq data with response after SWI, we used the scRNA-seq dataset (10x) for cells from cortical GM at 5dpSWI, which was kindly provided by Koupourtidou, Schwarz et al., 2023. The module scores for each of the annotated cell type were calculated based on the top 25 DEGs using the AddModuleScore function in Seurat. The statistics for comparison was performed with GraphPad Prism 9.5 with Kruskal-wallis test and Dunn's test for multiple comparison was performed.

Other Resources

Software and Algorithms	
Resource	Identifier
ImageJ	https://imagej.net/Downloads

Imaris 9.7.2	Access to software provided by Core Facility Bioimaging, Biomedical Center, LMU (https://imaris.oxinst.com/)
ZEN software, Zeiss	https://www.zeiss.com/microscopy/en_us/products/microscopesoftware/zen.html
Microsoft Excel	https://www.microsoft.com/en-gb/
GraphPad Prism 9.5	https://www.graphpad.com/
Affinity Designer 1.1	https://affinity.serif.com/en-us/designer/
RStudio	https://rstudio.com
R ggplot2	https://ggplot2.tidyverse.org
Seurat (v4.3)	https://github.com/satijalab/seurat/blob/HEAD/vignettes/install.Rmd
enrichGO (ClusterProfiler)	https://bioconductor.org/packages/release/bioc/vignettes/clusterProfiler/inst/doc/clusterProfiler.html
rrvgo	https://www.micropublication.org/journals/biology/micropub-biology-000811

References

- Bakken, T.E., Jorstad, N.L., Hu, Q., Lake, B.B., Tian, W., Kalmbach, B.E., Crow, M., Hodge, R.D., Krienen, F.M., Sorensen, S.A., Eggermont, J., Yao, Z., Aevermann, B.D., Aldridge, A.I., Bartlett, A., Bertagnolli, D., Casper, T., Castanon, R.G., Crichton, K., Daigle, T.L., Dalley, R., Dee, N., Dembrow, N., Diep, D., Ding, S.-L., Dong, W., Fang, R., Fischer, S., Goldman, M., Goldy, J., Graybuck, L.T., Herb, B.R., Hou, X., Kancherla, J., Kroll, M., Lathia, K., Van Lew, B., Li, Y.E., Liu, C.S., Liu, H., Lucero, J.D., Mahurkar, A., McMillen, D., Miller, J.A., Moussa, M., Nery, J.R., Nicovich, P.R., Niu, S.-Y., Orvis, J., Osteen, J.K., Owen, S., Palmer, C.R., Pham, T., Plongthongkum, N., Poirion, O., Reed, N.M., Rimorin, C., Rivkin, A., Romanow, W.J., Sedeño-Cortés, A.E., Siletti, K., Somasundaram, S., Sulc, J., Tieu, M., Torkelson, A., Tung, H., Wang, X., Xie, F., Yanny, A.M., Zhang, R., Ament, S.A., Behrens, M.M., Bravo, H.C., Chun, J., Dobin, A., Gillis, J., Hertzano, R., Hof, P.R., Höllt, T., Horwitz, G.D., Keene, C.D., Kharchenko, P.V., Ko, A.L., Lelieveldt, B.P., Luo, C., Mukamel, E.A., Pinto-Duarte, A., Preissl, S., Regev, A., Ren, B., Scheuermann, R.H., Smith, K., Spain, W.J., White, O.R., Koch, C., Hawrylycz, M., Tasic, B., Macosko, E.Z., McCarroll, S.A., Ting, J.T., Zeng, H., Zhang, K., Feng, G., Ecker, J.R., Linnarsson, S., Lein, E.S., 2021. Comparative cellular analysis of motor cortex in human, marmoset and mouse. *Nature* 598, 111–119. <https://doi.org/10.1038/s41586-021-03465-8>
- Bayraktar, O.A., Bartels, T., Holmqvist, S., Kleshchevnikov, V., Martirosyan, A., Polioudakis, D., Ben Haim, L., Young, A.M.H., Batiuk, M.Y., Prakash, K., Brown, A., Roberts, K., Paredes, M.F., Kawaguchi, R., Stockley, J.H., Sabeur, K., Chang, S.M., Huang, E., Hutchinson, P., Ullian, E.M., Hemberg, M., Coppola, G., Holt, M.G., Geschwind, D.H., Rowitch, D.H., 2020. Astrocyte layers in the mammalian cerebral cortex revealed by a single-cell in situ transcriptomic map. *Nat. Neurosci.* 23, 500–509. <https://doi.org/10.1038/s41593-020-0602-1>
- Boisvert, M.M., Erikson, G.A., Shokhirev, M.N., Allen, N.J., 2018. The Aging Astrocyte Transcriptome from Multiple Regions of the Mouse Brain. *Cell Rep.* 22, 269–285. <https://doi.org/10.1016/j.celrep.2017.12.039>
- Breunig, C.T., Neuner, A.M., Giehl-Schwab, J., Wurst, W., Götz, M., Stricker, S.H., 2018. A Customizable Protocol for String Assembly gRNA Cloning (STAgR). *J. Vis. Exp.* 58556. <https://doi.org/10.3791/58556>
- Cadwell, C.R., Palasantza, A., Jiang, X., Berens, P., Deng, Q., Yilmaz, M., Reimer, J., Shen, S., Bethge, M., Tolias, K.F., Sandberg, R., Tolias, A.S., 2016. Electrophysiological, transcriptomic and morphologic profiling of single neurons using Patch-seq. *Nat. Biotechnol.* 34, 199–203. <https://doi.org/10.1038/nbt.3445>
- Cadwell, C.R., Scala, F., Li, S., Livrizzi, G., Shen, S., Sandberg, R., Jiang, X., Tolias, A.S., 2017. Multimodal profiling of single-cell morphology, electrophysiology, and gene expression using Patch-seq. *Nat. Protoc.* 12, 2531–2553. <https://doi.org/10.1038/nprot.2017.120>
- Cheng, Y.-T., Luna-Figueroa, E., Woo, J., Chen, H.-C., Lee, Z.-F., Harmanci, A.S., Deneen, B., 2023. Inhibitory input directs astrocyte morphogenesis through glial GABABR. *Nature* 617, 369–376. <https://doi.org/10.1038/s41586-023-06010-x>
- Deneen, B., Ho, R., Lukaszewicz, A., Hochstim, C.J., Gronostajski, R.M., Anderson, D.J., 2006. The Transcription Factor NFIA Controls the Onset of Gliogenesis in the Developing Spinal Cord. *Neuron* 52, 953–968. <https://doi.org/10.1016/j.neuron.2006.11.019>
- Endo, F., Kasai, A., Soto, J.S., Yu, X., Qu, Z., Hashimoto, H., Gradinaru, V., Kawaguchi, R., Khakh, B.S., 2022. Molecular basis of astrocyte diversity and morphology across the

- CNS in health and disease. *Science* 378, eadc9020.
<https://doi.org/10.1126/science.adc9020>
- Escartin, C., Galea, E., Lakatos, A., O’Callaghan, J.P., Petzold, G.C., Serrano-Pozo, A., Steinhäuser, C., Volterra, A., Carmignoto, G., Agarwal, A., Allen, N.J., Araque, A., Barbeito, L., Barzilai, A., Bergles, D.E., Bonvento, G., Butt, A.M., Chen, W.-T., Cohen-Salmon, M., Cunningham, C., Deneen, B., De Strooper, B., Díaz-Castro, B., Farina, C., Freeman, M., Gallo, V., Goldman, J.E., Goldman, S.A., Götz, M., Gutiérrez, A., Haydon, P.G., Heiland, D.H., Hol, E.M., Holt, M.G., Iino, M., Kastanenka, K.V., Kettenmann, H., Khakh, B.S., Koizumi, S., Lee, C.J., Liddelow, S.A., MacVicar, B.A., Magistretti, P., Messing, A., Mishra, A., Molofsky, A.V., Murai, K.K., Norris, C.M., Okada, S., Oliet, S.H.R., Oliveira, J.F., Panatier, A., Parpura, V., Pekna, M., Pekny, M., Pellerin, L., Perea, G., Pérez-Nievas, B.G., Pfrieger, F.W., Poskanzer, K.E., Quintana, F.J., Ransohoff, R.M., Riquelme-Perez, M., Robel, S., Rose, C.R., Rothstein, J.D., Rouach, N., Rowitch, D.H., Semyanov, A., Sirko, S., Sontheimer, H., Swanson, R.A., Vitorica, J., Wanner, I.-B., Wood, L.B., Wu, J., Zheng, B., Zimmer, E.R., Zorec, R., Sofroniew, M.V., Verkhratsky, A., 2021. Reactive astrocyte nomenclature, definitions, and future directions. *Nat. Neurosci.* 24, 312–325. <https://doi.org/10.1038/s41593-020-00783-4>
- Fantauzzo, K.A., Christiano, A.M., 2012. Trps1 activates a network of secreted Wnt inhibitors and transcription factors crucial to vibrissa follicle morphogenesis. *Development* 139, 203–214. <https://doi.org/10.1242/dev.069971>
- Fantauzzo, K.A., Kurban, M., Levy, B., Christiano, A.M., 2012. Trps1 and Its Target Gene Sox9 Regulate Epithelial Proliferation in the Developing Hair Follicle and Are Associated with Hypertrichosis. *PLoS Genet.* 8, e1003002. <https://doi.org/10.1371/journal.pgen.1003002>
- Frik, J., Merl-Pham, J., Plesnila, N., Mattugini, N., Kjell, J., Kraska, J., Gómez, R.M., Hauck, S.M., Sirko, S., Götz, M., 2018. Cross-talk between monocyte invasion and astrocyte proliferation regulates scarring in brain injury. *EMBO Rep.* 19, e45294. <https://doi.org/10.15252/embr.201745294>
- Gibson, D.G., 2011. Enzymatic Assembly of Overlapping DNA Fragments, in: *Methods in Enzymology*. Elsevier, pp. 349–361. <https://doi.org/10.1016/B978-0-12-385120-8.00015-2>
- Glasgow, S.M., Carlson, J.C., Zhu, W., Chaboub, L.S., Kang, P., Lee, H.K., Clovis, Y.M., Lozzi, B.E., McEvelly, R.J., Rosenfeld, M.G., Creighton, C.J., Lee, S.-K., Mohila, C.A., Deneen, B., 2017. Glia-specific enhancers and chromatin structure regulate NFIA expression and glioma tumorigenesis. *Nat. Neurosci.* 20, 1520–1528. <https://doi.org/10.1038/nn.4638>
- Hammond, T.R., McEllin, B., Morton, P.D., Raymond, M., Dupree, J., Gallo, V., 2015. Endothelin-B Receptor Activation in Astrocytes Regulates the Rate of Oligodendrocyte Regeneration during Remyelination. *Cell Rep.* 13, 2090–2097. <https://doi.org/10.1016/j.celrep.2015.11.002>
- Hasel, P., Rose, I.V.L., Sadick, J.S., Kim, R.D., Liddelow, S.A., 2021. Neuroinflammatory astrocyte subtypes in the mouse brain. *Nat. Neurosci.* 24, 1475–1487. <https://doi.org/10.1038/s41593-021-00905-6>
- Heinrich, C., Bergami, M., Gascón, S., Lepier, A., Viganò, F., Dimou, L., Sutor, B., Berninger, B., Götz, M., 2014. Sox2-Mediated Conversion of NG2 Glia into Induced Neurons in the Injured Adult Cerebral Cortex. *Stem Cell Rep.* 3, 1000–1014. <https://doi.org/10.1016/j.stemcr.2014.10.007>
- Hol, E.M., Pekny, M., 2015. Glial fibrillary acidic protein (GFAP) and the astrocyte intermediate filament system in diseases of the central nervous system. *Curr. Opin. Cell Biol.* 32, 121–130. <https://doi.org/10.1016/j.ceb.2015.02.004>

- Huang, A.Y.-S., Woo, J., Sardar, D., Lozzi, B., Bosquez Huerta, N.A., Lin, C.-C.J., Felice, D., Jain, A., Paulucci-Holthausen, A., Deneen, B., 2020. Region-Specific Transcriptional Control of Astrocyte Function Oversees Local Circuit Activities. *Neuron* 106, 992-1008.e9. <https://doi.org/10.1016/j.neuron.2020.03.025>
- Kang, P., Lee, H.K., Glasgow, S.M., Finley, M., Donti, T., Gaber, Z.B., Graham, B.H., Foster, A.E., Novitsch, B.G., Gronostajski, R.M., Deneen, B., 2012. Sox9 and NFIA Coordinate a Transcriptional Regulatory Cascade during the Initiation of Gliogenesis. *Neuron* 74, 79–94. <https://doi.org/10.1016/j.neuron.2012.01.024>
- Klum, S., Zaouter, C., Alekseenko, Z., Björklund, Å.K., Hagey, D.W., Ericson, J., Muhr, J., Bergsland, M., 2018. Sequentially acting SOX proteins orchestrate astrocyte- and oligodendrocyte-specific gene expression. *EMBO Rep.* 19, e46635. <https://doi.org/10.15252/embr.201846635>
- Koupourtidou, C., Veronika Schwarz, Aliee, H., Frerich, S., Fischer-Sternjak, J., Bocchi, R., Simon-Ebert, T., Dichgans, M., Götz, M., Theis, F., Ninkovic, J., 2023. Shared inflammatory glial cell signature after brain injury, revealed by spatial, temporal and cell-type-specific profiling of the murine cerebral cortex (preprint). *Neuroscience*. <https://doi.org/10.1101/2023.02.24.529840>
- Lanjakornsiripan, D., Pior, B.-J., Kawaguchi, D., Furutachi, S., Tahara, T., Katsuyama, Y., Suzuki, Y., Fukazawa, Y., Gotoh, Y., 2018. Layer-specific morphological and molecular differences in neocortical astrocytes and their dependence on neuronal layers. *Nat. Commun.* 9, 1623. <https://doi.org/10.1038/s41467-018-03940-3>
- Laug, D., Huang, T.-W., Huerta, N.A.B., Huang, A.Y.-S., Sardar, D., Ortiz-Guzman, J., Carlson, J.C., Arenkiel, B.R., Kuo, C.T., Mohila, C.A., Glasgow, S.M., Lee, H.K., Deneen, B., 2019. Nuclear factor I-A regulates diverse reactive astrocyte responses after CNS injury. *J. Clin. Invest.* 129, 4408–4418. <https://doi.org/10.1172/JCI127492>
- Malik, T.H., 2001. Transcriptional repression and developmental functions of the atypical vertebrate GATA protein TRPS1. *EMBO J.* 20, 1715–1725. <https://doi.org/10.1093/emboj/20.7.1715>
- Mattugini, N., Bocchi, R., Scheuss, V., Russo, G.L., Torper, O., Lao, C.L., Götz, M., 2019. Inducing Different Neuronal Subtypes from Astrocytes in the Injured Mouse Cerebral Cortex. *Neuron* 103, 1086-1095.e5. <https://doi.org/10.1016/j.neuron.2019.08.009>
- Mira, R.G., Lira, M., Cerpa, W., 2021. Traumatic Brain Injury: Mechanisms of Glial Response. *Front. Physiol.* 12, 740939. <https://doi.org/10.3389/fphys.2021.740939>
- Ohba, S., He, X., Hojo, H., McMahon, A.P., 2015. Distinct Transcriptional Programs Underlie Sox9 Regulation of the Mammalian Chondrocyte. *Cell Rep.* 12, 229–243. <https://doi.org/10.1016/j.celrep.2015.06.013>
- Ohlig, S., Clavreul, S., Thorwirth, M., Simon-Ebert, T., Bocchi, R., Ulbricht, S., Kannayian, N., Rossner, M., Sirko, S., Smialowski, P., Fischer-Sternjak, J., Götz, M., 2021a. Molecular diversity of diencephalic astrocytes reveals adult astrogenesis regulated by Smad4. *EMBO J.* 40. <https://doi.org/10.15252/emboj.2020107532>
- Ohlig, S., Clavreul, S., Thorwirth, M., Simon-Ebert, T., Bocchi, R., Ulbricht, S., Kannayian, N., Rossner, M., Sirko, S., Smialowski, P., Fischer-Sternjak, J., Götz, M., 2021b. Molecular diversity of diencephalic astrocytes reveals adult astrogenesis regulated by Smad4. *EMBO J.* 40, e107532. <https://doi.org/10.15252/emboj.2020107532>
- Palii, C.G., Cheng, Q., Gillespie, M.A., Shannon, P., Mazurczyk, M., Napolitani, G., Price, N.D., Ranish, J.A., Morrissey, E., Higgs, D.R., Brand, M., 2019. Single-Cell Proteomics Reveal that Quantitative Changes in Co-expressed Lineage-Specific Transcription Factors Determine Cell Fate. *Cell Stem Cell* 24, 812-820.e5. <https://doi.org/10.1016/j.stem.2019.02.006>
- Platt, R.J., Chen, S., Zhou, Y., Yim, M.J., Swiech, L., Kempton, H.R., Dahlman, J.E., Parnas, O., Eisenhaure, T.M., Jovanovic, M., Graham, D.B., Jhunjunwala, S., Heidenreich,

- M., Xavier, R.J., Langer, R., Anderson, D.G., Hacoheh, N., Regev, A., Feng, G., Sharp, P.A., Zhang, F., 2014. CRISPR-Cas9 Knockin Mice for Genome Editing and Cancer Modeling. *Cell* 159, 440–455. <https://doi.org/10.1016/j.cell.2014.09.014>
- Puntambekar, S.S., Saber, M., Lamb, B.T., Kokiko-Cochran, O.N., 2018. Cellular players that shape evolving pathology and neurodegeneration following traumatic brain injury. *Brain. Behav. Immun.* 71, 9–17. <https://doi.org/10.1016/j.bbi.2018.03.033>
- Sadick, J.S., O’Dea, M.R., Hasel, P., Dykstra, T., Faustin, A., Liddelow, S.A., 2022. Astrocytes and oligodendrocytes undergo subtype-specific transcriptional changes in Alzheimer’s disease. *Neuron* 110, 1788-1805.e10. <https://doi.org/10.1016/j.neuron.2022.03.008>
- Sanchez-Gonzalez, R., Koupourtidou, C., Lepko, T., Zambusi, A., Novoselc, K.T., Durovic, T., Aschenbroich, S., Schwarz, V., Breunig, C.T., Straka, H., Huttner, H.B., Irmeler, M., Beckers, J., Wurst, W., Zwergal, A., Schauer, T., Straub, T., Czopka, T., Trümbach, D., Götz, M., Stricker, S.H., Ninkovic, J., 2022. Innate Immune Pathways Promote Oligodendrocyte Progenitor Cell Recruitment to the Injury Site in Adult Zebrafish Brain. *Cells* 11, 520. <https://doi.org/10.3390/cells11030520>
- Sardar, D., Chen, H.-C., Reyes, A., Varadharajan, S., Jain, A., Mohila, C., Curry, R., Lozzi, B., Rajendran, K., Cervantes, A., Yu, K., Jalali, A., Rao, G., Mack, S.C., Deneen, B., 2022. Sox9 directs divergent epigenomic states in brain tumor subtypes. *Proc. Natl. Acad. Sci.* 119, e2202015119. <https://doi.org/10.1073/pnas.2202015119>
- Sirko, S., Irmeler, M., Gascón, S., Bek, S., Schneider, S., Dimou, L., Obermann, J., De Souza Paiva, D., Poirier, F., Beckers, J., Hauck, S.M., Barde, Y., Götz, M., 2015. Astrocyte reactivity after brain injury—: The role of galectins 1 and 3. *Glia* 63, 2340–2361. <https://doi.org/10.1002/glia.22898>
- Sun, W., Cornwell, A., Li, J., Peng, S., Osorio, M.J., Aalling, N., Wang, S., Benraiss, A., Lou, N., Goldman, S.A., Nedergaard, M., 2017. SOX9 Is an Astrocyte-Specific Nuclear Marker in the Adult Brain Outside the Neurogenic Regions. *J. Neurosci.* 37, 4493–4507. <https://doi.org/10.1523/JNEUROSCI.3199-16.2017>
- Tan, Z., Niu, B., Tsang, K.Y., Melhado, I.G., Ohba, S., He, X., Huang, Y., Wang, C., McMahon, A.P., Jauch, R., Chan, D., Zhang, M.Q., Cheah, K.S.E., 2018. Synergistic co-regulation and competition by a SOX9-GLI-FOXA phasic transcriptional network coordinate chondrocyte differentiation transitions. *PLOS Genet.* 14, e1007346. <https://doi.org/10.1371/journal.pgen.1007346>
- Tiwari, N., Pataskar, A., Péron, S., Thakurela, S., Sahu, S.K., Figueres-Oñate, M., Marichal, N., López-Mascaraque, L., Tiwari, V.K., Berninger, B., 2018. Stage-Specific Transcription Factors Drive Astrogliogenesis by Remodeling Gene Regulatory Landscapes. *Cell Stem Cell* 23, 557-571.e8. <https://doi.org/10.1016/j.stem.2018.09.008>
- Ung, K., Huang, T.-W., Lozzi, B., Woo, J., Hanson, E., Pekarek, B., Tepe, B., Sardar, D., Cheng, Y.-T., Liu, G., Deneen, B., Arenkiel, B.R., 2021. Olfactory bulb astrocytes mediate sensory circuit processing through Sox9 in the mouse brain. *Nat. Commun.* 12, 5230. <https://doi.org/10.1038/s41467-021-25444-3>
- Watson, D.J., Kobinger, G.P., Passini, M.A., Wilson, J.M., Wolfe, J.H., 2002. Targeted Transduction Patterns in the Mouse Brain by Lentivirus Vectors Pseudotyped with VSV, Ebola, Mokola, LCMV, or MuLV Envelope Proteins. *Mol. Ther.* 5, 528–537. <https://doi.org/10.1006/mthe.2002.0584>
- Weng, Q., Wang, Jincheng, Wang, Jiajia, He, D., Cheng, Z., Zhang, F., Verma, R., Xu, L., Dong, X., Liao, Y., He, X., Potter, A., Zhang, L., Zhao, C., Xin, M., Zhou, Q., Aronow, B.J., Blackshear, P.J., Rich, J.N., He, Q., Zhou, W., Suvà, M.L., Waclaw, R.R., Potter, S.S., Yu, G., Lu, Q.R., 2019. Single-Cell Transcriptomics Uncovers Glial Progenitor Diversity and Cell Fate Determinants during Development and

- Gliomagenesis. *Cell Stem Cell* 24, 707-723.e8.
<https://doi.org/10.1016/j.stem.2019.03.006>
- Witwicki, R.M., Ekram, M.B., Qiu, X., Janiszewska, M., Shu, S., Kwon, M., Trinh, A., Frias, E., Ramadan, N., Hoffman, G., Yu, K., Xie, Y., McAllister, G., McDonald, R., Golji, J., Schlabach, M., deWeck, A., Keen, N., Chan, H.M., Ruddy, D., Rejtar, T., Sovath, S., Silver, S., Sellers, W.R., Jagani, Z., Hogarty, M.D., Roberts, C., Brown, M., Stegmaier, K., Long, H., Shivdasani, R.A., Pellman, D., Polyak, K., 2018. TRPS1 Is a Lineage-Specific Transcriptional Dependency in Breast Cancer. *Cell Rep.* 25, 1255-1267.e5. <https://doi.org/10.1016/j.celrep.2018.10.023>
- Wuelling, M., Schneider, S., Schröther, V.A., Waterkamp, C., Hoffmann, D., Vortkamp, A., 2020. Wnt5a is a transcriptional target of Gli3 and Trps1 at the onset of chondrocyte hypertrophy. *Dev. Biol.* 457, 104–118. <https://doi.org/10.1016/j.ydbio.2019.09.012>
- Yang, Y., Gomez, N., Infarinato, N., Adam, R.C., Sribour, M., Baek, I., Laurin, M., Fuchs, E., 2023. The pioneer factor SOX9 competes for epigenetic factors to switch stem cell fates. *Nat. Cell Biol.* <https://doi.org/10.1038/s41556-023-01184-y>
- Zamboni, M., Llorens-Bobadilla, E., Magnusson, J.P., Frisén, J., 2020. A Widespread Neurogenic Potential of Neocortical Astrocytes Is Induced by Injury. *Cell Stem Cell* 27, 605-617.e5. <https://doi.org/10.1016/j.stem.2020.07.006>
- Zhang, Y., Chen, K., Sloan, S.A., Bennett, M.L., Scholze, A.R., O'Keefe, S., Phatnani, H.P., Guarnieri, P., Caneda, C., Ruderisch, N., Deng, S., Liddelow, S.A., Zhang, C., Daneman, R., Maniatis, T., Barres, B.A., Wu, J.Q., 2014. An RNA-Sequencing Transcriptome and Splicing Database of Glia, Neurons, and Vascular Cells of the Cerebral Cortex. *J. Neurosci.* 34, 11929–11947.
<https://doi.org/10.1523/JNEUROSCI.1860-14.2014>

Figure 1

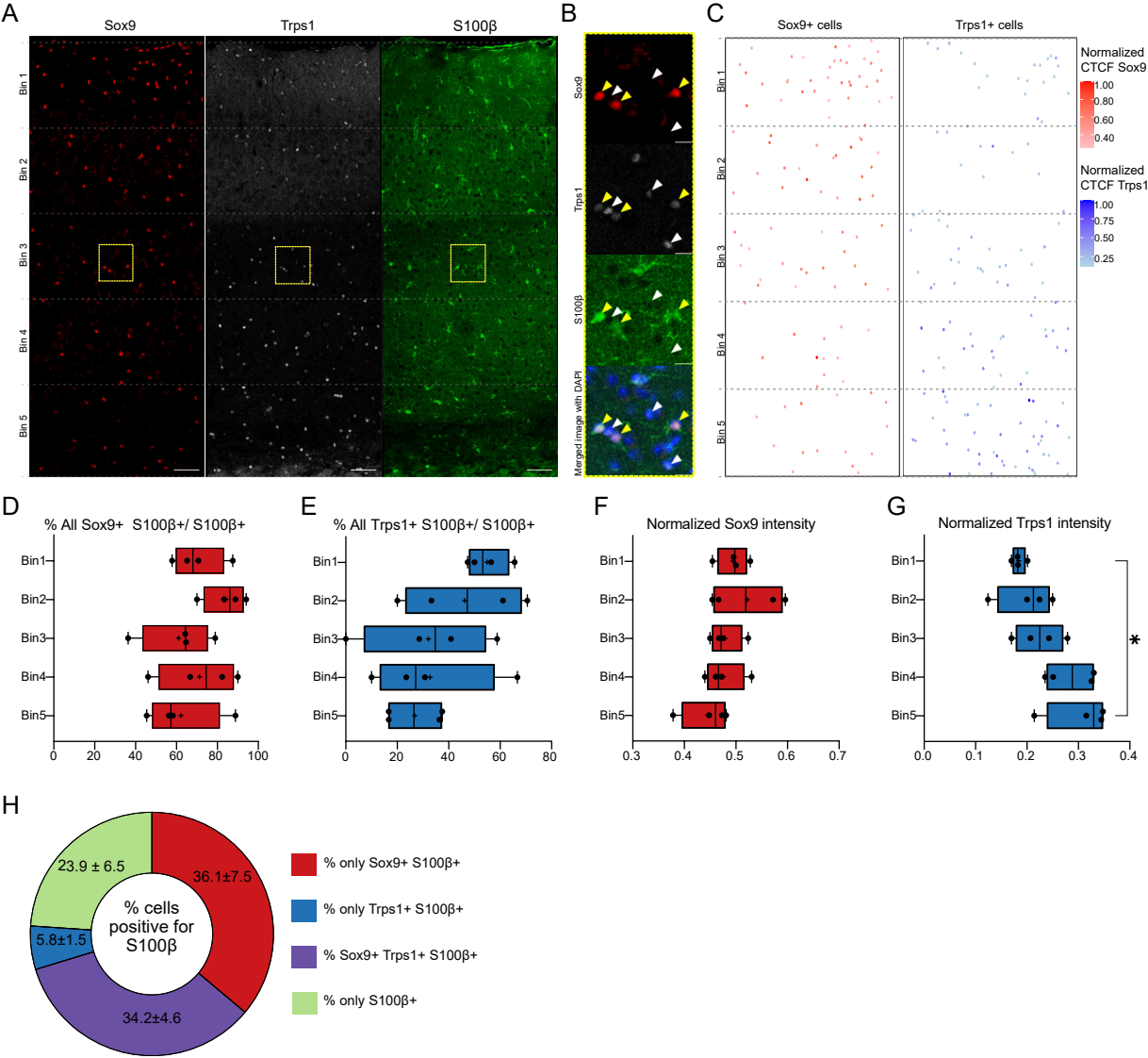


Figure 2

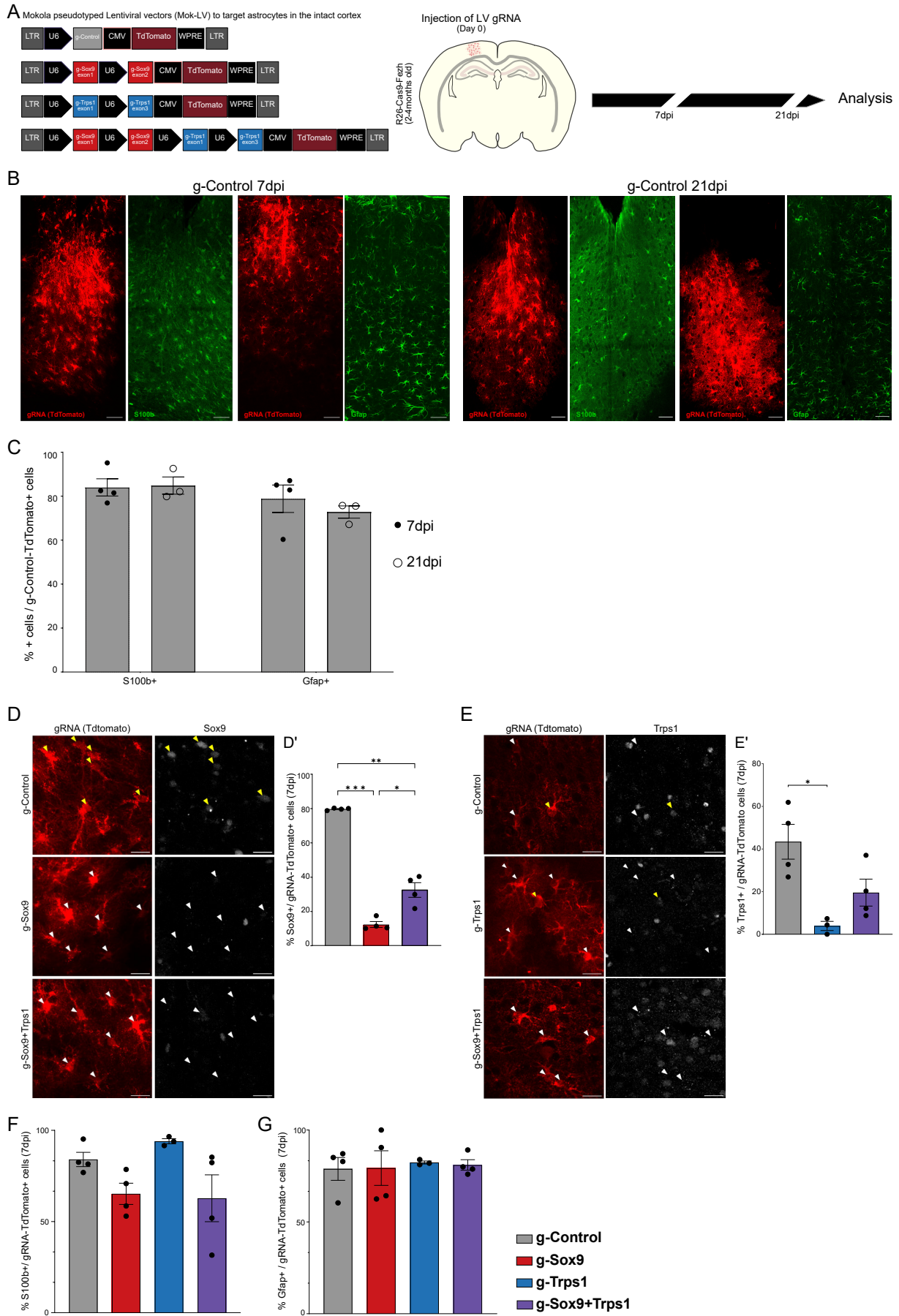


Figure 3

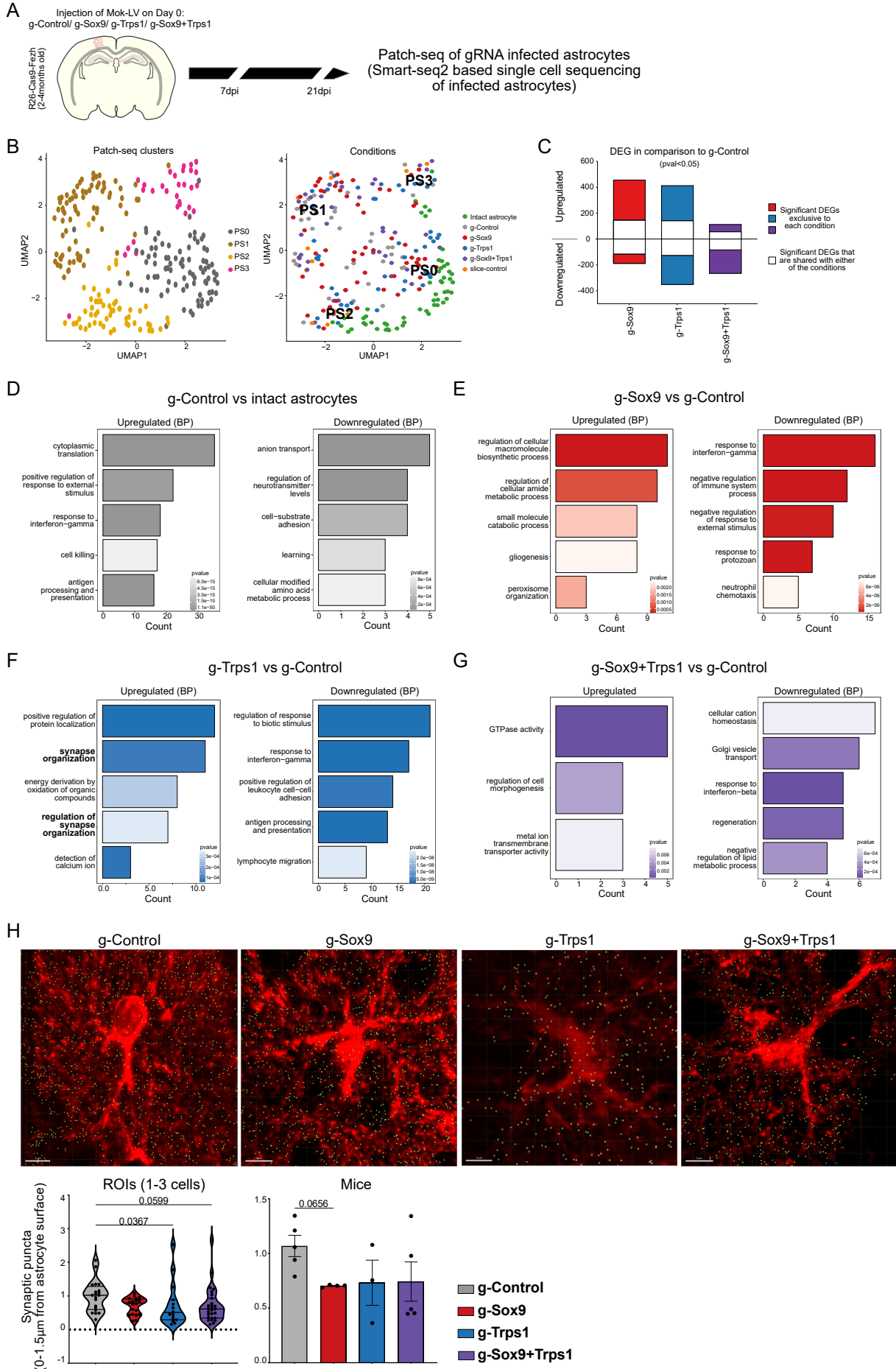


Figure 4

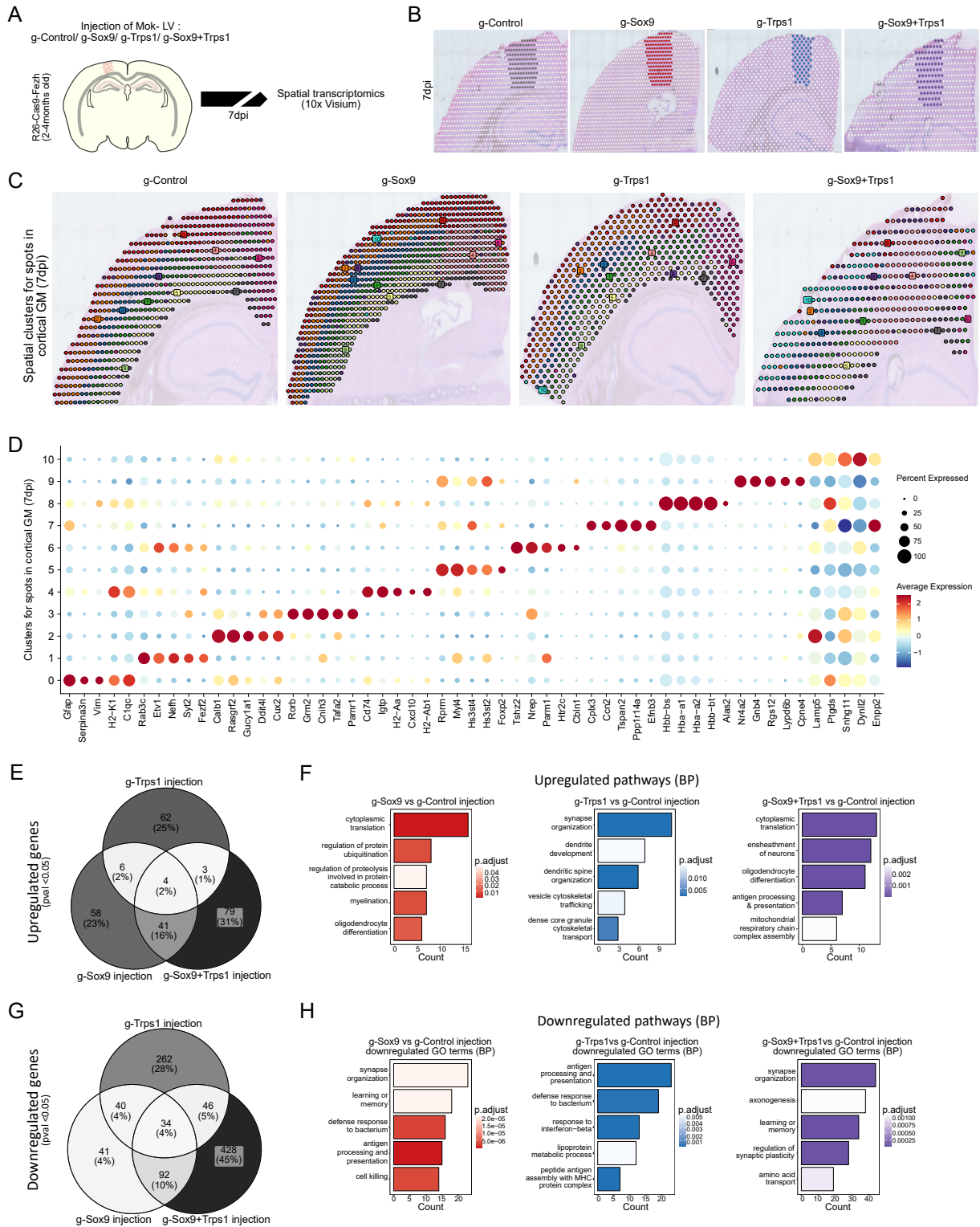
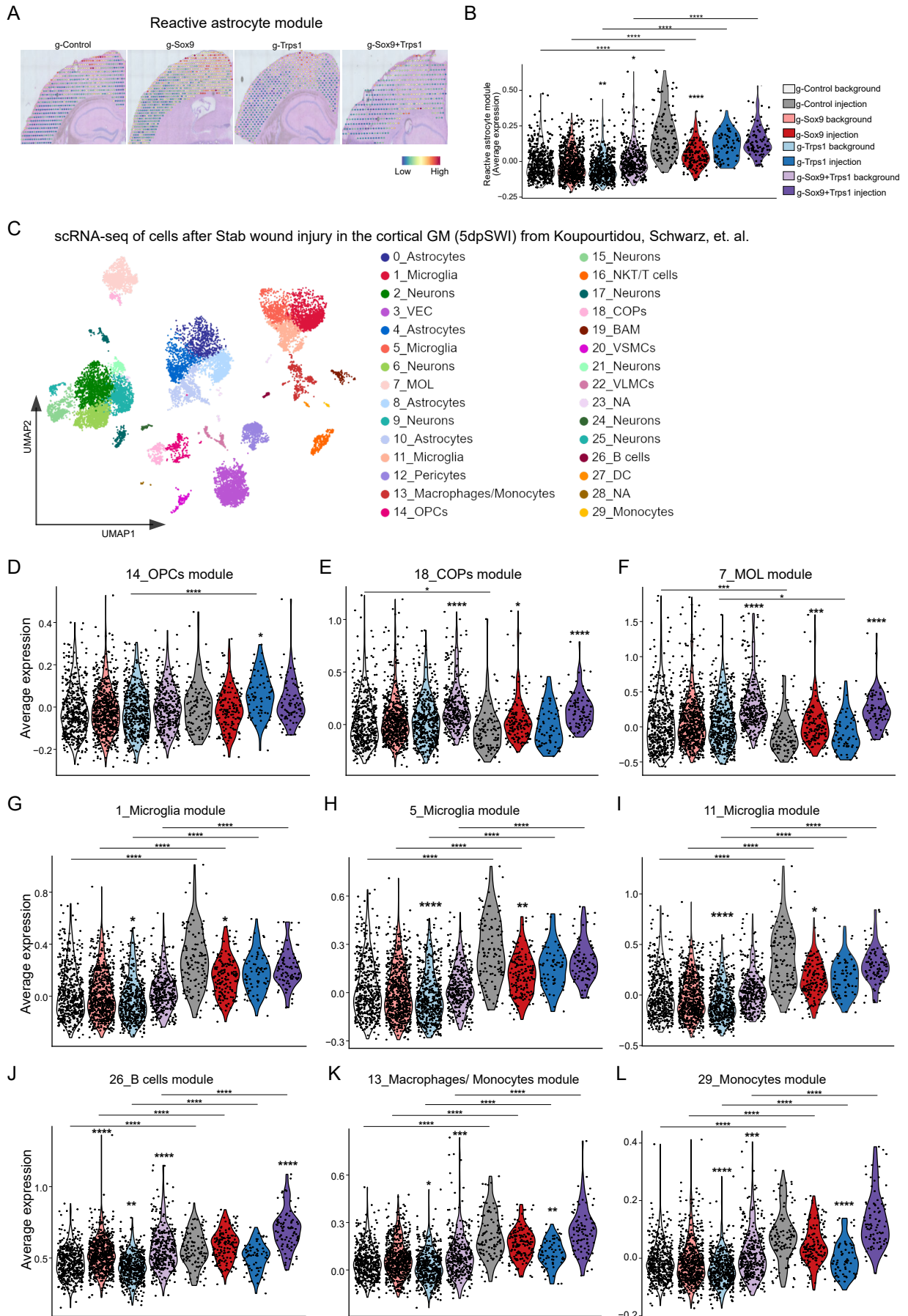
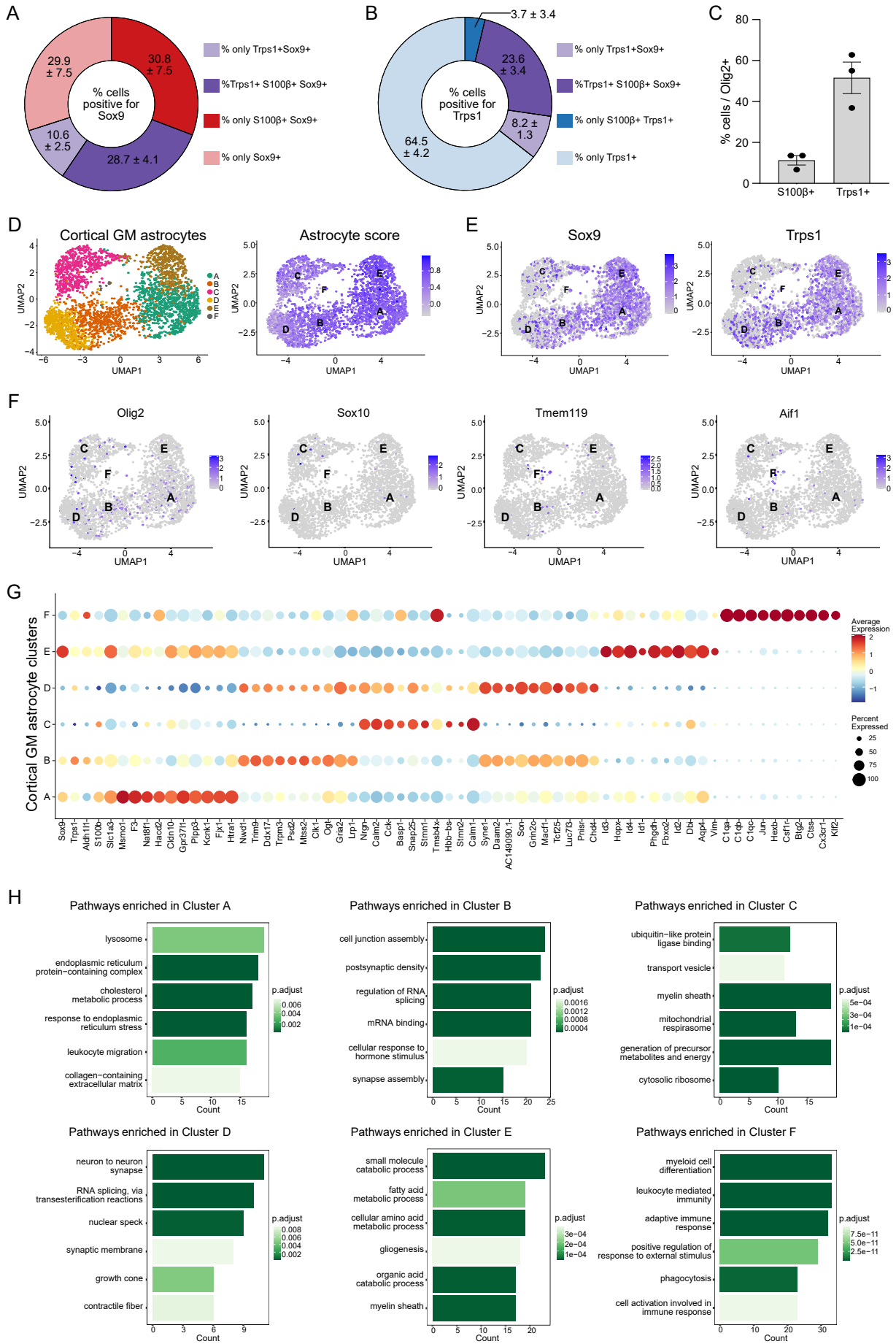


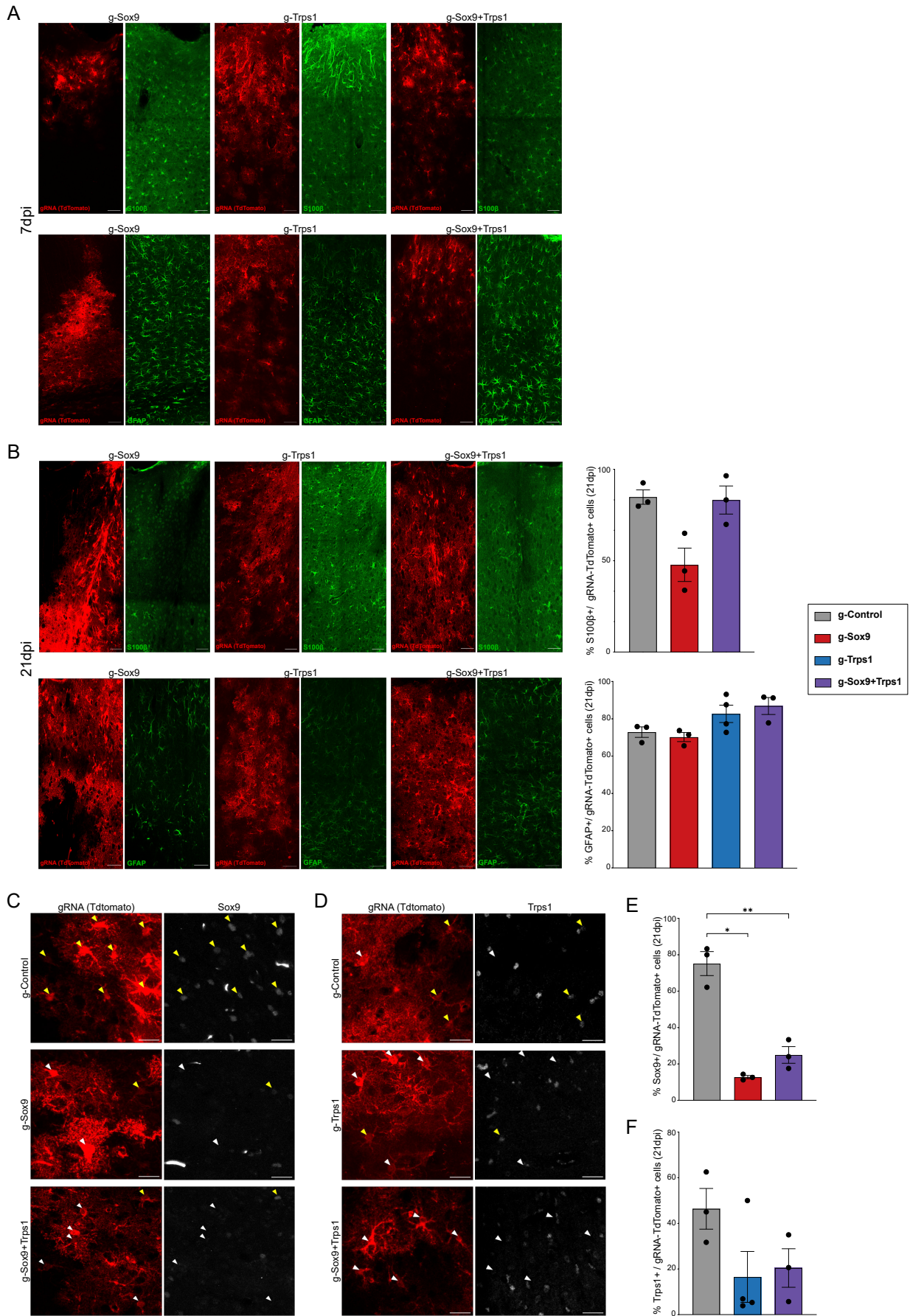
Figure 5



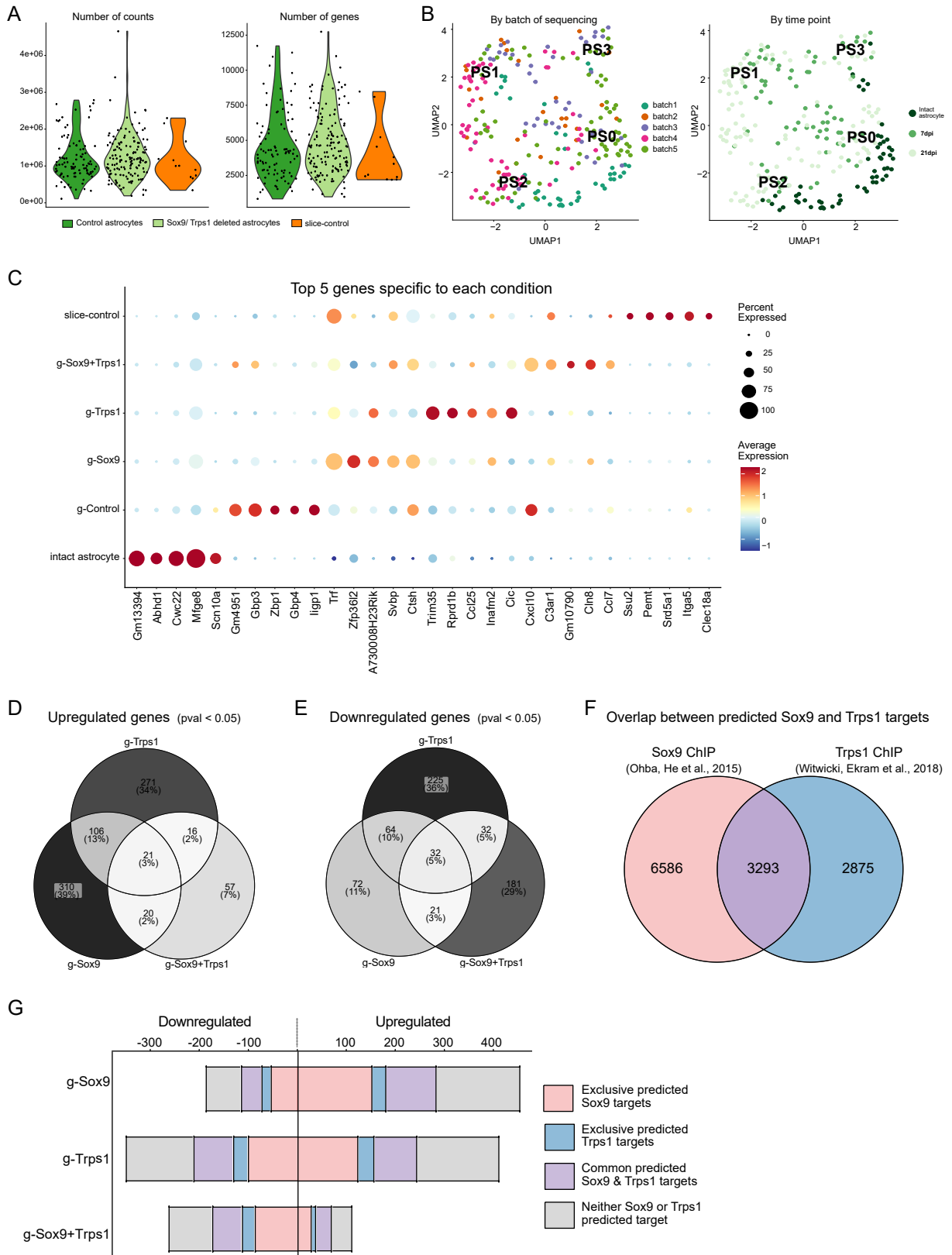
Extended data Figure 1 (Related to Figure 1)



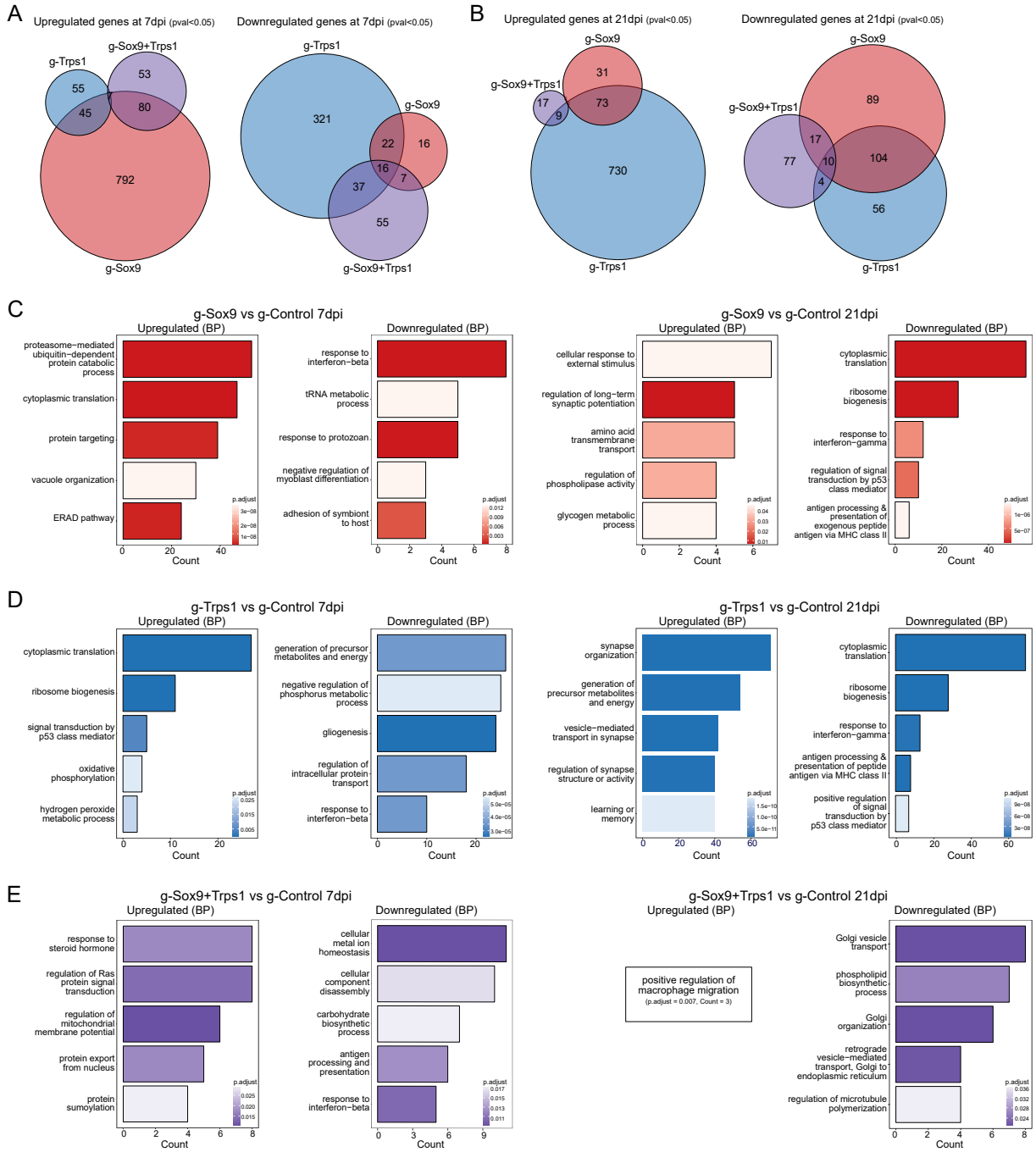
Extended data Figure 2 (Related to Figure 2)



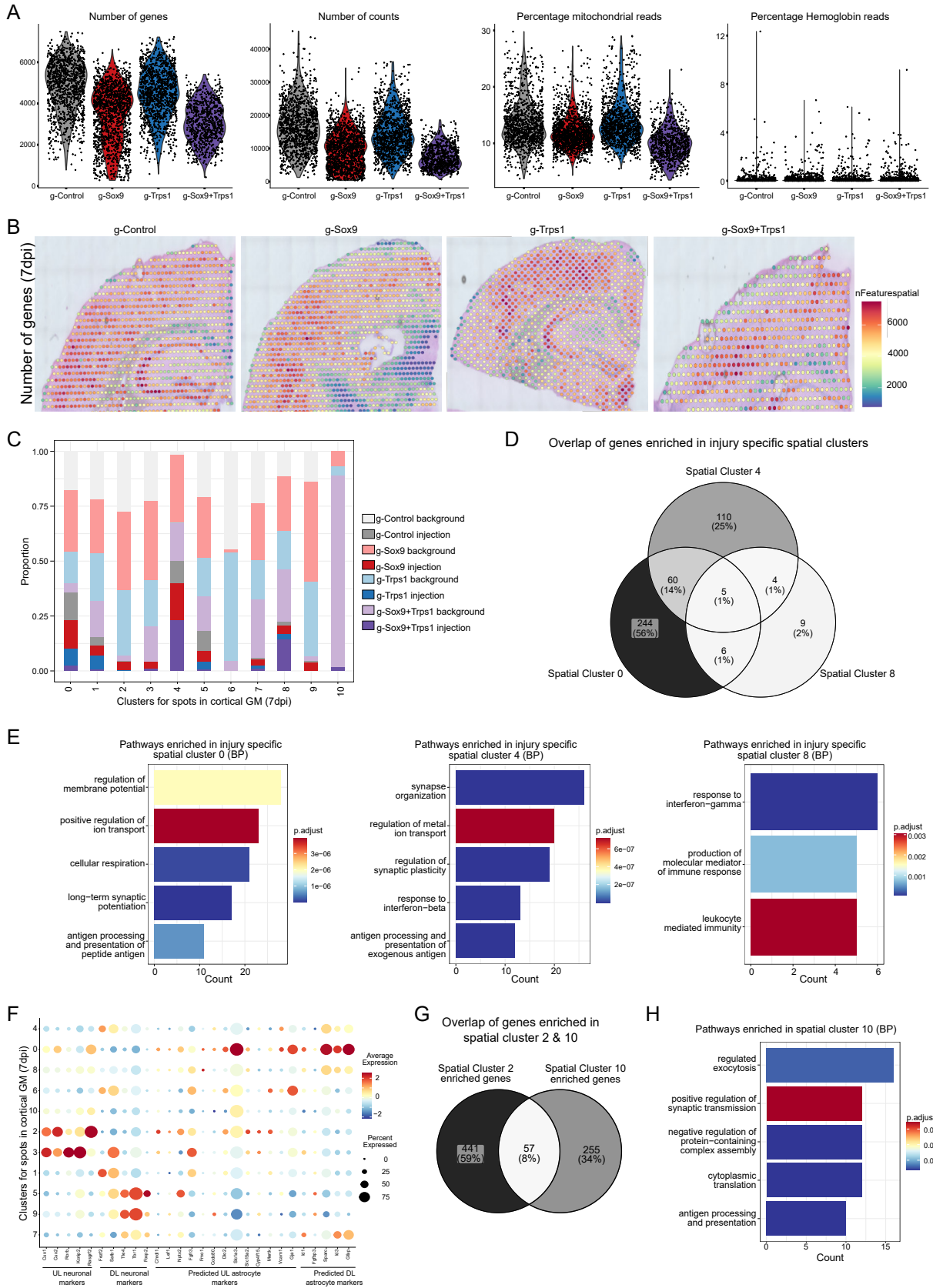
Extended data Figure 3 (Related to Figure 3)



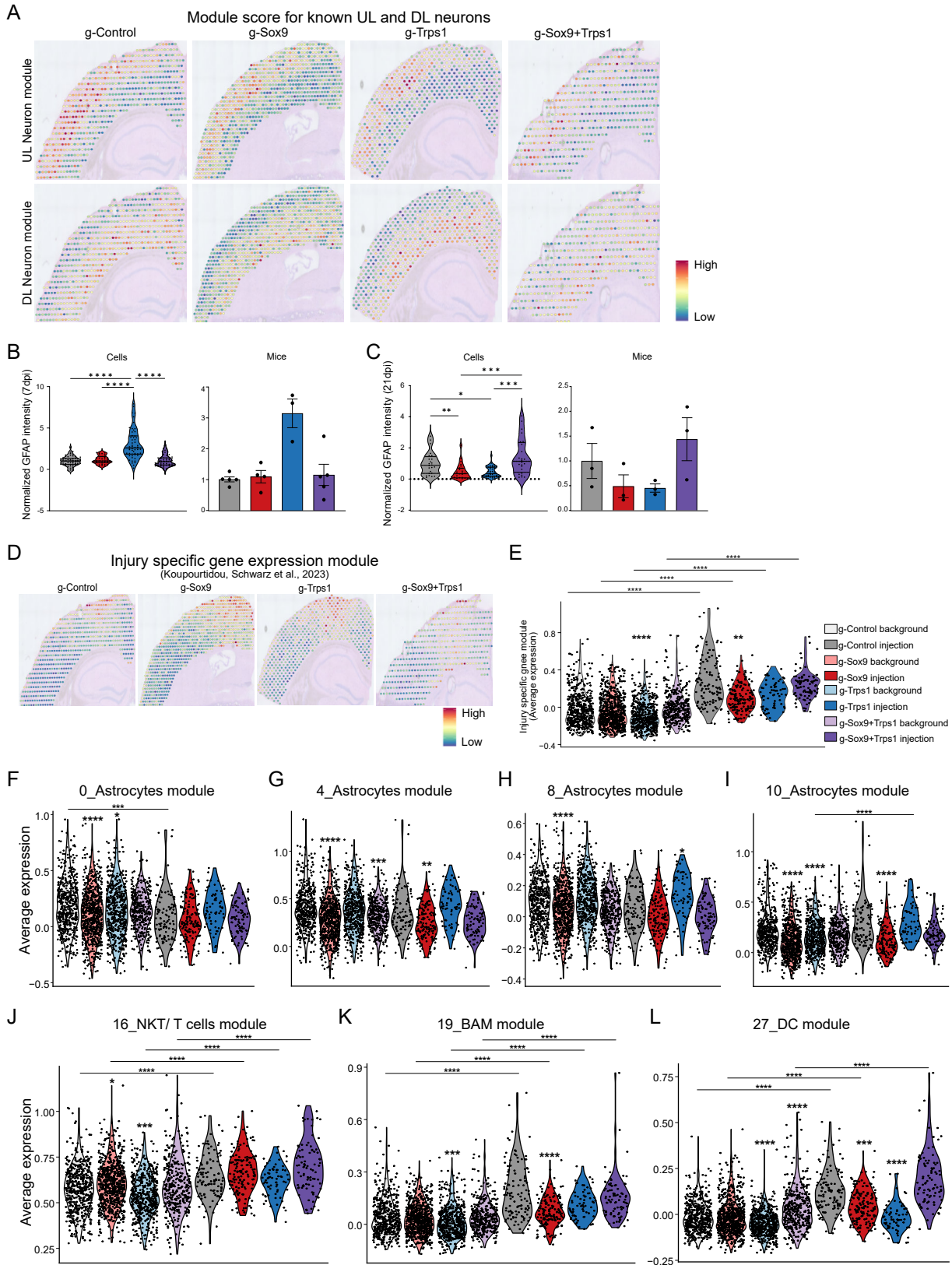
Extended data Figure 4 (Related to Figure 3)



Extended data Figure 5 (Related to Figure 4)



Extended data Figure 6 (Related to Figure 5)



3. DISCUSSION

My PhD projects focused on identifying methods to improve direct neuronal reprogramming of astrocytes and understanding the molecular mechanisms governing the starter cell (astrocyte) identity and functions.

3.1 Metabolic and mitochondrial remodeling are crucial to the success of astrocyte to neuron fate conversion

Metabolic plasticity characterized by a shift from aerobic glycolysis to oxidative phosphorylation has been observed during developmental differentiation of neuronal progenitors (Lorenz and Prigione, 2017; Zheng et al., 2016). Similarly, a shift in metabolism has also been observed during adult neural stem cell activation (Knobloch et al., 2017; Llorens-Bobadilla et al., 2015; Wani et al., 2022), showing this to be an essential step in adult neurogenesis as well. Astrocytes have been shown to be metabolically similar to NSCs (Götz et al., 2015), they have a higher preference for glycolysis and FAO while neurons prefer oxidative phosphorylation (Bolaños, 2016; Magistretti and Allaman, 2018; Rose et al., 2020). Thus, conversion of astrocytes to neurons by direct reprogramming would require this successful metabolic shift. As explained earlier, direct neuronal reprogramming of astrocytes also elicits massive cell death due to ROS production, thus it was of interest to understand how the mitochondria and metabolism affects direct neuronal reprogramming of astrocytes.

3.1.1 Astrocytes and neurons have a distinct mitochondrial proteome

To understand how the mitochondria of astrocytes and neurons differ to support their preferred metabolic pathways, we characterized the mitochondrial proteome of *in vitro* cultured postnatal cortical astrocytes and E14 derived cortical neurons by liquid chromatography-tandem mass spectrometry (LC-MS/MS). Analysis revealed significant differences in the entire proteome as well as the mitochondrial proteome of astrocytes when compared to neurons. In general, around 20% of the mitoproteome showed an enrichment in either astrocytes or neurons. Gene ontology analysis to understand the functional relevance of the differences in the mitoproteome revealed that astrocytes had proteins specific to processes like “fatty acid beta-oxidation”, “cellular lipid catabolic process” in line with known astrocyte functions of metabolic support of neurons by these pathways (Ioannou et al., 2019; Van Deijk et al., 2017). On the other hand, proteins

enriched in the neuronal mitoproteome showed enrichment for terms like “mitochondrial RNA metabolic process” and “tRNA metabolic process”.

A previous study had characterized the mitoproteome of astrocytes and neurons (Purkinje cells and granule cells) of the cerebellum. Similar to our findings, they identified that the mitoproteomes differed significantly, even between the two neuronal cell types (Fecher et al., 2019). There were similarities between the mitoproteome of cortical astrocytes from our study and that of the cerebellar astrocytes in their study (with around 60% overlap), and pathways like fatty acid oxidation with common regulators like Cpt1a, Cpt2 enriched in both. The differences in the mitoproteome between the two studies likely arise from the fact that astrocytes and neurons are distinct between the brain regions (Endo et al., 2022; Herrero-Navarro et al., 2021).

3.1.2. Mitochondria undergoes dynamic remodeling during direct neuronal reprogramming of astrocytes

First, we observed that the morphology of astrocyte mitochondria was vastly different from that of reprogrammed neurons. Astrocytes had ramified and elongated mitochondria, while the successfully reprogrammed iNs had smaller and round mitochondria. Neurons are known to have smaller and round mitochondria, especially in the axonal compartment (Mendelsohn et al., 2022; Misgeld and Schwarz, 2017), while astrocytes have more ramified mitochondrial networks (Gollihue and Norris, 2020; Motori et al., 2013). This is also supported by the enrichment of mitochondrial fusion protein Mitofusin 1 (Mfn1) in the astrocyte mitoproteome. Thus, successful reprogramming also involves structural remodeling of the mitochondria. Such structural remodeling of mitochondria has been observed even during neurogenesis, cells with higher levels of mitochondrial fission are indicative of a neuronal fate while cells with higher levels of mitochondrial fusion are primed for self-renewal (Iwata et al., 2020).

It can be hypothesized that conversion of cell fate from astrocyte to neurons must involve downregulation of astrocyte-enriched mitoproteins and a concomitant increase in the expression of neuron-enriched mitoproteins. To validate if this hypothesis holds true, we verified if the expression of proteins detected in the mitoproteome show a dynamic change in expression over the course of neuronal reprogramming. By immunostainings, we characterized the expression levels of astrocyte-enriched mitoproteins Sfxn5 and CpoX or neuronal mitoproteins Prdx2 and Gls, in astrocytes transduced with either control or *Ascl1* for reprogramming *in vitro*, over a period of 7 days. Cells transduced with the control virus

continued to express *Sfxn5* and *Cpox* throughout. On the other hand, *Ascl1* transduced cells undergoing successful reprogramming showed downregulation of these proteins on Day 5 and Day 7, but not earlier. Interestingly, *Ascl1* transduced cells that continued to display a characteristic astrocyte morphology (i.e., cells that failed to reprogram) continued to express *Sfxn5* or *Cpox*. Upregulation of the neuron-enriched mitoproteins was observed already on Day 3 and significant differences in the expression of these proteins could be clearly seen between successfully reprogramming cells and others on Day 5 and Day 7. This suggests that changes in the mitoproteome is a crucial step for successful neuronal reprogramming.

Previous studies have demonstrated that *Ascl1* and *Ngn2*, the commonly used reprogramming TFs induce neurogenic programs rapidly, as early as 24 and 48h after transduction (Kempf, Knelles, Hersbach et al., 2021; Masserdotti et al., 2015). Time-lapse analysis of astrocytes undergoing reprogramming had revealed cell death of astrocytes between 25 and 75h of reprogramming (Gascón, Murenu et al., 2016). Our time course analysis of the expression of neuron specific mitoproteins showed significant upregulation of *Prdx2* only on Day 3 (72h). Although *Gls* was significantly upregulated on Day 1 itself, the expression levels of this protein did not match that of endogenous neurons. This inadequate and delayed expression of neuronal mitoproteins along with persistent low-level expression of astrocyte-enriched mitoproteins could be a reason for inefficient reprogramming. Thus, we explored if earlier expression of neuronal mitoproteins improves the efficiency of reprogramming.

3.1.3 Early induction of neuron-enriched mitoproteins aids direct neuronal reprogramming

Among the neuron-enriched mitoproteins, we chose *Prdx2* (Peroxiredoxin 2) and *Sod1* (Superoxide Dismutase 1), that are known to play protective antioxidant roles (Boulos et al., 2007; Eleutherio et al., 2021; Liu et al., 2020). Additionally, we chose *Acot7* (Acyl-CoA Thioesterase 7), *Slc25a22* (Solute Carrier Family 25 Member 22), *Pgam5* (PGAM Family Member 5, Mitochondrial Serine/Threonine Protein Phosphatase), *Arg2* (Arginase 2), *Gls* (Glutaminase) and *Mgst3* (Microsomal Glutathione S-Transferase 3). For comparison, we also chose two astrocyte-enriched mitoproteins that have an antioxidant role, *Prdx6* (Peroxiredoxin 6, paralog to the neuron enriched *Prdx2*) and *Mgst1* (Microsomal Glutathione S-Transferase 1, paralog to the neuron enriched *Mgst3*) and chose *Dnm3* (Dynamin 3), which is not mitochondrially enriched, but may still be higher expressed in neurons. We induced expression of these genes by a CRISPRa (dCas9) mediated strategy. For this, we used mice expressing

Aldh111-Cre driven astrocyte specific dCas9-VPR (Rosa26-loxP-Stop-LoxP-dCas9VPR-SAM mice, generated in the study Giehrl-Schwab et al., 2022). Two gRNAs per candidate gene, targeting regions in close proximity to the transcriptional start sites (TSS) were multiplexed (targeting either one or two candidates at a time) in a single construct (Breunig et al., 2018). The gRNAs plasmids were transfected along with the plasmid expressing *Ascl1* to understand the effects on direct neuronal reprogramming of astrocytes *in vitro*.

Interestingly, *Ascl1* mediated neuronal reprogramming was significantly improved by early induction of neuron enriched *Sod1* alone or *Sod1* along with *Prdx2* (but not by *Prdx2* alone). While this showed the highest improvement in reprogramming efficiency, induction of other neuronal mitoproteins like *Arg2*, *Mgst3*, *Pgam5* and *Slc25a22* improved the reprogramming efficiency moderately. Surprisingly, not all neuron-enriched mitoproteins improved the efficiency, early induction of *Acot7*, *Gls* or *Prdx2* alone had no effect. Even though *Prdx6* and *Mgst1* have antioxidant functions and are very similar to the neuronal *Mgst3* and *Prdx2*, induction of these astrocyte-enriched mitoproteins did not improve reprogramming, highlighting the need for not just any protein with anti-oxidant function. Similarly, induction of *Dnm3* that is not enriched in the mitochondria had no beneficial effect. Apart from increasing the reprogramming efficiency, we observed that early induction some of the selected mitoproteins resulted in iNs with more complex morphology, which can be a measure of neuronal maturity. In addition to improving the reprogramming efficiency maximally, the condition of *Ascl1+Prdx2+Sod1* resulted in iNs that had longer cable length and branches. While the condition of *Ascl1+Slc25a22* improved the reprogramming efficiency minimally, this resulted in neurons with the most complex morphology.

In addition to aiding in the mitochondrial remodeling during the process of neuronal reprogramming, the combination of *Prdx2+Sod1* most likely improves reprogramming by also conferring antioxidant effects (Boulos et al., 2007; Eleutherio et al., 2021; Liu et al., 2020). By similarity to *Mgst1* (Maeda et al., 2005), *Mgst3* may also have an anti-oxidative effect, and this could contribute to the mild improvement in reprogramming in the condition of *Ascl1+Mgst3*, at least partly. On the other hand, the improvement in the condition of *Ascl1+Pgam5* could be due to its ability to promote mitophagy, thus helping in structural remodeling of mitochondria which is required during neuronal reprogramming and also protect from cell death (Lu et al., 2016, 2014; Ma et al., 2020). *Slc25a22*, a mitochondrial glutamate carrier, has been implicated in epilepsy and seizures (Molinari et al., 2009; Poduri et al., 2013), and the combination of *Ascl1+Slc25a22* gives neurons with the most morphological complexity. *Slc25a22* has been

shown to prevent ferroptosis in other cell types (Liu et al., 2023), and may have similar functions in reprogrammed neurons. While early induction of Slc25a22 may not be involved in establishment of neuronal fate, this may provide the reprogrammed neurons with higher resistance to metabolic stress which may permit higher level of morphological maturation. Interestingly, the condition Ascl1+Gls showed no improvement in reprogramming, highlighting that the process of glutamine synthesis does not affect neuronal reprogramming. On the other hand, not much is known about Acot7 or Arg2; Acot7 may regulate lipid retention in neurons (Ellis et al., 2013) but the condition of Ascl1+Acot7 did not improve reprogramming, and we did not observe an impact on the neuronal morphology of iNs in this condition either. Overall, although we have demonstrated that early induction of certain neuron enriched mitochondrial proteins can be beneficial, the exact roles and mechanisms by which each of them may impact this process is yet to be explored in finer detail.

To gain further understanding of how early induction of neuron-enriched mitoproteins influences the dynamics of neuronal reprogramming, we performed continuous single-cell live imaging of astrocytes undergoing Ascl1 mediated reprogramming, starting at 28h after transfection and monitored the process until 168h (7 days). We chose the condition that improved the reprogramming efficiency maximally, i.e., the condition of Ascl1+Prdx2+Sod1 and compared it to the reprogramming dynamics of astrocytes transfected only with Ascl1.

Surprisingly, we could identify more cells with a neuronal morphology already by 72h in the condition of Ascl1+Prdx2+Sod1 and many of these survive until the end of the experiment. In the condition of Ascl1 only, many neurons acquired a neuronal morphology by this time point as well, but they did not survive; only the slow-reprogramming cells (cells that begin to exhibit neuronal morphology after 72h) survived until the end of the experiment. Thus, the duration of survival (lifespan) of the iNs (both of the cells that die before the end of experiment and the ones that survive till the end of experiment) is significantly increased in the condition of Ascl1+Prdx2+Sod1 than in the reprogramming condition with Ascl1 only. This indicates that co-activation of Prdx2 and Sod1 with Ascl1 confers the cells with better mechanisms to cope with the sharp increase in ROS and the increased metabolic demand associated with the process of direct neuronal reprogramming. Intriguingly, Prdx2 and Sod1 had a positive effect only on the lifespan of the reprogrammed cells and had no significant impact on the non-reprogrammed cells. This highlights that the beneficial role of these mitoproteins may be limited to the cell-type they are enriched in. Notably, the cell death of reprogrammed iNs was not completely abolished in the condition of Ascl1+Prdx2+Sod1, many of the fast-reprogramming cells died

also in this condition. The difference in the efficiency arises from more cells being recruited for reprogramming at the earlier time points in this condition. These results are similar to the observation made earlier; both Bcl2 and the drug forskolin improved Ascl1 mediated reprogramming by accelerating the speed of the process and improved the survival of the iNs (Gascón, Murenu et al., 2016).

Thus, reprogramming efficiency and the quality/ maturity of the reprogrammed neurons (measured here based on morphological criteria) can be improved by helping the process of metabolic and mitochondrial remodeling, highlighting this to be a crucial step in cell fate conversion.

3.1.4 Inhibiting astrocyte specific metabolic pathways improves direct neuronal reprogramming

While early induction of neuron-enriched mitoproteins improved reprogramming, we also wanted to understand if downregulation of an astrocyte specific metabolic pathway would improve reprogramming. Astrocyte mitoproteome was highly enriched for genes related to fatty acid β -oxidation (FAO), both in our data of the cortical astrocytes and in the mitoproteome data of cerebellar astrocytes (Fecher et al., 2019). Thus, we decided to block FAO by pharmacological inhibition of Cpt1a (carnitine palmitoyltransferase 1A, which is required for transport of long chain fatty acids into mitochondria) with the drug etomoxir (Jernberg et al., 2017) to understand the impact on direct neuronal reprogramming.

We performed *in vitro* reprogramming experiments with Ascl1 and Ngn2 and etomoxir was added at varying concentrations (1, 25 and 100 μ M). Addition of etomoxir resulted in a sharp increase in the efficiency of both Ascl1 and Ngn2 mediated reprogramming. In the case of astrocytes undergoing Ngn2 mediated reprogramming, 1 μ M of etomoxir showed a slight increase in the reprogramming efficiency, and this was significantly increased at the concentration of 25 μ M; but further increase in etomoxir concentration was not beneficial. On the other hand, in the Ascl1 mediated reprogramming, 1 μ M of etomoxir showed no improvement, but the improvement was sustained at both 25 and 100 μ M of the drug concentration. This shows a context dependent effect of etomoxir in improving reprogramming efficiency. Interestingly, etomoxir has been shown to have a dose dependent effect in other cells as well. Above a concentration of 5 μ M, etomoxir triggered acute ROS production in T cells and was no longer just an inhibitor of FAO (O'Connor et al., 2018). However, it is to be noted that the dose limit may also be cell type dependent, as concentrations in the range of 50-200 μ M

have been used in other studies before (Knobloch et al., 2017). Nonetheless, if etomoxir induced an increase in ROS production at the concentrations we used, we might not observe an increase in reprogramming. To see if the effect of FAO inhibition is masked by etomoxir induced ROS production, we treated astrocytes undergoing Ascl1 mediated reprogramming with etomoxir (1, 25 μ M) and vitamin E (α -tocotrienol, ROS scavenger). However, we observed no improvement in the efficiency of reprogramming. In fact, addition of α -tocotrienol abolished the improvement in reprogramming efficiency observed with etomoxir alone. Thus, low levels of ROS may in fact be beneficial to successful reprogramming.

Similar to astrocytes, adult NSCs display high levels of FAO and downregulation of the same was shown to promote exit from quiescence (Knobloch et al., 2017). Impaired FAO has been observed in autism and rare inherited metabolic diseases where NSC self-renewal is affected (Xie et al., 2016). Interestingly, blocking FAO by inhibiting Cpt1a was not beneficial to adult hippocampal neurogenesis, as it induced cell death (Knobloch et al., 2017). Instead, increasing levels of a metabolite malonyl-CoA was more beneficial in NSC activation, as it only decreased FAO and did not block the pathway entirely. Given how similar astrocytes are to adult NSCs (Götz et al., 2015), this alternate strategy for FAO inhibition may be more beneficial during direct neuronal reprogramming as well, and would have to be explored in the future.

In conclusion, we were able to demonstrate that astrocytes and neurons have a distinct mitoproteome, which is more suited to cater to the metabolic needs of these different cell types. Cell fate conversion from astrocytes to neurons would thus require efficient and timely remodeling of mitochondria and the metabolic pathways. This has also been observed in direct neuronal differentiation of embryonic stem cells recently (Ordureau et al., 2021).

The absence of timely upregulation of the neuron specific mitoproteins and failure to downregulate astrocyte specific mitoproteins could be a major contributor to the failure of reprogramming. Downregulation of starter cell type specific metabolic pathways (like FAO inhibition) or early induction of neuron specific mitoproteins could help the cells undergoing reprogramming to adapt to the increased metabolic burden during the conversion process.

3.2 Astrocyte specific Sox9, Trps1 deletion affects glial crosstalk and injury response

As explained earlier, it is imperative to understand the mechanisms governing astrocyte identity and functions to eventually devise better strategies for both astrocytes based regenerative therapies and for improving direct neuronal reprogramming of astrocytes. While the roles of TFs in astrocyte development have been studied in quite some detail (Kang, Lee et al., 2012; Tiwari, Pataskar et al., 2018), how they influence the functions and identity of mature astrocytes remains poorly understood.

In Natarajan et al., we decided to focus on two TFs Sox9 (SRY-Box Transcription Factor 9) and Trps1 (Transcriptional Repressor GATA Binding 1), to understand how they influence astrocyte functions.

3.2.1 Intra-regional heterogeneity in the expression of individual TFs at protein and RNA levels

As Trps1 is a novel TF in the context of glial cells, we first characterized its expression in the adult cortical GM by immunostaining with other astrocyte specific proteins. We observed that around 40% of the S100 β ⁺ astrocytes or Sox9⁺ astrocytes were immunopositive for Trps1. Intriguingly, around 50% of Olig2⁺ cells were also found to be immunopositive for Trps1. Previously, Trps1 was found to be expressed in both astrocytes and oligodendroglial lineage (PDGFR α ⁺) cells during early postnatal development and was predicted as a transcriptional regulator of both these cell types (Weng, Wang et al., 2019). Olig2 mainly labels oligodendrocyte lineage cells in the adult cortex (Dimou et al., 2008), and this points to the possibility that Trps1 may be expressed in both astrocyte and oligodendroglial lineage cells even in the adult brain. This reveals that Trps1 may be a pan-glial TF and not just an astrocyte specific TF. However, it must be noted that a small fraction of Olig2⁺ cells have been shown to give rise to astrocytes (Dimou et al., 2008). Thus, it would be interesting to study if Trps1 is explicitly expressed in Olig2⁺ cells that give rise to astrocytes in the adult cortex, or if it is independent of the fate.

Bin-wise characterization of the distribution of Sox9 or Trps1 positive S100 β ⁺ astrocytes revealed no layer specific bias for the number of S100 β ⁺ astrocytes expressing Sox9. On the other hand, the number S100 β ⁺ astrocytes expressing Trps1 was slightly higher (although not significant) in the upper layers (UL) than in the deeper layers (DL) of the cortex. Several studies

have noted cortical layer specific astrocyte gene expression (Bayraktar et al., 2020; Lanjakornsiripan, Pior, Kawaguchi et al., 2018) and they are influenced by the layer specific signaling from the cortical neurons during postnatal development. In the future, it would be interesting to explore the potential cause and the impact of this mild UL bias for Trps1 expression in the astrocytes of the adult brain, and if this bias can be detected already during early postnatal stages, or if this is specific to mature astrocytes in the adult cortex.

In addition, we also characterized the expression level of these TFs at single cell protein level by fluorescence intensity quantifications after immunohistochemistry. This revealed a widespread variation in the expression of these TFs throughout the cortical GM. Similar to the percentages of S100 β ⁺ astrocytes expressing Sox9, the Sox9-low or Sox9-high cells displayed no bias in their distribution across the bins. Nevertheless, significantly more Trps1-low cells were present in Bin1 (UL) than in Bin5 (DL). While most previous studies have demonstrated inter- and intra-regional astrocyte heterogeneity at the transcriptome level (Bayraktar et al., 2020; Boisvert et al., 2018; Endo et al., 2022; Lanjakornsiripan, Pior, Kawaguchi et al., 2018; Ohlig, Clavreul et al., 2021), such heterogeneity in the levels of individual TFs at the level of protein has not been observed before. This could be an important feature, as the levels of a TF expression may dictate the extent to which downstream gene cascades are activated or inhibited. For example, in chondrocytes, Sox9 has been shown to promote gene expression by engaging with promoter regions indirectly via a basal transcriptional complex (referred to as Class I engagement), or by directly binding enhancer elements as a Sox9 dimer (referred to as Class II engagement) (Ohba, He et al., 2015). It can be hypothesized that the expression levels of TFs like Sox9 may confer a preference for the type of engagement and thus influence different downstream cascades. Similarly Trps1, though initially identified as a transcriptional repressor (Fantauzzo et al., 2012; Malik, 2001) can act as a transcriptional activator. The activator function of Trps1 may be achieved by binding directly to promoter regions of its targets (Fantauzzo and Christiano, 2012), or may be achieved by association with a transcriptional activator like Gli3 (Wuelling et al., 2020). The function of Trps1 as an activator or as a repressor may be highly dependent on the cell type and the availability of transcriptional complexes. In some breast cancer cell lines, Trps1 has been shown to bind open chromatin regions, with H3K27ac mark. However, Trps1 loss in this context resulted in both activation and repression of some of these genes (Witwicki, Ekram et al., 2018). Given this versatile nature of Trps1 in controlling downstream cascades, the levels of Trps1 expression may influence the nature of interactions as well.

We also observed that the cortical GM astrocytes displayed remarkable intra-regional heterogeneity, similar to the astrocytes of the diencephalon (Ohlig, Clavreul et al., 2021). Strikingly, we also observed variations in the levels of Sox9 and Trps1 at the RNA level within the astrocytes of the cortical GM. Due to technical limitations, we have been unable to directly draw a correlation between the RNA and protein levels, to see if the cells/ clusters with lower levels of Sox9 and Trps1 RNA correspond to cells with lower Sox9 and Trps1 protein levels or vice versa; and if the predicted cluster specific functions are related to Sox9 and Trps1 levels. Even still, it is exciting that we can observe intra-regional heterogeneity in the expression levels of key TFs at the level of single cell protein and RNA in cortical GM.

While we have focused mainly on cortical GM astrocytes so far, it would be interesting to characterize Trps1 expression in other brain regions as well in the future. In other lineages, Trps1 has been shown to influence cell proliferation and survival (Elster, Tollot et al., 2018; Witwicki, Ekram et al., 2018; Yang et al., 2021). Thus it would be interesting to see if there are more astrocytes expressing Trps1 in the diencephalon, where adult astrogenesis persists at low levels (Ohlig, Clavreul et al., 2021); or if the cortical juxtavascular astrocytes that proliferate upon injury (Sirko, Behrendt et al., 2013) express higher levels of Trps1.

3.2.2 Sox9 and Trps1 deletion reveals crucial roles in adult cortical astrocytes

To shed light on the roles of Sox9 and Trps1 in adult cortical GM astrocytes, we deleted these TFs either one at a time or both simultaneously using a CRISPR/ Cas9 approach. Astrocyte targeting was achieved by use of Mokola pseudotyped lentivirus (Mok-LV) (Watson et al., 2002). Our study demonstrates that this is an efficient way to target astrocytes in the adult cortex.

While we observed a quick and efficient loss of the targeted TFs, loss of Sox9 and Trps1 did not alter the identity of astrocytes visibly as they continued to express bonafide astrocyte markers like S100 β and GFAP at both 7 and 21dpi. Cell identity may be tightly regulated by the presence of several elaborate TF networks that reinforce the cell identity (Holmberg and Perlmann, 2012). Thus, loss of Sox9 or Trps1 may not have altered the astrocyte identity drastically. Nonetheless, Patch-seq based single cell sequencing (scRNA-seq) of control and Sox9/ Trps1 deleted astrocytes revealed that the loss of these key TFs triggered significant changes in the astrocyte transcriptome.

Sox9 deletion resulted in more upregulated genes, while Trps1 deletion resulted in comparable number of up and downregulated genes, fitting with Trps1's versatile role as both a

transcriptional activator (Fantauzzo and Christiano, 2012; Witwicki, Ekram et al., 2018; Wuelling et al., 2020) and repressor (Elster, Tollot et al., 2018; Fantauzzo et al., 2012; Malik, 2001) in other lineages. Interestingly, simultaneous Sox9 and Trps1 deletion resulted in fewer differentially expressed genes (DEGs), with much lower number of genes significantly upregulated. This raises the possibility that Sox9 may be required to activate genes that are de-repressed upon loss of Trps1. In other cell types, Sox9 and Trps1 have been shown to regulate each other; Trps1 has been shown to repress Sox9 (Fantauzzo et al., 2012; Shibata et al., 2016), while Sox9 has been shown to activate Trps1 (Tan, Niu et al., 2018). This implicates that Sox9 and Trps1 are involved in similar transcriptional cascades, often involving other factors related to Hedgehog signaling pathway. In our Patch-seq based scRNA-seq, we did not see a significant direct regulation of Sox9 or Trps1 upon deletion of the other. Nevertheless, the fact that simultaneous deletion of Sox9 and Trps1 abolishes the effects seen by single deletion of Sox9 or Trps1 points to their involvement in related transcriptional cascades in astrocytes too. In the future, it may be interesting to study the interplay between these two TFs at the molecular level in astrocytes, by performing ChIP for Trps1 and Sox9 in Sox9 or Trps1 deleted astrocytes respectively. This may give us more insights into how they influence astrocyte identity, functions and heterogeneity.

Gene ontology (GO) analysis to understand the functional relevance of Sox9, Trps1 deletion revealed that several pathways related to key astrocyte functions such as synapse organization and immune response were regulated in all the conditions (Sox9, Trps1 or Sox9+Trps1 deletion). Interestingly, Sox9 and Trps1 deletion conditions showed upregulation of the GO term “gliogenesis” (with enrichment of genes like *Fgfr3*, *Hes5*, *Zfp365*, *Hes1*). We had previously noticed that Sox9 and Trps1 deleted cells continue to express hallmark astrocyte proteins like S100 β and GFAP, and this further reinforces the possibility that the glial identity is maintained rather stably even in the absence of Sox9 or Trps1, by upregulation of alternate glial specific genes.

As the Patch-seq based scRNA-seq revealed upregulation of synapse related pathways, we verified the effect of astrocyte specific Sox9, Trps1 loss on the surrounding synapses by performing immunostaining for synaptophysin and Homer1. Although the number of pre- and post-synaptic puncta were not affected by astrocyte specific Sox9 or Trps1 deletion, the number of synaptic puncta (i.e. pre-synaptic puncta co-localizing with post-synaptic puncta) was significantly reduced in the immediate vicinity of Trps1 or Sox9 and Trps1 deleted astrocytes. It is indeed surprising that the number of synaptic puncta seem to reduce in the neurons while

the Patch-seq scRNA-seq data revealed upregulation of synapse related pathways from the point of astrocytes. It is possible that Sox9, Trps1 deleted astrocytes upregulate synapse related pathways to compensate for the fewer synapses in the surroundings. Nevertheless, this indicates a broad tissue level effect of astrocyte manipulation by TF deletion. So far, we have mainly focused on changes in excitatory synapses, as an excitatory post-synaptic marker (Homer1) was used for this analysis. It is possible that Sox9, Trps1 loss has a different effect on inhibitory post-synapses, especially because Sox9 has been shown to regulate response to inhibitory neurons during postnatal development of olfactory bulb astrocytes (Cheng et al., 2023). Thus, it would be interesting to see the effect of Sox9, Trps1 loss on inhibitory synapses in the adult cortex. Furthermore, the effects of Sox9 and Trps1 in synapse maintenance may also be verified by electrophysiological characterization of the surrounding neurons in the future.

The role of Sox9 by deletion has already been explored in the adult brain (Ung, Huang et al., 2021) and during postnatal astrocyte development (Cheng et al., 2023). However, both these studies noticed a significant impact only in the astrocytes of the olfactory bulb. During postnatal astrocyte development, Sox9 deletion reduced the expression of *Gabbr1* in the olfactory bulb astrocytes, reducing their sensitivity to respond to the synaptic activity of inhibitory neurons in the surrounding, which consequently affected the morphological maturation of the astrocytes in this region (Cheng et al., 2023). In the adult olfactory bulb astrocytes, Sox9 deletion resulted in impaired calcium signaling and affected the sensory processing neural circuits and no prominent effects were observed in the adult cortical astrocytes. On the other hand, we notice several intrinsic astrocyte functions related to synapse maintenance and immune response being impacted upon Sox9, Trps1 deletion. It is to be noted that our experimental paradigm for Sox9 (and Trps1) deletion is drastically different from the Cre mediated deletion performed by Ung, Huang et al., 2021. Our experiment involves injection of Mok-LV encoding gRNAs against the TF of interest for eventual deletion by CRISPR strategy. This may be disadvantageous on certain accounts: only a limited number of cells are targeted and there may be a relative unpredictability in the nature of indels while targeting mostly post-mitotic cells. However, in our case, the TF deletion is accompanied by a “mild injury” like condition. Our Patch-seq based scRNA-seq revealed an injury response signature in all our experimental conditions (Control, Sox9/ Trps1 deletion) in comparison to adult astrocytes collected from the intact cortex of *Aldh111-eGFP* animals. Although our experimental paradigm does not involve an invasive injury like that of a SWI, the mild injury of Mok-LV injection and the response to lentivirus (Mattugini, Bocchi et al., 2019) seems to be sufficient to trigger this response. As a result, Gene

ontology (GO) terms like “response to interferon- gamma”, “antigen processing and presentation” were upregulated in the gRNA control (g-Control) astrocytes in comparison to the intact astrocytes. Thus, our experimental paradigm can also be used to understand how Sox9 and Trps1 mediate astrocyte response to injury and inflammation caused by the Mok-LV injection. It is possible that this injury/ inflammatory environment challenges the astrocytes and the effect of Sox9, Trps1 loss is more prominent and sheds light on astrocytic functions that are compromised in the absence of key TFs like Sox9 and Trps1. Cortical astrocytes may in general be more resistant to gene perturbations, deletion of *Rbpj-k* (Magnusson et al., 2020), Sox9 (Ung, Huang et al., 2021) and Nfia (Huang, Woo et al., 2020) elicited no significant change, *Rbpj-k* knockdown in cortical astrocytes had an observable effect only when combined with a SWI (Zamboni et al., 2020).

3.2.3 Astrocyte specific Sox9 and Trps1 loss affects injury response of several cells in the tissue microenvironment

As we observed a broader tissue level effect in the number of synapses in the regions surrounding Sox9/ Trps1 deleted astrocytes, we wanted to understand how the tissue microenvironment is affected upon astrocyte manipulation by TF deletion. Another motivator for this was that the Patch-seq based scRNA-seq had indicated downregulation of immune response related pathways in astrocytes after Sox9, Trps1 deletion. While astrocytes respond to injury (Koupourtidou, Schwarz et al., 2023), inflammation (Hasel et al., 2021), degenerative diseases (Sadick, O'Dea et al., 2022) and ageing (Boisvert et al., 2018; Clarke et al., 2018); other glial and immune cells respond to these conditions as well (Mira et al., 2021). Even more importantly, astrocytes play a key role in signaling to the other glial and immune cells and modulate response in the injury environment (Domingues et al., 2016; Frik et al., 2018; Guttenplan et al., 2021; Hammond, McEllin et al., 2015; Koupourtidou, Schwarz et al., 2023; Linnerbauer et al., 2020; Linnerbauer and Rothhammer, 2020). Thus, we wanted to understand how impaired immune response in Sox9, Trps1 deleted astrocytes affect the tissue microenvironment.

In our effort to understand the tissue level changes upon Sox9/ Trps1 deletion in astrocytes, we performed spatial transcriptomics (10x Visium, stRNA-seq) of the adult mouse cortex. This revealed a very unexpected effect on oligodendrocytes; deletion of Sox9 alone or Sox9 along with Trps1, but not Trps1 resulted in upregulation of genes related to the term “oligodendrocyte differentiation” (*Olig1*, *Enpp2*, *Tspan2*, etc). In addition, comparison of the Mok-LV injection

regions for Sox9 or Trps1 deletion with the control injection region revealed downregulation of immune response related pathways in the entire region. On the other hand, concomitant deletion of Sox9 and Trps1 revealed upregulation of the same at the tissue level. It is possible that when both Sox9 and Trps1 are deleted, other immune cells in the tissue environment upregulate immune response, either because of or as a compensation for the astrocyte's inability to mediate immune response. Overall, this reveals dynamic changes in the tissue microenvironment upon astrocyte specific TF deletion, possibly due to altered glial crosstalk.

To understand the overall changes in all the cell types that respond to injury, we compared our stRNA-seq data after astrocyte specific Sox9, Trps1 deletion with the scRNA-seq data of cells from cortical GM after a SWI (Koupourtidou, Schwarz et al., 2023). Our Patch-seq based scRNA-seq had already revealed the presence of an injury associated transcriptional signature in all the conditions. Further comparison of our stRNA-seq data with the scRNA-seq data of cells from cortical GM at 5dpSWI (days post SWI) revealed the same, and confirmed the presence of injury specific spatial clusters, presence of reactive astrocytes, activated microglia and other immune cells at the site of Mok-LV injection. However, the extent to which these glial or immune cell types were present changed drastically depending on which TF was deleted. In conditions where only Sox9 or Trps1 was deleted, significantly less representation of microglia, monocytes, T cells or DC was observed, and this could be the reason behind the attenuated immune response in these conditions. The changes in microglial activation in Sox9 or Trps1 deletion condition is intriguing, as microglia are thought to induce astrocyte reactivity (Liddelow et al., 2017). Reduced microglial activation would be expected to result in reduced astrocyte activation as well, but we observe a reduction in astrocyte reactivity only after Sox9 deletion and not Trps1 deletion. It has been shown that limiting monocyte invasion in a cortical SWI paradigm is beneficial as it promotes astrocyte proliferation and faster recovery of the BBB (Frik et al., 2018). Thus, reduced activation of microglia and the reduced representation of monocytes and other immune cells may point towards faster resolution of the injury response in tissue where Sox9 or Trps1 is deleted.

On the other hand, we observed an increased representation of B cells, monocytes and dendritic cells (DC) in the tissue after simultaneous Sox9, Trps1 deletion, possibly contributing to the exacerbated immune response at the tissue level in this condition. Although we could previously not detect T or B cells among the invading immune cells at 3dpSWI based on fluorescence activated cell sorting (FACS) for CD19 and CD3+ cells respectively (Frik et al., 2018), we detect the presence of cells with T and B cells transcriptional signature in the 5dpSWI scRNA-

seq data (Koupourtidou, Schwarz et al., 2023). It is interesting that we see an increase in the representation of B cells; they may have beneficial or detrimental roles in the CNS. In case of stroke, migrating B cells may support functional recovery (Ortega et al., 2020), but in autoimmune diseases like multiple sclerosis (MS), B cell depletion may be beneficial (Li et al., 2018; Sabatino et al., 2019). Thus, in the context of Sox9 and Trps1 where immune response is exacerbated at the tissue level also due to an increased representation of monocytes and DC, it is difficult to assess whether this may be beneficial or not.

In line with the observation that GO terms related to “oligodendrocyte differentiation” was upregulated in Sox9 or Sox9+Trps1 deletion conditions, we observed an increase in the representation of genes enriched in committed oligodendrocyte progenitors and myelinating oligodendrocytes in these conditions. In healthy conditions, astrocytes signal to oligodendrocyte progenitor cells (OPC) and promote proliferation or differentiation and subsequent myelination (see reviews Domingues et al., 2016; Nutma et al., 2020). Several astrocyte secreted factors promote oligodendrocyte development (Pang et al., 2013), like fibroblast growth factor (FGF) (Oh et al., 1997), Timp-1 (Jiang et al., 2016), semaphorins (Su et al., 2023), extracellular vesicles (Willis et al., 2020). On the other hand, in inflammatory or injury conditions astrocytes may promote OPC proliferation and differentiation by expression of Cxcl12 (Patel et al., 2012), or inhibit the same by expressing high levels of Ednrb (Hammond, McEllin et al., 2015); see *Figure 5* for an overview of signaling pathways that may be beneficial or detrimental to OPC differentiation and remyelination under inflammatory conditions. It would be interesting to understand which (of these known or a novel) pathway contributes to increased oligodendrocyte differentiation after Sox9 or Sox9+Trps1 deletion. Overall, one could hypothesize that deletion of Sox9 alone, may be beneficial by limiting monocyte invasion and promoting oligodendrocyte differentiation, and thus most likely repair.

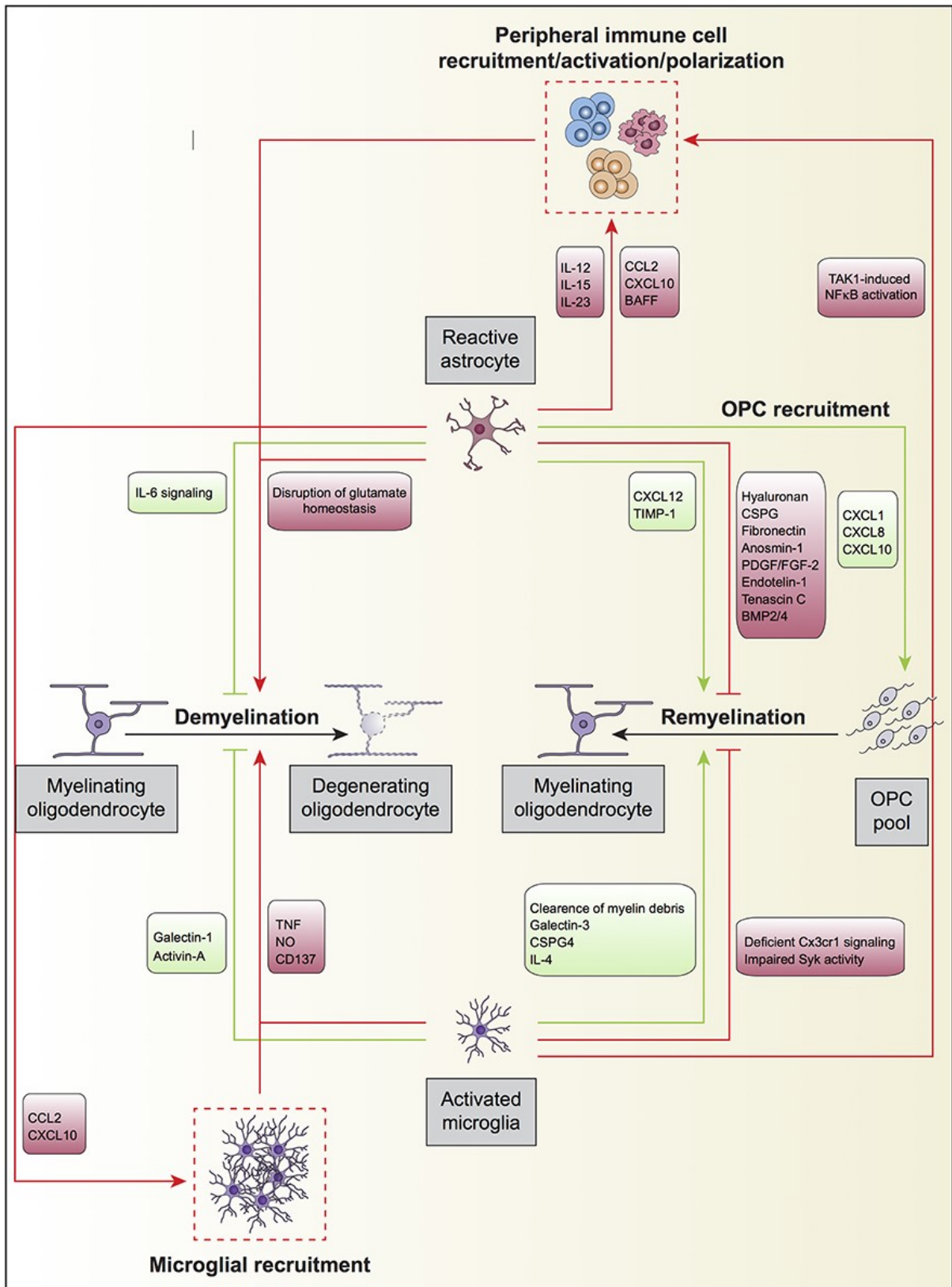


Figure 5. Overview of glial crosstalk in inflammatory conditions (red and green lines indicate signaling between cells that inhibit or promote OPC recruitment and remyelination)

respectively). This image is from Domingues et al., 2016, an open-access article distributed under the terms of the Creative Commons Attribution License.

In conclusion, we observed striking variations in the levels of individual TFs like Sox9 and Trps1 at single cell protein and RNA levels within the astrocytes of the cortical GM and demonstrate their importance in mediating key astrocyte functions. While loss of these TFs did not alter the identity of the astrocytes (by inducing de-differentiation into neural stem cells or trans-differentiation to other glial cell types), it severely influences astrocytic functions and we unveiled unexpected widespread effects on other cells such as oligodendrocytes and immune cells in the tissue microenvironment. Understanding the downstream targets that seem to increase oligodendrocyte differentiation in Sox9 deletion conditions may be beneficial to identifying therapeutic targets for diseases like multiple sclerosis where demyelination is a hallmark feature. Indeed, these downstream targets can also be exploited to improve myelination of reprogrammed or transplanted neurons and improve the therapeutic outcome.

3.3 Concluding remarks

We would benefit greatly by bridging our gap in the understanding of astrocyte identity, heterogeneity and the mechanisms that underlie the process of direct neuronal reprogramming. Recent work demonstrating that the regional identity of astrocytes is carried over to the reprogrammed neurons (Herrero-Navarro et al., 2021) and the dynamics of reprogramming is highly dependent on the source of astrocyte origin within the CNS (Kempf, Knelles, Hersbach et al., 2021) reiterate this. Most interestingly, even during *in vivo* direct neuronal reprogramming, layer specific neurons may arise from layer specific astrocytes of the cortex (Mattugini, Bocchi et al., 2019), but the exact nature of this is yet to be understood. Given the diverse roles of astrocytes in brain homeostasis, and the growing recognition of their implications in disease etiology (Franklin et al., 2021), astrocytes themselves can be a target of therapy in certain conditions. All of these advocate for the need of further studies into astrocyte identity, heterogeneity and functions and their impact on neuronal reprogramming.

My PhD studies demonstrate the need for understanding astrocyte identity and functions as well. In the first project, we showed that one unique facet of astrocyte identity, their preference

for glycolytic and fatty acid β -oxidation is supported by a distinct mitochondrial proteome that supports these metabolic pathways. Successful fate conversion from astrocytes to neurons would require downregulation of these unique astrocyte functions accompanied by simultaneous upregulation of factors that are unique and supportive of metabolic pathways emblematic to neurons. Aiding the establishment of neuronal mitochondria by early expression of neuron enriched mitochondrial proteins or downregulation of astrocyte specific metabolic pathways improved the outcome of direct neuronal reprogramming of astrocytes.

To understand the identity and functions of astrocytes better, we studied the role of two central astrocyte TFs in the cortex GM. We noticed that these TFs are heterogeneously expressed and future studies to explore their relevance in conferring intra-regional heterogeneity may be essential. In our current study, we unraveled the roles of these TFs by deleting them in the cortex GM and observed that several astrocyte functions related to synapse maintenance and immune response were altered. Unexpectedly, deletion of these factors resulted in non-cell autonomous effects, with increased oligodendrocyte proliferation and altered immune cell response in the tissue microenvironment. It can be hypothesized that in the Sox9 deletion condition, functional recovery may be improved due to diminished immune response and increased oligodendrocyte differentiation. In the future, it would be interesting to extend this study to the context of reprogramming and see how the dynamics is altered when overexpression of neurogenic TFs is combined with astrocyte specific deletion of TFs essential for principal astrocyte functions.

4. REFERENCES

- Allen, N.J., Eroglu, C., 2017. Cell Biology of Astrocyte-Synapse Interactions. *Neuron* 96, 697–708. <https://doi.org/10.1016/j.neuron.2017.09.056>
- Anderson, M.A., Burda, J.E., Ren, Y., Ao, Y., O’Shea, T.M., Kawaguchi, R., Coppola, G., Khakh, B.S., Deming, T.J., Sofroniew, M.V., 2016. Astrocyte scar formation aids central nervous system axon regeneration. *Nature* 532, 195–200. <https://doi.org/10.1038/nature17623>
- Aydin, B., Kakumanu, A., Rossillo, M., Moreno-Estellés, M., Garipler, G., Ringstad, N., Flames, N., Mahony, S., Mazzoni, E.O., 2019. Proneural factors *Ascl1* and *Neurog2* contribute to neuronal subtype identities by establishing distinct chromatin landscapes. *Nat. Neurosci.* 22, 897–908. <https://doi.org/10.1038/s41593-019-0399-y>
- Babos, K.N., Galloway, K.E., Kisler, K., Zitting, M., Li, Y., Shi, Y., Quintino, B., Chow, R.H., Zlokovic, B.V., Ichida, J.K., 2019. Mitigating Antagonism between Transcription and Proliferation Allows Near-Deterministic Cellular Reprogramming. *Cell Stem Cell* 25, 486–500.e9. <https://doi.org/10.1016/j.stem.2019.08.005>
- Bandler, R.C., Vitali, I., Delgado, R.N., Ho, M.C., Dvoretzkova, E., Ibarra Molinas, J.S., Frazel, P.W., Mohammadkhani, M., Machold, R., Maedler, S., Liddelow, S.A., Nowakowski, T.J., Fishell, G., Mayer, C., 2022. Single-cell delineation of lineage and genetic identity in the mouse brain. *Nature* 601, 404–409. <https://doi.org/10.1038/s41586-021-04237-0>
- Bardehle, S., Krüger, M., Buggenthin, F., Schwausch, J., Ninkovic, J., Clevers, H., Snippert, H.J., Theis, F.J., Meyer-Luehmann, M., Bechmann, I., Dimou, L., Götz, M., 2013. Live imaging of astrocyte responses to acute injury reveals selective juxtavascular proliferation. *Nat. Neurosci.* 16, 580–586. <https://doi.org/10.1038/nn.3371>
- Batiuk, M.Y., Martirosyan, A., Wahis, J., de Vin, F., Marneffe, C., Kusserow, C., Koeppen, J., Viana, J.F., Oliveira, J.F., Voet, T., Ponting, C.P., Belgard, T.G., Holt, M.G., 2020. Identification of region-specific astrocyte subtypes at single cell resolution. *Nat. Commun.* 11, 1220. <https://doi.org/10.1038/s41467-019-14198-8>
- Bayraktar, O.A., Bartels, T., Holmqvist, S., Kleshchevnikov, V., Martirosyan, A., Polioudakis, D., Ben Haim, L., Young, A.M.H., Batiuk, M.Y., Prakash, K., Brown, A., Roberts, K., Paredes, M.F., Kawaguchi, R., Stockley, J.H., Sabeur, K., Chang, S.M., Huang, E., Hutchinson, P., Ullian, E.M., Hemberg, M., Coppola, G., Holt, M.G., Geschwind, D.H., Rowitch, D.H., 2020. Astrocyte layers in the mammalian cerebral cortex revealed by a single-cell in situ transcriptomic map. *Nat. Neurosci.* 23, 500–509. <https://doi.org/10.1038/s41593-020-0602-1>
- Berninger, B., Costa, M.R., Koch, U., Schroeder, T., Sutor, B., Grothe, B., Götz, M., 2007. Functional Properties of Neurons Derived from *In Vitro* Reprogrammed Postnatal Astroglia. *J. Neurosci.* 27, 8654–8664. <https://doi.org/10.1523/JNEUROSCI.1615-07.2007>
- Blanco-Suarez, E., Liu, T.-F., Kopelevich, A., Allen, N.J., 2018. Astrocyte-Secreted Chordin-like 1 Drives Synapse Maturation and Limits Plasticity by Increasing Synaptic GluA2 AMPA Receptors. *Neuron* 100, 1116–1132.e13. <https://doi.org/10.1016/j.neuron.2018.09.043>

- Bocchi, R., Masserdotti, G., Götz, M., 2022. Direct neuronal reprogramming: Fast forward from new concepts toward therapeutic approaches. *Neuron* 110, 366–393. <https://doi.org/10.1016/j.neuron.2021.11.023>
- Boisvert, M.M., Erikson, G.A., Shokhirev, M.N., Allen, N.J., 2018. The Aging Astrocyte Transcriptome from Multiple Regions of the Mouse Brain. *Cell Rep.* 22, 269–285. <https://doi.org/10.1016/j.celrep.2017.12.039>
- Bolaños, J.P., 2016. Bioenergetics and redox adaptations of astrocytes to neuronal activity. *J. Neurochem.* 139, 115–125. <https://doi.org/10.1111/jnc.13486>
- Boulos, S., Meloni, B.P., Arthur, P.G., Bojarski, C., Knuckey, N.W., 2007. Peroxiredoxin 2 overexpression protects cortical neuronal cultures from ischemic and oxidative injury but not glutamate excitotoxicity, whereas Cu/Zn superoxide dismutase 1 overexpression protects only against oxidative injury. *J. Neurosci. Res.* 85, 3089–3097. <https://doi.org/10.1002/jnr.21429>
- Breunig, C.T., Neuner, A.M., Giehl-Schwab, J., Wurst, W., Götz, M., Stricker, S.H., 2018. A Customizable Protocol for String Assembly gRNA Cloning (STAgR). *J. Vis. Exp.* 58556. <https://doi.org/10.3791/58556>
- Briggs, R., King, T.J., 1952. Transplantation of living nuclei from blastula cells into enucleated frogs' eggs. *Proc. Natl. Acad. Sci.* 38, 455–463. <https://doi.org/10.1073/pnas.38.5.455>
- Buffo, A., Rite, I., Tripathi, P., Lepier, A., Colak, D., Horn, A.-P., Mori, T., Götz, M., 2008. Origin and progeny of reactive gliosis: A source of multipotent cells in the injured brain. *Proc. Natl. Acad. Sci.* 105, 3581–3586. <https://doi.org/10.1073/pnas.0709002105>
- Buffo, A., Vosko, M.R., Ertürk, D., Hamann, G.F., Jucker, M., Rowitch, D., Götz, M., 2005. Expression pattern of the transcription factor Olig2 in response to brain injuries: Implications for neuronal repair. *Proc. Natl. Acad. Sci.* 102, 18183–18188. <https://doi.org/10.1073/pnas.0506535102>
- Bustos, L.M., Sattler, R., 2023. The Fault in Our Astrocytes - cause or casualties of proteinopathies of ALS/FTD and other neurodegenerative diseases? *Front. Mol. Med.* 3, 1075805. <https://doi.org/10.3389/fmmed.2023.1075805>
- Caldwell, A.L.M., Sancho, L., Deng, J., Bosworth, A., Miglietta, A., Diedrich, J.K., Shokhirev, M.N., Allen, N.J., 2022. Aberrant astrocyte protein secretion contributes to altered neuronal development in multiple models of neurodevelopmental disorders. *Nat. Neurosci.* 25, 1163–1178. <https://doi.org/10.1038/s41593-022-01150-1>
- Carlén, M., Meletis, K., Göritz, C., Darsalia, V., Evergren, E., Tanigaki, K., Amendola, M., Barnabé-Heider, F., Yeung, M.S.Y., Naldini, L., Honjo, T., Kokaia, Z., Shupliakov, O., Cassidy, R.M., Lindvall, O., Frisén, J., 2009. Forebrain ependymal cells are Notch-dependent and generate neuroblasts and astrocytes after stroke. *Nat. Neurosci.* 12, 259–267. <https://doi.org/10.1038/nm.2268>
- Carter, J.L., Halmai, J.A.N.M., Fink, K.D., 2020. The iNs and Outs of Direct Reprogramming to Induced Neurons. *Front. Genome Ed.* 2, 7. <https://doi.org/10.3389/fgeed.2020.00007>

Cates, K., McCoy, M.J., Kwon, J.-S., Liu, Y., Abernathy, D.G., Zhang, B., Liu, S., Gontarz, P., Kim, W.K., Chen, S., Kong, W., Ho, J.N., Burbach, K.F., Gabel, H.W., Morris, S.A., Yoo, A.S., 2021. Deconstructing Stepwise Fate Conversion of Human Fibroblasts to Neurons by MicroRNAs. *Cell Stem Cell* 28, 127-140.e9. <https://doi.org/10.1016/j.stem.2020.08.015>

Chanda, S., Ang, C.E., Davila, J., Pak, C., Mall, M., Lee, Q.Y., Ahlenius, H., Jung, S.W., Südhof, T.C., Wernig, M., 2014. Generation of Induced Neuronal Cells by the Single Reprogramming Factor ASCL1. *Stem Cell Rep.* 3, 282–296. <https://doi.org/10.1016/j.stemcr.2014.05.020>

Chen, Y.-C., Ma, N.-X., Pei, Z.-F., Wu, Z., Do-Monte, F.H., Keefe, S., Yellin, E., Chen, M.S., Yin, J.-C., Lee, G., Minier-Toribio, A., Hu, Y., Bai, Y.-T., Lee, K., Quirk, G.J., Chen, G., 2020. A NeuroD1 AAV-Based Gene Therapy for Functional Brain Repair after Ischemic Injury through In Vivo Astrocyte-to-Neuron Conversion. *Mol. Ther.* 28, 217–234. <https://doi.org/10.1016/j.yymthe.2019.09.003>

Cheng, Y.-T., Luna-Figueroa, E., Woo, J., Chen, H.-C., Lee, Z.-F., Harmanci, A.S., Deneen, B., 2023. Inhibitory input directs astrocyte morphogenesis through glial GABABR. *Nature* 617, 369–376. <https://doi.org/10.1038/s41586-023-06010-x>

Chever, O., Djukic, B., McCarthy, K.D., Amzica, F., 2010. Implication of K_{ir} 4.1 Channel in Excess Potassium Clearance: An *In Vivo* Study on Anesthetized Glial-Conditional K_{ir} 4.1 Knock-Out Mice. *J. Neurosci.* 30, 15769–15777. <https://doi.org/10.1523/JNEUROSCI.2078-10.2010>

Clarke, L.E., Liddelow, S.A., Chakraborty, C., Münch, A.E., Heiman, M., Barres, B.A., 2018. Normal aging induces A1-like astrocyte reactivity. *Proc. Natl. Acad. Sci.* 115. <https://doi.org/10.1073/pnas.1800165115>

Clavreul, S., Abdeladim, L., Hernández-Garzón, E., Niculescu, D., Durand, J., Ieng, S.-H., Barry, R., Bonvento, G., Beaupaire, E., Livet, J., Loulier, K., 2019. Cortical astrocytes develop in a plastic manner at both clonal and cellular levels. *Nat. Commun.* 10, 4884. <https://doi.org/10.1038/s41467-019-12791-5>

Cornelissen, L.M., Drenth, A.P., van der Burg, E., de Bruijn, R., Pritchard, C.E.J., Huijbers, I.J., Zwart, W., Jonkers, J., 2020. TRPS1 acts as a context-dependent regulator of mammary epithelial cell growth/differentiation and breast cancer development. *Genes Dev.* 34, 179–193. <https://doi.org/10.1101/gad.331371.119>

Davis, R.L., Weintraub, H., Lassar, A.B., 1987. Expression of a single transfected cDNA converts fibroblasts to myoblasts. *Cell* 51, 987–1000. [https://doi.org/10.1016/0092-8674\(87\)90585-X](https://doi.org/10.1016/0092-8674(87)90585-X)

Dimou, L., Simon, C., Kirchhoff, F., Takebayashi, H., Götz, M., 2008. Progeny of Olig2-Expressing Progenitors in the Gray and White Matter of the Adult Mouse Cerebral Cortex. *J. Neurosci.* 28, 10434–10442. <https://doi.org/10.1523/JNEUROSCI.2831-08.2008>

Djukic, B., Casper, K.B., Philpot, B.D., Chin, L.-S., McCarthy, K.D., 2007. Conditional Knock-Out of K_{ir} 4.1 Leads to Glial Membrane Depolarization, Inhibition of Potassium and Glutamate Uptake, and Enhanced Short-Term Synaptic Potentiation. *J. Neurosci.* 27, 11354–11365. <https://doi.org/10.1523/JNEUROSCI.0723-07.2007>

- Domingues, H.S., Portugal, C.C., Socodato, R., Relvas, J.B., 2016. Oligodendrocyte, Astrocyte, and Microglia Crosstalk in Myelin Development, Damage, and Repair. *Front. Cell Dev. Biol.* 4. <https://doi.org/10.3389/fcell.2016.00071>
- Eleutherio, E.C.A., Silva Magalhães, R.S., De Araújo Brasil, A., Monteiro Neto, J.R., De Holanda Paranhos, L., 2021. SOD1, more than just an antioxidant. *Arch. Biochem. Biophys.* 697, 108701. <https://doi.org/10.1016/j.abb.2020.108701>
- Ellis, J.M., Wong, G.W., Wolfgang, M.J., 2013. Acyl coenzyme A thioesterase 7 regulates neuronal fatty acid metabolism to prevent neurotoxicity. *Mol. Cell. Biol.* 33, 1869–1882. <https://doi.org/10.1128/MCB.01548-12>
- Elster, D., Tollot, M., Schlegelmilch, K., Ori, A., Rosenwald, A., Sahai, E., von Eyss, B., 2018. TRPS1 shapes YAP/TEAD-dependent transcription in breast cancer cells. *Nat. Commun.* 9, 3115. <https://doi.org/10.1038/s41467-018-05370-7>
- Endo, F., Kasai, A., Soto, J.S., Yu, X., Qu, Z., Hashimoto, H., Gradinaru, V., Kawaguchi, R., Khakh, B.S., 2022. Molecular basis of astrocyte diversity and morphology across the CNS in health and disease. *Science* 378, eadc9020. <https://doi.org/10.1126/science.adc9020>
- Eraso-Pichot, A., Brasó-Vives, M., Golbano, A., Menacho, C., Claro, E., Galea, E., Masgrau, R., 2018. GSEA of mouse and human mitochondriomes reveals fatty acid oxidation in astrocytes. *Glia* 66, 1724–1735. <https://doi.org/10.1002/glia.23330>
- Falk, S., Götz, M., 2017. Glial control of neurogenesis. *Curr. Opin. Neurobiol.* 47, 188–195. <https://doi.org/10.1016/j.conb.2017.10.025>
- Falkner, S., Grade, S., Dimou, L., Conzelmann, K.-K., Bonhoeffer, T., Götz, M., Hübener, M., 2016. Transplanted embryonic neurons integrate into adult neocortical circuits. *Nature* 539, 248–253. <https://doi.org/10.1038/nature20113>
- Fantauzzo, K.A., Christiano, A.M., 2012. *Trps1* activates a network of secreted Wnt inhibitors and transcription factors crucial to vibrissa follicle morphogenesis. *Development* 139, 203–214. <https://doi.org/10.1242/dev.069971>
- Fantauzzo, K.A., Kurban, M., Levy, B., Christiano, A.M., 2012. *Trps1* and Its Target Gene *Sox9* Regulate Epithelial Proliferation in the Developing Hair Follicle and Are Associated with Hypertrichosis. *PLoS Genet.* 8, e1003002. <https://doi.org/10.1371/journal.pgen.1003002>
- Fecher, C., Trovò, L., Müller, S.A., Snaidero, N., Wettmarshausen, J., Heink, S., Ortiz, O., Wagner, I., Kühn, R., Hartmann, J., Karl, R.M., Konnerth, A., Korn, T., Wurst, W., Merkler, D., Lichtenthaler, S.F., Perocchi, F., Misgeld, T., 2019. Cell-type-specific profiling of brain mitochondria reveals functional and molecular diversity. *Nat. Neurosci.* 22, 1731–1742. <https://doi.org/10.1038/s41593-019-0479-z>
- Franklin, H., Clarke, B.E., Patani, R., 2021. Astrocytes and microglia in neurodegenerative diseases: Lessons from human in vitro models. *Prog. Neurobiol.* 200, 101973. <https://doi.org/10.1016/j.pneurobio.2020.101973>
- Frik, J., Merl-Pham, J., Plesnila, N., Mattugini, N., Kjell, J., Kraska, J., Gómez, R.M., Hauck, S.M., Sirko, S., Götz, M., 2018. Cross-talk between monocyte invasion and astrocyte

- proliferation regulates scarring in brain injury. *EMBO Rep.* 19, e45294. <https://doi.org/10.15252/embr.201745294>
- Gascón, S., Masserdotti, G., Russo, G.L., Götz, M., 2017. Direct Neuronal Reprogramming: Achievements, Hurdles, and New Roads to Success. *Cell Stem Cell* 21, 18–34. <https://doi.org/10.1016/j.stem.2017.06.011>
- Gascón, S., Murenu, E., Masserdotti, G., Ortega, F., Russo, G.L., Petrik, D., Deshpande, A., Heinrich, C., Karow, M., Robertson, S.P., Schroeder, T., Beckers, J., Irmeler, M., Berndt, C., Angeli, J.P.F., Conrad, M., Berninger, B., Götz, M., 2016. Identification and Successful Negotiation of a Metabolic Checkpoint in Direct Neuronal Reprogramming. *Cell Stem Cell* 18, 396–409. <https://doi.org/10.1016/j.stem.2015.12.003>
- Ge, W.-P., Jia, J.-M., 2016. Local production of astrocytes in the cerebral cortex. *Neuroscience* 323, 3–9. <https://doi.org/10.1016/j.neuroscience.2015.08.057>
- Ge, W.-P., Miyawaki, A., Gage, F.H., Jan, Y.N., Jan, L.Y., 2012. Local generation of glia is a major astrocyte source in postnatal cortex. *Nature* 484, 376–380. <https://doi.org/10.1038/nature10959>
- Giehl-Schwab, J., Giesert, F., Rauser, B., Lao, C.L., Hembach, S., Lefort, S., Ibarra, I.L., Koupourtidou, C., Luecken, M.D., Truong, D.J., Fischer-Sternjak, J., Masserdotti, G., Prakash, N., Ninkovic, J., Höltter, S.M., Vogt Weisenhorn, D.M., Theis, F.J., Götz, M., Wurst, W., 2022. Parkinson’s disease motor symptoms rescue by CRISPRa-reprogramming astrocytes into GABAergic neurons. *EMBO Mol. Med.* 14, e14797. <https://doi.org/10.15252/emmm.202114797>
- Gollihue, J.L., Norris, C.M., 2020. Astrocyte mitochondria: Central players and potential therapeutic targets for neurodegenerative diseases and injury. *Ageing Res. Rev.* 59, 101039. <https://doi.org/10.1016/j.arr.2020.101039>
- Götz, M., Sirko, S., Beckers, J., Irmeler, M., 2015. Reactive astrocytes as neural stem or progenitor cells: In vivo lineage, In vitro potential, and Genome-wide expression analysis. *Glia* 63, 1452–1468. <https://doi.org/10.1002/glia.22850>
- Guo, Z., Zhang, L., Wu, Z., Chen, Y., Wang, F., Chen, G., 2014. In Vivo Direct Reprogramming of Reactive Glial Cells into Functional Neurons after Brain Injury and in an Alzheimer’s Disease Model. *Cell Stem Cell* 14, 188–202. <https://doi.org/10.1016/j.stem.2013.12.001>
- Gurdon, J.B., 1962. The developmental capacity of nuclei taken from intestinal epithelium cells of feeding tadpoles. *J. Embryol. Exp. Morphol.* 10, 622–640.
- Gurdon, J.B., Elsdale, T.R., Fischberg, M., 1958. Sexually Mature Individuals of *Xenopus laevis* from the Transplantation of Single Somatic Nuclei. *Nature* 182, 64–65. <https://doi.org/10.1038/182064a0>
- Guttenplan, K.A., Weigel, M.K., Prakash, P., Wijewardhane, P.R., Hasel, P., Rufen-Blanchette, U., Münch, A.E., Blum, J.A., Fine, J., Neal, M.C., Bruce, K.D., Gitler, A.D., Chopra, G., Liddelow, S.A., Barres, B.A., 2021. Neurotoxic reactive astrocytes induce cell death via saturated lipids. *Nature* 599, 102–107. <https://doi.org/10.1038/s41586-021-03960-y>

- Hammond, T.R., McEllin, B., Morton, P.D., Raymond, M., Dupree, J., Gallo, V., 2015. Endothelin-B Receptor Activation in Astrocytes Regulates the Rate of Oligodendrocyte Regeneration during Remyelination. *Cell Rep.* 13, 2090–2097. <https://doi.org/10.1016/j.celrep.2015.11.002>
- Han, R.T., Kim, R.D., Molofsky, A.V., Liddelow, S.A., 2021. Astrocyte-immune cell interactions in physiology and pathology. *Immunity* 54, 211–224. <https://doi.org/10.1016/j.immuni.2021.01.013>
- Hasel, P., Rose, I.V.L., Sadick, J.S., Kim, R.D., Liddelow, S.A., 2021. Neuroinflammatory astrocyte subtypes in the mouse brain. *Nat. Neurosci.* 24, 1475–1487. <https://doi.org/10.1038/s41593-021-00905-6>
- Heinrich, C., Bergami, M., Gascón, S., Lepier, A., Viganò, F., Dimou, L., Sutor, B., Berninger, B., Götz, M., 2014. Sox2-Mediated Conversion of NG2 Glia into Induced Neurons in the Injured Adult Cerebral Cortex. *Stem Cell Rep.* 3, 1000–1014. <https://doi.org/10.1016/j.stemcr.2014.10.007>
- Heinrich, C., Blum, R., Gascón, S., Masserdotti, G., Tripathi, P., Sánchez, R., Tiedt, S., Schroeder, T., Götz, M., Berninger, B., 2010. Directing Astroglia from the Cerebral Cortex into Subtype Specific Functional Neurons. *PLoS Biol.* 8, e1000373. <https://doi.org/10.1371/journal.pbio.1000373>
- Heins, N., Malatesta, P., Cecconi, F., Nakafuku, M., Tucker, K.L., Hack, M.A., Chapouton, P., Barde, Y.-A., Götz, M., 2002. Glial cells generate neurons: the role of the transcription factor Pax6. *Nat. Neurosci.* 5, 308–315. <https://doi.org/10.1038/nn828>
- Heithoff, B.P., George, K.K., Phares, A.N., Zuidhoek, I.A., Munoz-Ballester, C., Robel, S., 2021. Astrocytes are necessary for blood–brain barrier maintenance in the adult mouse brain. *Glia* 69, 436–472. <https://doi.org/10.1002/glia.23908>
- Herrero-Navarro, Á., Puche-Aroca, L., Moreno-Juan, V., Sempere-Ferrández, A., Espinosa, A., Susín, R., Torres-Masjoan, L., Leyva-Díaz, E., Karow, M., Figueres-Oñate, M., López-Mascaraque, L., López-Atalaya, J.P., Berninger, B., López-Bendito, G., 2021. Astrocytes and neurons share region-specific transcriptional signatures that confer regional identity to neuronal reprogramming. *Sci. Adv.* 7, eabe8978. <https://doi.org/10.1126/sciadv.abe8978>
- Hersbach, B.A., Fischer, D.S., Masserdotti, G., Deeksha, Mojžišová, K., Waltzhöni, T., Rodriguez-Terrones, D., Heinig, M., Theis, F.J., Götz, M., Stricker, S.H., 2022. Probing cell identity hierarchies by fate titration and collision during direct reprogramming. *Mol. Syst. Biol.* 18, e11129. <https://doi.org/10.15252/msb.202211129>
- Hochstim, C., Deneen, B., Lukaszewicz, A., Zhou, Q., Anderson, D.J., 2008. Identification of Positionally Distinct Astrocyte Subtypes whose Identities Are Specified by a Homeodomain Code. *Cell* 133, 510–522. <https://doi.org/10.1016/j.cell.2008.02.046>
- Holmberg, J., Perlmann, T., 2012. Maintaining differentiated cellular identity. *Nat. Rev. Genet.* 13, 429–439. <https://doi.org/10.1038/nrg3209>

- Hösli, L., Zuend, M., Bredell, G., Zanker, H.S., Porto De Oliveira, C.E., Saab, A.S., Weber, B., 2022. Direct vascular contact is a hallmark of cerebral astrocytes. *Cell Rep.* 39, 110599. <https://doi.org/10.1016/j.celrep.2022.110599>
- Hu, X., Qin, S., Huang, X., Yuan, Y., Tan, Z., Gu, Y., Cheng, X., Wang, D., Lian, X.-F., He, C., Su, Z., 2019. Region-Restrict Astrocytes Exhibit Heterogeneous Susceptibility to Neuronal Reprogramming. *Stem Cell Rep.* 12, 290–304. <https://doi.org/10.1016/j.stemcr.2018.12.017>
- Huang, A.Y.-S., Woo, J., Sardar, D., Lozzi, B., Bosquez Huerta, N.A., Lin, C.-C.J., Felice, D., Jain, A., Paulucci-Holthausen, A., Deneen, B., 2020. Region-Specific Transcriptional Control of Astrocyte Function Oversees Local Circuit Activities. *Neuron* 106, 992-1008.e9. <https://doi.org/10.1016/j.neuron.2020.03.025>
- Ioannou, M.S., Jackson, J., Sheu, S.-H., Chang, C.-L., Weigel, A.V., Liu, H., Pasolli, H.A., Xu, C.S., Pang, S., Matthies, D., Hess, H.F., Lippincott-Schwartz, J., Liu, Z., 2019. Neuron-Astrocyte Metabolic Coupling Protects against Activity-Induced Fatty Acid Toxicity. *Cell* 177, 1522-1535.e14. <https://doi.org/10.1016/j.cell.2019.04.001>
- Iwata, R., Casimir, P., Vanderhaeghen, P., 2020. Mitochondrial dynamics in postmitotic cells regulate neurogenesis. *Science* 369, 858–862. <https://doi.org/10.1126/science.aba9760>
- Jernberg, J.N., Bowman, C.E., Wolfgang, M.J., Scafidi, S., 2017. Developmental regulation and localization of carnitine palmitoyltransferases (CPTs) in rat brain. *J. Neurochem.* 142, 407–419. <https://doi.org/10.1111/jnc.14072>
- Jiang, P., Chen, C., Liu, X.-B., Pleasure, D.E., Liu, Y., Deng, W., 2016. Human iPSC-Derived Immature Astroglia Promote Oligodendrogenesis by Increasing TIMP-1 Secretion. *Cell Rep.* 15, 1303–1315. <https://doi.org/10.1016/j.celrep.2016.04.011>
- Kang, P., Lee, H.K., Glasgow, S.M., Finley, M., Donti, T., Gaber, Z.B., Graham, B.H., Foster, A.E., Novitsch, B.G., Gronostajski, R.M., Deneen, B., 2012. Sox9 and NFIA Coordinate a Transcriptional Regulatory Cascade during the Initiation of Gliogenesis. *Neuron* 74, 79–94. <https://doi.org/10.1016/j.neuron.2012.01.024>
- Karow, M., Camp, J.G., Falk, S., Gerber, T., Pataskar, A., Gac-Santel, M., Kageyama, J., Brazovskaja, A., Garding, A., Fan, W., Riedemann, T., Casamassa, A., Smiyakin, A., Schichor, C., Götz, M., Tiwari, V.K., Treutlein, B., Berninger, B., 2018. Direct pericyte-to-neuron reprogramming via unfolding of a neural stem cell-like program. *Nat. Neurosci.* 21, 932–940. <https://doi.org/10.1038/s41593-018-0168-3>
- Kelley, K.W., Ben Haim, L., Schirmer, L., Tyzack, G.E., Tolman, M., Miller, J.G., Tsai, H.-H., Chang, S.M., Molofsky, A.V., Yang, Y., Patani, R., Lakatos, A., Ullian, E.M., Rowitch, D.H., 2018. Kir4.1-Dependent Astrocyte-Fast Motor Neuron Interactions Are Required for Peak Strength. *Neuron* 98, 306-319.e7. <https://doi.org/10.1016/j.neuron.2018.03.010>
- Kempf, J., Knelles, K., Hersbach, B.A., Petrik, D., Riedemann, T., Bednarova, V., Janjic, A., Simon-Ebert, T., Enard, W., Smialowski, P., Götz, M., Masserdotti, G., 2021. Heterogeneity of neurons reprogrammed from spinal cord astrocytes by the proneural factors Ascl1 and Neurogenin2. *Cell Rep.* 36, 109409. <https://doi.org/10.1016/j.celrep.2021.109409>

- Khacho, M., Clark, A., Svoboda, D.S., Azzi, J., MacLaurin, J.G., Meghaizel, C., Sesaki, H., Lagace, D.C., Germain, M., Harper, M.-E., Park, D.S., Slack, R.S., 2016. Mitochondrial Dynamics Impacts Stem Cell Identity and Fate Decisions by Regulating a Nuclear Transcriptional Program. *Cell Stem Cell* 19, 232–247. <https://doi.org/10.1016/j.stem.2016.04.015>
- Kikuchi, T., Morizane, A., Doi, D., Magotani, H., Onoe, H., Hayashi, T., Mizuma, H., Takara, S., Takahashi, R., Inoue, H., Morita, S., Yamamoto, M., Okita, K., Nakagawa, M., Parmar, M., Takahashi, J., 2017. Human iPS cell-derived dopaminergic neurons function in a primate Parkinson's disease model. *Nature* 548, 592–596. <https://doi.org/10.1038/nature23664>
- Klum, S., Zaouter, C., Alekseenko, Z., Björklund, Å.K., Hagey, D.W., Ericson, J., Muhr, J., Bergsland, M., 2018. Sequentially acting SOX proteins orchestrate astrocyte- and oligodendrocyte-specific gene expression. *EMBO Rep.* 19, e46635. <https://doi.org/10.15252/embr.201846635>
- Knobloch, M., Pilz, G.-A., Ghesquière, B., Kovacs, W.J., Wegleiter, T., Moore, D.L., Hruzova, M., Zamboni, N., Carmeliet, P., Jessberger, S., 2017. A Fatty Acid Oxidation-Dependent Metabolic Shift Regulates Adult Neural Stem Cell Activity. *Cell Rep.* 20, 2144–2155. <https://doi.org/10.1016/j.celrep.2017.08.029>
- Koupourtidou, C., Veronika Schwarz, Aliee, H., Frerich, S., Fischer-Sternjak, J., Bocchi, R., Simon-Ebert, T., Dichgans, M., Götz, M., Theis, F., Ninkovic, J., 2023. Shared inflammatory glial cell signature after brain injury, revealed by spatial, temporal and cell-type-specific profiling of the murine cerebral cortex (preprint). *Neuroscience*. <https://doi.org/10.1101/2023.02.24.529840>
- Lanjakornsiripan, D., Pior, B.-J., Kawaguchi, D., Furutachi, S., Tahara, T., Katsuyama, Y., Suzuki, Y., Fukazawa, Y., Gotoh, Y., 2018. Layer-specific morphological and molecular differences in neocortical astrocytes and their dependence on neuronal layers. *Nat. Commun.* 9, 1623. <https://doi.org/10.1038/s41467-018-03940-3>
- Laug, D., Huang, T.-W., Huerta, N.A.B., Huang, A.Y.-S., Sardar, D., Ortiz-Guzman, J., Carlson, J.C., Arenkiel, B.R., Kuo, C.T., Mohila, C.A., Glasgow, S.M., Lee, H.K., Deneen, B., 2019. Nuclear factor I-A regulates diverse reactive astrocyte responses after CNS injury. *J. Clin. Invest.* 129, 4408–4418. <https://doi.org/10.1172/JCI127492>
- Lee, J.-H., Kim, J., Noh, S., Lee, H., Lee, S.Y., Mun, J.Y., Park, H., Chung, W.-S., 2021. Astrocytes phagocytose adult hippocampal synapses for circuit homeostasis. *Nature* 590, 612–617. <https://doi.org/10.1038/s41586-020-03060-3>
- Lee, Q.Y., Mall, M., Chanda, S., Zhou, B., Sharma, K.S., Schaukowitch, K., Adrian-Segarra, J.M., Grieder, S.D., Karetka, M.S., Wapinski, O.L., Ang, C.E., Li, R., Südhof, T.C., Chang, H.Y., Wernig, M., 2020. Pro-neuronal activity of Myod1 due to promiscuous binding to neuronal genes. *Nat. Cell Biol.* 22, 401–411. <https://doi.org/10.1038/s41556-020-0490-3>
- Li, R., Patterson, K.R., Bar-Or, A., 2018. Reassessing B cell contributions in multiple sclerosis. *Nat. Immunol.* 19, 696–707. <https://doi.org/10.1038/s41590-018-0135-x>
- Liddelw, S.A., Guttenplan, K.A., Clarke, L.E., Bennett, F.C., Bohlen, C.J., Schirmer, L., Bennett, M.L., Münch, A.E., Chung, W.-S., Peterson, T.C., Wilton, D.K., Frouin, A., Napier,

B.A., Panicker, N., Kumar, M., Buckwalter, M.S., Rowitch, D.H., Dawson, V.L., Dawson, T.M., Stevens, B., Barres, B.A., 2017. Neurotoxic reactive astrocytes are induced by activated microglia. *Nature* 541, 481–487. <https://doi.org/10.1038/nature21029>

Linnerbauer, M., Rothhammer, V., 2020. Protective Functions of Reactive Astrocytes Following Central Nervous System Insult. *Front. Immunol.* 11, 573256. <https://doi.org/10.3389/fimmu.2020.573256>

Linnerbauer, M., Wheeler, M.A., Quintana, F.J., 2020. Astrocyte Crosstalk in CNS Inflammation. *Neuron* 108, 608–622. <https://doi.org/10.1016/j.neuron.2020.08.012>

Liu, J., Su, G., Gao, J., Tian, Y., Liu, X., Zhang, Z., 2020. Effects of Peroxiredoxin 2 in Neurological Disorders: A Review of its Molecular Mechanisms. *Neurochem. Res.* 45, 720–730. <https://doi.org/10.1007/s11064-020-02971-x>

Liu, J., Wu, X., Lu, Q., 2022. Molecular divergence of mammalian astrocyte progenitor cells at early gliogenesis. *Development* 149, dev199985. <https://doi.org/10.1242/dev.199985>

Liu, Y., Miao, Q., Yuan, J., Han, S., Zhang, P., Li, S., Rao, Z., Zhao, W., Ye, Q., Geng, J., Zhang, X., Cheng, L., 2015. Ascl1 Converts Dorsal Midbrain Astrocytes into Functional Neurons In Vivo. *J. Neurosci.* 35, 9336–9355. <https://doi.org/10.1523/JNEUROSCI.3975-14.2015>

Liu, Y., Wang, Y., Lin, Z., Kang, R., Tang, D., Liu, J., 2023. SLC25A22 as a Key Mitochondrial Transporter Against Ferroptosis by Producing Glutathione and Monounsaturated Fatty Acids. *Antioxid. Redox Signal.* 39, 166–185. <https://doi.org/10.1089/ars.2022.0203>

Llorens-Bobadilla, E., Zhao, S., Baser, A., Saiz-Castro, G., Zwadlo, K., Martin-Villalba, A., 2015. Single-Cell Transcriptomics Reveals a Population of Dormant Neural Stem Cells that Become Activated upon Brain Injury. *Cell Stem Cell* 17, 329–340. <https://doi.org/10.1016/j.stem.2015.07.002>

Lorenz, C., Prigione, A., 2017. Mitochondrial metabolism in early neural fate and its relevance for neuronal disease modeling. *Curr. Opin. Cell Biol.* 49, 71–76. <https://doi.org/10.1016/j.ceb.2017.12.004>

Lu, W., Karuppagounder, S.S., Springer, D.A., Allen, M.D., Zheng, L., Chao, B., Zhang, Y., Dawson, V.L., Dawson, T.M., Lenardo, M., 2014. Genetic deficiency of the mitochondrial protein PGAM5 causes a Parkinson's-like movement disorder. *Nat. Commun.* 5, 4930. <https://doi.org/10.1038/ncomms5930>

Lu, W., Sun, J., Yoon, J.S., Zhang, Y., Zheng, L., Murphy, E., Mattson, M.P., Lenardo, M.J., 2016. Mitochondrial Protein PGAM5 Regulates Mitophagic Protection against Cell Necroptosis. *PLOS ONE* 11, e0147792. <https://doi.org/10.1371/journal.pone.0147792>

Ma, K., Zhang, Z., Chang, R., Cheng, H., Mu, C., Zhao, T., Chen, L., Zhang, C., Luo, Q., Lin, J., Zhu, Y., Chen, Q., 2020. Dynamic PGAM5 multimers dephosphorylate BCL-xL or FUNDC1 to regulate mitochondrial and cellular fate. *Cell Death Differ.* 27, 1036–1051. <https://doi.org/10.1038/s41418-019-0396-4>

- Maeda, A., Crabb, J.W., Palczewski, K., 2005. Microsomal glutathione S-transferase 1 in the retinal pigment epithelium: protection against oxidative stress and a potential role in aging. *Biochemistry* 44, 480–489. <https://doi.org/10.1021/bi048016f>
- Magistretti, P.J., Allaman, I., 2018. Lactate in the brain: from metabolic end-product to signalling molecule. *Nat. Rev. Neurosci.* 19, 235–249. <https://doi.org/10.1038/nrn.2018.19>
- Magnusson, J.P., Göritz, C., Tatarishvili, J., Dias, D.O., Smith, E.M.K., Lindvall, O., Kokaia, Z., Frisén, J., 2014. A latent neurogenic program in astrocytes regulated by Notch signaling in the mouse. *Science* 346, 237–241. <https://doi.org/10.1126/science.346.6206.237>
- Magnusson, J.P., Zamboni, M., Santopolo, G., Mold, J.E., Barrientos-Somarribas, M., Talavera-Lopez, C., Andersson, B., Frisén, J., 2020. Activation of a neural stem cell transcriptional program in parenchymal astrocytes. *eLife* 9, e59733. <https://doi.org/10.7554/eLife.59733>
- Malik, T.H., 2001. Transcriptional repression and developmental functions of the atypical vertebrate GATA protein TRPS1. *EMBO J.* 20, 1715–1725. <https://doi.org/10.1093/emboj/20.7.1715>
- Masserdotti, G., Gillotin, S., Sutor, B., Drechsel, D., Irmeler, M., Jørgensen, H.F., Sass, S., Theis, F.J., Beckers, J., Berninger, B., Guillemot, F., Götz, M., 2015. Transcriptional Mechanisms of Proneural Factors and REST in Regulating Neuronal Reprogramming of Astrocytes. *Cell Stem Cell* 17, 74–88. <https://doi.org/10.1016/j.stem.2015.05.014>
- Matsuda, T., Irie, T., Katsurabayashi, S., Hayashi, Y., Nagai, T., Hamazaki, N., Adefuin, A.M.D., Miura, F., Ito, T., Kimura, H., Shirahige, K., Takeda, T., Iwasaki, K., Imamura, T., Nakashima, K., 2019. Pioneer Factor NeuroD1 Rearranges Transcriptional and Epigenetic Profiles to Execute Microglia-Neuron Conversion. *Neuron* 101, 472–485.e7. <https://doi.org/10.1016/j.neuron.2018.12.010>
- Mattugini, N., Bocchi, R., Scheuss, V., Russo, G.L., Torper, O., Lao, C.L., Götz, M., 2019. Inducing Different Neuronal Subtypes from Astrocytes in the Injured Mouse Cerebral Cortex. *Neuron* 103, 1086–1095.e5. <https://doi.org/10.1016/j.neuron.2019.08.009>
- Mendelsohn, R., Garcia, G.C., Bartol, T.M., Lee, C.T., Khandelwal, P., Liu, E., Spencer, D.J., Husar, A., Bushong, E.A., Phan, S., Perkins, G., Ellisman, M.H., Skupin, A., Sejnowski, T.J., Rangamani, P., 2022. Morphological principles of neuronal mitochondria. *J. Comp. Neurol.* 530, 886–902. <https://doi.org/10.1002/cne.25254>
- Mira, R.G., Lira, M., Cerpa, W., 2021. Traumatic Brain Injury: Mechanisms of Glial Response. *Front. Physiol.* 12, 740939. <https://doi.org/10.3389/fphys.2021.740939>
- Misgeld, T., Schwarz, T.L., 2017. Mitostasis in Neurons: Maintaining Mitochondria in an Extended Cellular Architecture. *Neuron* 96, 651–666. <https://doi.org/10.1016/j.neuron.2017.09.055>
- Molinari, F., Kaminska, A., Fiermonte, G., Boddaert, N., Raas-Rothschild, A., Plouin, P., Palmieri, L., Brunelle, F., Palmieri, F., Dulac, O., Munnich, A., Colleaux, L., 2009. Mutations in the mitochondrial glutamate carrier *SLC25A22* in neonatal epileptic encephalopathy with

suppression bursts. *Clin. Genet.* 76, 188–194. <https://doi.org/10.1111/j.1399-0004.2009.01236.x>

Molofsky, A.V., Kelley, K.W., Tsai, H.-H., Redmond, S.A., Chang, S.M., Madireddy, L., Chan, J.R., Baranzini, S.E., Ullian, E.M., Rowitch, D.H., 2014. Astrocyte-encoded positional cues maintain sensorimotor circuit integrity. *Nature* 509, 189–194. <https://doi.org/10.1038/nature13161>

Monterey, M.D., Wei, H., Wu, X., Wu, J.Q., 2021. The Many Faces of Astrocytes in Alzheimer’s Disease. *Front. Neurol.* 12, 619626. <https://doi.org/10.3389/fneur.2021.619626>

Morris, S.A., 2016. Direct lineage reprogramming via pioneer factors; a detour through developmental gene regulatory networks. *Development* 143, 2696–2705. <https://doi.org/10.1242/dev.138263>

Motori, E., Puyal, J., Toni, N., Ghanem, A., Angeloni, C., Malaguti, M., Cantelli-Forti, G., Berninger, B., Conzelmann, K.-K., Götz, M., Winklhofer, K.F., Hrelia, S., Bergami, M., 2013. Inflammation-Induced Alteration of Astrocyte Mitochondrial Dynamics Requires Autophagy for Mitochondrial Network Maintenance. *Cell Metab.* 18, 844–859. <https://doi.org/10.1016/j.cmet.2013.11.005>

Nagao, M., Ogata, T., Sawada, Y., Gotoh, Y., 2016. Zbtb20 promotes astrocytogenesis during neocortical development. *Nat. Commun.* 7, 11102. <https://doi.org/10.1038/ncomms11102>

Niu, W., Zang, T., Smith, D.K., Vue, T.Y., Zou, Y., Bachoo, R., Johnson, J.E., Zhang, C.-L., 2015. SOX2 Reprograms Resident Astrocytes into Neural Progenitors in the Adult Brain. *Stem Cell Rep.* 4, 780–794. <https://doi.org/10.1016/j.stemcr.2015.03.006>

Nutma, E., Van Gent, D., Amor, S., Peferoen, L.A.N., 2020. Astrocyte and Oligodendrocyte Cross-Talk in the Central Nervous System. *Cells* 9, 600. <https://doi.org/10.3390/cells9030600>

O’Connor, R.S., Guo, L., Ghassemi, S., Snyder, N.W., Worth, A.J., Weng, L., Kam, Y., Philipson, B., Trefely, S., Nunez-Cruz, S., Blair, I.A., June, C.H., Milone, M.C., 2018. The CPT1a inhibitor, etomoxir induces severe oxidative stress at commonly used concentrations. *Sci. Rep.* 8, 6289. <https://doi.org/10.1038/s41598-018-24676-6>

Oh, L.Y.S., Goodyer, C.G., Olivier, A., Yong, V.W., 1997. The promoting effects of bFGF and astrocyte extracellular matrix on process outgrowth by adult human oligodendrocytes are mediated by protein kinase C. *Brain Res.* 757, 236–244. [https://doi.org/10.1016/S0006-8993\(97\)00224-2](https://doi.org/10.1016/S0006-8993(97)00224-2)

Ohba, S., He, X., Hojo, H., McMahon, A.P., 2015. Distinct Transcriptional Programs Underlie Sox9 Regulation of the Mammalian Chondrocyte. *Cell Rep.* 12, 229–243. <https://doi.org/10.1016/j.celrep.2015.06.013>

Ohlig, S., Clavreul, S., Thorwirth, M., Simon-Ebert, T., Bocchi, R., Ulbricht, S., Kannayian, N., Rossner, M., Sirko, S., Smialowski, P., Fischer-Sternjak, J., Götz, M., 2021. Molecular diversity of diencephalic astrocytes reveals adult astrogenesis regulated by Smad4. *EMBO J.* 40, e107532. <https://doi.org/10.15252/embj.2020107532>

- Ordureau, A., Kraus, F., Zhang, J., An, H., Park, S., Ahfeldt, T., Paulo, J.A., Harper, J.W., 2021. Temporal proteomics during neurogenesis reveals large-scale proteome and organelle remodeling via selective autophagy. *Mol. Cell* 81, 5082-5098.e11. <https://doi.org/10.1016/j.molcel.2021.10.001>
- Ortega, S.B., Torres, V.O., Latchney, S.E., Whoolery, C.W., Noorbhai, I.Z., Poinsette, K., Selvaraj, U.M., Benson, M.A., Meeuwissen, A.J.M., Plautz, E.J., Kong, X., Ramirez, D.M., Ajay, A.D., Meeks, J.P., Goldberg, M.P., Monson, N.L., Eisch, A.J., Stowe, A.M., 2020. B cells migrate into remote brain areas and support neurogenesis and functional recovery after focal stroke in mice. *Proc. Natl. Acad. Sci.* 117, 4983–4993. <https://doi.org/10.1073/pnas.1913292117>
- Pang, Y., Fan, L.-W., Tien, L.-T., Dai, X., Zheng, B., Cai, Z., Lin, R.C.S., Bhatt, A., 2013. Differential roles of astrocyte and microglia in supporting oligodendrocyte development and myelination in vitro. *Brain Behav.* 3, 503–514. <https://doi.org/10.1002/brb3.152>
- Pataskar, A., Jung, J., Smialowski, P., Noack, F., Calegari, F., Straub, T., Tiwari, V.K., 2016. NeuroD1 reprograms chromatin and transcription factor landscapes to induce the neuronal program. *EMBO J.* 35, 24–45. <https://doi.org/10.15252/embj.201591206>
- Patel, J.R., Williams, J.L., Muccigrosso, M.M., Liu, L., Sun, T., Rubin, J.B., Klein, R.S., 2012. Astrocyte TNFR2 is required for CXCL12-mediated regulation of oligodendrocyte progenitor proliferation and differentiation within the adult CNS. *Acta Neuropathol. (Berl.)* 124, 847–860. <https://doi.org/10.1007/s00401-012-1034-0>
- Pereira, M., Birtele, M., Shrigley, S., Benitez, J.A., Hedlund, E., Parmar, M., Ottosson, D.R., 2017. Direct Reprogramming of Resident NG2 Glia into Neurons with Properties of Fast-Spiking Parvalbumin-Containing Interneurons. *Stem Cell Rep.* 9, 742–751. <https://doi.org/10.1016/j.stemcr.2017.07.023>
- Poduri, A., Heinzen, E.L., Chitsazzadeh, V., Lasorsa, F.M., Elhosary, P.C., LaCoursiere, C.M., Martin, E., Yuskaitis, C.J., Hill, R.S., Atabay, K.D., Barry, B., Partlow, J.N., Bashiri, F.A., Zeidan, R.M., Elmalik, S.A., Kabiraj, M.M.U., Kothare, S., Stöberg, T., McTague, A., Kurian, M.A., Scheffer, I.E., Barkovich, A.J., Palmieri, F., Salih, M.A., Walsh, C.A., 2013. *SLC25A22* is a novel gene for migrating partial seizures in infancy: Poduri et al: *SLC25A22* Mutation in MPSI. *Ann. Neurol.* 74, 873–882. <https://doi.org/10.1002/ana.23998>
- Rose, J., Brian, C., Pappa, A., Panayiotidis, M.I., Franco, R., 2020. Mitochondrial Metabolism in Astrocytes Regulates Brain Bioenergetics, Neurotransmission and Redox Balance. *Front. Neurosci.* 14, 536682. <https://doi.org/10.3389/fnins.2020.536682>
- Ruiz, S., Panopoulos, A.D., Herrerías, A., Bissig, K.-D., Lutz, M., Berggren, W.T., Verma, I.M., Izpisua Belmonte, J.C., 2011. A High Proliferation Rate Is Required for Cell Reprogramming and Maintenance of Human Embryonic Stem Cell Identity. *Curr. Biol.* 21, 45–52. <https://doi.org/10.1016/j.cub.2010.11.049>
- Russo, G.L., Sonsalla, G., Natarajan, P., Breunig, C.T., Bulli, G., Merl-Pham, J., Schmitt, S., Giehl-Schwab, J., Giesert, F., Jastroch, M., Zischka, H., Wurst, W., Stricker, S.H., Hauck, S.M., Masserdotti, G., Götz, M., 2021. CRISPR-Mediated Induction of Neuron-Enriched Mitochondrial Proteins Boosts Direct Glia-to-Neuron Conversion. *Cell Stem Cell* 28, 524-534.e7. <https://doi.org/10.1016/j.stem.2020.10.015>

- Sabatino, J.J., Pröbstel, A.-K., Zamvil, S.S., 2019. B cells in autoimmune and neurodegenerative central nervous system diseases. *Nat. Rev. Neurosci.* 20, 728–745. <https://doi.org/10.1038/s41583-019-0233-2>
- Sadick, J.S., O’Dea, M.R., Hasel, P., Dykstra, T., Faustin, A., Liddel, S.A., 2022. Astrocytes and oligodendrocytes undergo subtype-specific transcriptional changes in Alzheimer’s disease. *Neuron* 110, 1788-1805.e10. <https://doi.org/10.1016/j.neuron.2022.03.008>
- Sánchez-González, R., Bribián, A., López-Mascaraque, L., 2020. Cell Fate Potential of NG2 Progenitors. *Sci. Rep.* 10, 9876. <https://doi.org/10.1038/s41598-020-66753-9>
- Schweitzer, J.S., Song, B., Herrington, T.M., Park, T.-Y., Lee, N., Ko, S., Jeon, J., Cha, Y., Kim, K., Li, Q., Henschliffe, C., Kaplitt, M., Neff, C., Rapalino, O., Seo, H., Lee, I.-H., Kim, J., Kim, T., Petsko, G.A., Ritz, J., Cohen, B.M., Kong, S.-W., Leblanc, P., Carter, B.S., Kim, K.-S., 2020. Personalized iPSC-Derived Dopamine Progenitor Cells for Parkinson’s Disease. *N. Engl. J. Med.* 382, 1926–1932. <https://doi.org/10.1056/NEJMoa1915872>
- Shibata, A., Tanahashi, K., Sugiura, K., Akiyama, M., 2016. TRPS1 haploinsufficiency results in increased STAT3 and SOX9 mRNA expression in hair follicles in trichorhinophalangeal syndrome. *J. Dermatol. Sci.* 84, e57. <https://doi.org/10.1016/j.jdermsci.2016.08.178>
- Sirko, S., Behrendt, G., Johansson, P.A., Tripathi, P., Costa, M.R., Bek, S., Heinrich, C., Tiedt, S., Colak, D., Dichgans, M., Fischer, I.R., Plesnila, N., Staufienbiel, M., Haass, C., Snayyan, M., Saghatelian, A., Tsai, L.-H., Fischer, A., Grobe, K., Dimou, L., Götz, M., 2013. Reactive Glia in the Injured Brain Acquire Stem Cell Properties in Response to Sonic Hedgehog. *Cell Stem Cell* 12, 426–439. <https://doi.org/10.1016/j.stem.2013.01.019>
- Sirko, S., Irmeler, M., Gascón, S., Bek, S., Schneider, S., Dimou, L., Obermann, J., De Souza Paiva, D., Poirier, F., Beckers, J., Hauck, S.M., Barde, Y., Götz, M., 2015. Astrocyte reactivity after brain injury—: The role of galectins 1 and 3. *Glia* 63, 2340–2361. <https://doi.org/10.1002/glia.22898>
- Smith, D.K., Yang, J., Liu, M.-L., Zhang, C.-L., 2016. Small Molecules Modulate Chromatin Accessibility to Promote NEUROG2-Mediated Fibroblast-to-Neuron Reprogramming. *Stem Cell Rep.* 7, 955–969. <https://doi.org/10.1016/j.stemcr.2016.09.013>
- Sofroniew, M.V., 2020. Astrocyte Reactivity: Subtypes, States, and Functions in CNS Innate Immunity. *Trends Immunol.* 41, 758–770. <https://doi.org/10.1016/j.it.2020.07.004>
- Stolt, C.C., Lommes, P., Sock, E., Chaboissier, M.-C., Schedl, A., Wegner, M., 2003. The Sox9 transcription factor determines glial fate choice in the developing spinal cord. *Genes Dev.* 17, 1677–1689. <https://doi.org/10.1101/gad.259003>
- Su, Y., Wang, X., Yang, Y., Chen, L., Xia, W., Hoi, K.K., Li, H., Wang, Q., Yu, G., Chen, X., Wang, S., Wang, Y., Xiao, L., Verkhatsky, A., Fancy, S.P.J., Yi, C., Niu, J., 2023. Astrocyte endfoot formation controls the termination of oligodendrocyte precursor cell perivascular migration during development. *Neuron* 111, 190-201.e8. <https://doi.org/10.1016/j.neuron.2022.10.032>

Tan, Z., Niu, B., Tsang, K.Y., Melhado, I.G., Ohba, S., He, X., Huang, Y., Wang, C., McMahon, A.P., Jauch, R., Chan, D., Zhang, M.Q., Cheah, K.S.E., 2018. Synergistic co-regulation and competition by a SOX9-GLI-FOXA phasic transcriptional network coordinate chondrocyte differentiation transitions. *PLOS Genet.* 14, e1007346. <https://doi.org/10.1371/journal.pgen.1007346>

Tiwari, N., Pataskar, A., Péron, S., Thakurela, S., Sahu, S.K., Figueres-Oñate, M., Marichal, N., López-Mascaraque, L., Tiwari, V.K., Berninger, B., 2018. Stage-Specific Transcription Factors Drive Astroglialogenesis by Remodeling Gene Regulatory Landscapes. *Cell Stem Cell* 23, 557-571.e8. <https://doi.org/10.1016/j.stem.2018.09.008>

Torper, O., Ottosson, D.R., Pereira, M., Lau, S., Cardoso, T., Grealish, S., Parmar, M., 2015. In Vivo Reprogramming of Striatal NG2 Glia into Functional Neurons that Integrate into Local Host Circuitry. *Cell Rep.* 12, 474–481. <https://doi.org/10.1016/j.celrep.2015.06.040>

Treutlein, B., Lee, Q.Y., Camp, J.G., Mall, M., Koh, W., Shariati, S.A.M., Sim, S., Neff, N.F., Skotheim, J.M., Wernig, M., Quake, S.R., 2016. Dissecting direct reprogramming from fibroblast to neuron using single-cell RNA-seq. *Nature* 534, 391–395. <https://doi.org/10.1038/nature18323>

Ung, K., Huang, T.-W., Lozzi, B., Woo, J., Hanson, E., Pekarek, B., Tepe, B., Sardar, D., Cheng, Y.-T., Liu, G., Deneen, B., Arenkiel, B.R., 2021. Olfactory bulb astrocytes mediate sensory circuit processing through Sox9 in the mouse brain. *Nat. Commun.* 12, 5230. <https://doi.org/10.1038/s41467-021-25444-3>

Van Deijk, A.-L.F., Camargo, N., Timmerman, J., Heistek, T., Brouwers, J.F., Mogavero, F., Mansvelder, H.D., Smit, A.B., Verheijen, M.H.G., 2017. Astrocyte lipid metabolism is critical for synapse development and function in vivo: van Deijk et al. *Glia* 65, 670–682. <https://doi.org/10.1002/glia.23120>

Velychko, S., Adachi, K., Kim, K.-P., Hou, Y., MacCarthy, C.M., Wu, G., Schöler, H.R., 2019. Excluding Oct4 from Yamanaka Cocktail Unleashes the Developmental Potential of iPSCs. *Cell Stem Cell* 25, 737-753.e4. <https://doi.org/10.1016/j.stem.2019.10.002>

Vierbuchen, T., Ostermeier, A., Pang, Z.P., Kokubu, Y., Südhof, T.C., Wernig, M., 2010. Direct conversion of fibroblasts to functional neurons by defined factors. *Nature* 463, 1035–1041. <https://doi.org/10.1038/nature08797>

Vong, K.I., Leung, C.K.Y., Behringer, R.R., Kwan, K.M., 2015. Sox9 is critical for suppression of neurogenesis but not initiation of gliogenesis in the cerebellum. *Mol. Brain* 8, 25. <https://doi.org/10.1186/s13041-015-0115-0>

Wang, H., Yang, Y., Liu, J., Qian, L., 2021. Direct cell reprogramming: approaches, mechanisms and progress. *Nat. Rev. Mol. Cell Biol.* 22, 410–424. <https://doi.org/10.1038/s41580-021-00335-z>

Wang, J., Chen, S., Pan, C., Li, G., Tang, Z., 2022. Application of Small Molecules in the Central Nervous System Direct Neuronal Reprogramming. *Front. Bioeng. Biotechnol.* 10, 799152. <https://doi.org/10.3389/fbioe.2022.799152>

- Wani, G.A., Sprenger, H.-G., Ndoci, K., Chandragiri, S., Acton, R.J., Schatton, D., Kochan, S.M.V., Sakthivelu, V., Jevtic, M., Seeger, J.M., Müller, S., Giavalisco, P., Rugarli, E.I., Motori, E., Langer, T., Bergami, M., 2022. Metabolic control of adult neural stem cell self-renewal by the mitochondrial protease YME1L. *Cell Rep.* 38, 110370. <https://doi.org/10.1016/j.celrep.2022.110370>
- Wapinski, O.L., Lee, Q.Y., Chen, A.C., Li, R., Corces, M.R., Ang, C.E., Treutlein, B., Xiang, C., Baubet, V., Suchy, F.P., Sankar, V., Sim, S., Quake, S.R., Dahmane, N., Wernig, M., Chang, H.Y., 2017. Rapid Chromatin Switch in the Direct Reprogramming of Fibroblasts to Neurons. *Cell Rep.* 20, 3236–3247. <https://doi.org/10.1016/j.celrep.2017.09.011>
- Wapinski, O.L., Vierbuchen, T., Qu, K., Lee, Q.Y., Chanda, S., Fuentes, D.R., Giresi, P.G., Ng, Y.H., Marro, S., Neff, N.F., Drechsel, D., Martynoga, B., Castro, D.S., Webb, A.E., Südhof, T.C., Brunet, A., Guillemot, F., Chang, H.Y., Wernig, M., 2013. Hierarchical Mechanisms for Direct Reprogramming of Fibroblasts to Neurons. *Cell* 155, 621–635. <https://doi.org/10.1016/j.cell.2013.09.028>
- Watson, D.J., Kobinger, G.P., Passini, M.A., Wilson, J.M., Wolfe, J.H., 2002. Targeted Transduction Patterns in the Mouse Brain by Lentivirus Vectors Pseudotyped with VSV, Ebola, Mokola, LCMV, or MuLV Envelope Proteins. *Mol. Ther.* 5, 528–537. <https://doi.org/10.1006/mthe.2002.0584>
- Wattananit, S., Tornero, D., Graubardt, N., Memanishvili, T., Monni, E., Tatarishvili, J., Miskinyte, G., Ge, R., Ahlenius, H., Lindvall, O., Schwartz, M., Kokaia, Z., 2016. Monocyte-Derived Macrophages Contribute to Spontaneous Long-Term Functional Recovery after Stroke in Mice. *J. Neurosci.* 36, 4182–4195. <https://doi.org/10.1523/JNEUROSCI.4317-15.2016>
- Weng, Q., Wang, Jincheng, Wang, Jiajia, He, D., Cheng, Z., Zhang, F., Verma, R., Xu, L., Dong, X., Liao, Y., He, X., Potter, A., Zhang, L., Zhao, C., Xin, M., Zhou, Q., Aronow, B.J., Blackshear, P.J., Rich, J.N., He, Q., Zhou, W., Suvà, M.L., Waclaw, R.R., Potter, S.S., Yu, G., Lu, Q.R., 2019. Single-Cell Transcriptomics Uncovers Glial Progenitor Diversity and Cell Fate Determinants during Development and Gliomagenesis. *Cell Stem Cell* 24, 707–723.e8. <https://doi.org/10.1016/j.stem.2019.03.006>
- Willis, C.M., Nicaise, A.M., Bongarzone, E.R., Givogri, M., Reiter, C.R., Heintz, O., Jellison, E.R., Sutter, P.A., TeHennepe, G., Ananda, G., Vella, A.T., Crocker, S.J., 2020. Astrocyte Support for Oligodendrocyte Differentiation can be Conveyed via Extracellular Vesicles but Diminishes with Age. *Sci. Rep.* 10, 828. <https://doi.org/10.1038/s41598-020-57663-x>
- Witwicki, R.M., Ekram, M.B., Qiu, X., Janiszewska, M., Shu, S., Kwon, M., Trinh, A., Frias, E., Ramadan, N., Hoffman, G., Yu, K., Xie, Y., McAllister, G., McDonald, R., Golji, J., Schlabach, M., deWeck, A., Keen, N., Chan, H.M., Ruddy, D., Rejtar, T., Sovath, S., Silver, S., Sellers, W.R., Jagani, Z., Hogarty, M.D., Roberts, C., Brown, M., Stegmaier, K., Long, H., Shivdasani, R.A., Pellman, D., Polyak, K., 2018. TRPS1 Is a Lineage-Specific Transcriptional Dependency in Breast Cancer. *Cell Rep.* 25, 1255–1267.e5. <https://doi.org/10.1016/j.celrep.2018.10.023>
- Wuelling, M., Kaiser, F.J., Buelens, L.A., Braunholz, D., Shivdasani, R.A., Depping, R., Vortkamp, A., 2009. Trps1, a regulator of chondrocyte proliferation and differentiation,

interacts with the activator form of Gli3. *Dev. Biol.* 328, 40–53.
<https://doi.org/10.1016/j.ydbio.2009.01.012>

Wuelling, M., Schneider, S., Schröther, V.A., Waterkamp, C., Hoffmann, D., Vortkamp, A., 2020. Wnt5a is a transcriptional target of Gli3 and Trps1 at the onset of chondrocyte hypertrophy. *Dev. Biol.* 457, 104–118. <https://doi.org/10.1016/j.ydbio.2019.09.012>

Xie, Z., Jones, A., Deeney, J.T., Hur, S.K., Bankaitis, V.A., 2016. Inborn Errors of Long-Chain Fatty Acid β -Oxidation Link Neural Stem Cell Self-Renewal to Autism. *Cell Rep.* 14, 991–999. <https://doi.org/10.1016/j.celrep.2016.01.004>

Yang, J., Liu, X., Huang, Y., He, L., Zhang, W., Ren, J., Wang, Y., Wu, J., Wu, X., Shan, L., Yang, X., Sun, L., Liang, J., Zhang, Y., Shang, Y., 2021. TRPS1 drives heterochromatic origin refring and cancer genome evolution. *Cell Rep.* 34, 108814.
<https://doi.org/10.1016/j.celrep.2021.108814>

Yang, T., Dai, Y., Chen, G., Cui, S., 2020. Dissecting the Dual Role of the Glial Scar and Scar-Forming Astrocytes in Spinal Cord Injury. *Front. Cell. Neurosci.* 14, 78.
<https://doi.org/10.3389/fncel.2020.00078>

Yin, J.-C., Zhang, L., Ma, N.-X., Wang, Y., Lee, G., Hou, X.-Y., Lei, Z.-F., Zhang, F.-Y., Dong, F.-P., Wu, G.-Y., Chen, G., 2019. Chemical Conversion of Human Fetal Astrocytes into Neurons through Modulation of Multiple Signaling Pathways. *Stem Cell Rep.* 12, 488–501. <https://doi.org/10.1016/j.stemcr.2019.01.003>

Zamboni, M., Llorens-Bobadilla, E., Magnusson, J.P., Frisé, J., 2020. A Widespread Neurogenic Potential of Neocortical Astrocytes Is Induced by Injury. *Cell Stem Cell* 27, 605–617.e5. <https://doi.org/10.1016/j.stem.2020.07.006>

Zhang, L., Yin, J.-C., Yeh, H., Ma, N.-X., Lee, G., Chen, X.A., Wang, Y., Lin, L., Chen, L., Jin, P., Wu, G.-Y., Chen, G., 2015. Small Molecules Efficiently Reprogram Human Astroglial Cells into Functional Neurons. *Cell Stem Cell* 17, 735–747.
<https://doi.org/10.1016/j.stem.2015.09.012>

Zheng, X., Boyer, L., Jin, M., Mertens, J., Kim, Y., Ma, L., Ma, L., Hamm, M., Gage, F.H., Hunter, T., 2016. Metabolic reprogramming during neuronal differentiation from aerobic glycolysis to neuronal oxidative phosphorylation. *eLife* 5, e13374.
<https://doi.org/10.7554/eLife.13374>

Zhu, X., Bergles, D.E., Nishiyama, A., 2008. NG2 cells generate both oligodendrocytes and gray matter astrocytes. *Development* 135, 145–157. <https://doi.org/10.1242/dev.004895>

Declaration of Author contributions

1. Russo, G. L., Sonsalla, G.[#], **Natarajan, P.[#]**, Breunig, C. T., Bulli, G., Merl-Pham, J., Schmitt, S., Giehl-Schwab, J., Giesert, F., Jastroch, M., Zischka, H., Wurst, W., Stricker, S. H., Hauck, S. M., Masserdotti, G.^{*}, & Götz, M.^{*} (2021) “CRISPR-Mediated Induction of Neuron-Enriched Mitochondrial Proteins Boosts Direct Glia-to- Neuron Conversion” *Cell Stem Cell*, 28(3): 524–534.e7.

These authors contributed equally

***Co-last author**

M.G. conceived and designed the project. G.L.R. and G.M. shaped the project, and G.L.R. performed experiments and analysis. G.S. contributed to the time course analysis. **P.N. performed and analyzed the experiment with etomoxir, gRNA, and continuous live imaging.** C.T.B. and S.H.S. provided CRISPR-Cas expertise and developed and designed the STAgR approach, and C.T.B. helped with cloning of the constructs. G.B. performed western blots. J.M.-P. and S.M.H. provided proteomics expertise and performed experiments and analysis. S.S. and H.Z. performed mitochondrial isolation and electron microscopy. J.G.-S., F.G., and W.W. generated and provided dCAM transgenic mice. M.J. provided expertise regarding metabolism and Seahorse analysis. G.M. analyzed the data; provided expertise and training of G.L.R., G.S., P.N., and G.B. regarding reprogramming; and co-directed the project together with M.G. G.L.R., G.M., and M.G. wrote the manuscript, **and all authors contributed corrections and comments.**

My contribution to this publication in detail:

All the experiments for the data in Figure 3, Figure 4, Figure S2, and Figure S4 were performed and analyzed by me, with help and guidance from G.M for statistical analysis and data visualization.

2. **Poornemaa Natarajan**^{1,2,3,4}, Christina Koupourtidou^{2,3,5}, Thibault de Resseguier¹, Riccardo Bocchi^{1,2,6}, Judith Fischer-Sternjak^{1,2}, Sarah Gleiss¹, Diana Rodrigues¹, Mike Myoga¹, Jovica Ninkovic^{5,7}, Giacomo Masserdotti^{1,2*}, Magdalena Götz^{1,2,7*#}

“Single cell deletion and analysis of the transcription factors Sox9 and Trps1 reveals novel functions in astrocyte”

Manuscript ready for submission

*Co-last author, # Correspondence to magdalena.goetz@helmholtz-munich.de

M.G. and G.M. conceived and designed the project. **P.N contributed to shaping the project, performed all experiments and data analysis.** C.K. helped performing stRNA-seq experiment, C.K. and J.N. provided the 5dpSWI scRNA-seq dataset for comparison with stRNA-seq data. T.D.R. characterized Trps1 expression in Olig2+ cells and contributed to the GFAP intensity analysis. R.B. helped with animal experiments, R.B. and J.F-S. provided the intact adult cortical GM scRNA-seq dataset. S.G., D.F. and M.M. performed the collection of cells for Patch-seq based scRNA-seq experiment. **P.N., G.M. and M.G. wrote the manuscript.** M.G. provided all the funding.

Signature of supervisor: Prof. Dr. Magdalena Götz

Dr. Gianluca Luigi Russo (first author of Publication 1)

Signature of PhD candidate: Poornemaa Natarajan

Poornema Natarajan

email: poornema.natarajan@helmholtz-munich.de

RESEARCH EXPERIENCE

- 10/2018- present* PhD student in Dr Magdalena Götz's lab
(Affiliated to the Graduate program at IMPRS-LS and Graduate School of systemic Neurosciences, LMU)
- 10/2015- 09/2016* EMBL Mouse Biology Unit, Monterotondo, Italy
Post: Project student in Dr Cornelius Gross' lab
Project: Molecular changes in the prefrontal cortex underlying adaptations to social adversity
- 08/2013 - 05/2015* Institute of Genomics and Integrative Biology, New Delhi
Post: Project assistant in Dr. Munia Ganguli's lab
Projects: Gene delivery using cell penetrating peptides/ small molecules, with an emphasis on delivery to skin
- 12/2012 - 05/2013* *Bachelor Thesis:* "Non-viral vector systems for biomolecule delivery to skin" in CSIR- IGIB, New Delhi under the guidance of Dr Munia Ganguli.
- 05/2012 - 07/2012* Summer fellowship in IIT Madras

EDUCATION

- 10/2017- 09/2018* Fast-track/ Masters in Neuroscience at the Graduate School of Systemic Neurosciences, LMU, Germany
GPA: 1.7 (1year, 60 credits)
- 07/2009 - 05/2013* SASTRA UNIVERSITY (www.sastra.edu),
Degree course - B.Tech in Industrial Biotechnology (231 credits, 4-year course)
CGPA - 8.33/10 (First class with Distinction, Dean's merit Scholarship for Top 3-10% students)
- 20/05/2009* All India Senior School Certificate Examination, CBSE
(Qualifying exam for entry into a University, Percentage: 80.6)

CORE COMPETENCIES

Advanced: Mice handling and stereotactic surgeries, cell culture, data analysis using R (single cell and spatial transcriptomic datasets), immunofluorescence, confocal microscopy

Intermediate: Fluorescence activated cell sorting, in situ hybridization (RNAscope), cloning, Smart-seq2 based single-cell sequencing protocols

Beginner: library preparation for droplet-based single-cell sequencing (10x), Retro and lentiviral productions, western blotting and immunoprecipitation (Ribo-seq)

CONFERENCES

- First prize for Best Poster Presentation Award for poster titled “*Exploring transcriptional cascades in cortical astrocytes: the role of Sox9 and Trps1*” at FENS/ The Brain Conference on *Establishment and Maintenance of Brain Cell States*, Rungstedgaard, Denmark, April 2023
- Presented poster titled “*Exploring transcriptional cascades in cortical astrocytes: the role of Sox9 and Trps1*” at the XVI European Meeting on Glial Cells in Health and Disease in Berlin (GLIA 2023)
- Virtual participation and poster presentation in Cold Spring Harbor Laboratory Conference Glia in Health & Disease, 2022 and XV European Meeting on Glial Cells in Health and Disease 2021

REFEREES

- Dr Magdalena Götz, Dept of Physiological Genomics, Biomedical Center, LMU, Email: magdalena.goetz@helmholtz-muenchen.de
- Dr Giacomo Masserdotti, Dept of Physiological Genomics, Biomedical Center, LMU Email: giacomo.masserdotti@bmc.med.lmu.de
- Dr Cornelius Gross (Senior Scientist), EMBL Mouse Biology Unit, Via E Ramarini, Monterotondo 00015, Italy Email: gross@embl.it
- Dr Munia Ganguli (Senior Scientist), CSIR- Institute of Genomics & Integrative Biology, New Delhi, India; Email: mganguli@igib.in

List of Publications

- **Natarajan, P.**, Koupourtidou, C., de Resseguier, T., Bocchi, R., Fischer-Sternjak, J., Gleiss, S., Rodrigues, D., Myoga, M., Ninkovic, J., Masserdotti, G., Götz, M. Single cell deletion and analysis of the transcription factors Sox9 and Trps1 reveals novel functions in astrocyte.
Manuscript in preparation
- Russo, G.L., Sonsalla, G.*, **Natarajan, P.***, Breunig, C.T., Bulli, G., Merl-Pham, J., Schmitt, S., Giehl-Schwab, J., Giesert, F., Jastroch, M., Zischka, H., Wurst, W., Stricker, S.H., Hauck, S.M., Masserdotti, G., Götz, M., 2021. CRISPR-Mediated Induction of Neuron-Enriched Mitochondrial Proteins Boosts Direct Glia-to-Neuron Conversion. *Cell Stem Cell* 28, 524-534.e7.
<https://doi.org/10.1016/j.stem.2020.10.015>
- Nisakar, D., Vij, M., Pandey, T., **Natarajan, P.**, Sharma, R., Mishra, S., Ganguli, M., 2019. Deciphering the Role of Chondroitin Sulfate in Increasing the Transfection Efficiency of Amphipathic Peptide-Based Nanocomplexes. *ACS Biomater. Sci. Eng.* 5, 45–55. <https://doi.org/10.1021/acsbiomaterials.8b00069>
- Vij, M., **Natarajan, P.**, Pattnaik, B.R., Alam, S., Gupta, N., Santhiya, D., Sharma, R., Singh, A., Ansari, K.M., Gokhale, R.S., Natarajan, V.T., Ganguli, M., 2016. Noninvasive topical delivery of plasmid DNA to the skin using a peptide carrier. *J. Controlled Release* 222, 159–168. <https://doi.org/10.1016/j.jconrel.2015.12.017>
- Vij, M.*, **Natarajan, P.***, Yadav, A.K., Patil, K.M., Pandey, T., Gupta, N., Santhiya, D., Kumar, V.A., Fernandes, M., Ganguli, M., 2016. Efficient Cellular Entry of (r-x-r)- Type Carbamate-Plasmid DNA Complexes and Its Implication for Noninvasive Topical DNA Delivery to Skin. *Mol. Pharm.* 13, 1779–1790.
<https://doi.org/10.1021/acs.molpharmaceut.5b00915>

Eidesstattliche Versicherung/Affidavit

Hiermit versichere ich an Eides statt, dass ich die vorliegende Dissertation **“EXPLORING MOLECULAR MECHANISMS DICTATING ASTROCYTE IDENTITIY AND IMPLICATIONS FOR NEURONAL REPROGRAMMING”** selbstständig angefertigt habe, mich außer der angegebenen keiner weiteren Hilfsmittel bedient und alle Erkenntnisse, die aus dem Schrifttum ganz oder annähernd übernommen sind, als solche kenntlich gemacht und nach ihrer Herkunft unter Bezeichnung der Fundstelle einzeln nachgewiesen habe.

I hereby confirm that the dissertation **“EXPLORING MOLECULAR MECHANISMS DICTATING ASTROCYTE IDENTITIY AND IMPLICATIONS FOR NEURONAL REPROGRAMMING”** is the result of my own work and that I have only used sources or materials listed and specified in the dissertation.

München , den

Munich, date

Munich, 21.08.2023

Unterschrift

Signature

Poornemaa Natarajan

Acknowledgements

This feels surreal. For where I come from, the circumstances in which I grew up, I would have never imagined that I would be doing a PhD, especially in a lab like this. I feel nothing other than an overwhelming gratitude for this life, all the people and the opportunities that have been given to me. First, I would like to thank the IMPRS-LS and Magdalena that saw some potential in my PhD application and decided to give me a chance to come and work here. I would be remiss if I did not thank the GSN, for without their option to do a “Fast-track”, I would have never been eligible to start a PhD in Germany.

Once again, I would like to thank Magdalena for this opportunity to work in the most enriching scientific environment, it feels like I was handed a golden ticket. Thank you for being a huge inspiration, your passion and enthusiasm for science (and life) is infectious. I would also like to thank you for being patient and kind with me through these years, I am truly grateful for this opportunity and I have so much to learn from you.

The other person who has been immensely patient and kind with me throughout this journey is my co-supervisor Giacomo. Thank you for checking on me often, for sitting beside me and helping me comprehend tricky data, for always being there for my last minute corrections, for patiently listening to all my incoherent ideas and guiding me to do the more sensible things and ensuring I was always (mostly) on track and not too distracted. Your dedication and hard work is formidable, and I have so much to learn from you.

Thanks to Florence and Francois for being the most supportive TAC members, I am grateful for the discussions and your keen insights into the project. This PhD journey would have been impossible without the support and kindness of the incredible people who work here. I would like to thank Arek for his generosity and help with the Cas9 mice. Within the department, I would like to thank Tatiana for teaching and helping with astrocyte cultures, for being a calming presence on extremely stressful experimental days involving cell culture or 10x; Manja for teaching me animal surgeries and helping with perfusions; Ines for helping out with often complicated stretches of STAgR cloning, Paulina for the virus productions. Special shout out also to Yvette and Riccardo for taking the time to teach me surgeries or helping with animal surgeries in the beginning, your kindness is highly appreciated. I am also grateful to all the other technicians and the people in the lab who are always so kind and offer to help in any way possible. I am grateful to all the lab meetings, data clubs, and by extension all the people for the stimulating discussions, I continue to learn from every one of you.

I am also filled with gratitude for all the amazing individuals who have made the non-scientific part of this journey beautiful. “Matteo’s minions”, you guys are the best of the best and I cannot comprehend how I got so lucky. Bob, thank you for “adopting” me as a friend, I will forever cherish our conversations, the pizza and wine evenings with you and the other minions. I am manifesting for the day when you and I will go to Sicily and ride on a Vespa (of course, with Matteo screaming in the background). Matteo, thanks for bringing drama (and immense happiness) to my life. I love discussing (borderline arguing) about everything with you, be it science or the rules for drinking cappuccino after lunchtime. Giulia, WE ARE LUCKY GIRLS! Thank you for always being around, you are the most wonderful person, your determination is inspiring. Florencia, thanks you for the splendid discussions and being an amazing presence. From you, I am trying to learn the art of caring without being consumed by it all. Gio, you are a ball of energy, thanks for being my coffee partner, you always make me smile. Fabio, thank you for being the sunshine of the office, your energy is infectious and I love going for “lunch” with you. I am also extremely grateful for the friendships and conversations with Daniela, Fernanda, Yiling, Maroussia, Ana, Yvette, Gulzar, Luisa, Chulan and Fatma, other past members of the lab Sonia, Gia, Judith, Gianluca, Riccardo and Alwyn.

Outside of Munich, I am grateful for the constant support from Munia Ganguli and Cornelius Gross. I am grateful for the opportunities you gave me and I admire your enthusiasm for science.

Coming to life outside of lab, I am forever grateful for the friendship of Sandhya, Durga, Sai, Ritu, Zsofi, Dhanya, Avleen, Florian and many others over the years. I always looked forward to Friday evenings in the past years, thanks to Snetanz and Abhinaya. Thank you for teaching me how to dance and more importantly, how to be myself unapologetically. Sharanya, thank you for your kindness, amazing food and being the best brunch partner.

Moving to my support systems, I am immensely indebted to Sarah. Sam, thank you for coming into my life when I was almost about to give up on Munich. Swedhu, thank you for your presence, I am so happy that we have been together in this long journey of Madras to Munich/EU. Vishnu, thank you for the BEST conversations ever, all the silliness and most importantly for introducing me to SP and initiating me into advaita. Anuroop, thank you for initiating me into R. From being a great movie buddy to listening to all my insecurities and encouraging me, you have helped me immensely, I am grateful for your presence. Vivek, thank you for being my “friend” and making me your family. I will be eternally grateful to Sneha, I

am so grateful for the sisterhood we share. I cannot imagine having gone through the past years without your love and constant virtual support. I love you and I cannot wait to meet my Krishna. Anu and Girish, thank you for being an unwavering pillar of support. The faith you have in me and the love you shower me with makes me speechless. Maithreyi, thank you for existing. You have taught me how to love, the mere thought of you fills me with joy and hope. Amma, thank you for everything. Your love and prayers will always guide me, thanks for teaching me the joy of existence. Appa, thatha and paati, thank you for loving me so unconditionally ALWAYS.

எத்தனை கோடி இன்பம் வைத்தாய்!

Poornemaa

20.08.23